

✓
CONTROL OF COORDINATION THROUGH 3,5-SUBSTITUENTS OF THE PYRAZOLE
RINGS IN PYRAZOLYLMETHYLPYRIDINE LIGANDS AND OXO-BRIDGED
DIMANGANESE SYSTEMS OF RELEVANCE TO BIOLOGY

A Thesis Submitted
in Partial Fulfilment of the Requirements
for the Degree of
DOCTOR OF PHILOSOPHY

by
Tapan Kumar Lal

to the
DEPARTMENT OF CHEMISTRY
INDIAN INSTITUTE OF TECHNOLOGY KANPUR
March, 1996

*Dedicated to
my parents*

- 8 AUG 1997
CENTRAL LIBRARY
I. I. T., KANPUR
A 12363

✓ CHM-1996-D-LAL-CON

STATEMENT

I hereby declare that the matter embodied in this thesis is the result of investigations carried out by me in this Department of Chemistry, Indian Institute of Technology, Kanpur, India under the supervision of Prof. R. N. Mukherjee.

In keeping with the general practice of reporting scientific observations, due acknowledgements have been made wherever the work described is based on the findings of other investigators.



Tapan Kumar Lal

I. I. T. Kanpur

March, 1996

DEPARTMENT OF CHEMISTRY
INDIAN INSTITUTE OF TECHNOLOGY , KANPUR
INDIA

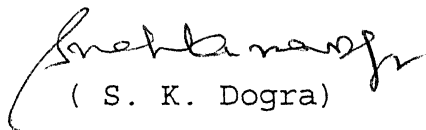
CERTIFICATE - I

This is to certify that Mr. Tapan Kumar Lal (Roll Number 9120765) has satisfactorily completed all the courses required for the Ph.D. degree program and obtained C.P.I. of 9.00

These courses include:

CHM 646 Bio-inorganic Chemistry
CHM 612 Frontiers in Organic Chemistry
CHM 625 Principles of Physical Chemistry
CHM 605 Principles of Organic Chemistry
CHM 645 Principles of Inorganic Chemistry
CHM 664 Modern Physical Methods in Chemistry
CHM 800 General Seminar
CHM 801 Special Seminar
CHM 900 Post Graduate Research

Mr. Tapan Kumar Lal successfully completed his Ph. D. qualifying examination in September 1993.


(S. K. Dogra)

Head

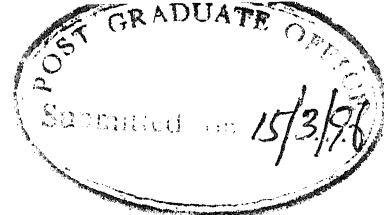
Department of Chemistry
I. I. T. Kanpur


(P. Guptabhaya)

Convenor

Departmental Post Graduate
Committee

Department of Chemistry
I. I. T. Kanpur



CERTIFICATE - II

It is certified that the work contained in the thesis entitled "Control of Coordination Through 3,5-Substituents of the Pyrazole Rings in Pyrazolylmethylpyridine Ligands and Oxo-bridged Dimanganese Systems of Relevance to Biology" by Mr. Tapan Kumar Lal, has been carried out under my supervision and that this work has not been submitted elsewhere for a degree.

R.N. Mukherjee
15/03.96

Signature of Supervisor

(Prof. R. N. Mukherjee)

Chemistry

I.I.T. Kanpur

March, 1996

ACKNOWLEDGEMENTS

It is a great privilege for me to record my profound gratitude to my thesis supervisor, Prof. R. N. Mukherjee who inspired and encouraged me through his guidance, constructive suggestions, and critical comments during my research program. I am really indebted to him for his untiring efforts in providing me a good spadework in my research career.

I am highly indebted to Prof. J. Iqbal and Prof. P. K. Bharadwaj of this department for their help and valuable suggestions. I express my sincere thanks to Prof. S. Sarkar, Prof. N. Sathyamurthy, Prof. S. Manogaran, and other faculty members in this department for their help and suggestions.

I would like to thank my senior labmates for various help and the nice homogeneous association I had with them. My special thank goes to Dr. S. Mahapatra who introduced me to ways and language of laboratory techniques and helped me in the initial stages of my work. Thanks are also due to Dr. N. Gupta, Dr. K. Ramesh, Dr. M. Ray, and Dr. Z. Shirin for useful discussions, help, suggestions and cooperation.

I would like to express my thanks to Apurba Patra and Debalina Ghosh for various help and discussions during the completion of my work. I also thank Saptarshi Roy, Rajeev Gupta, Rajdeep Das, and Rupa Mukhopadhyay for their help.

I wish to acknowledge the valuable help received from Prof. S. Mitra (TIFR, Bombay) for variable temperature magnetic susceptibility measurements and his invaluable suggestions in the

set up of our magnetism system. I am also thankful to Prof R. M. Buchanan (University of Lousville, Lousville, Kentucky, USA) for one X-ray structure.

I extend my sincere thank to Mr. Nayab Ahmed, Mr. Bausar and Mr D. K. Kannaujia for helping me in recording NMR, IR, and EPR spectra respectively.

I thank to Mr. L. P. Tripathi, Mr. V. N. Katiyar, Mr. B. N. Shukla, and Mr. U. S. Mishra of this department for all the help I got from them. I also thank Mr. V. K Gupta for tracing of figures.

I thank my friends Justin, Ramsharan, Samarda, Gagan, Shibu, Susanta, Rabin, Arpita, Subit, Raghu, Kapurida, Goutam, Dipak and others in the department and Hall 4 who made my stay at IIT Kanpur, a most eventful one.

I also like to take this opportunity to thank Mrs. Mukherjee for making my stay here homely and lively.

I find myself at a loss for words in expressing my heartfelt gratitude to my adored parents, brothers, sisters and other family members for providing tremendous moral support and encouragement for completion of my work.

T.K. Lal

Tapan Kumar Lal

SYNOPSIS

The thesis entitled "Control of Coordination through 3,5-Substituents of the Pyrazole Rings in Pyrazolylmethylpyridine Ligands and Oxo-bridged Dimanganese Systems of Relevance to Biology" has been divided into five chapters.

Chapter I (Introduction) presents an overview of the known coordination chemistry of selected bidentate (in some cases tridentate also) nitrogen donor ligands containing pyridine and pyrazole as donor sites. The impetus of majority of these studies using polypyridyl ligands arises from the standpoint of catalytic, redox, and photoredox properties of a variety of transition-metal complexes and ruthenium complexes in particular.

Now a given ligand system can be subtly modified by the following strategies. They include: (i) the placement of both a π -accepting heterocyclic ring such as pyridine and a π -donor heterocyclic ring such as pyrazole. This would give rise to a situation in which both a hard donor center and a soft donor center would be present and (ii) by placing an aliphatic spacer between the two different kinds of heterocyclic rings so as to prevent electronic communication from one heterocyclic ring to another. Obviously, such ligands could be utilized to suitably fine tune the properties of their complexes. A survey of the literature reveals that systematic chemistry has not been developed using these types of bidentate ligand systems.

This chapter also covers a brief outline of the biological implications of copper nitrite reductases and the oxo-bridged dimanganese cores and thus provides the scope of the present work. The work presented in subsequent chapters stems mainly from the following facts: (a) there were no reports on systematic studies of steric effect imposed by the bidentate pyrazolylmethylpyridine ligands on the formation of 1:1, 1:2, and 1:3 (metal-to-ligand ratio) complexes of Co(II) and Ni(II), (b) reports of Cu(II) complexes with variable stereochemistry using bidentate ligands is comparatively limited, (c) mononuclear Cu(II) complexes with nitrite ligation is expected to mimic structural/functional properties of copper containing nitrite reductases. The number of such complexes is limited, and (d) oxo-bridged dimanganese cores are believed to be present in *pseudo*-catalases (Mn-catalases) and water-oxidizing complex in photosystem II; model studies of these core structures are of contemporary interest. Each of these problems has been dealt with in the subsequent chapters.

Chapter II demonstrates the effect of methyl substituents at the 3,5-positions of pyrazole rings using two non-planar bidentate nitrogen donor ligands 2-(pyrazole-1-ylmethyl)pyridine and 2-(3,5-dimethylpyrazole-1-ylmethyl)pyridine. In the course of this investigation several *pseudo*-tetrahedral with $M^{II}N_2Cl_2$ coordination sphere and a series of *pseudo*-octahedral with $M^{II}N_4Cl_2$ and $M^{II}N_6$ coordination spheres of high-spin Co(II) and Ni(II) have been synthesized. The metal coordination environments in *pseudo*-tetrahedral and *pseudo*-octahedral Co(II) have been revealed by X-ray

diffraction studies. The metal coordination environments in the solution-state of a *pseudo*-tetrahedral Co(II) and a *pseudo*-octahedral Ni(II) complex have been determined by ^1H NMR spectral studies. For *pseudo*-octahedral Ni(II) complexes an estimation of $10D_q$ values revealed that increased steric crowding decreases the value of $10D_q$ for these two bidentate ligands.

Chapter III deals with the effect of methyl substituents at 3,5-positions of pyrazole rings of the above-mentioned ligands on the $\text{Cu}^{\text{II}}\text{N}_4$ coordination environment. Various stereochemical features such as distorted trigonal bipyramidal, distorted square pyramidal geometries around Cu(II) with $\text{Cu}^{\text{II}}\text{N}_4\text{X}$ ($\text{X} = \text{Cl}^-$, NO_2^- , SCN^- , and N_3^-) coordination sphere have been achieved using the methyl substituted ligand. For grossly $\text{Cu}^{\text{II}}\text{N}_4$ coordination sphere the Cu(II)/Cu(I) reduction potentials are quite high. For a penta-coordinate complex with $\text{Cu}^{\text{II}}\text{N}_4(\text{NO}_2^-)$ coordination a novel electrochemistry has been demonstrated for the first time which is very interesting so far as the functional modeling of copper containing nitrite reductases are concerned.

Chapter IV describes synthesis, characterization, highest Cu(II)/Cu(I) redox potentials of two novel pentacoordinate Cu(II) complexes having $\text{Cu}^{\text{II}}\text{N}_5$ coordination sphere where all coordinating nitrogens are from heterocyclic rings. Copper(II) coordination environment (distorted square pyramidal) of a sterically congested complex has been revealed by X-ray diffraction studies.

Syntheses, spectroscopy, and electrochemistry of tribridged dimanganese complexes containing $\{\text{Mn}^{\text{III}}_2(\mu\text{-O})(\mu\text{-OAc})_2\}^{2+}$ and $\{\text{Mn}^{\text{IV}}_2(\mu\text{-O})_2(\mu\text{-OAc})\}^{3+}$ cores using a pyridine-rich facially capping ligand MeL have been described in Chapter V. The coordination environment around the manganese atoms of the mixed-valent dimanganese core has been revealed by X-ray diffraction studies. Novel and interesting electrochemistry of the $\{\text{Mn}^{\text{III}}_2-(\mu\text{-O})-(\mu\text{-OAc})_2\}^{2+}$ core have been demonstrated. Interesting redox interconversion studies among three triply-bridged dimanganese cores have been presented. For the first time a high yield synthesis of $\{\text{Mn}^{\text{III}}_2(\mu\text{-O})(\mu\text{-OAc})_2\}^{2+}$ core from $\{\text{Mn}^{\text{III}}\text{Mn}^{\text{IV}}(\mu\text{-O})_2(\mu\text{-OAc})\}^{2+}$ core has been achieved using glacial acetic acid. Chloride-ligated dimanganese (IV,IV) species has been generated in MeCN solution and electrochemistry of the same has been studied in MeCN. Oxidation of water by the $\{\text{Mn}^{\text{IV}}_2(\mu\text{-O})_2(\mu\text{-OAc})\}^{3+}$ core has been demonstrated.

CONTENTS

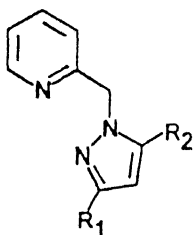
STATEMENT		iii
CERTIFICATE - I		iv
CERTIFICATE - II		v
ACKNOWLEDGEMENTS		vi
SYNOPSIS		viii
CHAPTER I	Introduction	1
CHAPTER II	Cobalt(II) and Nickel(II) Complexes of Pyrazolymethylpyridine Ligands: Synthesis, Structure, and Reactivities	31
CHAPTER III	Cu(II) Complexes of Pyrazolymethylpyridine Ligands: Synthesis, Structure, and Redox Properties	92
CHAPTER IV	Five-Coordinate Cu(II) Complexes using Pyrazolymethylpyridine and Bis(pyrazolymethyl)pyridine Ligands: Synthesis, Structure, and Redox Properties	155
CHAPTER V	Chemistry of New Triply Bridged Dimanganese(III) and Dimanganese(IV) Complexes with $\{\text{Mn}^{\text{III}}_2(\mu\text{-O})(\mu\text{-OAc})_2\}^{2+}$ and $\{\text{Mn}^{\text{IV}}_2(\mu\text{-O})_2(\mu\text{-OAc})\}^{3+}$ Cores	176
REFERENCES		225
APPENDIX		239
FUTURE SCOPE OF THIS WORK		250

CHAPTER I

INTRODUCTION

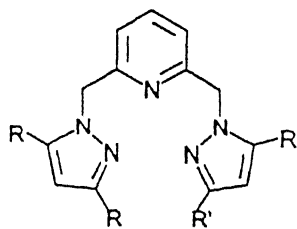
I.1 Purpose of the Present Investigation

The primary concern of this thesis is twofold. (i) To develop an extensive transition metal chemistry utilizing, primarily, two bidentate pyrazolylmethylpyridine ligands, I and II. However, the tridentate ligands, III and IV, a closely similar variety of I and II, have also been used in one case. (ii) To demonstrate a rich oxo-bridged binuclear manganese chemistry of relevance to the water oxidation center of photosystem II of the photosynthetic apparatus and manganese containing catalases and *pseudo*-catalases, using a pyridine-rich facially capping tridentate nitrogen donor ligand, V.



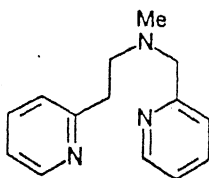
$R_1 = R_2 = H$, H_2pp (I)

$R_1 = R_2 = Me$, Me_2pp (II)



$R = R' = H$, H_4bpp (III)

$R = R' = Me$, Me_4bpp (IV)



MeL (V)

I.2 Scope of the Work

In what follows we describe selected examples of known chelate chemistry utilizing bidentate nitrogen donor ligands of relevance to the present investigation. This background information allows one to appreciate the uniqueness of the ligands chosen in the present work. The design of new organic ligands capable of coordinating metal ions efficiently deserves an appreciation on its own merit but the ultimate challenge lies in the fruitful use of such ligands to develop new interesting chemistry of greater importance to chemists in general and inorganic chemists in particular.

I.2.1 Challenging Coordination Chemistry Utilizing Selected Bidentate Ligands Containing Pyridine/Pyrazole Rings

In this section the focus has been made mainly on the bidentate ligand systems. However, for a meaningful comparison, some closely similar tridentate ligands are also included.

I.2.1.1. Ligands having π -Conjugation Between Two Aromatic Nitrogen Heterocycles: Diimine systems

I.2.1.1.1 Ligands Containing Pyridine Rings (Figures I.1, I.2 and I.3):

Bidentate heterocyclic ligands, such as 2,2'-bipyridine (bpy) (1) and 1,10-phenanthroline (phen) (2) have long been used as ligands in transition metal coordination chemistry.^{1,2} These family of ligands hold a considerable importance in coordination chemistry because of their ability to form stable tris-complexes with variety of transition metals. Within this family, photochemi-

cal and electrochemical properties of tris(2,2'-bipyridine)ruthenium(II), $[\text{Ru}(\text{bpy})_3]^{2+}$ have been the subject of a large number of studies because of its potential use as a photocatalyst,³ and various substituents have been introduced to the bipyridine moiety in order to "tune" the photochemical and/or electrochemical properties of the complexes.⁴⁻⁶

The introduction of sterically hindering or directing substituents on to multidentate nitrogen donor ligands may have longer range consequences on the reactivity of many of the transition metal complexes which utilize such ligands.⁷⁻¹⁷ For example, recent work with $\text{Cu}(\text{dpphen})$ (dpphen = 2,9-diphenyl-1,10-phenanthroline (3)) complexes has shown that the phenyl substituents of dpphen significantly influence the manner in which the copper complex binds to DNA as well as influence the excited state life-times.^{18,19} In addition, complexes of Rh and Ir which incorporate dmphen (dmphen = 2,9-dimethyl-1,10-phenanthroline (4)) have been proven to be efficient water gas shift catalysts²⁰ while $\text{cis-}[\text{Ru}^{\text{VI}}(\text{dmphen})_2\text{O}_2](\text{PF}_6)_2$ has been studied in the oxidation of organic substrates.²¹ Similarly, bpy ligands have extensively been modified (5-7) (to introduce steric effect) synthetically.²²⁻²⁸ Ruthenium coordination complexes utilizing the bpy and substituted bpy ligands have been studied in relation to their remarkable reactivity which is manifested in the photo-production of H_2 and O_2 from water and their use in photo-chemical cells to convert and store solar energy.²⁹ The steric crowding caused by the H-atoms on the benzo rings markedly changes the metal chelating properties of biq (2,2'-biquinoline (8)) and pq (2-(2'-pyridyl)quinoline (9)).^{30a,30b} In particular a single benzo substitution of bpy to

form pq changes the tris complex with iron(II) from low spin in $\text{Fe}(\text{bpy})_3^{2+}$ to essentially high spin in $\text{Fe}(\text{pq})_3^{2+}$, while double benzo substitution to form big so increases the steric hindrance that the tris complex $\text{Fe}(\text{big})_3^{2+}$ could not be prepared.^{30c} Klassen et al.^{30d} have shown the effect of the benzo substituents on the absorption and emission spectra of the tris(big) complexes of Ru(II) and Os(II). Goodwin and co-workers have reported^{30e-30g} influence of the steric effect of substituents within a chelate group on the stability and electronic ground state of Fe(II) tris-complexes using 6-methyl-2,2'-bipyridine (10), pq, dmbpy, and 2-methyl-1,10-phenanthroline (11). They have also shown^{30h} the effect of introduction of six-membered chelate ring on electronic ground state of Fe(II) complex of phen using the substituted phen ligand, 1,10-phenanthroline-2-yl-(pyridin-2-yl)amine (12).

Investigations of the structural effects caused by the 6,6''-disubstitution of terpy (2,2': 6,6''-terpyridine (13)) (14-15) ligands on transition metal complex reactivity are relatively rare.³¹⁻³³ Ruthenium complexes which utilizes terpy ligands have been proven catalytically to oxidise H_2O to molecular oxygen^{15,34} and to act as oxygen-atom transfer agents for the oxidation of benzyl alcohol and norbornene.^{35a-35c} Thummel and co-workers have shown influence of remote substituents on the properties of bis(terpy)ruthenium(II) complexes³⁶ and they have investigated^{37a,37b} the interrelationship between ligand conformation and coordination geometry for the Ru(II) complexes of 3,3' annealated derivatives of 2-(2'-pyridyl)quinoline (16), 2-(2'-pyridyl)-1,8-naphthyridine (17), annealated derivatives of terpy (18) and related systems. Planar tridentate terheteroaro-

matic analogue of terpyridine (19-24) are less common,³⁸⁻⁴⁶ complexes of these ligands which contain two excessive pyrazole rings, have very different properties to those of terpyridyl complexes.

The ability to constrain sterically the access of a substrate to an active transition metal centre has been proposed to be of importance in the development of substrate-specific catalyst.^{20,21}

Che et al. have shown that the complexes trans- $[\text{Ru}^{\text{III}}(\text{L})_2(\text{OH})(\text{H}_2\text{O})](\text{ClO}_4)_2$ ^{47a} (L = phen or 5,5'-dimethyl-2,2'-bipyridine (25)), cis- $[\text{Ru}^{\text{II}}(6,6'\text{-Cl}_2\text{bpy})_2(\text{OH}_2)_2]^{2+}$ ^{47b} (6,6'-Cl₂-bpy = 6,6'-dichloro-2,2'-bipyridine (26)), and $[\text{Ru}^{\text{II}}(\text{terpy})(6,6'\text{-Cl}_2\text{bpy})(\text{H}_2\text{O})]^{2+}$ ^{47c} are useful catalysts which can oxidize organic substrates chemically or electrochemically in good yield. They have also shown^{47d} that the mono-oxoruthenium(IV) complex, $[\text{Ru}^{\text{IV}}(\text{L})(\text{bpy})\text{O}]^{2+}$ (L = 1,4,7-trimethyl-1,4,7-triazacyclononane (27)) is a competent oxidant for alkane (styrene, norbornene) epoxidation. Che and co-workers also reported⁴⁸ PhIO oxidation of organic substrates (norbornene, styrene, cyclohexene etc.) catalyzed by $[\text{Ru}^{\text{III}}(\text{N}_4\text{O})(\text{OH}_2)](\text{ClO}_4)_2$ (N₄OH = bis(2-(2-pyridyl)ethyl)(2-hydroxy-2-(2-pyridyl)ethyl)amine) (28). The sterically crowded complex, cis- $[\text{Ru}^{\text{II}}(\text{dmphen})_2\text{S}_2](\text{PF}_6)_2$, S = Me₃CN or H₂O) is capable of hydroxylating methane under mild reaction conditions utilizing H₂O₂ as the primary oxidant have been shown⁴⁹ by Drago et al.

Thorp and co-workers have shown⁵⁰ that complexes based on $\text{Ru}(\text{terpy})(\text{L})\text{OH}_2^{2+}$ (L = η^2 -tpt, phen, dppz, tmen; tpt = 2, 4, 6-tripyridyltriazine (29), dppz=dipyridophenazine (30) and tmen= N,

N,N', N'-tetramethylethylenediamine) (31) can all be reversibly oxidized to their $\text{Ru}^{\text{IV}}\text{O}$ forms, which are component DNA cleavage agents. Chaires and co-workers have shown^{51a} the interaction of Δ - and Λ - $[\text{Ru}(\text{phen})_2\text{dppz}]^{2+}$ with DNA. Linkletter and Chin have shown^{51b} that the two methyl groups of dmphen ligand in $[\text{Cu}(\text{dmphen})(\text{H}_2\text{O})_2]^{2+}$ not only prevent dimerization but also activate the complex for RNA hydrolysis and they have shown that this complex is currently most effective transition metal complex for hydrolyzing RNA. Bernhart et al. have demonstrated^{51c} that depending upon the size of the bulky groups of 2,9-dialkyl-1,10-phenanthroline, in $[\text{Cu}(\text{dap})_2]^+$ distortion varies from ideal tetrahedral geometry.

I.2.1.1.2 Ligands Containing Both Pyridine and Pyrazole Rings (Figures I.2, I.3 and I.4):

Recently^{52,53} bidentate ligands containing pyridine and pyrazole rings have been shown to have different properties to those of bpy and phen because of presence of both six-membered π -deficient and five-membered π -excessive heterocycles. Pyrazole-containing ligands have been the focus of much recent attention.³⁸ As for example, Rae et al. have reported^{54a} the occurrence of a thermallyinduced spin transition in $\text{Fe}(\text{II})$ tris-complex of N^1 -(pyridin-2-yl)-3,5-dimethylpyrazole (32).

I.2.1.1.3 Ligands Containing Pyridine and/or Other Heterocyclic Rings (Figures I.4 and I.5):

In recent years there have been many studies of transition metal complexes of biheteroaromatic ligand in which one pyri-

dine ring of bpy is replaced by other nitrogen heterocycles.^{54b,54c} Both π -deficient six-membered nitrogen heterocycles (azines) and π -excessive five-membered heterocycles (azoles) have been employed as ligand components (33-54), and the properties of resulting complexes have been found to depend markedly on the specific heterocycle involved.^{54b,54c}

I.2.1.2 Ligands having Two Nitrogen Heterocycles Joined by a Bridging Group: Absence of Diimine Moiety (Figure I.5):

Coordination chemistry of Cu(II) as well as photo-physical and electrochemical properties of Ru(II) complexes have been developed⁵⁵⁻⁶⁵ using bidentate ligands containing >NH or >CO group between the two heterocyclic rings (55-61). In such cases chemistry and electronic properties are quite different than that of bpy and phen since here electron (π or n-electron(s)) can flow only between the bridging group and any one of the heterocyclic rings.

Geldard et al. have shown⁶⁰ that with the increased steric interaction between ligands (due to (i) increase in the number of methyl groups near donor site and/or (ii) in going from 6-membered to 5-membered ring) in Cu(II) complexes of general formula $[\text{Cu}(\text{HL})_2](\text{ClO}_4)_2$ (HL = 2-pyridyl-2'-pyrimidylamine (55), 2-pyridyl-2'-thiazolylamine (56), 2-pyridyl-2'-(4'-methylthiazolyl)amine (57), and 2-(6-methylpyridyl)-2'-(4'-methylthiazolyl)amine (58)) the geometry becomes more towards tetrahedral.

I.2.1.3 Ligands having Two Aromatic Nitrogen Heterocycles: π -Conjugation Absent (Figures I.6 and I.7)

Bidentate nitrogen donor heterocyclic ligands containing an "insulator" (or spacer) such as $-\text{CH}_2-\text{CH}_2-$ (62-63) and; $>\text{CR}_2$ ($\text{R} = \text{H}, \text{Me}, \text{Et}, \text{OMe}$ etc.) (64-81) groups between two heterocycles have been used recently in coordination^{66-70,78} and organometallic⁷¹ chemistry. Thus due to presence of any "insulator" prevents π -conjugation between two heterocycles (i.e. electron can not flow from one heterocycle to the other) and thereby electronic properties of these ligands are quite different. The chemistry of the complexes formed by these ligands differ markedly to those of bpy, phen, and their analogs.

I.2.1.3.1 Ligands Containing Pyridine Rings (Figure I.6):

Recently^{66-71,78} coordination and interesting organometallic chemistry have been developed using dipyridylmethanes (64-68).

I.2.1.3.2 Ligands Containing Pyrazole Rings (Figure I.6):

Ligands containing pyrazole rings have been shown⁷¹⁻⁷⁷ to greatly modify the properties of complexes. This results from the fact that the π -excessive five-membered nitrogen heterocycles have significantly different π -donor/acceptor properties to the π -deficient six membered nitrogen heterocycles (69-76). Recently Shiu et al. have shown⁷⁷ the contribution of steric effect of the bidentate ligand, bis(3,5-dimethylpyrazolyl-1-yl)methane in $[\text{Mo}(\text{L})(\text{CO})_2(\text{NO})(\text{MeOH})]^+$ towards the formation of various types of products using a variety of nucleophiles.

I.2.1.3.3 Ligands Containing Both Pyridine and Pyrazole Rings

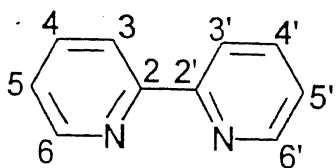
(Figures I.6 and I.7):

Very little coordination chemistry has been developed^{39,79-85} using these kinds of nitrogen donor heterocyclic ligands. They are of special importance due to the presence of (i) two different kinds of π -systems within one ligand and (ii) "insulator" (i.e. $>CR_2$ group as spacer) between those π -systems (77-81).

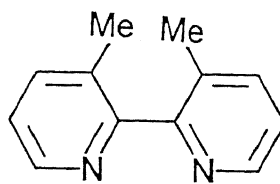
In spite of the important catalytic properties of complexes of bidentate nitrogen heterocycles, such as bpy, only recently⁸⁰⁻⁸⁵ attempts have been made to synthesize chiral derivatives of polyheterocyclic ligands (82-83). Steel et al^{39,79} have reported the synthesis and study of a variety of polydentate ligands comprising nitrogen heterocycles fused to a bornyl framework.

It is worth mentioning here that during the last five years or so from our laboratory studies were made to identify the steric effect of methyl substituent(s) adjacent to donor atoms in groups of bis-ligated high-spin complexes of type $[ML_2]^{2+}$ ($M = Fe(II), Co(II)$ or $Ni(II)$) using a new family of three tridentate bis(pyrazolylmethyl)pyridine ligands (84-86).^{86,89-92}

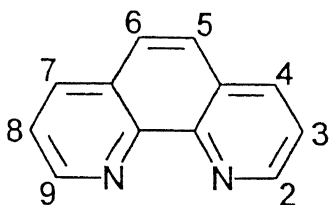
The effect has been identified by investigating the trends in the energies of the ligand field spectral transitions,^{86,89} the M^{III}/M^{II} redox potentials ($M = Mn, Fe$ or Co),^{86,87,91} the temperature dependence of the spin-state properties of $Fe(II)$ complexes,⁹⁰ and the X-ray structural properties of a bis(ligand) $Fe(II)$ complex of an unsymmetrical tridentate bis-(pyrazolylmethyl)pyridine ligand (85).⁹²



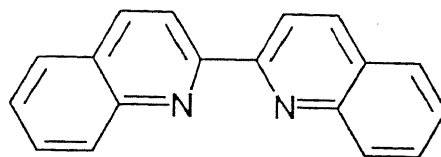
(1)



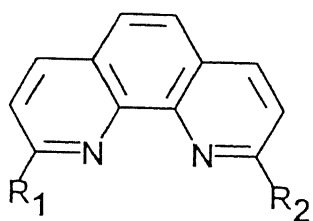
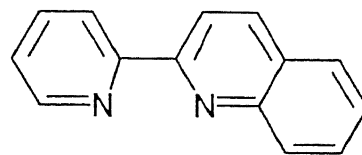
(7)



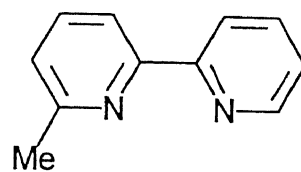
(2)



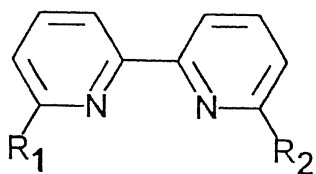
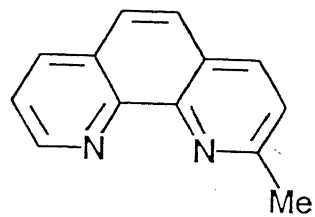
(8)


 $R_1 = R_2 = \text{Ph} \quad (3)$
 $R_1 = R_2 = \text{Me} \quad (4)$


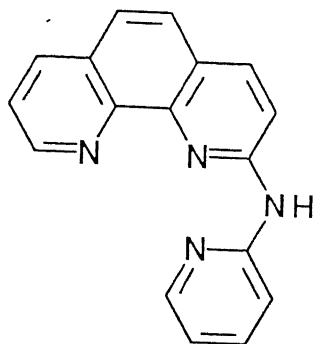
(9)



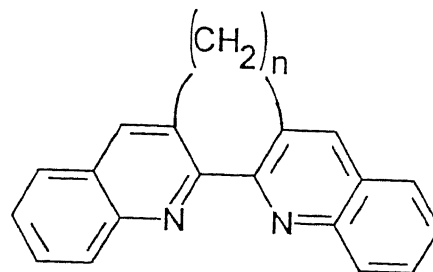
(10)


 $R_1 = R_2 = \text{Me} \quad (5)$
 $R_1 = R_2 = \text{NH}_2 \quad (6)$


(11)

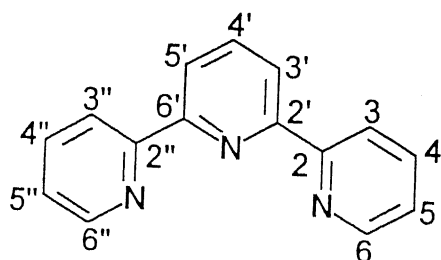


(12)

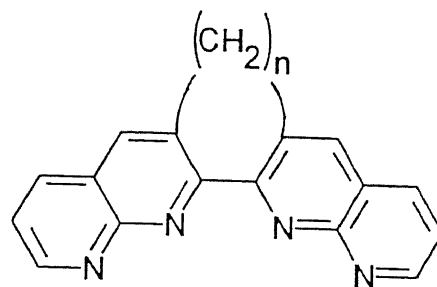


n = 1-4

(16)

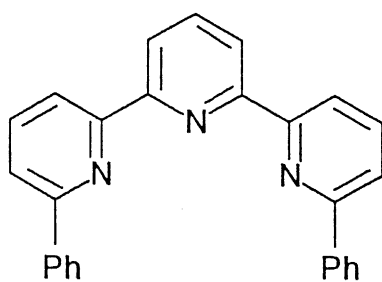


(13)

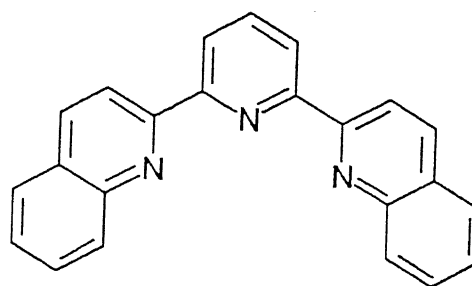


n = 1-4

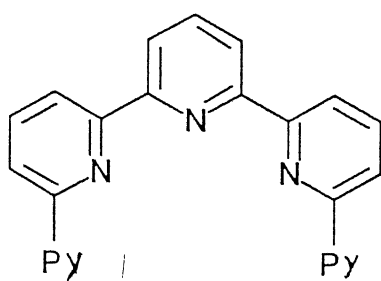
(17)



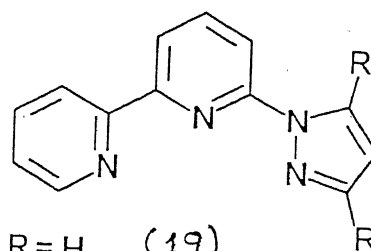
(14)



(18)

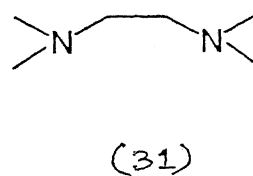
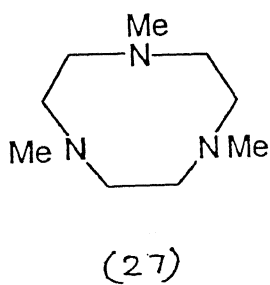
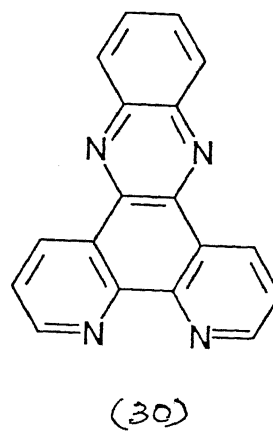
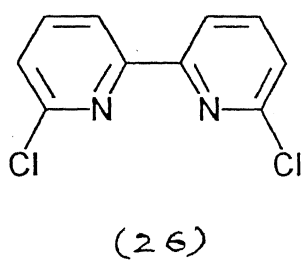
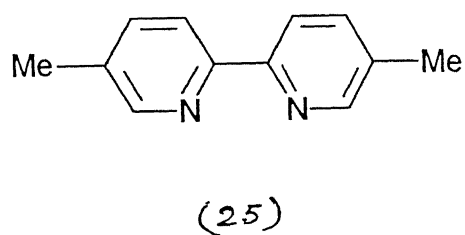
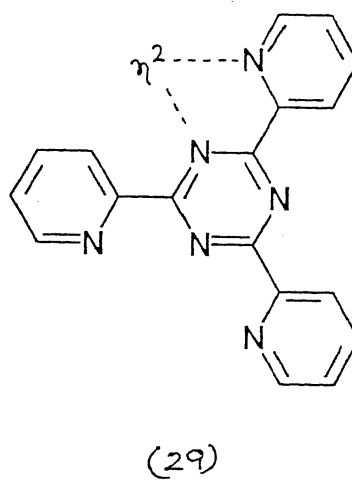
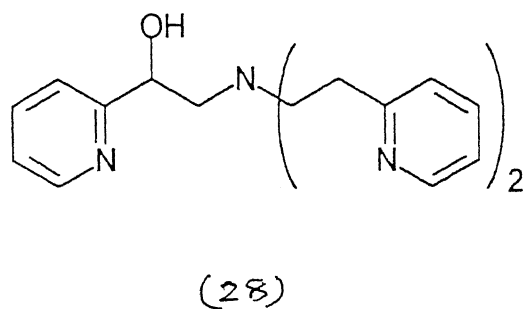
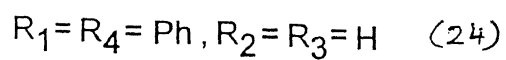
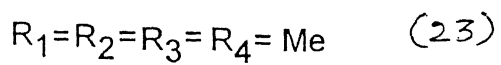
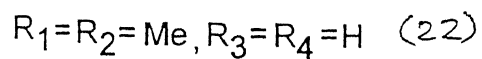
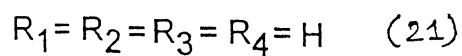
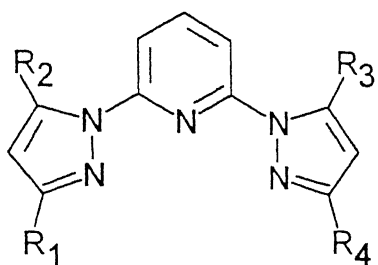


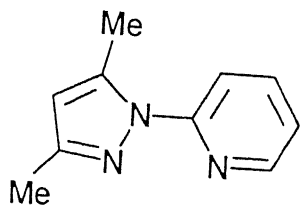
(15)



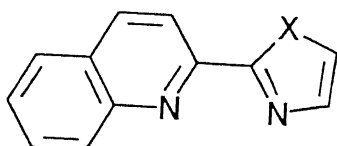
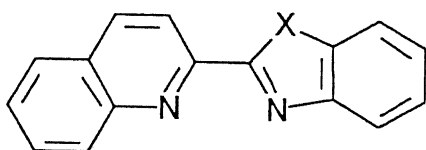
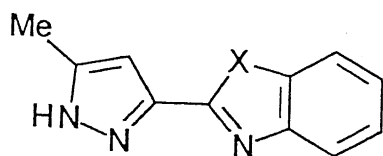
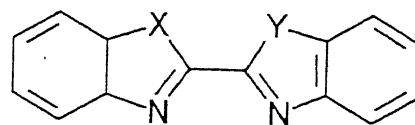
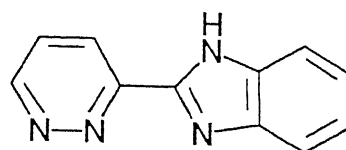
R = H (19)

R = Me (20)

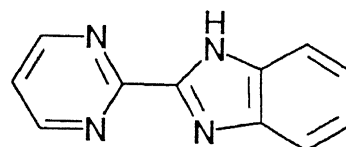




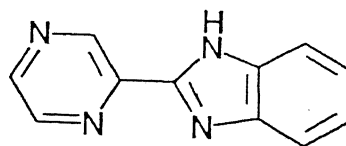
(32)

 $X = \text{NH}$ (33) $X = \text{O}$ (34) $X = \text{S}$ (35) $X = \text{NH}$ (36) $X = \text{O}$ (37) $X = \text{S}$ (38) $X = \text{NH}$ (39) $X = \text{S}$ (40) $X = Y = \text{NH}$ (41) $X = Y = \text{O}$ (42) $X = Y = \text{S}$ (43) $X = \text{NH}, Y = \text{O}$ (44) $X = \text{NH}, Y = \text{S}$ (45) $X = \text{O}, Y = \text{S}$ (46)

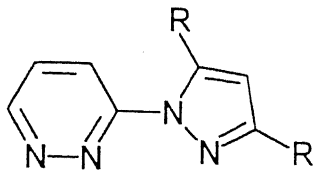
(47)



(48)

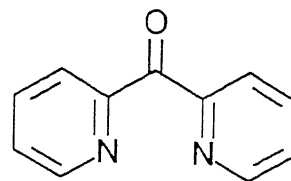


(49)

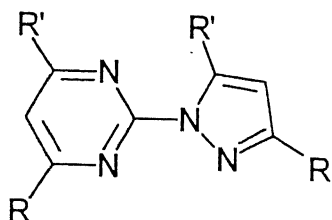


R = H (50)

R = Me (51)



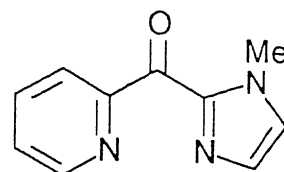
(59)



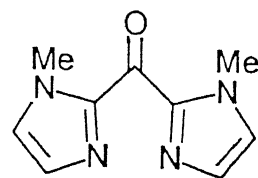
R = R' = H (52)

R = R' = Me (53)

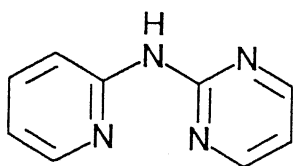
R = Me R' = OMe (54)



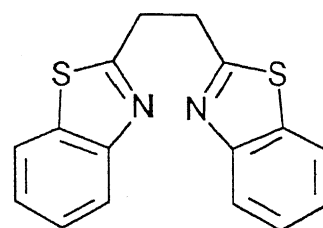
(60)



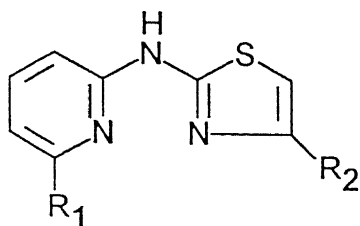
(61)



(55)



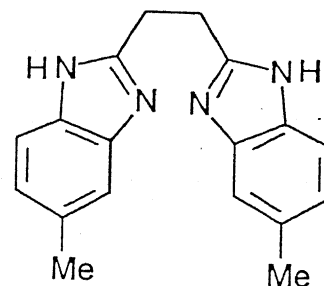
(62)



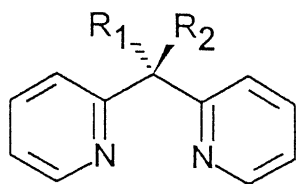
R₁ = R₂ = H (56)

R₁ = H, R₂ = Me (57)

R₁ = R₂ = Me (58)



(63)



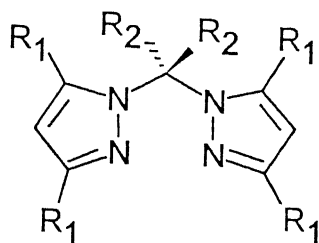
$R_1 = R_2 = H$ (64)

$R_1 = H, R_2 = Me$ (65)

$R_1 = R_2 = Et$ (66)

$R_1 = Me, R_2 = OH$ (67)

$R_1 = Me, R_2 = OMe$ (68)

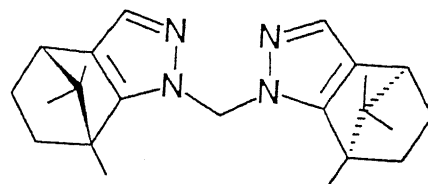


$R_1 = R_2 = H$ (69)

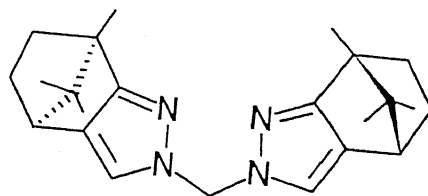
$R_1 = Me, R_2 = H$ (70)

$R_1 = H, R_2 = Me$ (71)

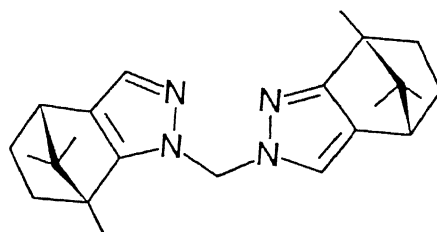
$R_1 = Bu^t, R_2 = H$ (72)



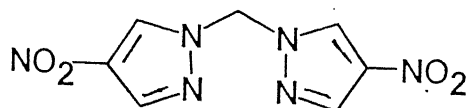
(74)



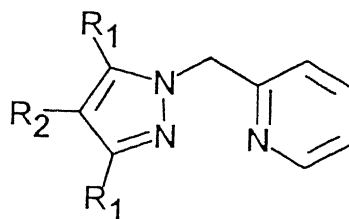
(75)



(76)



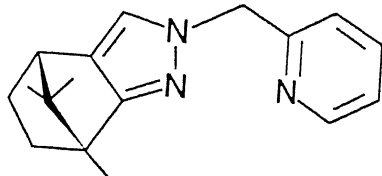
(73)



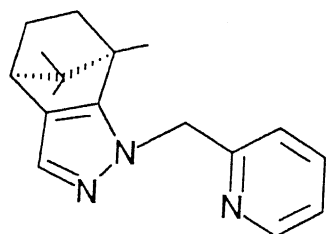
$R_1 = R_2 = H$ (77)

$R_1 = Me, R_2 = H$ (78)

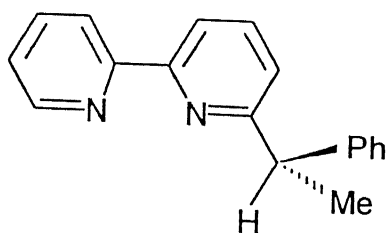
$R_1 = R_2 = Me$ (79)



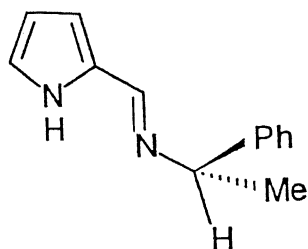
(80)



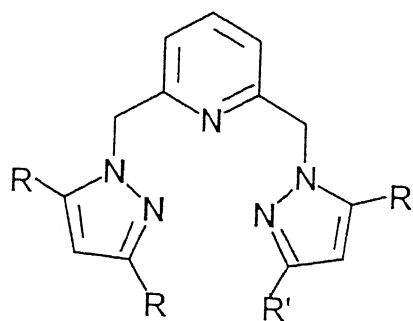
(81)



(82)



(83)



$R = R' = H$ (84)

$R = H, R' = Me$ (85)

$R = R' = Me$ (86)

1.2.1.4 The Specific Problems Considered Based on the Above

Background:

1.2.1.4.1 Identification of Ligand Substituents Induced Steric Effect

The coordination properties of poly(pyrazolyl)borates received widespread attention since its first report by Trofimenko in 1966.⁷² However, the chelate chemistry of other pyrazole-based ligands has attracted attention only during the last decade (see above). An interesting point to note from the above literature survey is the following. Majority of recently reported bidentate heterocyclic nitrogen donor ligand chemistry is dominated by the exploitation of steric factors of the ligand substituents.

In the subsequent chapters (chapters II and III) an extensive coordination chemistry using the ligands (I and II) is described. The present ligands were chosen so as to introduce the following two features: (i) pyrazole ring substituents near the donor site to provide steric constraints in the resulting complexes and (ii) incorporation of other coordinating group (pyridine) to pyrazole ring(s), by use of methylene group(s) as spacer to exert more flexibility.

Single-crystal X-ray crystallography has been utilized as a probe to identify the steric effect of the ring methyl substituents in the representative metal complexes. Metal ions used are Co(II), Ni(II), and Cu(II).

1.2.1.4.2 Preliminary Catalytic Oxidation of Organic Substrates by Four-coordinate Co(II) Complexes with Dioxygen at 298 K

An attempt has been made to investigate the possible

catalytic oxidation chemistry using cobalt(II) complexes toward suitable organic substrates. The results are described in chapter II.

1.2.1.4.3 Structure, Reactivity, and Redox Properties of Grossly Four- and Five Coordinate Cu(II) Complexes

In chapter III the coordination chemistry of interesting Cu(II) complexes having grossly $\text{Cu}^{\text{II}}\text{N}_4$ and $\text{Cu}^{\text{II}}\text{N}_4(\text{X})$ coordination spheres are described.

1.2.2 Copper Containing Nitrite Reductase

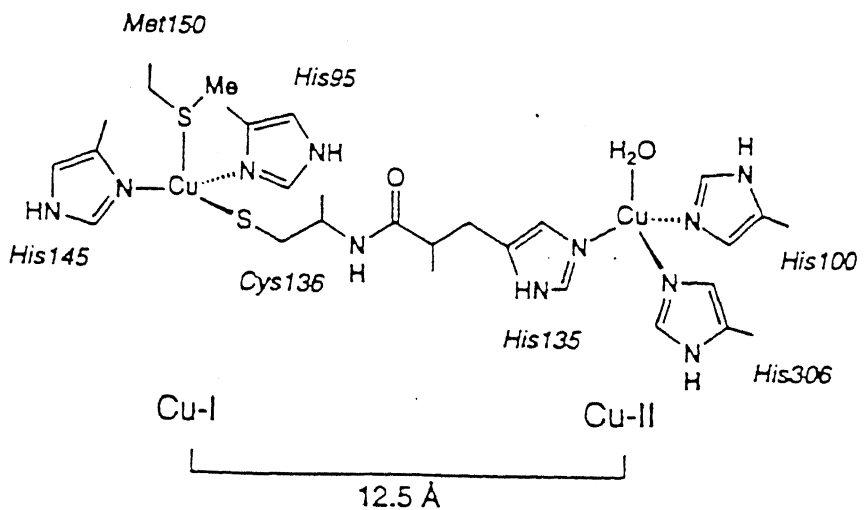
The denitrification process, i.e., the bacterial dissimilatory reduction of nitrate and nitrite to NO , N_2O , and N_2 , occupies a central position in the global nitrogen cycle and in one type of nitrite reductases copper is present in the active site.⁹³ Substrate binding and subsequent redox transformations occur at a single copper site in the protein which is coordinated to three histidines and water or hydroxide ligand in a *pseudo-tetrahedral* geometry.⁹⁴ A variety of structurally characterized model complexes for comparison of corresponding properties with appropriate forms of the enzymes are now available in the literature^{95a-h} (Scheme I.1).

1.2.2.1 Synthetic Model for Copper Containing Nitrite Reductase

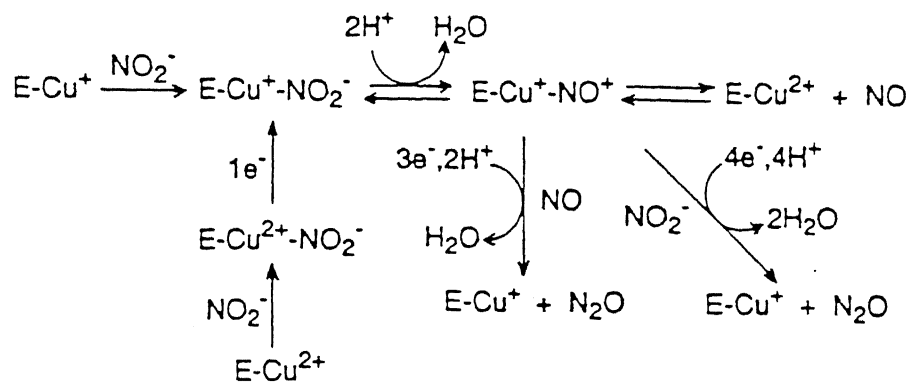
(Figure I.8):

The supporting ligands utilized so far to model such chemistry using mononuclear copper(II) complexes are of three general types: tris(pyrazolel)hydroborate derivative,^{95a-c,e,f} (87,88) 1,4,7-triazacyclononane derivative (89),^{95d} and tripodal

Scheme I. 1



Schematic representation of the copper sites in Nitrite Reductase from Achromobacter cycloclastes



Proposed mechanism for nitrite reduction by Nitrite Reductase

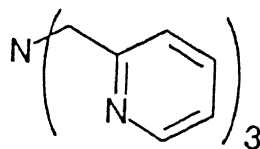
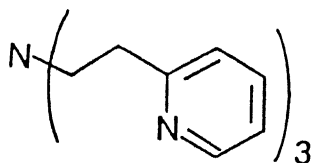
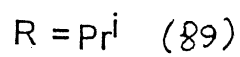
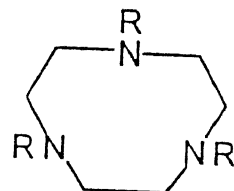
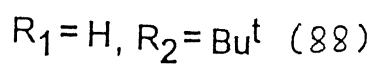
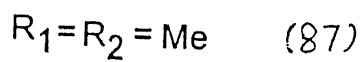
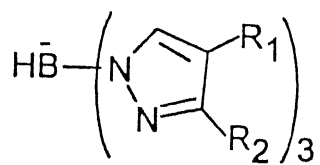


Figure I. 8

ligands providing three pyridine and a tertiary amine nitrogen (90,91).^{95g,h}

I.2.2.2 *Specific Problem Considered Based on the Above*

Background:

An interesting nitrite-bound copper(II) chemistry as a bioinorganic model for copper containing nitrite reductase has been described in chapter III utilizing the ligand, II.

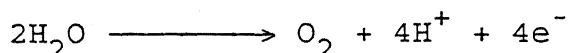
I.2.3 *Coordination Chemistry of Two Novel Five Coordinate Cu(II) Complexes*

In addition to the ligands I and II, two tridentate ligands H₄bpp (III) and Me₄bpp (IV) have been utilized to develop a novel five-coordinate copper chemistry where all five coordinations to Cu(II) center are provided by heterocyclic ring nitrogens. The results are described in chapter IV.

I.2.4 *Oxo-bridged Dimanganese Chemistry of Biological Relevance*

I.2.4.1 Water Oxidation Center in Photosynthetic Apparatus:

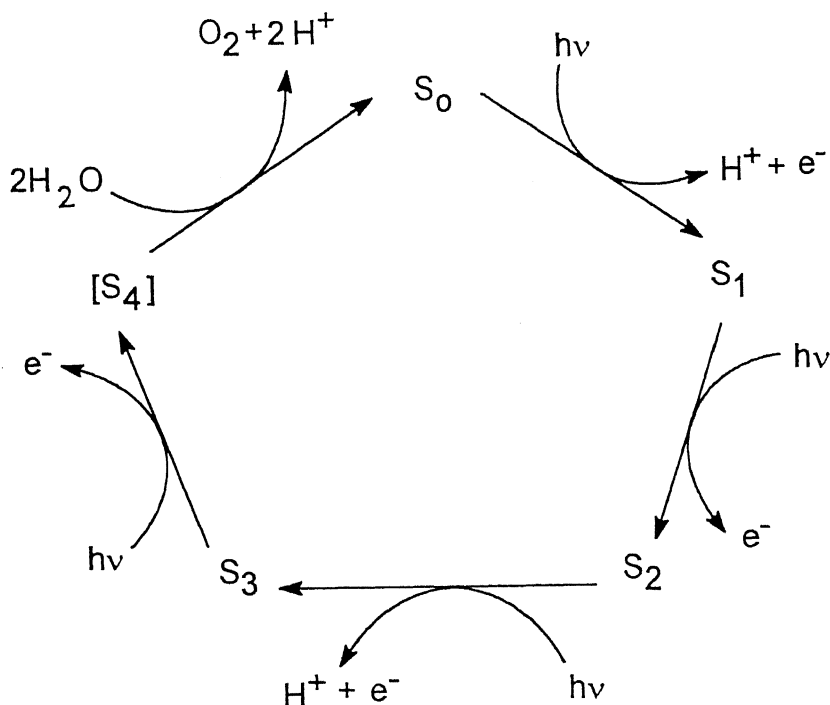
Higher plants and cyanobacteria can generate chemical energy from light. In the water-oxidizing-photosynthesis^{96a-c} this conversion proceeds by light-induced, trans membrane charge separation of protons and electron at the reaction centers photosystem I (PSI) and photosystem II (PSII), during which water is oxidized in the active site of PSII.



The mechanism of oxygen evolution in PSII^{96a,96d-108}

is typically discussed in terms of the so-called 'S-states'. The model is based on a measurement of oxygen release after a series of short flashes of light,^{109,110} so that, in each reaction centre, there is a single charge separation event taking place per flash. The yield of oxygen in response to short flashes of light shows a characteristic oscillation pattern with a periodicity of four flashes. To account for this result, it was proposed¹¹⁰ that PSII cycles through five states (S_0 -[S_4]) (Scheme I.2).

Scheme I.2



The intermediate states are each defined by the number of electrons extracted from the water-oxidizing complex of PS II. The species which is oxidized in each of the S-transitions appears to be a tetramanganese cluster, except possibly for the $S_2 \longrightarrow S_3$

transition, where something other than the manganese may be oxidized. The identity of this other species is unknown, although EPR evidence had implicated a protein residue close to the manganese cluster,¹¹¹⁻¹¹⁵ possibly a histidine residue.¹¹⁶

One essential feature of Scheme I.1 is that during the $S_0 \longrightarrow S_3$ transitions, water is not oxidized. Water oxidation apparently takes place only after the third step in one concerted four-electron reaction or two two-electron reactions.¹¹⁷⁻¹¹⁹ The water is oxidized only in $[S_4]$ state.

During this process, the cluster goes through five oxidation state S_{0-4} , the index of which refers to the number of oxidizing equivalent stored.

Recently, Klein et al.¹¹¹⁻¹¹⁶ have from their EXAFS experiment proposed a structural model which is summarized in Figure I.9. The site would contain two di- μ -oxo units linked by a μ -oxo-bis- μ -carboxylate bridge. The Mn-Mn distances would be $Mn_a - Mn_b = Mn_c - Mn_d = 2.7 \text{ \AA}$ and $Mn_b - Mn_c = 3.3 \text{ \AA}$.

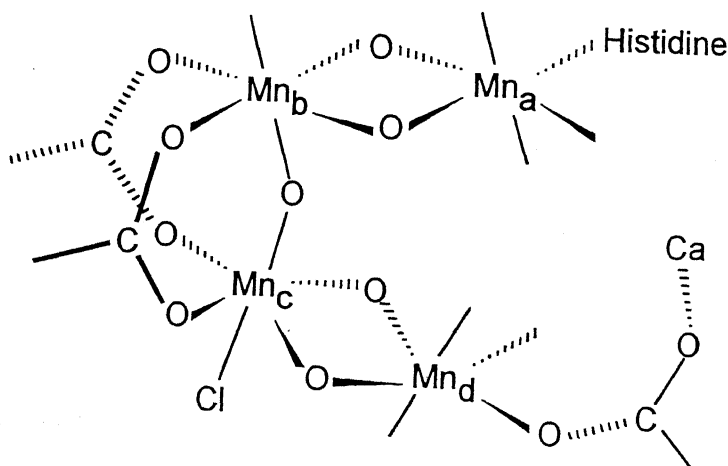


Figure I.9 Klein's model for the OEC

The catalytic chemistry is accompanied by redox chemistry with II, III and IV oxidation states of manganese. Hence studies on high-valent dinuclear oxomanganese clusters, especially the di- μ -oxo-bridged Mn^{III}_2 , $\text{Mn}^{\text{III}}\text{Mn}^{\text{IV}}$ and Mn^{IV}_2 clusters, are particularly relevant.

I.2.4.2 Catalases and pseudo-Catalases:

Oxo-bridged cluster of Mn have been shown to occur in the active site of the catalases, pseudo-catalases and ribonucleotide reductases.

I.2.4.3 Synthetic Oxo-Bridged Dimanganese Chemistry:

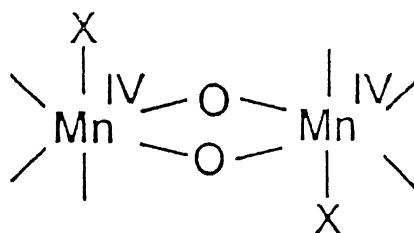
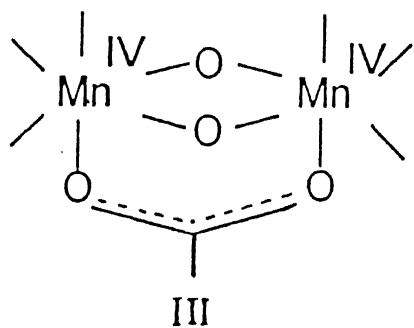
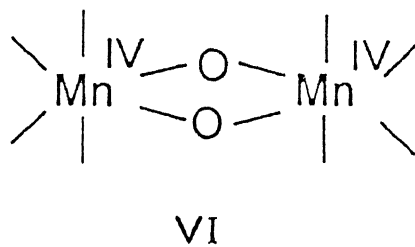
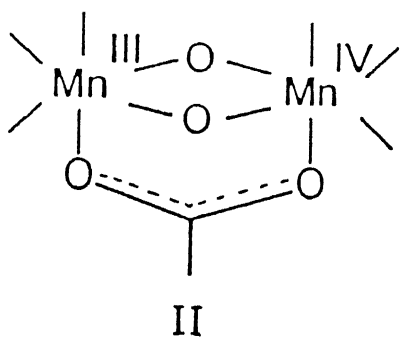
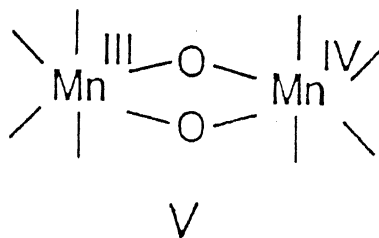
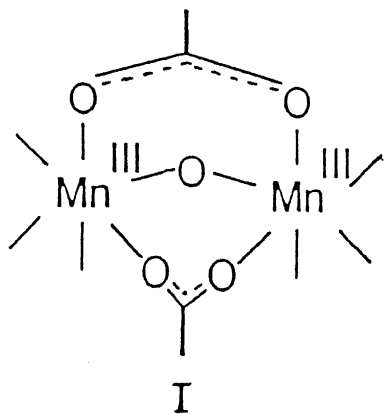
The oxo-bridged manganese cores in various oxidation levels are mainly classified by the structural types I, II, III, IV, V, VI, VII, and VIII, (Figures I.10, I.11, I.12, I.13, I.14, I.15 and I.16)

I.2.4.4 Specific Problem Considered Based on the Above

Background:

In chapter V an exhaustive binuclear oxo-bridged manganese chemistry from the standpoint of above-mentioned synthetic analogue approach to bioinorganic chemistry has been described. The terminal ligand used to hold the following core structures is V. Syntheses, characterization, and spectroscopic studies of the binuclear cores $\{\text{Mn}_2^{\text{III}}(\mu\text{-O})(\mu\text{-OAc})_2\}^{2+}$, $\{\text{Mn}^{\text{III}}\text{Mn}^{\text{IV}}(\mu\text{-O})_2(\mu\text{-OAc})\}^{2+}$, and $\{\text{Mn}_2^{\text{IV}}(\mu\text{-O})_2(\mu\text{-OAc})\}^{3+}$ and chemical/electrochemical interconversions among these cores are the principal theme of this chapter.

Selected Structural Types



$X = Cl^-$ $X = OH^-$
 $X = F^-$

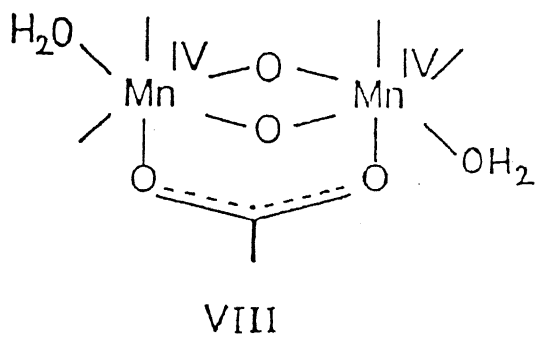
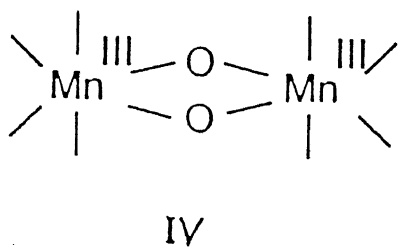
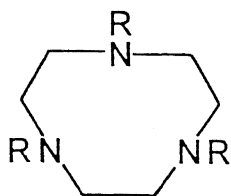


Figure T. 12

Ligand used for structural type I



R = H (TACN)

R = Me (Me₃TACN)

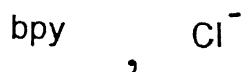
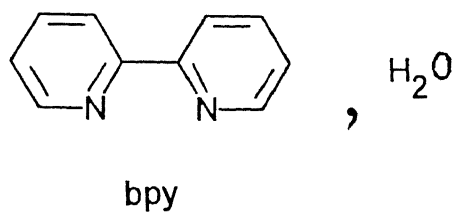
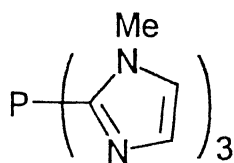
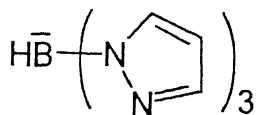
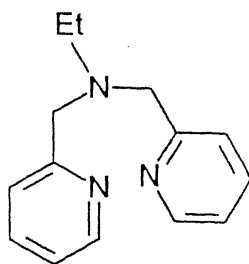
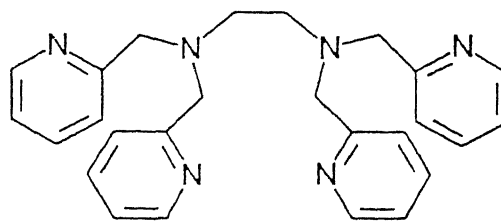


Figure 1.11

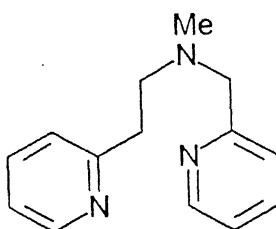
Ligand used for structural type II



bpea



tpen



MeL

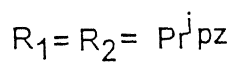
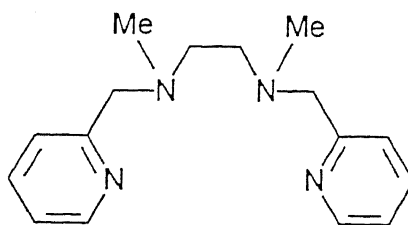
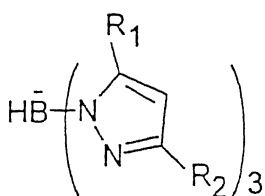
Ligand used for structural type III

bpea

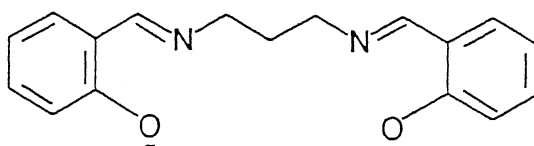
tpen

bpy , H_2O

Ligand used for structural type IV

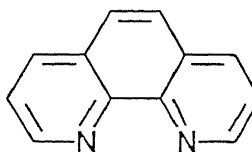


Ligand used for structural type V



salpn

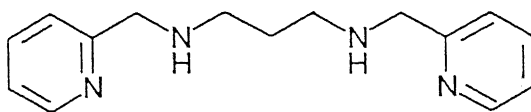
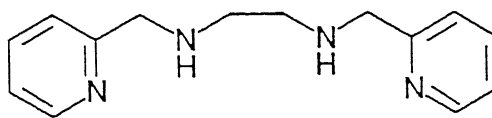
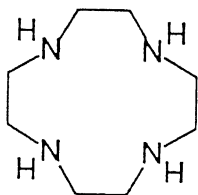
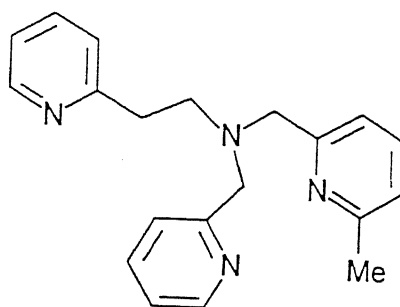
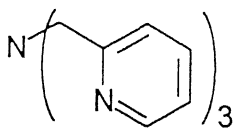
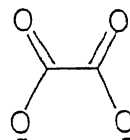
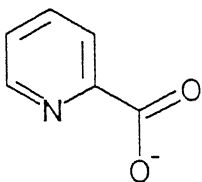
bpy



phen

Ligand used for structural type VI

Salpn



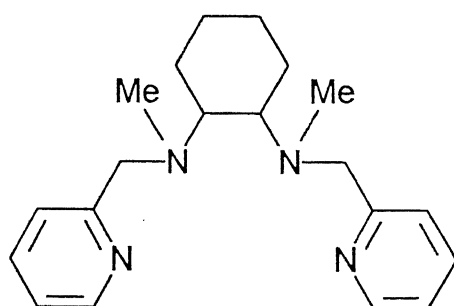
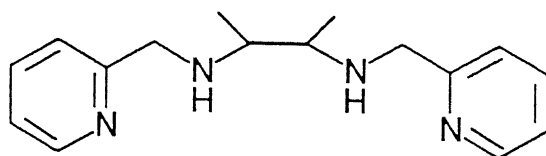


Figure 1.15

Ligand used for structural type VII

TACN , OH^-

TACN , Cl^-

bpy , Cl^-

Ligand used for structural type VIII

bpy

CHAPTER II

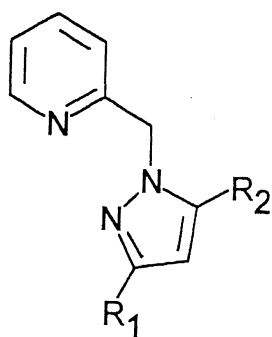
Cobalt(II) and Nickel(II) Complexes of Pyrazolylmethylpyridine Ligands: Synthesis, Structure, and Reactivity

In this chapter the effect of methyl substituents at the 3- and 5-positions of pyrazole rings of the non-planar ligands H_2pp and Me_2pp on the formation of 1:1, 1:2 and 1:3 (metal-to-ligand ratio) complexes of Co(II) and Ni(II) are investigated. An attempt has also been made to investigate the possible catalytic oxidation chemistry using cobalt(II) complexes toward suitable organic substrates.

II.1 Experimental Section

II.1.1 Solvents and Reagents

Solvents and reagents were obtained from commercial sources and used without further purification unless otherwise stated. Water was deionized and then distilled from alkaline permanganate. Acetonitrile was dried by distillation over CaH_2 . For electrochemical experiments (see below) further purification was achieved by $KMnO_4/Li_2CO_3$ treatment¹²⁰ followed by distillation over P_4O_{10} . Chloroform and dichloromethane were made acid free by washing first with sodium bicarbonate solution then five to six times with water followed by keeping over anhydrous calcium chloride for 24 h and distilled. Ethanol and methanol were distilled from $Mg(OC_2H_5)_2$ and $Mg(OCH_3)_2$ respectively. Diethyl ether was dried first with



$R_1 = R_2 = H$, H₂pp (I)

$R_1 = R_2 = Me$, Me₂pp (II)

anhydrous CaCl_2 and then refluxed with and distilled over sodium. Benzene was first stirred with concentrated sulphuric acid until it was free from thiophene. To remove acid it was then shaken twice with water, once with 10% Na_2CO_3 solution, again with water, and finally dried over anhydrous CaCl_2 and stored over sodium. N,N'-dimethylformamide (DMF) was kept over alumina (neutral) for 24h and distilled in vacuo. Tetra-n-butylammonium perchlorate (TBAP) was prepared from tetra-n-butylammonium bromide and 70% aqueous perchloric acid. This was recrystallized from ethanol and dried in vacuo. Dinitrogen was purified by bubbling through an alkaline dithionite solution.¹²¹

II.1.2 Measurements

IR spectra were recorded in KBr disks with the help of a Perkin Elmer 320 or M-580 IR spectrophotometer. Electronic spectra were measured with a Perkin Elmer Lambda 2 spectrophotometer and solid state electronic spectra (reflectance spectra) were measured using paraffin oil with the same spectrophotometer. The ^1H NMR spectra were obtained on either a PMX-60 JEOL (60 MHz) instrument or a Brüker WP-80 (80 MHz) NMR spectrometer using CDCl_3 or CD_3CN solutions. The 400 MHz NMR spectra were measured in CD_3CN or $(\text{CD}_3)_2\text{CO}$ on a Brüker WM-400 (400 MHz) NMR spectrometer. This was obtained by the Analytical Facilities, Regional Sophisticated Instrumentation Centre, Lucknow, India. Solution magnetic susceptibility measurements were made by the usual NMR method¹²² with a PMX-60 Jeol (60 MHz) or Brüker WP-80 spectrometer and made use of the paramagnetic shift of the methyl protons of acetonitrile, methanol and the TMS reference as the measured NMR parameter using the Equation II.1

$$\text{Mass susceptibility } \chi_m = -\frac{3\Delta f}{2\pi f m} + \chi_o + \frac{\chi_o(d_o - d_s)}{m} \quad (\text{II.1})$$

where Δf is the frequency separation between the two TMS or solvent peaks in Hz, f is the frequency at which the proton resonances are being studied in Hz, m is the mass of substance contained in 1 ml of solution, χ_o is the mass susceptibility of the solvent, d_o is the density of the solvent and d_s that of solution. Final term involved in equation II.1 is negligible for the highly paramagnetic substances.

The temperature of the NMR probe was determined¹²³ using CH_3OH proton signals using Equation II.2

$$T = 435.5 - 1.193(\Delta f) - 29.3(\Delta f \times 10^{-2})^2 \quad (\text{II.2})$$

where Δf is the frequency difference between the peak positions of $-\text{CH}_3$ and $-\text{OH}$ protons, in Hz. Solvent susceptibilities¹²⁴ and diamagnetic corrections¹²⁵ were taken from literature tabulations.

Room temperature magnetic susceptibility data for some complexes were obtained on polycrystalline samples (powdered form) by the Faraday method using a locally built susceptometer in Professor S. Mitra's laboratory, Chemical Physics Group, Tata Institute of Fundamental Research (TIFR), Bombay, India and for rest of the complexes by the same method using a susceptometer (Electromagnet from Polytronic Corporation, Bombay; Sartorius balance Germany) equipped with a closed-cycle cryostat (CTI cryogenics, USA) in this laboratory; $\text{Hg}[\text{Co}(\text{SCN})_4]$, $[\text{Fe}(\text{acac})_3]$ and $\text{Cu}(\text{SO}_4)_2 \cdot 5\text{H}_2\text{O}$ were used as calibrants. Experimental susceptibility data were

corrected for diamagnetic contributions. Effective magnetic moments were calculated from $\mu_{\text{eff}} = 2.828 [\chi_M T]^{1/2}$, where χ_M is the corrected molar susceptibility. All the measurements were made at a fixed field strength and the field dependence of the magnetic susceptibility was not studied.

X-Band EPR spectra were recorded with a Varian E-109 C spectrometer fitted with a quartz Dewar for measurements at liquid dinitrogen temperature. The spectra were calibrated with the help of DPPH ($g = 2.0037$). Solution electrical conductivity measurements were made with an Elico (Hyderabad, India) Type CM 82 T conductivity bridge.

Cyclic voltammetric measurements were performed by using the PAR Model 370-4 electrochemistry system incorporating the following: Model 174A polarographic analyzer; Model 175 universal programmer; Model RE-0074 X-Y recorder. Differential pulse voltammetric experiments were carried out using the Model 174A polarographic analyzer. Potentials are reported at ~ 298 K referenced to an aqueous saturated calomel electrode (SCE) and are uncorrected for junction potentials. The solutions were $\sim 10^{-3}$ M in complex and 0.2 M in supporting electrolyte, TBAP. In acetonitrile solutions at a scan rate of 50 mVs^{-1} the above condition was found to give best performance with platinum and glassy carbon electrode for the $[\text{Fe}(\eta\text{-C}_5\text{H}_5)_2]^+ / [\text{Fe}(\eta\text{-C}_5\text{H}_5)_2]$ couple. At a platinum electrode the $E_{1/2}$ [$E_{1/2} = 0.5 (E_{\text{pa}} + E_{\text{pc}})$] and the peak-to-peak separation (ΔE_p) values are : MeCN, 0.40 V (80 mV).¹²⁶

A PAR G0021 glassy carbon electrode or a planar platinum-inlay electrode (Beckman Model 39273) was used as the working electrode. A sealed all-glass cell was used; measurement were made

under an atmosphere of dry dinitrogen. The auxiliary electrode, which consists of a platinum flag sealed in soft glass, and the reference electrode were separated from the working solution by means of fritted bridge filled with the same solvent and supporting electrolyte. Uncompensated solution resistance in the cell configuration was minimized by placing the tip of the reference electrode as close to the working electrode as possible.

Analytical thin layer chromatography was performed on silica gel (Acme) coated glass plates. Aldehyde and organic substrates for catalytic oxidation were purchased commercially and purified prior to use.

Caution! Although the preparation of the perchlorate salts described in this thesis has been done many times without incident, perchlorate salts of metal complexes with organic ligands have been known to explode spontaneously. Therefore, the preparation and handling of these salts deserve special care.

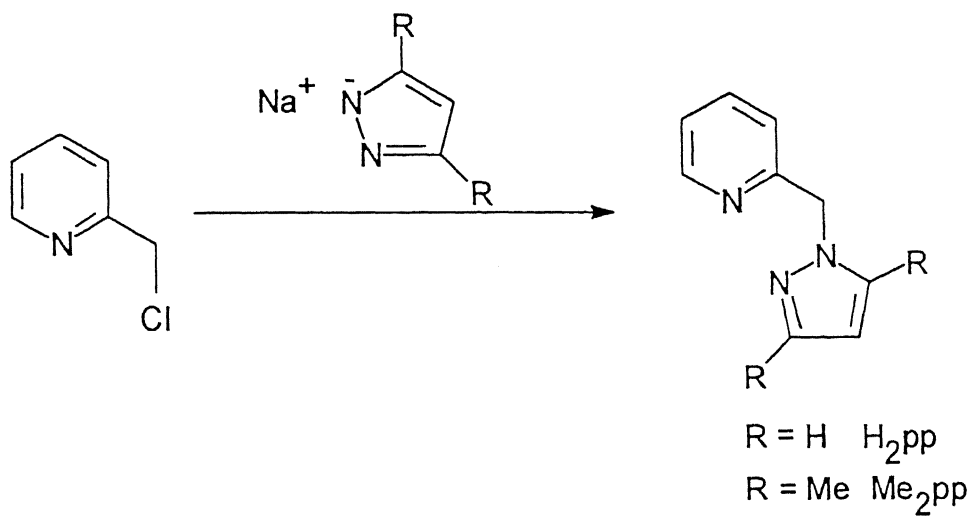
II.2 Syntheses of Ligands:

The bidentate ligands R_2pp were prepared in high yields by phase-transfer^{39,79} catalyzed coupling of pyrazole and 3,5-dimethylpyrazole by 2-(chloromethyl)pyridine and the structures were confirmed by 1H NMR (Scheme II.1).

II.2.1 2-(pyrazole-1-ylmethyl)pyridine, H_2pp (I)

A mixture of 2-(chloromethyl)pyridine (4g; 0.0244 mmol), pyrazole (1.66 g; 0.0244 mmol), benzene (280 mL), 40% aqueous sodium hydroxide (38 mL) and 40% aqueous tetra-n-butylammonium hydroxide (24 drops) was refluxed with stirring for 8 h and then stirred at 298 K for 12 h. The organic layer was separated, dried over

Scheme II.1



anhydrous sodium sulphate and evaporated under reduced pressure to yield 2-(pyrazol-1-ylmethyl)pyridine as an oil (yield 3.85 g, 99%). ^1H NMR (CDCl_3): 8.45(d), 7.50(m), 7.10(m), 6.90(d), 6.25(t) and 5.40(s) (Figure II.1).

II.2.2 2-(3,5-dimethyl pyrazol-1-ylmethyl)pyridine, Me_2pp (II)

This ligand was synthesized following the same method as that of H_2pp ; however, this time using substituted pyrazole instead of pyrazole. Yield 98%. ^1H NMR (CDCl_3): 8.45(d), 7.50(m), 7.10(m), 6.70(d), 5.80(s), 5.32(s), 2.18(s) and 2.15(s) (Figure II.2).

II.3 Syntheses of complexes

II.3.1 $[\text{Co}(\text{H}_2\text{pp})\text{Cl}_2]$

An ethanolic solution (8 mL) of H_2pp (0.122 g, 0.77 mmol) was added to an ethanolic solution (5 mL) of $\text{CoCl}_2 \cdot 6\text{H}_2\text{O}$ (0.1g, 0.77 mmol) dropwise while stirring. Stirring was continued for 15 min. The solvent was evaporated under vacuum. The blue solid thus obtained was washed several times with benzene and dried in vacuo. Yield (146 mg, 81%).

II.3.2 $[\text{Co}(\text{H}_2\text{pp})_2\text{Cl}_2] \cdot 4\text{H}_2\text{O}$

An ethanolic solution (3 mL) of H_2pp (0.150 g, 0.94 mmol) was added to an ethanolic solution (3 mL) of $\text{CoCl}_2 \cdot 6\text{H}_2\text{O}$ (0.1g, 0.42 mmol). The resulting reaction mixture was refluxed for 2 h and cooled to 298 K. Pink crystalline solid thus obtained was filtered, thoroughly washed with ethanol and dried in air at 298 K. Yield (92 mg, 50%). The single crystals suitable for X-ray diffraction studies were grown by slow evaporation from $\text{EtOH-H}_2\text{O}$ mixture.

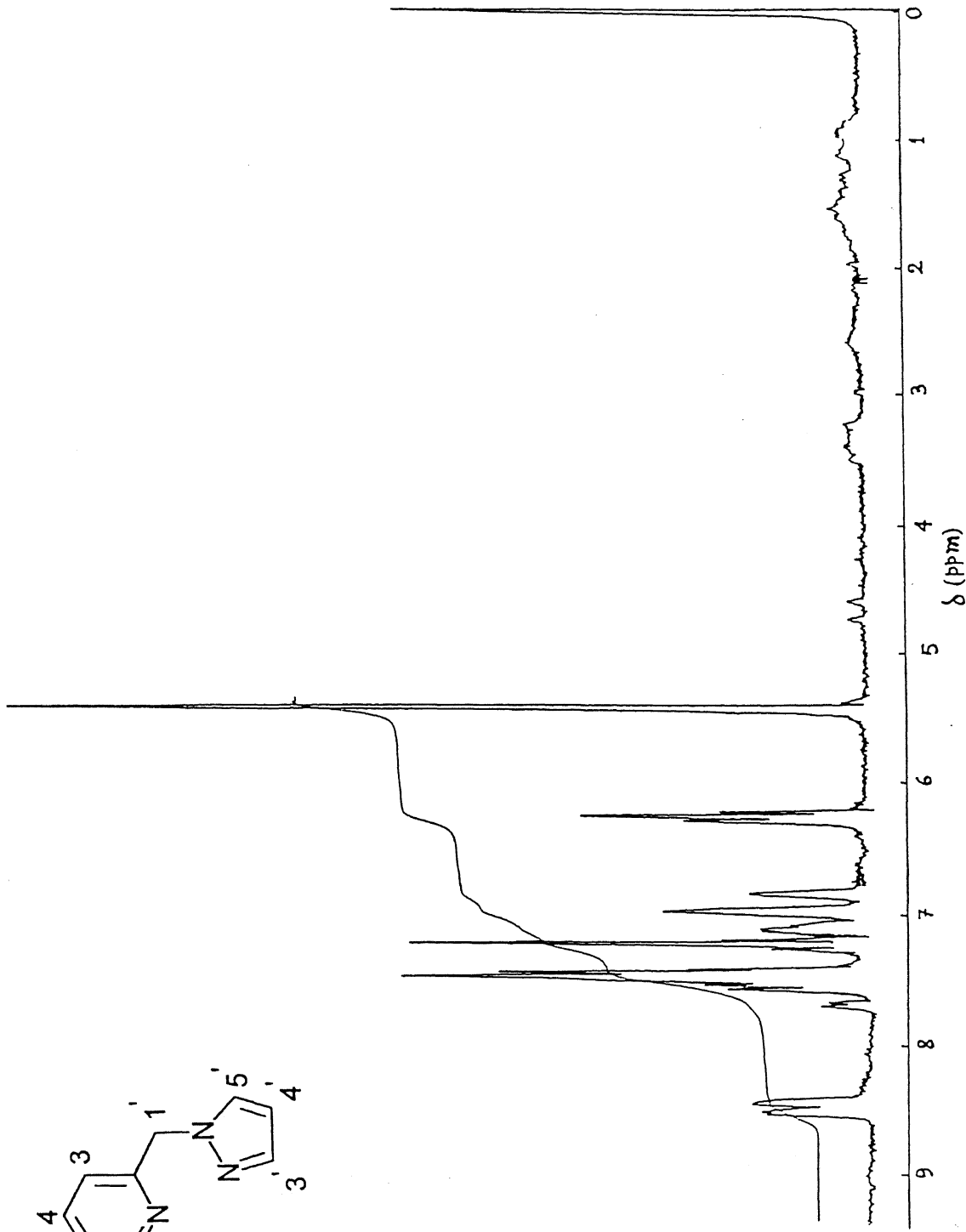
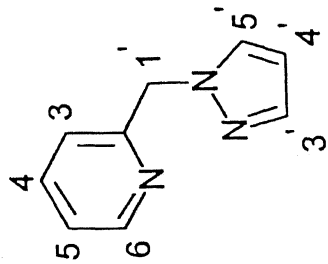


Figure II.1 ^1H NMR spectrum of 2-(pyrazol-1-yl methyl)pyridine (H_2pp) in CDCl_3

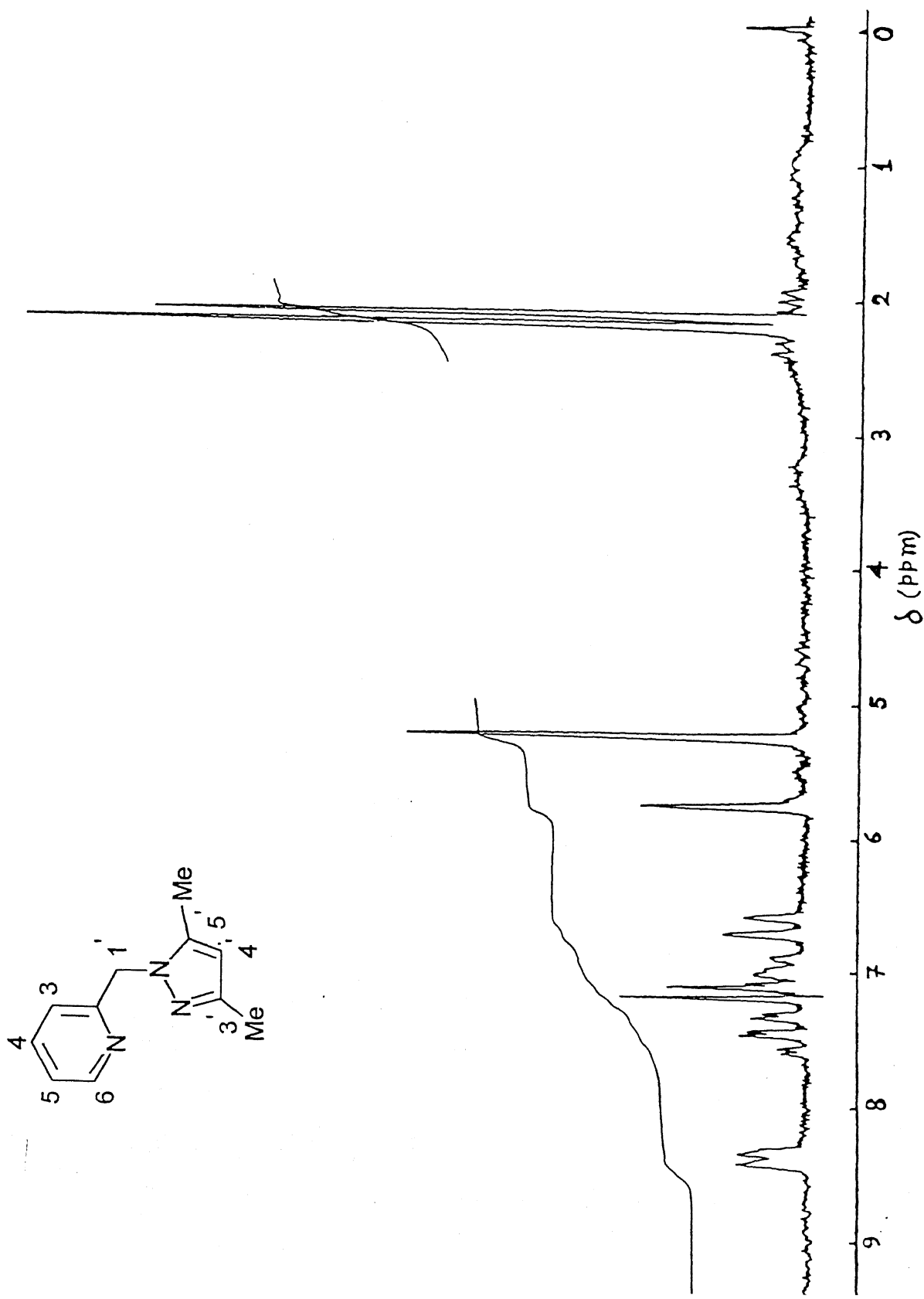


figure II.2 ¹H NMR spectrum of 2-(3,5-dimethylpyrazol-1-yl methyl)pyridine (Me₂pp) in CDCl₃

II.3.3 $[\text{Co}(\text{H}_2\text{pp})_3](\text{ClO}_4)_2 \cdot \text{H}_2\text{O}$

To an ethanolic solution (6 mL) of H_2pp (0.52g, 3.28 mmol) was added an ethanolic solution (6 mL) of $[\text{Co}(\text{H}_2\text{O})_6](\text{ClO}_4)_2$ (0.3g, 0.82 mmol). The resulting mixture was stirred for 3 h at 298 K and the solvent was stripped off. Orange crystalline solid was obtained by slow diffusion of diethyl ether to an acetonitrile (MeCN) solution of the resulting solid. It was filtered, washed thoroughly with diethyl ether and dried in vacuo. Yield (280 mg, 45%).

II.3.4 $[\text{Co}(\text{Me}_2\text{pp})\text{Cl}_2]$

To an ethanolic solution (2 mL) of $\text{CoCl}_2 \cdot 6\text{H}_2\text{O}$ (0.1g, 0.42 mmol) was added an ethanolic solution (5 mL) of Me_2pp (0.08g, 0.43 mmol). After 2 min stirring deep blue microcrystalline solid started to precipitate out. The solid thus obtained was filtered, washed with ethanol and dried in vacuo. Yield (0.1g, 75%). The single crystals suitable for X-ray diffraction studies were grown by slow diffusion of diethylether into a MeCN solution of the complex.

II.3.5 $[\text{Ni}(\text{H}_2\text{pp})_2\text{Cl}_2] \cdot 4\text{H}_2\text{O}$

An ethanolic solution (5 mL) of H_2pp (0.134 g, 0.843 mmol) was added dropwise to an ethanolic solution (5 mL) of $[\text{Ni}(\text{H}_2\text{O})_6]\text{Cl}_2$ (0.1g, 0.421 mmol) and the reaction mixture was magnetically stirred. It was then refluxed for 2 h, cooled to room temperature and the solvent evaporated under vacuo. The light green solid thus obtained was washed 2-3 times with CHCl_3 and once with acetone, and finally dried in air. Yield (145 mg, 77%).

II.3.6 $[\text{Ni}(\text{H}_2\text{pp})_3](\text{ClO}_4)_2 \cdot \text{H}_2\text{O}$

To an ethanolic solution (3 mL) of H_2pp (0.6g, 3.774

mmol) was added solid $[\text{Ni}(\text{H}_2\text{O})_6](\text{ClO}_4)_2$ (0.4g, 1.094 mmol) in portions while stirring the solution. The resulting mixture was stirred for 2 h at 298 K and the solvent was stripped off. Crystalline violet compound with blue tinge was obtained using layering technique from CH_3CN /petroleum ether at 273K. Yield (178 mg, 22%).

II.3.7 $[\text{Ni}(\text{Me}_2\text{pp})(\text{S})_2\text{Cl}_2] \cdot \text{H}_2\text{O}$ (S= EtOH or H_2O)

To an ethanolic solution (10 mL) of $[\text{Ni}(\text{H}_2\text{O})_6]\text{Cl}_2$ (0.1g, 0.0 mmol) was added an ethanolic solution (10 mL) of Me_2pp (0.08 g, 0.0 mmol) dropwise while magnetically stirring the mixture. The stirring was continued for 15 min at 298 K. The volume of the solution was reduced to ~2 mL and the resulting solution was kept at 273 K for 12 h. Light blue microcrystalline solid thus obtained was washed thoroughly with chloroform and finally dried in vacuo (in vacuum desiccator the color of the solid is light green). Yield (0.090 g).

II.3.8 $[\text{Ni}(\text{Me}_2\text{pp})_2\text{Cl}_2] \cdot 2\text{H}_2\text{O}$

A mixture of $[\text{Ni}(\text{H}_2\text{O})_6]\text{Cl}_2$ (0.5g, 2.1 mmol) and Me_2pp (0.787 g, 4.2 mmol) in 20 mL of ethanol was refluxed for 1h and then cooled to room temperature. The solvent of the resulting solution was reduced to ~ 5 mL and kept at 273 K overnight. Light blue solid thus obtained was washed 3-4 times with CHCl_3 , dried in vacuo. Yield (616 mg, 58%).

II.4 X-ray Data Collection and Structure Solution and Refinement

Crystals were mounted on glass fiber. Preliminary examination and data collection were performed with MoK_α radiation ($\lambda = 0.71073 \text{ \AA}$) on an Enraf-Nonius CAD4 Mach computer controlled

diffractometer equipped with a graphite monochromator. Data at 293 K were collected at this Department of Chemistry, Indian Institute of Technology (IIT), Kanpur, India.

Cell constants and the orientation matrix for data collection were obtained from least-squares refinement, using the setting angles of 25 reflections in the range $20 < 2\theta < 40$ for $[\text{Co}(\text{Me}_2\text{pp})\text{Cl}_2]$ and $12 < 2\theta < 30$ for $[\text{Co}(\text{H}_2\text{pp})_2\text{Cl}_2] \cdot 4\text{H}_2\text{O}$. Experimental details of crystal data, intensity measurements, structure solution and refinement are given in Tables II.1 a II.1 b .

As a check on crystal and electronic stability three representative reflections were measured every 97 reflections. The intensities of these standards remained constant within experimental error throughout data collection. Intensities were corrected for Lorentz and polarization effect. Anomalous dispersion was applied for all non-hydrogen atoms. Analytical absorption correction was applied to the data. The structure was refined by a full-matrix least-squares method on F with anisotropic thermal parameters used for the non-hydrogen atoms. Hydrogen atoms were located from the difference Fourier maps and included in the refinements with fixed isotropic thermal parameters. For $[\text{Co}(\text{H}_2\text{pp})_2\text{Cl}_2] \cdot 4\text{H}_2\text{O}$ two water molecules were located from the difference Fourier maps. However, for one water molecule (O(1w)) hydrogens could not be located. The function minimized was $\sum w(|F_o| - |F_c|)^2$ where F_o and F_c are the observed and calculated structure amplitudes, and the weight, w , is $4F_o^2/\sigma^2(F_o^2)$ for $[\text{Co}(\text{Me}_2\text{pp})\text{Cl}_2]$ and 1 for $[\text{Co}(\text{H}_2\text{pp})_2\text{Cl}_2] \cdot 4\text{H}_2\text{O}$. For $[\text{Co}(\text{Me}_2\text{pp})\text{Cl}_2]$ the refinement based on 154 parameters converged with $R = \sum |F_o| - |F_c| / \sum |F_o|$ and $R_w = [\sum w(|F_o| - |F_c|)^2 / \sum w|F_o|^2]^{1/2}$ values of

Table II.1a

EXPERIMENTAL DETAILS

A. CRYSTAL DATA

Empirical Formula	$\text{CoCl}_2\text{N}_3\text{C}_{11}\text{H}_{13}$
Formula Weight	316.33
Crystal Colour, Habit	Bright blue, block shaped
Crystal dimensions (mm^3)	0.5 x 0.2 x 0.1
Crystal System	Triclinic
Lattice Type	P
No. of reflections used for unit cell determination (2θ range)	25 reflections ($20 < 2\theta < 40$)
Lattice parameters	$a = 8.113(3)$, $b = 8.228(1)$, $c = 10.727(5)\text{\AA}$, $\alpha = 76.35(4)^\circ$, $\beta = 76.90(4)^\circ$, $\gamma = 75.99(3)^\circ$
Space Group	$P\bar{1}$ (No.2)
Z value	2
D_{calc} (g cm^{-3})	1.585
F_{000}	321.9
μ ($\text{MoK}\alpha$) (mm^{-1})	1.67
Transm Coef	0.7241-0.7260

B. INTENSITY MEASUREMENTS

Diffractometer	Cad4Mach
Radiation	$\text{MoK}\alpha$ ($\lambda = 0.71073\text{\AA}$)
Temperature	293K
Scan Type	$\theta - 2\theta$
Scan Rate	variable
Scan Width	$1.0 + 0.35 \tan \theta$
2θ range (deg)	2 - 50
No. of reflections measured ($2 < 2\theta < 50$)	2614

Contd.

No. of unique reflections	2339
Corrections	L_p , absorption(analytical)

C. STRUCTURE SOLUTION AND REFINEMENT

Structure Solution	Direct Method
Refinement	Full matrix, least squares
Function minimized	$\sum w(F_o - F_c)^2$
Anomalous dispersion	applied (for non H atoms)
No. of observations ($I > 3\sigma(I)$)	1987
No. of variables	154
Reflection/Parameter ratio	12.9
Residuals: $R; R_w$	0.032 ; 0.038
Goodness of fit indicator	3.525
Max shift/error in final cycle	0.1594×10^{-3}
Avg shift/error in final cycle	0.1148×10^{-4}
Maximum peak in final diff. map($e\text{\AA}^{-3}$)	0.36
Minimum peak in final diff. map($e\text{\AA}^{-3}$)	-0.43

Table II.1b

EXPERIMENTAL DETAILS

A. CRYSTAL DATA

Empirical Formula	$\text{CoCl}_2\text{O}_4\text{N}_6\text{C}_{18}\text{H}_{26}$
Formula Weight	519.93
Crystal Colour, Habit	Pink, irregular shaped
Crystal dimensions (mm^3)	0.3 x 0.2 x 0.2
Crystal System	Triclinic
Lattice Type	P
No. of reflections used for unit cell determination (2θ range)	25 reflections ($12. < 2\theta < 30$)
Lattice parameters	$a = 7.124(1)$, $b = 8.854(2)$, $c = 10.144(9)\text{\AA}$, $\alpha = 106.92(4)$, $\beta = 93.74(4)$, $\gamma = 111.29(2)^\circ$
Space Group	$P\bar{1}$ (No.2)
Z value	1
$D_{\text{calc}} (\text{g cm}^{-3})$	1.543
F_{000}	268.9
$\mu(\text{MoK}\alpha) (\text{mm}^{-1})$	1.03
Transm Coef	0.8235 - 0.8242

B. INTENSITY MEASUREMENTS

Diffractometer	Cad4Mach
Radiation	$\text{MoK}\alpha$ ($\lambda = 0.71073\text{\AA}$)
Temperature	293K
Scan Type	$\theta - 2\theta$
Scan Rate	variable
Scan Width	$0.8 + 0.35\tan\theta$
2θ range (deg)	2 - 50
No. of reflections measured ($2 < 2\theta < 50$)	2187

Contd.

No. of unique reflections	1973
Corrections	L_p , absorption(analytical)

C. STRUCTURE SOLUTION AND REFINEMENT

Structure Solution	Direct Method
Refinement	Full matrix, least squares
Function minimized	$\sum (F_o - F_c)^2$
Anomalous dispersion	applied (for non H atoms)
No. of observations ($I > 3\sigma(I)$)	1896
No. of variables	142
Reflection/Parameter ratio	13.4
Residuals: $R; R_w$	0.079 ; 0.099
Goodness of fit indicator	1.538
Max shift/error in final cycle	0.3165×10^{-4}
Avg shift/error in final cycle	0.3280×10^{-5}
Maximum peak in final diff. map($e\text{\AA}^{-3}$)	1.39; near O(1w)
Minimum peak in final diff. map($e\text{\AA}^{-3}$)	-1.54

0.032 and 0.038 respectively. For $[\text{Co}(\text{H}_2\text{pp})_2\text{Cl}_2] \cdot 4\text{H}_2\text{O}$ the refinement based on 142 parameters converged with $R = \sum |F_o| - |F_c| / \sum |F_o|$ and $R_w = 1$ (unit weight) values of 0.079 and 0.099 respectively. All calculations were performed using the Xtal 3.2 package¹²⁷ installed on a PC 486 computer.

II.5 Procedures^{128a-c} Used for Catalytic Oxidation of Organic Substrates and Isolation of Oxidized Products

II.5.1 Catalytic Transformation of *trans*-Stilbene

Unactivated organic substrate, *trans*-stilbene (0.15 g, 0.83 mmol) and 2-methyl propanaldehyde (0.15 g, 2.22 mmol) were added to a stirred solution of $[\text{Co}(\text{H}_2\text{pp})\text{Cl}_2]$ (1) (0.002 g, 6.92 μmol) in acetonitrile (20 ml). The mixture was stirred at 298 K under dioxygen balloon for 12 h. The solvent was evaporated in rotavapor and the residue was dissolved in ethylacetate (20 ml). The ethylacetate layer was washed with saturated NaHCO_3 (3 x 20 ml), brine solution (2 x 20 ml) and water (2 x 20 ml). The organic layer was dried over anhydrous Na_2SO_4 and the solvent was evaporated to yield oxidized product. Oxidized product was confirmed by ^1H NMR (Figure II.3).

For catalyst $[\text{Co}(\text{Me}_2\text{pp})\text{Cl}_2]$ (2) same method was followed (Figure II.3).

II.5.2 Catalytic Transformation of R(+) Limonene

For the catalytic transformations same method described above was followed. Here R(+) limonene was taken as the organic substrate (Figure II.4).

II.5.3 Catalytic Transformation of Indane

Following the same procedure as described above benzylic

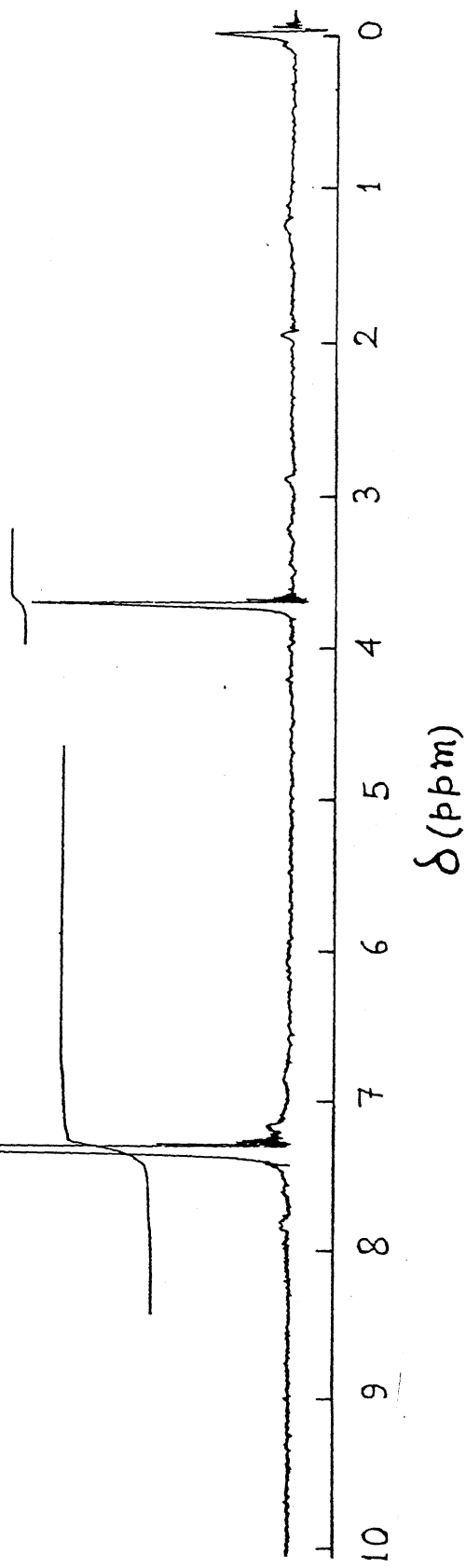
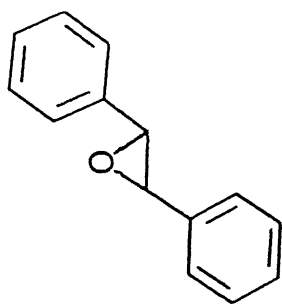


Figure 11.3 ^1H NMR spectrum of trans-stilbene oxide obtained by catalytic oxidation of trans-stilbene

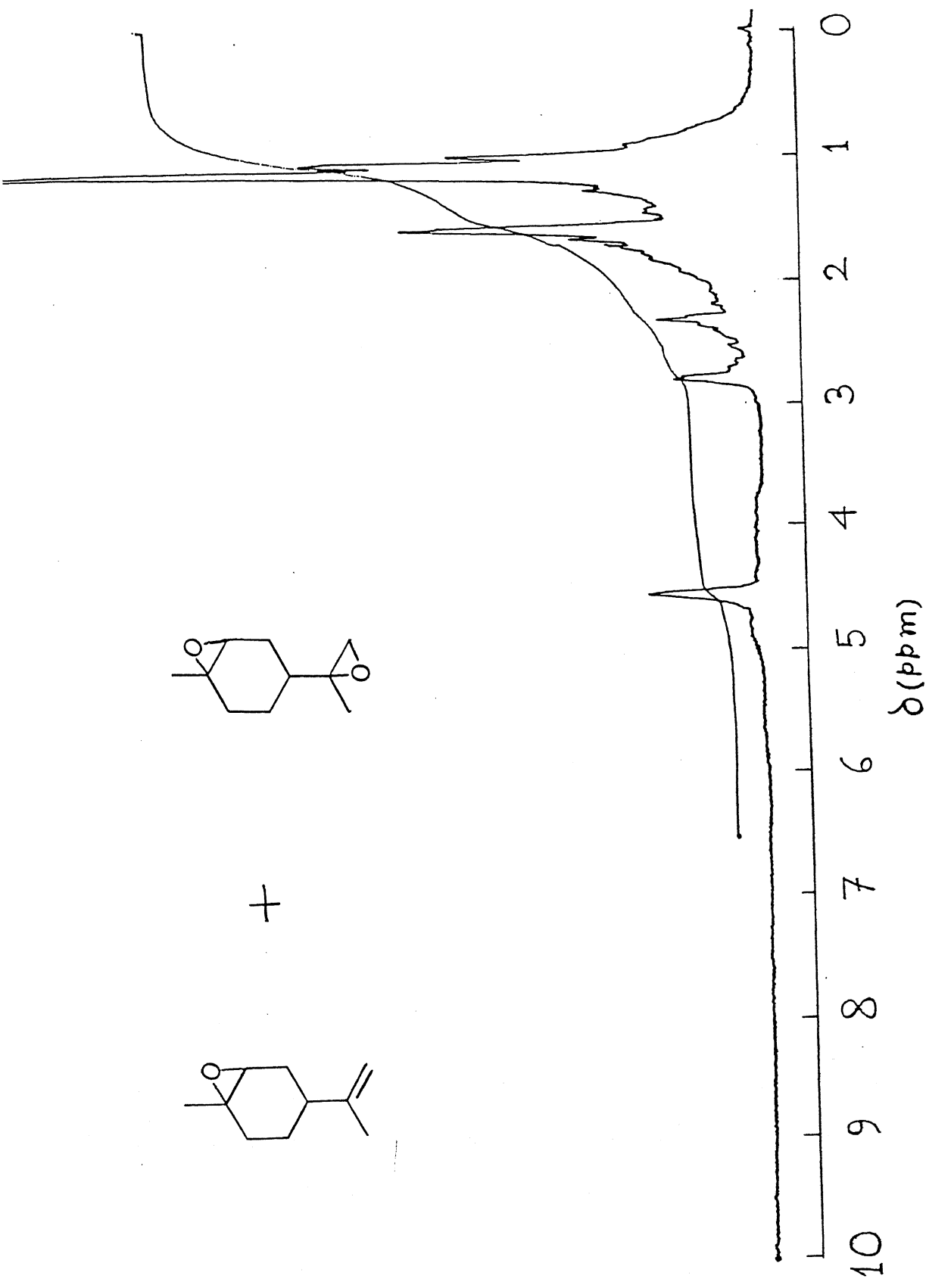


Figure II.4 ^1H NMR spectra of 1:1 mixture of (+) limonene oxide and diepoxide form of (+) limonene obtained by catalytic oxidation of R(+) limonene

oxidation of indane were carried out (Figure II.5). Additionally, one interesting point to be noted that when concentration of the substrate was 212 m M within 6 h conversion was completed. Whereas, generally substrate concentration were used as 42 m M in all cases and conversion were completed within 12h.

One of the above catalytic reactions (indane as substrate) was investigated in absence of catalyst (i.e. Co(II) complex) and no oxidized product was obtained.

II.6 ¹⁶Results and Discussion

II.6.1 Four- and Six-coordinate Cobalt(II) Complexes

II.6.1.1 Syntheses and their Preliminary Characterizations

The synthetic methods reported herein for the preparation of $[\text{Co}(\text{R}_2\text{pp})\text{Cl}_2]$, $[\text{Co}(\text{H}_2\text{pp})_2\text{Cl}_2] \cdot 4\text{H}_2\text{O}$ and $[\text{Co}(\text{H}_2\text{pp})_3](\text{ClO}_4)_2 \cdot \text{H}_2\text{O}$ are relatively straightforward. The stoichiometric reaction of $[\text{Co}(\text{H}_2\text{O})_6]\text{Cl}_2$ with appropriate bidentate ligand in ethanol affords 1:1 / 1:2 complexes. For the 1:3 complex, $[\text{Co}(\text{H}_2\text{O})_6](\text{ClO}_4)_2$ was used instead of $[\text{Co}(\text{H}_2\text{O})_6]\text{Cl}_2$. As expected, four- and six- coordinate complexes are blue and pink/orange respectively. The complexes are stable in air, except $[\text{Co}(\text{H}_2\text{pp})\text{Cl}_2]$ which is moisture sensitive.

Microanalysis (C, H, N) (Table II.1) as well as chloride estimation (gravimetric method) of the chlorocomplexes conformed to the said formulation. The complex $[\text{Co}(\text{H}_2\text{pp})_2\text{Cl}_2] \cdot 4\text{H}_2\text{O}$ displays $\nu(\text{OH})$ band at 3250 and 3150 (split band) cm^{-1} (Figure II.6) indicating presence of water molecules as solvent of crystallization and they are hydrogen bonded (vide infra). The complex

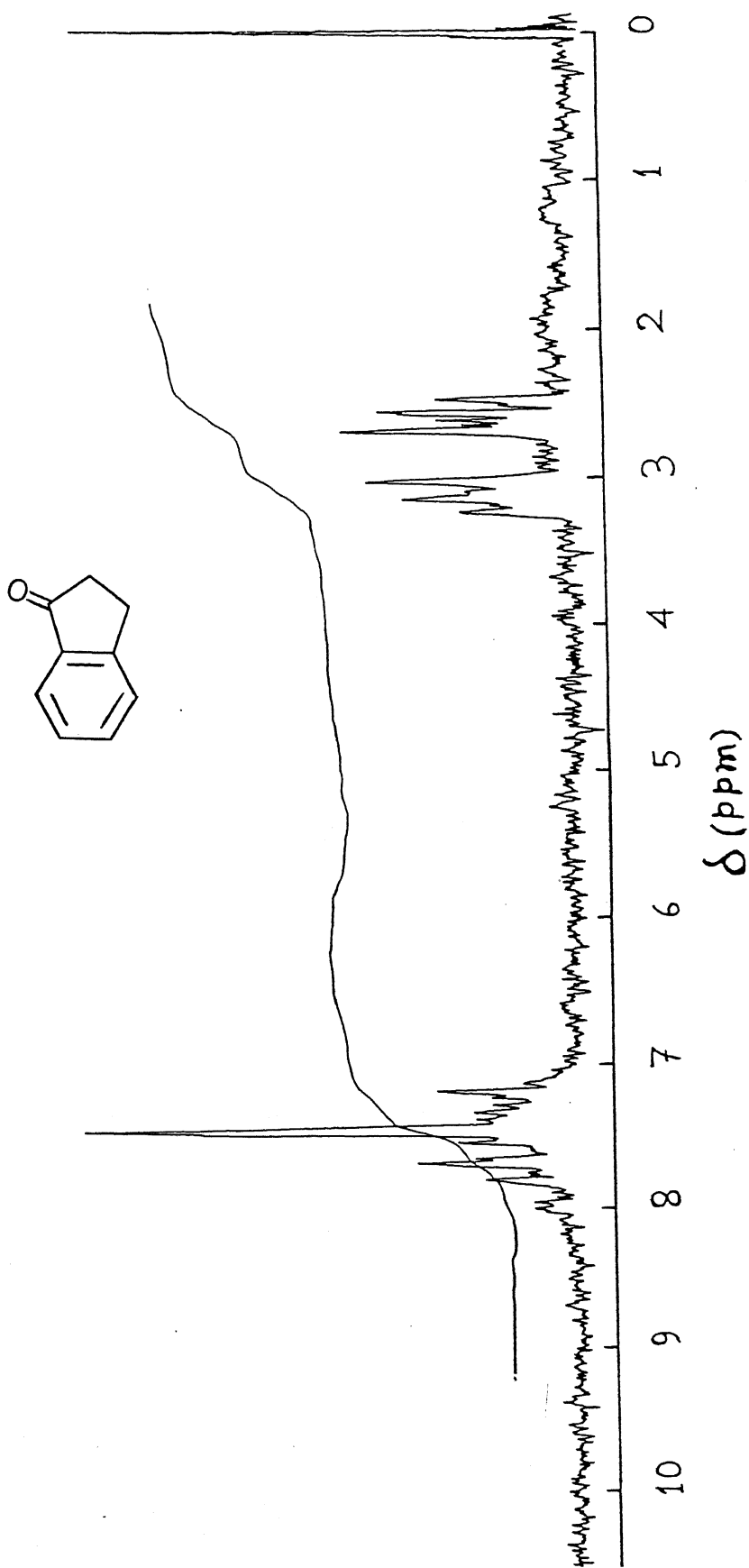


Figure 11.5 ^1H NMR spectrum of 1-indanone obtained by catalytic oxidation of indane

Table II.1: Microanalytical data of Cobalt(II) and Nickel(II)
Complexes

Complexes	Empirical Formula	Analysis ^a		
		% C	% H	% N
[Co(H ₂ pp)Cl ₂]	C ₉ H ₉ Cl ₂ N ₃ Co	37.42 (37.38)	3.13 (3.12)	14.53 (14.54)
[Co(H ₂ pp) ₂ Cl ₂] - .4H ₂ O	C ₁₈ H ₂₆ Cl ₂ N ₆ O ₄ Co	41.42 (41.54)	4.95 (5.00)	16.04 (16.16)
[Co(H ₂ pp) ₃] - (ClO ₄) ₂ .H ₂ O	C ₂₇ H ₂₉ Cl ₂ N ₉ O ₉ Co	42.90 (43.00)	3.82 (3.90)	16.55 (16.70)
[Co(Me ₂ pp)Cl ₂]	C ₁₁ H ₁₃ Cl ₂ N ₃ Co	41.50 (41.64)	4.20 (4.10)	13.10 (13.25)
[Ni(H ₂ pp) ₂ Cl ₂] - .4H ₂ O	C ₁₈ H ₂₆ Cl ₂ N ₆ O ₄ Ni	41.72 (41.56)	5.12 (5.00)	16.28 (16.16)
[Ni(Me ₂ pp) ₂ Cl ₂] - .2H ₂ O	C ₂₂ H ₃₀ Cl ₂ N ₆ O ₂ Ni	49.06 (48.92)	5.72 (5.56)	15.66 (15.56)
[Ni(H ₂ pp) ₃] (ClO ₄) ₂ .H ₂ O	C ₂₇ H ₂₉ Cl ₂ N ₉ O ₉ Ni	42.92 (43.05)	3.76 (3.85)	16.65 (16.74)

^aCalculated values in parentheses

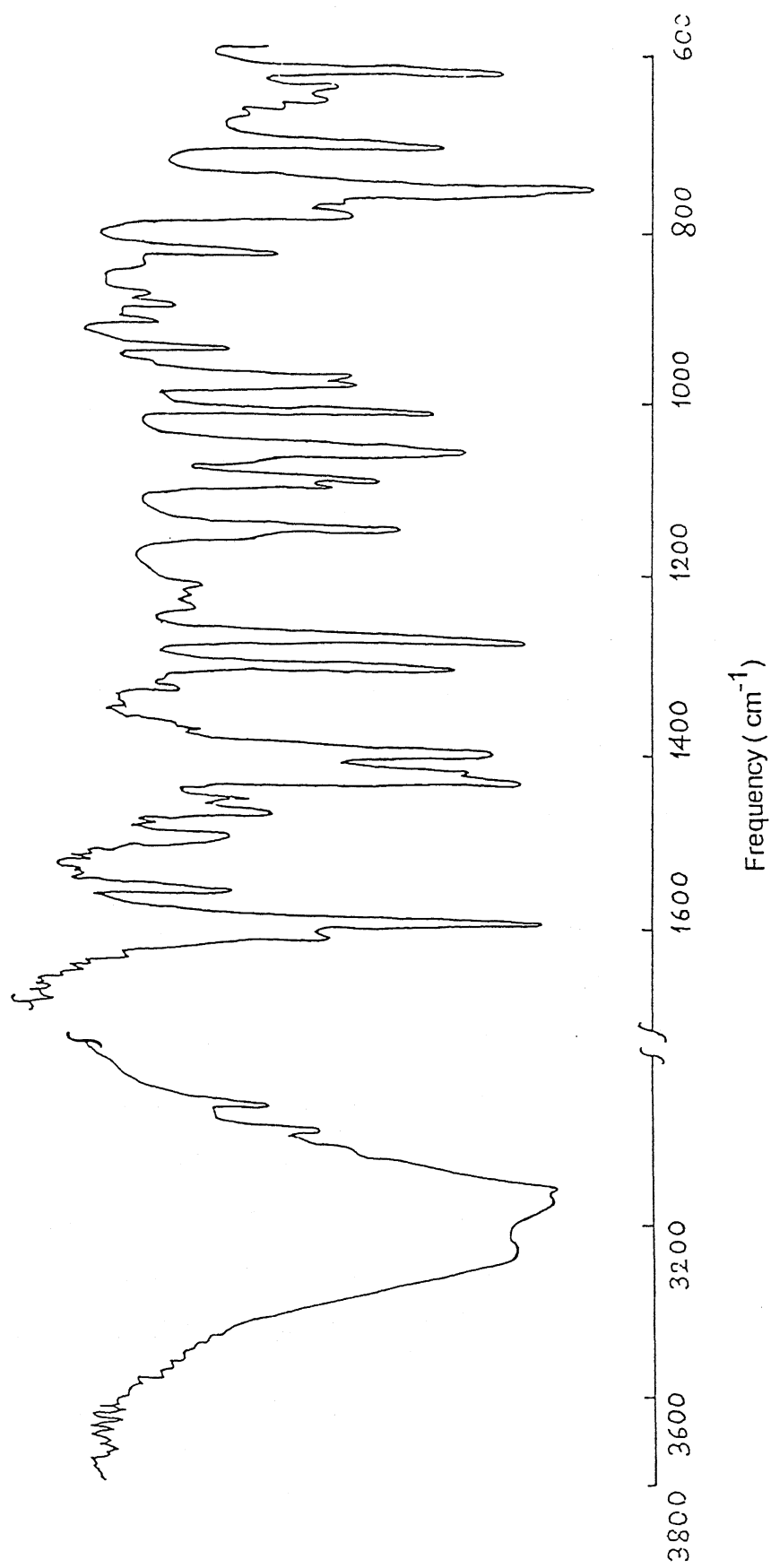


Figure 11.6 IR Spectrum of $[\text{Co}(\text{H}_2\text{pp})_2\text{Cl}_2] \cdot 4\text{H}_2\text{O}$

$[\text{Co}(\text{H}_2\text{pp})_3](\text{ClO}_4)_2 \cdot \text{H}_2\text{O}$ displays $\nu(\text{OH})$ band at 3400 cm^{-1} and $\nu(\text{ClO}_4^-)$ at 1100 and 620 cm^{-1} in its IR spectrum. The IR spectrum of this complex is shown in Figure II.7). The complexes $[\text{Co}(\text{R}_2\text{pp})\text{Cl}_2]$ are soluble in CH_2Cl_2 , MeCN and acetone retaining their original blue color as that in the solid state. Unlike $[\text{Co}(\text{Me}_2\text{pp})\text{Cl}_2]$ the complex $[\text{Co}(\text{H}_2\text{pp})\text{Cl}_2]$ is soluble in MeOH and EtOH to generate pink solutions. The complex $[\text{Co}(\text{H}_2\text{pp})_2\text{Cl}_2] \cdot 4\text{H}_2\text{O}$ is moderately soluble in MeOH and sparingly soluble in EtOH (the solid state color (pink) is retained in solution). The complex $[\text{Co}(\text{H}_2\text{pp})_2\text{Cl}_2] \cdot 4\text{H}_2\text{O}$ is sparingly soluble in CH_2Cl_2 , MeCN and acetone to form blue solutions. However, the tris-complex $[\text{Co}(\text{H}_2\text{pp})_3](\text{ClO}_4)_2 \cdot \text{H}_2\text{O}$ is highly soluble in polar organic solvents. Electrical conductivity data (Table II.2) in MeCN solution demonstrate the neutral nature of $[\text{Co}(\text{R}_2\text{pp})\text{Cl}_2]$ and 1:2 electrolytic^{129a} nature of $[\text{Co}(\text{H}_2\text{pp})_3](\text{ClO}_4)_2 \cdot \text{H}_2\text{O}$. The complex $[\text{Co}(\text{H}_2\text{pp})_2\text{Cl}_2] \cdot 4\text{H}_2\text{O}$ shows 1:1 electrolytic behavior in MeOH because partial chloride dissociation occurs in this solution (vide infra).

Solution-state magnetic susceptibility measurements using Evans' method reveal that the magnetic moments of four-coordinate chloro-complexes are in the range $4.65\text{--}4.71 \mu_{\text{B}}$, which is within the accepted range of high-spin tetrahedral cobalt(II) complexes with a ground term $^4\text{A}_2$.^{129b} Solid state magnetic moments are in the range $4.53\text{--}4.56 \mu_{\text{B}}$ which is close to that in solution. For six-coordinate complexes the range in the solution state is $4.90\text{--}5.25 \mu_{\text{B}}$ and the range in the solid state is $4.90\text{--}5.28 \mu_{\text{B}}$.

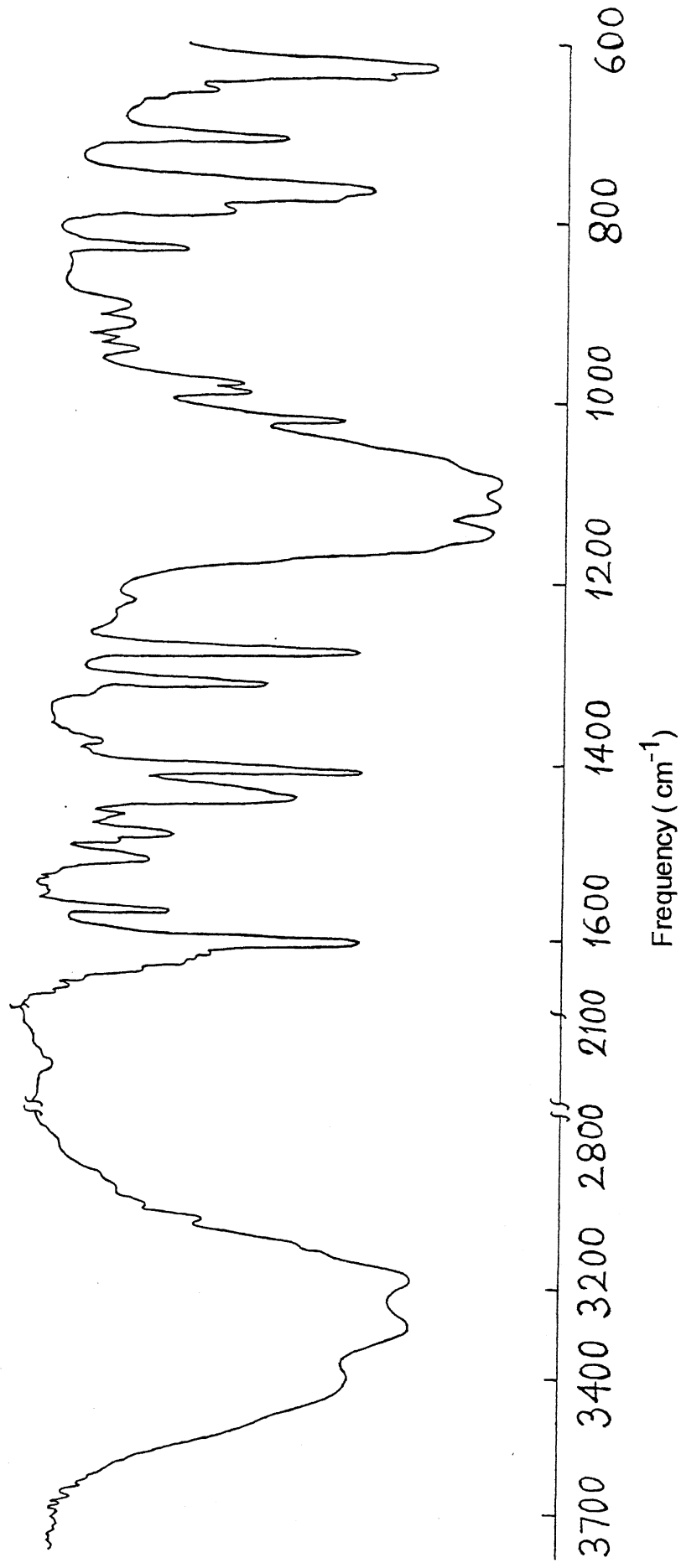


Figure II.7 IR Spectrum of $[\text{Co}(\text{H}_2\text{pp})_3](\text{ClO}_4)_2 \cdot \text{H}_2\text{O}$

Table II.2 Molar Conductance, Magnetic Moment and Electronic Spectral Data of Cobalt(II) and Nickel(II) Complexes at 298 K.

Complexes	Λ_M^c ($\Omega^{-1}\text{cm}^2\text{mol}^{-1}$)	$\mu_{\text{eff}}(\text{B.M.})^d$	$\lambda, \text{nm} (\epsilon, \text{M}^{-1}\text{cm}^{-1})$
$[\text{Co}(\text{H}_2\text{pp}) - \text{Cl}_2]^a$	12	4.65 (4.53)	1 100(9), 656(258), 630 (sh) (192), 590(171), 575 (sh) (150), 535(sh) (35), 515 (sh) (15), 268(sh) (2 990), 261(sh) (4,292), 255(4 610) (980 (sh), 550(sh), 520(sh), 490, 314(sh), 266) ^e
$[\text{Co}(\text{H}_2\text{pp})_2 - \text{Cl}_2] \cdot 4\text{H}_2\text{O}^b$	139	4.91 (4.91)	>1 100, 510(20), 490(sh) (18) (980(sh), 550(sh), 520(sh) 490, 314(sh), 266) ^e
$[\text{Co}(\text{H}_2\text{pp})_3] - (\text{ClO}_4)_2 \cdot \text{H}_2\text{O}^a$	296	5.25 (5.28)	1 038(6), 530(sh) (10), 504(sh) (15), 478(22), 301(sh) (840), 260 (6 658)
$[\text{Co}(\text{Me}_2\text{pp}) - \text{Cl}_2]^a$	11	4.71 (4.56)	1 000(20), 648(396), 625(sh) (334), 567(246), 533(sh) (80), 510(sh) (24), 267(sh) (3 260), 256(4 400) (650, 623(sh), 572, 540- (sh), 325(sh), 278(sh), 267) ^e

Table II.2 contd.

$[\text{Ni}(\text{H}_2\text{pp})_2^- \text{Cl}_2] \cdot 4\text{H}_2\text{O}^b$	70	2.98 (3.02)	972(13), 589(13.2), 362 (30.4), 267(sh) (4 506), 260(6 175), 255(sh) (5 543)
$[\text{Ni}(\text{H}_2\text{pp})_3] (\text{ClO}_4)_2 \cdot \text{H}_2\text{O}^b$	291	2.92	883(18), 550(25.6), 350 (49.5), 268(sh) (6 780), 261(9 362), 256(sh) (8 608)
$[\text{Ni}(\text{Me}_2\text{pp})_2^- \text{Cl}_2] \cdot 2\text{H}_2\text{O}^b$	75	2.85 (2.99)	1 005(6), 951(sh) (5), 620(6), 385(17), 268(sh) (5 068), 260(7 223), 255 (sh) (6 608)

^aMeasurements done in MeCN

^bMeasurements done in MeOH

^cExpected range for 1:1 and 1:2 electrolytes in MeCN are 120-160 and 220-300 $\Omega^{-1} \text{ cm}^2 \text{ mol}^{-1}$ respectively. Expected range for 1:1 and 1:2 electrolytes in MeOH are 80-115 and 160-220 $\Omega^{-1} \text{ cm}^2 \text{ mol}^{-1}$ respectively

^dMeasured using Evans' method and room temperature solid state values are in parentheses

^eRoom temperature solid state values are in parentheses

which are within the accepted range of high-spin octahedral cobalt(II) complexes with a ground term $^4T_{1g}$ (Table II.2).^{130,131}

II.6.1.2 Absorption Spectra

The ligand field spectral behavior of four- and six-coordinate cobalt(II) complexes were examined in solid state as well as in MeCN and MeOH solutions (Figures II.8-II.13). The data are presented in Table II.2.

Thus the four-coordinate complexes, $[Co(R_2pp)Cl_2]$ are *pseudo-tetrahedral*^{129b} in MeCN, CH_2Cl_2 , and acetone. The six-coordinate chloro-complex, $[Co(H_2pp)_2Cl_2] \cdot 4H_2O$ is *pseudo-octahedral*^{130,131} in MeOH and *pseudo-tetrahedral* in MeCN, CH_2Cl_2 , and acetone because these solutions are blue in color and absorption spectra of these solutions are similar to $[Co(H_2pp)Cl_2]$. Hence, the complex $[Co(H_2pp)_2Cl_2] \cdot 4H_2O$ loses a bidentate ligand in MeCN, CH_2Cl_2 , and acetone. Solid state electronic spectra of the complexes, $[Co(R_2pp)Cl_2]$ and $[Co(H_2pp)_2Cl_2] \cdot 4H_2O$ confirm *pseudo-tetrahedral* and *pseudo-octahedral* nature respectively.

The spectra of the tris-complex are similar to those observed for *pseudo-octahedral* high-spin cobalt(II) complexes.^{130,131}

II.6.1.3 Solution Structure of the High-spin $Co^{II}N_2Cl_2$ Coordination Sphere by 1H NMR Spectra

Solution structure of $[Co(Me_2pp)Cl_2]$ has been examined using 1H NMR spectroscopy. Proton NMR spectrum of this complex in $(CD_3)_2CO$ at 298 K is shown in Figure II.14 and the chemical shifts are listed in Table II.3. Peaks were observed in a wide

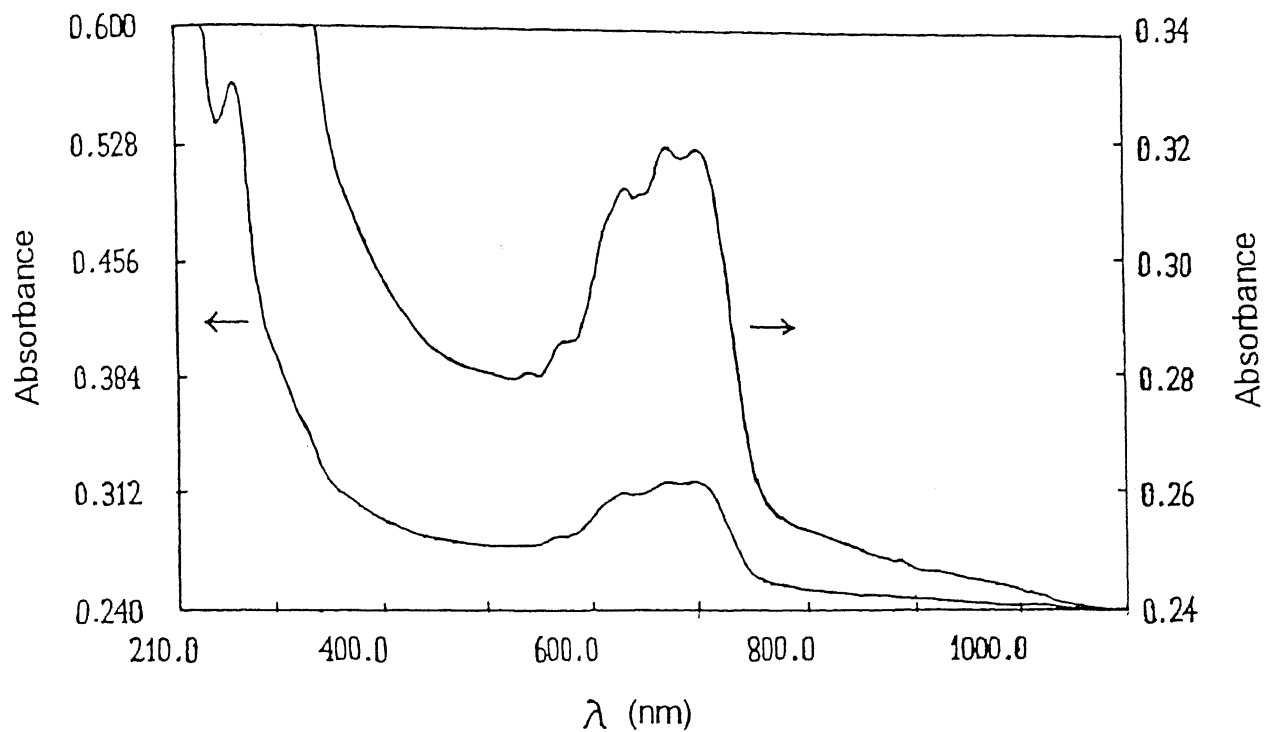
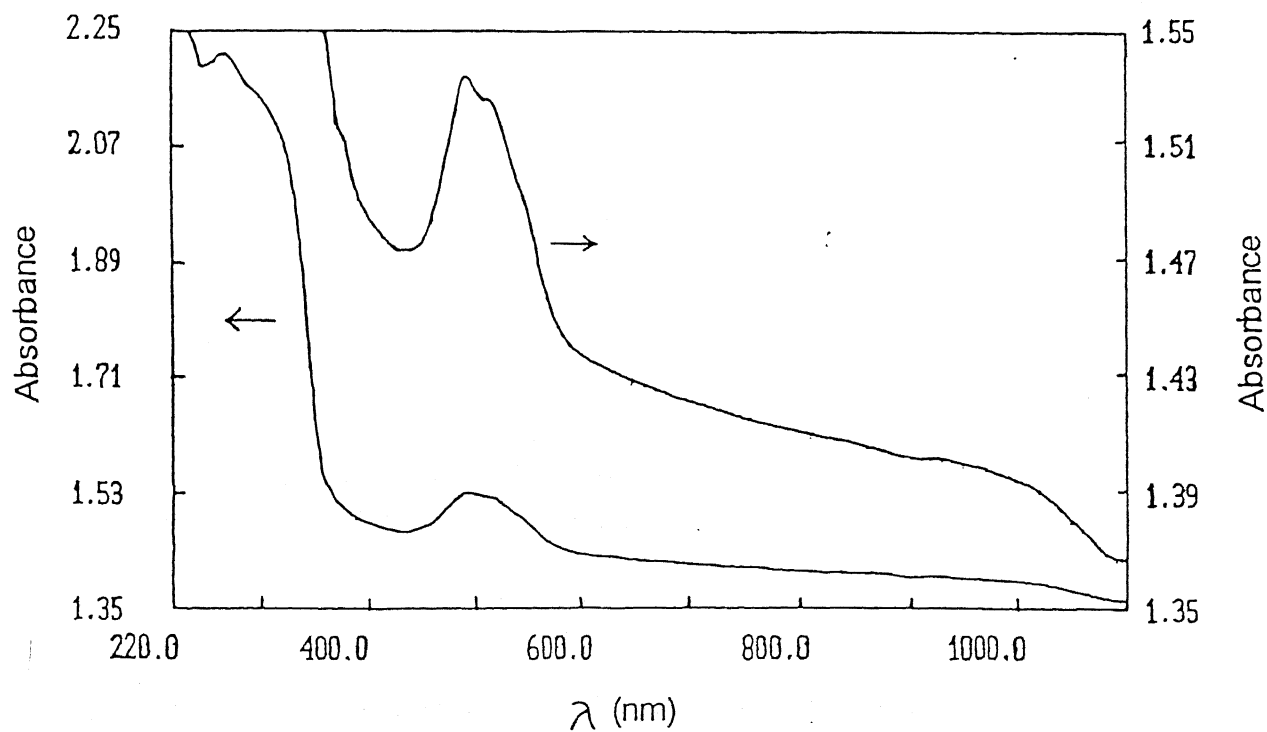


Figure II.8 Electronic Spectrum of $[\text{Co}(\text{H}_2\text{pp})\text{Cl}_2]$ in paraffin oil



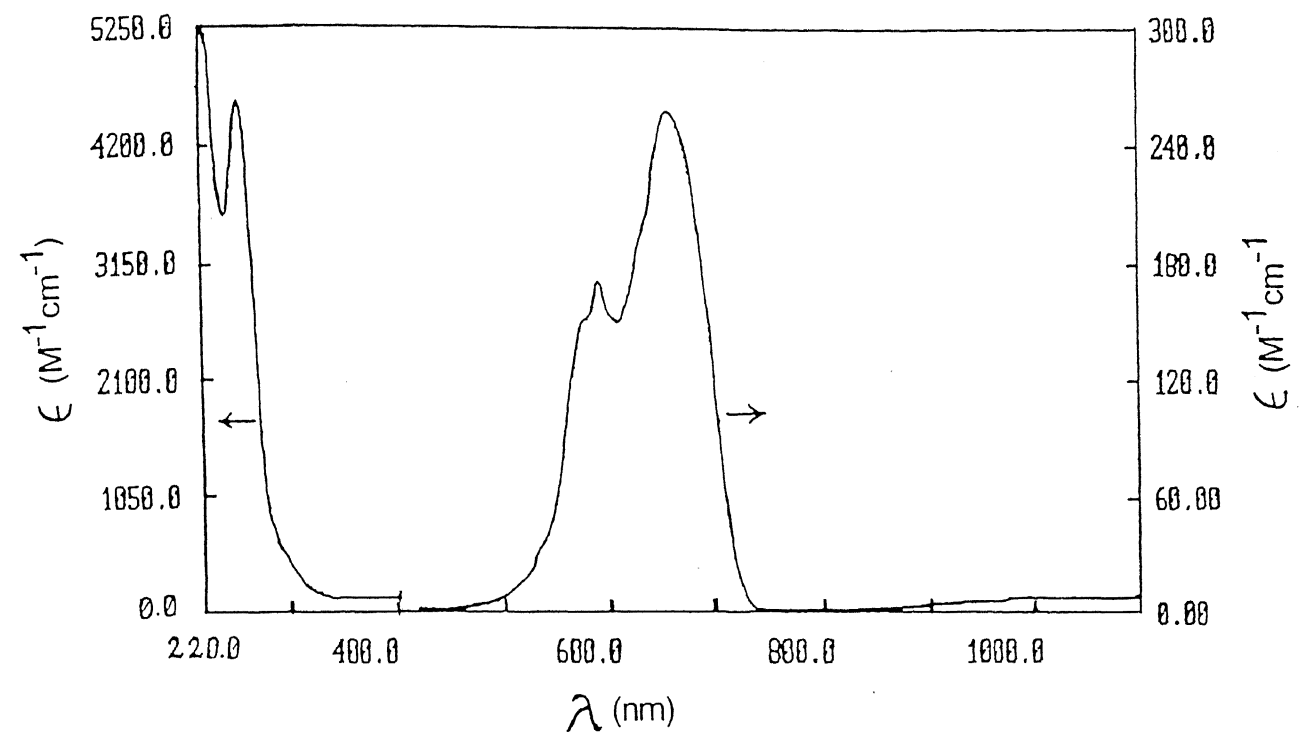


Figure II.10 Electronic Spectrum of $[\text{Co}(\text{H}_2\text{pp})\text{Cl}_2]$ in MeCN

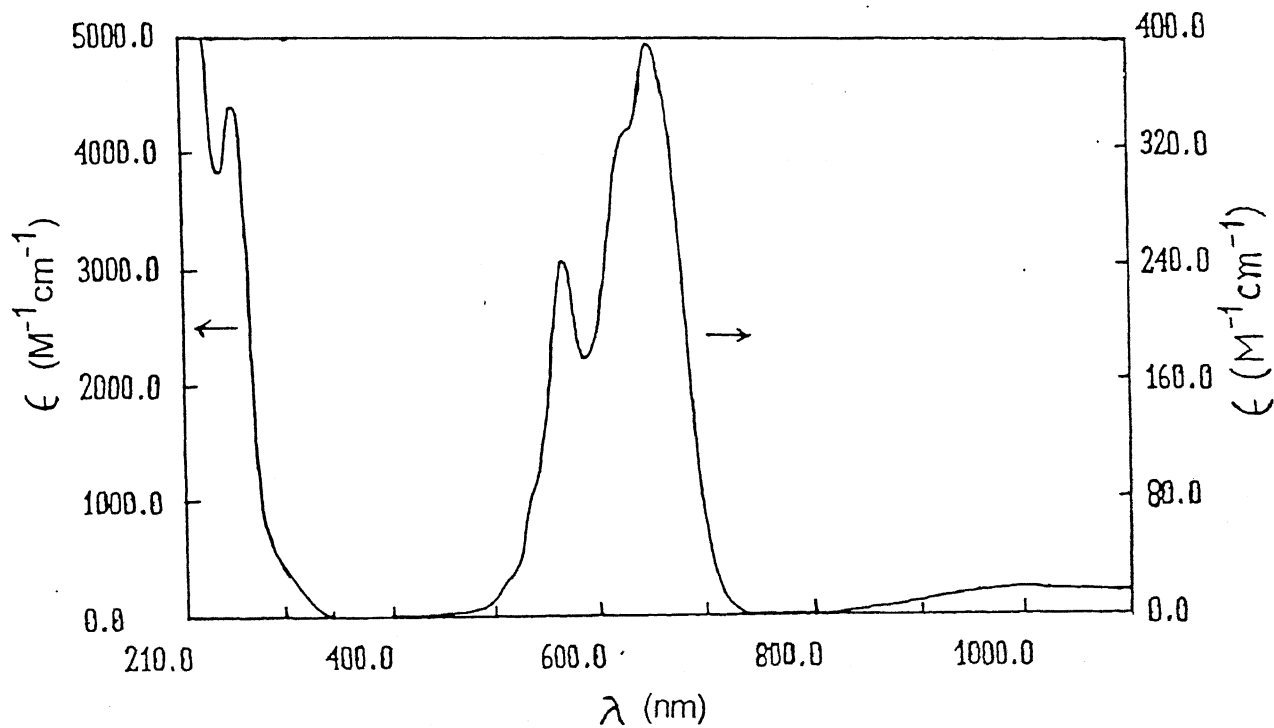


Figure II.11 Electronic Spectrum of $[\text{Co}(\text{Me}_2\text{pp})\text{Cl}_2]$ in MeCN

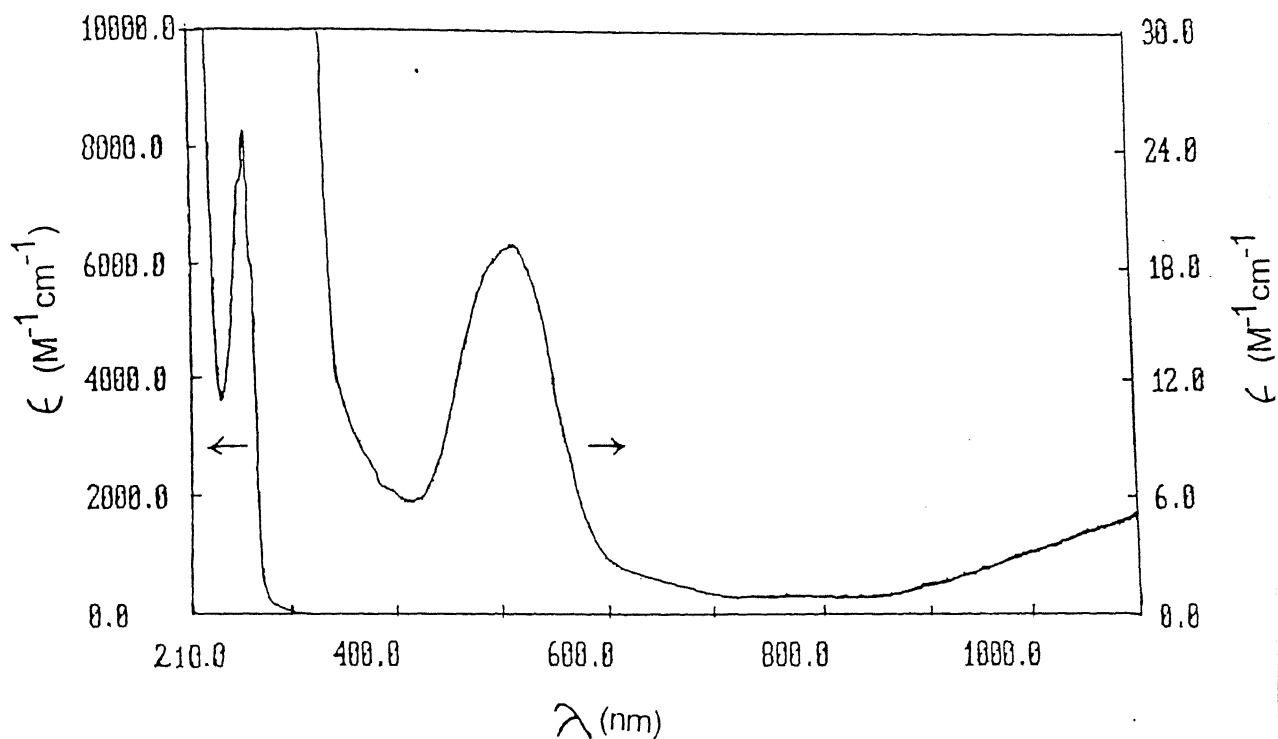


Figure II. 12 Electronic Spectrum of $[\text{Co}(\text{H}_2\text{pp})_2\text{Cl}_2] \cdot 4\text{H}_2\text{O}$ in MeOH

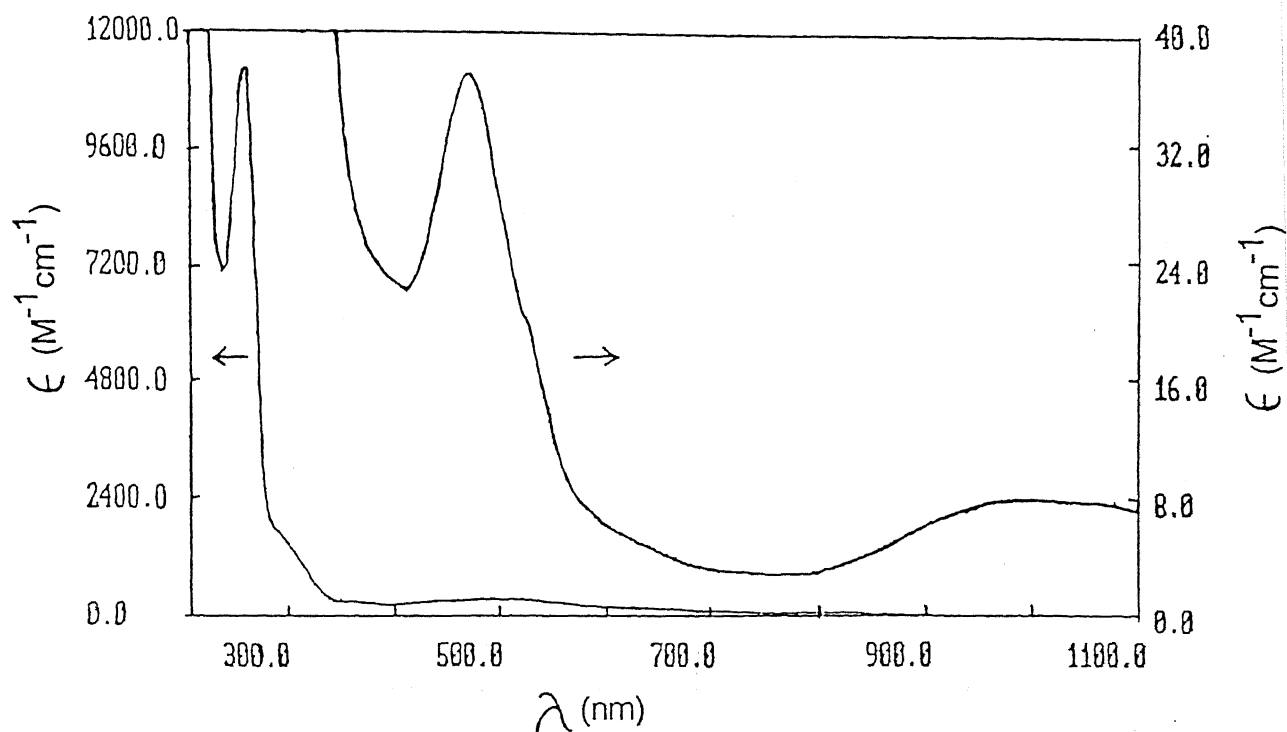


Figure II.13 Electronic Spectrum of $[\text{Co}(\text{H}_2\text{pp})_3](\text{ClO}_4)_2 \cdot \text{H}_2\text{O}$ in MeCN

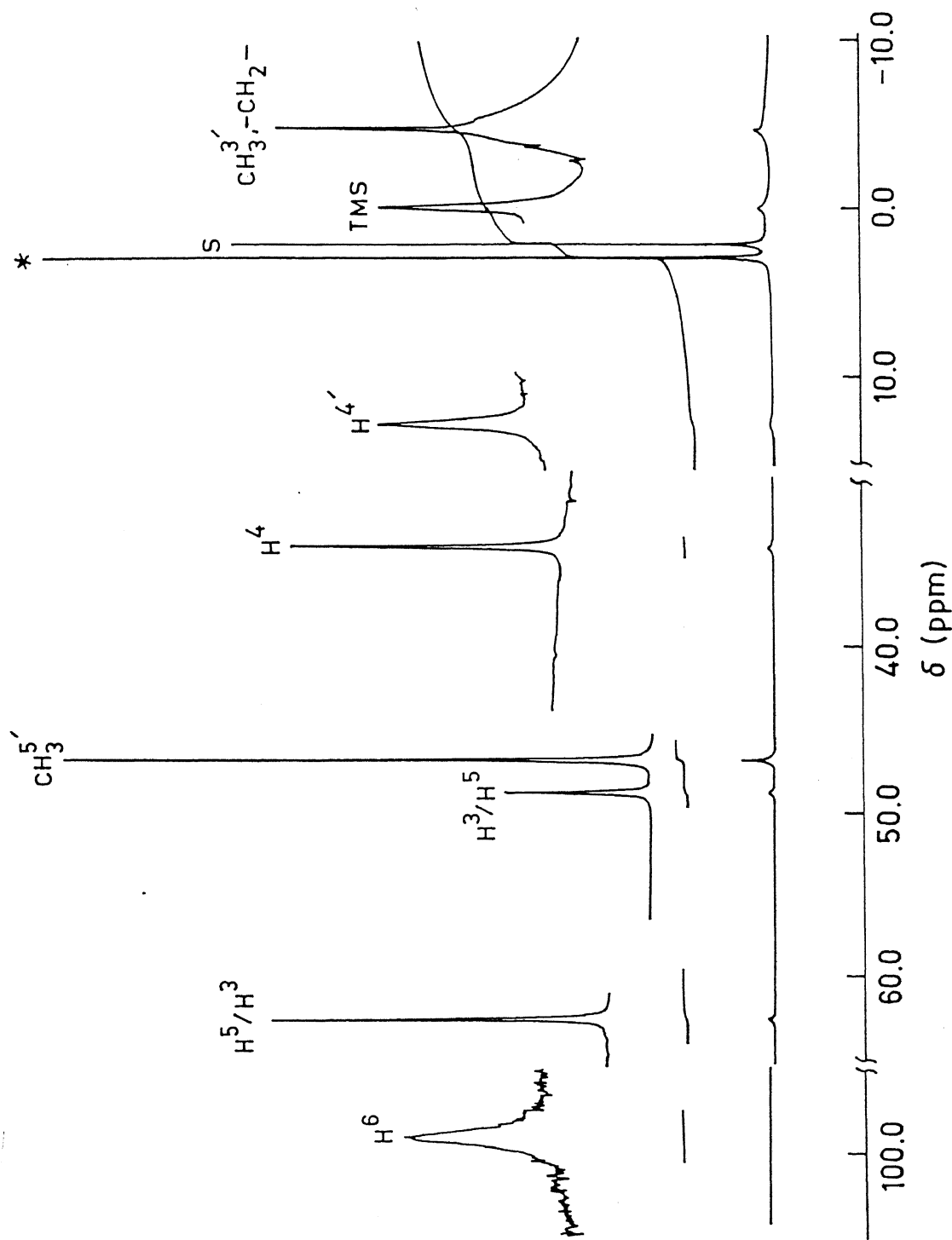


Figure II.14 400 MHz ^1H NMR Spectrum of $[\text{Co}(\text{Me}_2\text{pp})\text{Cl}_2]$ in CD_3COCD_3 (Solvent and Water Peaks Marked by S and * Respectively).

Table II.3 Proton NMR Chemical Shifts Relative to TMS for the
Cobalt(II) and Nickel(II) complexes

$[\text{Co}(\text{Me}_2\text{pp})\text{Cl}_2]$		$[\text{Ni}(\text{H}_2\text{pp})_3](\text{ClO}_4)_2 \cdot \text{H}_2\text{O}$	
δ (ppm)	assignment	δ (ppm)	assignment
99.25	H^6	58.65	H^6
62.62	H^5/H^3	55.75	H^3, H^5
48.75	H^3/H^5	50.00	$\text{H}^{4'}$
46.75	CH_3	48.75	$\text{H}^{5'}$
34.25	H^4	43.40	$\text{H}^{3'}$
12.75	$\text{H}^{4'}$	17.12	H^4
-4.75	CH_2, CH_3	-6.20	CH_2
		-11.25	2CH_2

range from -5 to +100 ppm and are well separated. The assignments (Table II.4) have been made on the basis of intensity, the effects of substitution of the methyl group for hydrogen, relative line widths and comparison with the spectra of the related systems.^{132,133} This ^1H NMR spectral behavior clearly demonstrates that in the complex the two heterocyclic rings are communicating electronically through the metal!

II.6.1.4 Description of Solid state Structure of $[\text{Co}(\text{Me}_2\text{pp})\text{Cl}_2]$ by X-ray

A perspective view (ORTEP) of the discrete complex and the atom labeling scheme is shown in Figure II.15. Table II.4 contain the essential bond distances and bond angles. Positional and isotropic thermal parameters are listed in Table II.5.

The complex $[\text{Co}(\text{Me}_2\text{pp})\text{Cl}_2]$ is a monomer. Each cobalt(II) ion is coordinated by two nitrogen atoms N(1) and N(3) from pyridyl and pyrazolyl rings of the ligand II and two chloride ions Cl(1) and Cl(2). The Co-N(pyridine) bond is longer than the Co-N(pyrazole) bond by 0.05 Å. This is quite common in these type of ligands.^{39,92} The cobalt atom exhibits pseudo-tetrahedral coordination, where the tetrahedron is somewhat distorted, especially the N(1)-Co-N(3) angle which is only $92.7(1)^\circ$. The Cl(1)-Co-Cl(2) angle has opened up to $116.00(5)^\circ$. The Cl(2)-Co-N(3) ($115.53(9)^\circ$) angle is also larger than the tetrahedral value. The pyridine and pyrazole rings are both planar and their mean planes are inclined to one another at an angle of 49.63° . It suggests that the six-membered chelate ring containing the cobalt atom exists in a boat conformation which is quite common in these

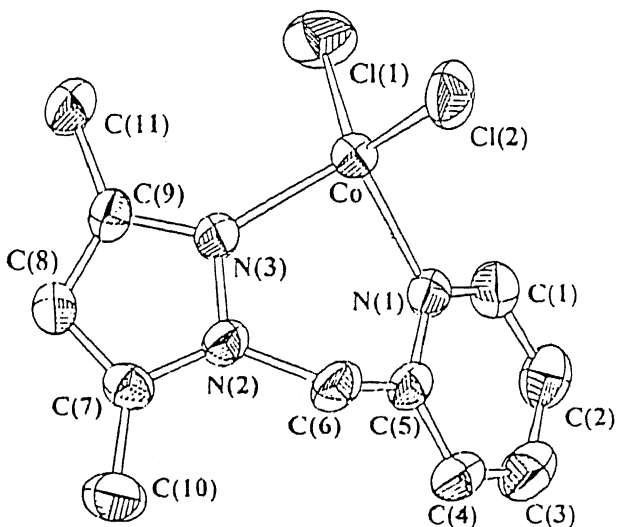


Figure II.15 ORTEP diagram of $[\text{Co}(\text{Me}_2\text{pp})\text{Cl}_2]$ showing the 50% probability thermal ellipsoids and atom labeling scheme

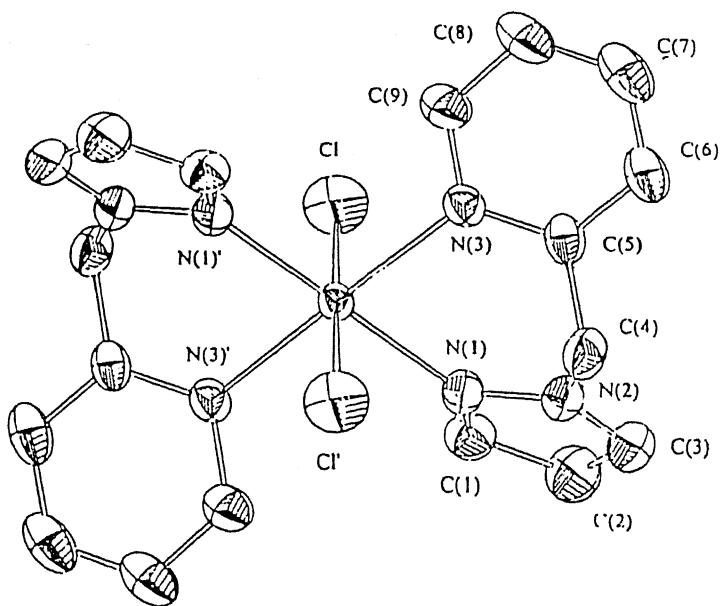


Figure II.16a ORTEP diagram of $[\text{Co}(\text{H}_2\text{pp})_2\text{Cl}_2] \cdot 4\text{H}_2\text{O}$ showing the 50% probability thermal ellipsoids and atom labeling scheme

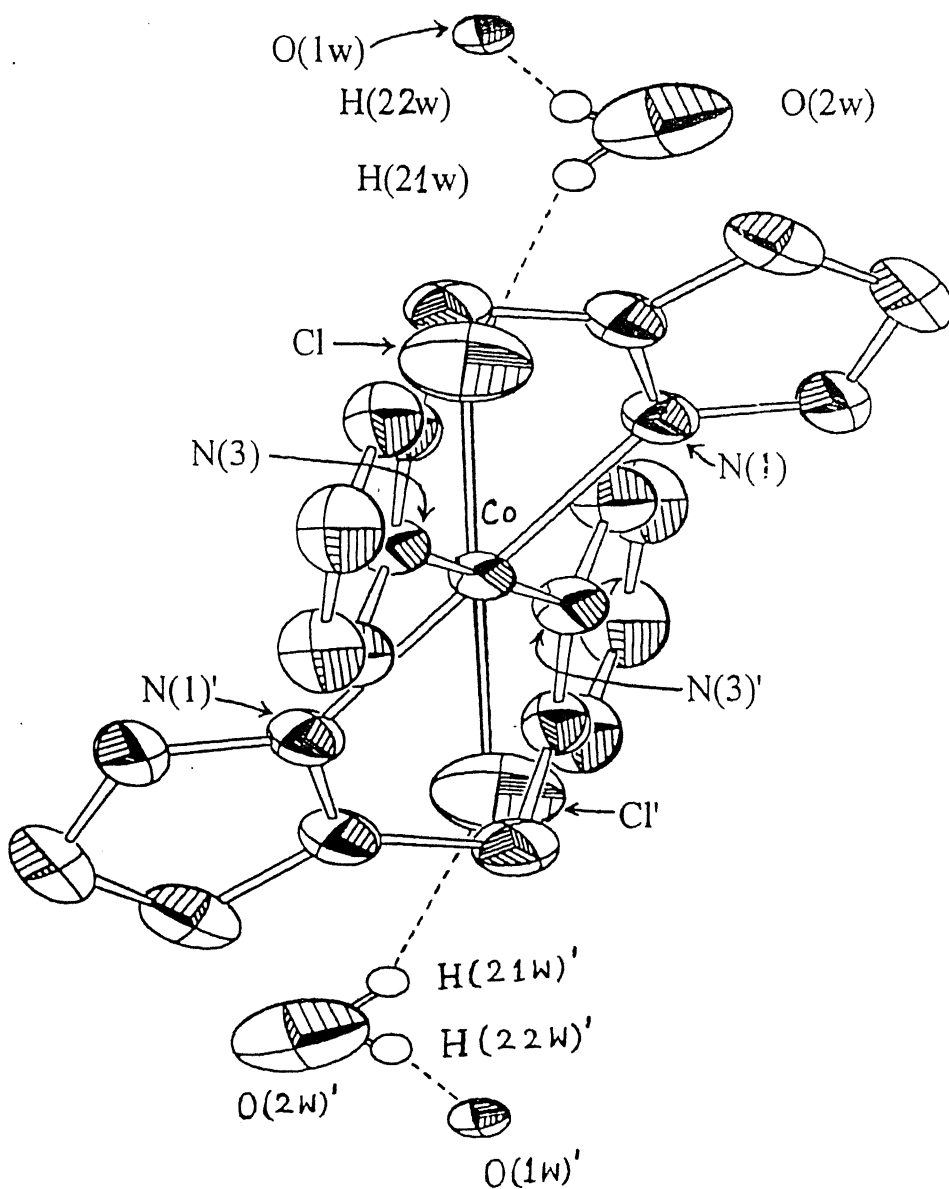


Figure II.16b ORTEP diagram of $[\text{Co}(\text{H}_2\text{pp})_2\text{Cl}_2] \cdot 4\text{H}_2\text{O}$ showing the hydrogen bondings

Table II.4

Bond Distances	(Angstroms)	Bond Angles	(degrees)
Co-Cl1	2.219 (1)	Cl1-Co-Cl2	116.00 (5)
Co-Cl2	2.224 (2)	Cl1-Co-N1	111.48 (8)
Co-N1	2.048 (2)	Cl1-Co-N3	110.98 (8)
Co-N3	1.998 (3)	Cl2-Co-N1	107.63 (9)
N1-C5	1.341 (4)	Cl2-Co-N3	115.53 (9)
N1-C1	1.335 (4)	N1-Co-N3	92.7 (1)
N3-N2	1.367 (3)	Co-N1-C5	119.9 (2)
N3-C9	1.346 (4)	Co-N1-C1	121.4 (2)
N2-C7	1.344 (5)	C5-N1-C1	118.7 (3)
N2-C6	1.460 (4)	Co-N3-N2	118.7 (2)
C8-C9	1.376 (5)	Co-N3-C9	135.3 (2)
C8-C7	1.372 (4)	N2-N3-C9	105.3 (3)
C9-C11	1.481 (4)	N3-N2-C7	111.5 (2)
C7-C10	1.480 (5)	N3-N2-C6	118.8 (3)
C5-C4	1.381 (5)	C7-N2-C6	129.4 (3)
C5-C6	1.509 (4)	C9-C8-C7	107.3 (3)
C4-C3	1.385 (5)	N3-C9-C8	109.8 (3)
C1-C2	1.370 (5)	N3-C9-C11	120.6 (3)
C3-C2	1.371 (6)	C8-C9-C11	129.6 (3)
		N2-C7-C8	106.2 (3)
		N2-C7-C10	123.0 (3)
		C8-C7-C10	130.9 (4)
		N1-C5-C4	121.8 (3)
		N1-C5-C6	117.3 (3)
		C4-C5-C6	120.8 (3)
		C5-C4-C3	118.6 (3)
		N1-C1-C2	122.9 (3)
		N2-C6-C5	113.4 (3)
		C4-C3-C2	119.6 (3)
		C1-C2-C3	118.5 (3)

Table II.5

Non-Hydrogen Positional and Isotropic Displacement Parameters

	x/a	y/b	z/c	U
Co	0.30947(6)	0.27754(5)	0.25371(5)	* 0.0400(2)
Cl(1)	0.2548(1)	0.4987(1)	0.0941(1)	* 0.0642(4)
Cl(2)	0.3958(1)	0.3310(1)	0.4198(1)	* 0.0632(4)
N(1)	0.4900(3)	0.0822(3)	0.1855(2)	* 0.039(1)
N(3)	0.1227(3)	0.1421(3)	0.3024(3)	* 0.038(1)
N(2)	0.1674(3)	-0.0318(3)	0.3335(3)	* 0.039(1)
C(8)	-0.1058(4)	0.0260(4)	0.3241(3)	* 0.042(1)
C(9)	-0.0465(4)	0.1761(4)	0.2965(3)	* 0.039(1)
C(7)	0.0314(4)	-0.1050(4)	0.3475(3)	* 0.040(1)
C(5)	0.4808(4)	-0.0802(4)	0.2413(3)	* 0.040(1)
C(4)	0.5991(5)	-0.2156(4)	0.1977(4)	* 0.053(1)
C(1)	0.6154(5)	0.1124(4)	0.0837(3)	* 0.048(1)
C(11)	-0.1398(5)	0.3543(5)	0.2620(4)	* 0.058(2)
C(10)	0.0425(5)	-0.2919(5)	0.3823(4)	* 0.060(2)
C(6)	0.3413(4)	-0.1097(4)	0.3591(3)	* 0.045(1)
C(3)	0.7305(5)	-0.1813(5)	0.0937(4)	* 0.060(2)
C(2)	0.7383(5)	-0.0152(5)	0.0356(3)	* 0.055(2)

type of ligands.^{39,79,92} We believe that this is due to the ligand-substituent induced steric effect.

II.6.1.5 Description of Solid-state Structure of $[\text{Co}(\text{H}_2\text{pp})_2\text{Cl}_2] \cdot 4\text{H}_2\text{O}$ by X-ray

An ORTEP diagram with atom labelling scheme is shown in Fig. II.16. Essential bond distances and bond angles are given in Table II.6. Positional and isotropic thermal parameters are listed in Table II.7. It's a monomer and the Cobalt atom sits on a crystallographically imposed inversion centre. The co-ordination environment around cobalt is distorted octahedron with the two chloride ions trans to each other. The remaining four positions are occupied by the pyridine/pyrazole nitrogen atoms of the two H_2pp ligands. As in $[\text{Co}(\text{Me}_2\text{pp})\text{Cl}_2]$ the Co-N(pyridine) is longer than Co-N(pyrazole) bond distances and the difference is 0.092 Å. The angles ranging from $85.7(2)^\circ$ to $180.0(3)^\circ$. The pyridine and pyrazole rings are each planar with the pyridine meanplane inclined to the pyrazole meanplane at an angle of 120.58° . As is the case for $[\text{Co}(\text{Me}_2\text{pp})\text{Cl}_2]$ and related structures the six-membered rings exist in boat conformations.

It is interesting to note here that (a) in $[\text{Co}(\text{H}_2\text{pp})_2\text{Cl}_2] \cdot 4\text{H}_2\text{O}$, Co-Cl, Co-N(pyridine) and Co-N(pyrazole) bond distances are longer compared to those in $[\text{Co}(\text{Me}_2\text{pp})\text{Cl}_2]$ and (b) in $[\text{Co}(\text{H}_2\text{pp})_2\text{Cl}_2] \cdot 4\text{H}_2\text{O}$, the angle between the pyridine and the pyrazole meanplane is higher than that obtained in $[\text{Co}(\text{Me}_2\text{pp})\text{Cl}_2]$. This is probably due to increased steric hindrance in $[\text{Co}(\text{H}_2\text{pp})_2\text{Cl}_2] \cdot 4\text{H}_2\text{O}$ though in this case two unsubstituted ligands (H_2pp) are coordinated.

Table II.6

Bond Distances		(Angstroms)	Bond Angles	(degrees)
Co-Cl	2.413 (4)	Cl-Co-N1	92.9 (2)	
Co-N1	2.106 (7)	Cl-Co-N3	89.9 (2)	
Co-N3	2.198 (6)	Cl-Co-Cl	180.0000	
Co-Cl	2.413 (4)	Cl-Co-N1	87.1 (2)	
Co-N1	2.106 (7)	Cl-Co-N3	90.1 (2)	
Co-N3	2.198 (6)	N1-Co-N3	94.3 (2)	
N1-N2	1.35 (1)	N1-Co-Cl	87.1 (2)	
N1-Cl	1.329 (9)	N1-Co-N1	180.0 (3)	
N2-C3	1.35 (1)	N1-Co-N3	85.7 (2)	
N2-C4	1.461 (9)	N3-Co-Cl	90.1 (2)	
N3-C5	1.34 (1)	N3-Co-N1	85.7 (2)	
N3-C9	1.348 (9)	N3-Co-N3	180.0 (3)	
C1-C2	1.38 (1)	Cl-Co-N1	92.9 (2)	
C2-C3	1.38 (1)	Cl-Co-N3	89.9 (2)	
C4-C5	1.51 (1)	N1-Co-N3	94.3 (2)	
C5-C6	1.38 (1)	Co-N1-N2	123.3 (4)	
C6-C7	1.36 (1)	Co-N1-Cl	129.8 (6)	
C7-C8	1.40 (2)	N2-N1-Cl	105.8 (7)	
C8-C9	1.37 (1)	N1-N2-C3	110.7 (6)	
O2w-H21w	.872 (9)	N1-N2-C4	120.9 (7)	
O2w-H22w	.88 (1)	C3-N2-C4	128.4 (8)	
		Co-N3-C5	123.4 (4)	
		Co-N3-C9	118.2 (6)	
		C5-N3-C9	117.5 (7)	
		N1-C1-C2	111.3 (7)	
		C1-C2-C3	104.9 (8)	
		N2-C3-C2	107.3 (9)	
		N2-C4-C5	111.7 (7)	
		N3-C5-C6	122.2 (7)	
		N3-C5-C4	117.5 (7)	
		C6-C5-C4	120.3 (8)	
		C5-C6-C7	120 (1)	
		C6-C7-C8	119.7 (9)	
		C7-C8-C9	117.2 (8)	
		N3-C9-C8	123.8 (9)	

Table II.7

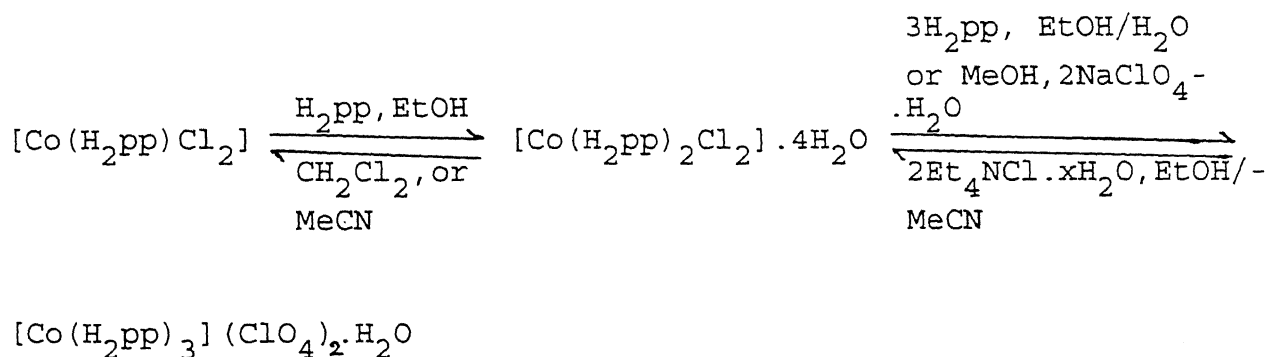
Non-Hydrogen Positional and Isotropic Displacement Parameters

	x/a	y/b	z/c	U
Co	1	0	0	* 0.0258(5)
Cl	0.7100(5)	0.0515(4)	0.0800(3)	* 0.081(2)
O(1w)	0.7148(6)	-0.4639(5)	0.4508(4)	* 0.019(2)
O(2w)	0.873(1)	0.2628(9)	0.3842(8)	* 0.076(4)
N(1)	0.8690(9)	-0.0247(8)	-0.2014(6)	* 0.033(3)
N(2)	0.961(1)	0.0813(8)	-0.2715(6)	* 0.035(3)
N(3)	1.1596(9)	0.2750(7)	0.0295(6)	* 0.032(2)
C(1)	0.678(1)	-0.116(1)	-0.2728(8)	* 0.038(3)
C(2)	0.645(1)	-0.073(1)	-0.3896(9)	* 0.050(4)
C(3)	0.830(1)	0.056(1)	-0.3857(8)	* 0.047(4)
C(4)	1.174(1)	0.207(1)	-0.2191(8)	* 0.040(3)
C(5)	1.198(1)	0.3352(9)	-0.0769(8)	* 0.033(3)
C(6)	1.263(1)	0.508(1)	-0.059(1)	* 0.045(4)
C(7)	1.292(1)	0.622(1)	0.071(1)	* 0.055(4)
C(8)	1.257(1)	0.564(1)	0.185(1)	* 0.049(4)
C(9)	1.189(1)	0.391(1)	0.1577(9)	* 0.041(3)

Two water protons are involved in hydrogen bonding: H(21w) is bonded to Cl since their bond distance (2.395 Å) is shorter than 3.00 Å, the sum of the van der Waals' radii and the angle at H(21w) is 125.31°; similarly, H(22w) is bonded to O(1w) (O(1w)-H(22w) bond distance is 2.155 Å and the sum of the van der Waals' radii is 2.60 Å) and the angle at H(22w) is 147.84°.

II.6.1.6 Stereochemical Interconversion Studies

Experiments performed to demonstrate stereochemical interconversions are as follows:



(i) When 1 is reacted with 1.25 (slightly greater than the stoichiometric requirement) of H₂pp in an appreciably polar solvent like ethanol [Co(H₂pp)₂Cl₂].4H₂O is formed. This clearly demonstrates stereochemical conversion from tetrahedral to octahedral. (ii) From the section II.4.1.1 we see that [Co(H₂pp)₂Cl₂].4H₂O is sparingly soluble in CH₂Cl₂, MeCN and acetone generating blue solutions. Electronic spectra of these solutions are characteristic of the tetrahedral co-ordination, as indicated by the strict similarity of the electronic spectrum of

$[\text{Co}(\text{H}_2\text{pp})\text{Cl}_2]$. It suggests preference of cobalt(II) for tetrahedral co-ordination. This may also be due to release of steric strain in these solvents. (iii) On reaction of $[\text{Co}(\text{H}_2\text{pp})_2\text{Cl}_2] \cdot 4\text{H}_2\text{O}$ with 3 equivalents of H_2pp in $\text{EtOH-H}_2\text{O}$ mixture or in MeOH in the presence of 2 equivalents of $\text{NaClO}_4 \cdot \text{H}_2\text{O}$ tris-complex $[\text{Co}(\text{H}_2\text{pp})_3](\text{ClO}_4)_2 \cdot \text{H}_2\text{O}$ is formed. This corroborates the conductivity behavior of $[\text{Co}(\text{H}_2\text{pp})_2\text{Cl}_2] \cdot 4\text{H}_2\text{O}$ in methanol (Section II.4.1.1). (iv) When $[\text{Co}(\text{H}_2\text{pp})_3](\text{ClO}_4)_2 \cdot \text{H}_2\text{O}$ is reacted with 2 equivalents of $\text{Et}_4\text{NCl} \cdot x\text{H}_2\text{O}$ in EtOH-MeCN mixture it transformed to $[\text{Co}(\text{H}_2\text{pp})_2\text{Cl}_2] \cdot 4\text{H}_2\text{O}$. This may be due to the fact that the resulting complex $[\text{Co}(\text{H}_2\text{pp})_2\text{Cl}_2] \cdot 4\text{H}_2\text{O}$ is more sterically relieved compared to the tris-ligated complex $[\text{Co}(\text{H}_2\text{pp})_3](\text{ClO}_4)_2 \cdot \text{H}_2\text{O}$.

II.6.1.7 Catalytic Oxidations of Various Organic Substrates by the 4-coordinated Co(II) Complexes

The complexes $[\text{Co}(\text{R}_2\text{pp})\text{Cl}_2]$ ($\text{R} = \text{H}$, 1; $\text{R} = \text{Me}$, 2) can oxidize various organic substrates efficiently and the reactions are catalytic in nature. Organic substrates used for catalytic oxidations are: *trans*-stilbene and $\text{R}(+)$ limonene for epoxydation and indane for benzylic oxidation.

Two pseudo-tetrahedral Co(II) complexes 1 and 2 are able to transform various types of C-C double bonds (i.e. alkenes e.g. *trans*-stilbene, limonene) to their epoxy form (epoxide) (Figures II.3-II.6; Table II.8) in good yield in presence of dioxygen and 2-methyl propanaldehyde as primary oxidant and activator respectively. Another function of the aldehyde is to act as sacrificial reducing agent. It is worth noting that catalytic turnovers are quite promising (Table II.8).

Table II.8 Catalytical Oxidation of Organic Substrates in MeCN by
 $[\text{Co}(\text{R}_2\text{pp})\text{Cl}_2$ (R=H, 1; R=Me, 2) with Dioxygen at 298 K

Catalyst	Substrate	Product(s)	Yield(%)	Turnover No. ^a
1	<u>trans</u> -stilbene	<u>trans</u> -stilbene oxide	100	130
2	<u>trans</u> -stilbene	<u>trans</u> -stilbene oxide	100	132
			50	
1	R(+) limonene	R(+)- limonene epoxides		110
			50	
			50	
2	R(+)limonene	R(+)- limonene epoxides		106
			50	
1	indane	1-indanone	100	190
2	indane	1-indanone	100	186

^aBased on metal complex over a period of 12h

A Proposed Mechanism

A possible mechanism for the catalytic oxidation of organic substrates is depicted in Scheme II.2 from the following observations. (i) Absorption spectral feature of $[\text{Co}(\text{Me}_2\text{pp})\text{Cl}_2]$ in MeCN (Table II.2) in presence of aldehyde and dioxygen changes completely (Figure II.17) along with the change in color from blue to green ($\lambda_{\text{max}}(\text{nm}, \text{MeCN}) = 690(\text{sh}), 651, 630(\text{sh}), 588, 576(\text{sh}), 558(\text{sh}), 532(\text{sh})$). This could be due to the formation of an oxygenated cobalt complex (most probably hydroperoxide species). It is worthnoting here that the color of Co(III)-bleomycin is green ($\lambda_{\text{max}}(\text{nm}, \text{water}) = 594$) when -OOH group is believed to be present as the sixth ligand.¹³⁴ (ii) Cyclic voltammetric studies (MeCN, platinum working electrode) indicate that $[\text{Co}(\text{Me}_2\text{pp})\text{Cl}_2]$ has an oxidative response at $\sim +1.40$ V which could be due to coordinated Cl^- oxidation along with oxidation of the metal center ($\text{Co}^{\text{III}}/\text{Co}^{\text{II}}$ process). In presence of aldehyde and dioxygen a broad reductive response at -0.5 V was observed for 2. As there was no response near -0.5 V for 2 without dioxygen and aldehyde this could be due to the formation of the species II (Scheme II.2). At this level of experimental information we are not in a position to convincingly identify this species.

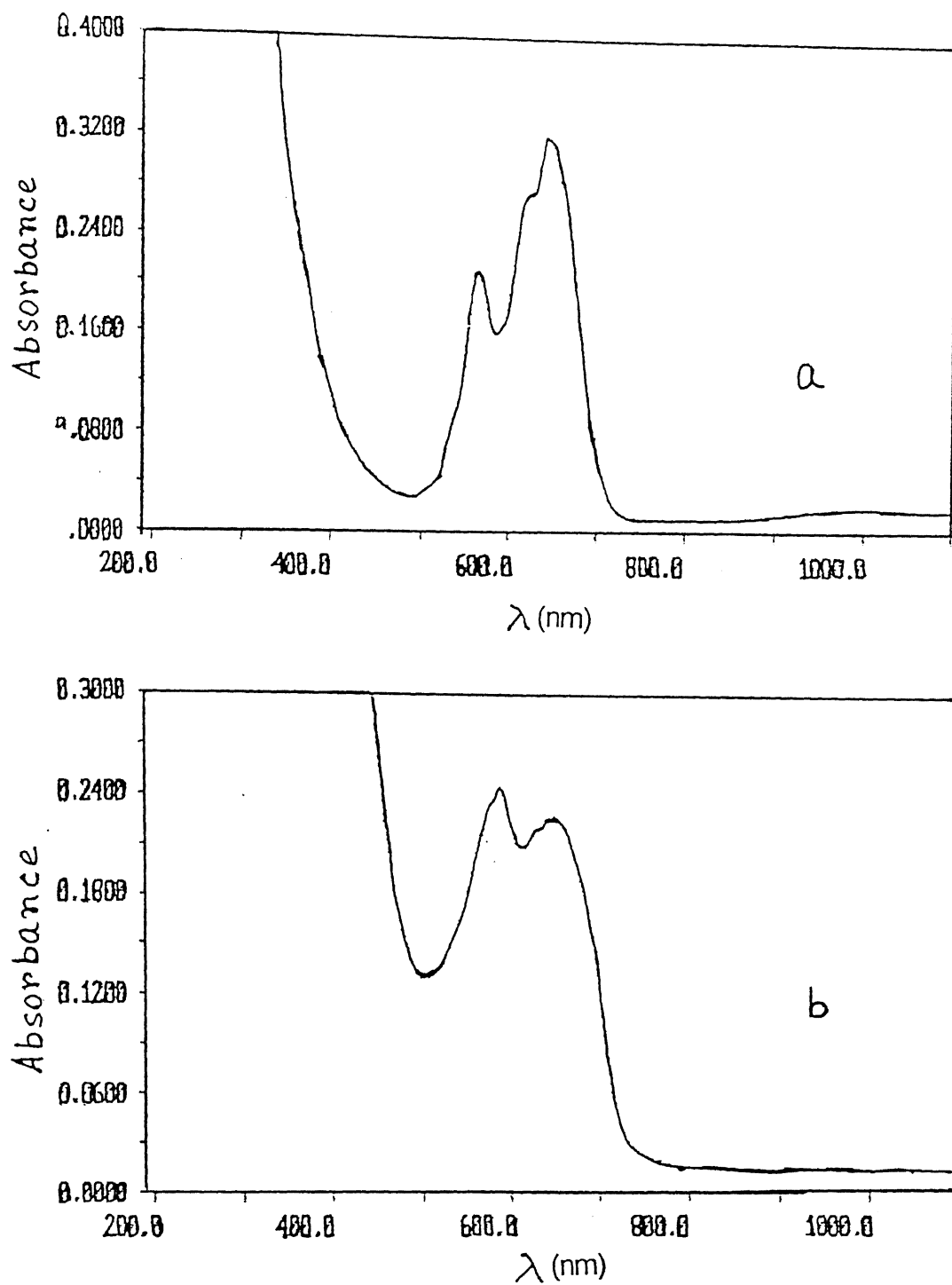
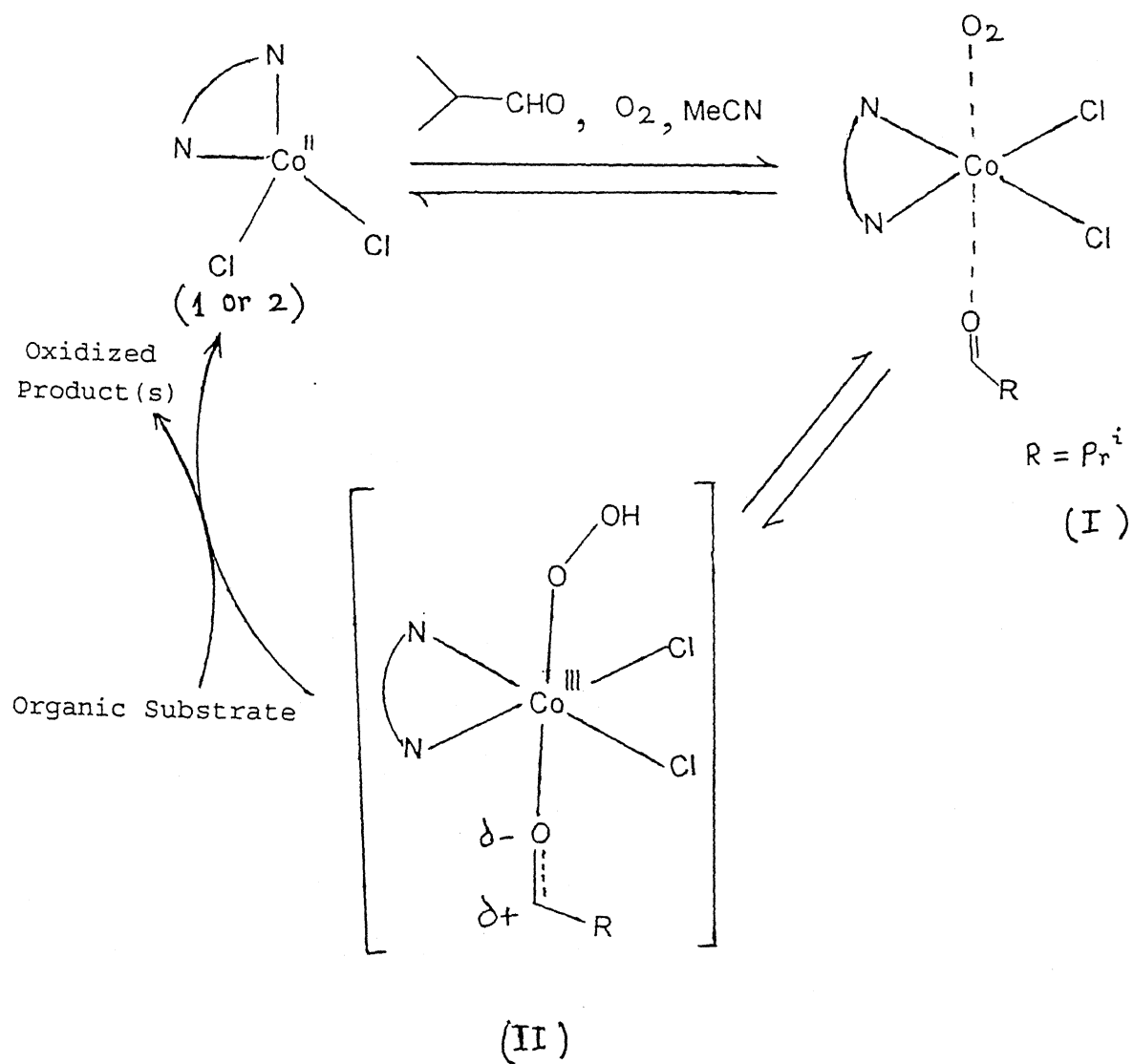


Figure II 17 Electronic spectra (in MeCN) of $[\text{Co}(\text{Me}_2\text{pp})\text{Cl}_2]$ before (a) and after (b) addition of 2-propanaldehyde and dioxxygen bubbling

Scheme II.2 Proposed mechanism of oxidation of organic substrate
by pseudo-tetrahedral Co(II) complexes, $[\text{Co}(\text{Me}_2\text{pp})\text{Cl}_2]$
($\text{R} = \text{H}$, 1 and $\text{R} = \text{Me}$, 2)



II.6.2 Six-coordinate Ni(II) Complexes

II.6.2.1 Synthesis and Characterization of Ni(II) Complexes

Reactions of $\text{NiCl}_2 \cdot 6\text{H}_2\text{O}$ with two equivalents of ligands H_2pp and Me_2pp in ethanol produced the complexes $[\text{Ni}(\text{R}_2\text{pp})_2\text{Cl}_2] \cdot x\text{H}_2\text{O}$ (when $\text{R} = \text{H}$, $x = 4$; $\text{R} = \text{Me}$, $x = 2$) and the reaction of $\text{Ni}(\text{ClO})_4 \cdot 6\text{H}_2\text{O}$ with three equivalents of H_2pp in ethanol resulted in the formation of the complex $[\text{Ni}(\text{H}_2\text{pp})_3](\text{ClO}_4)_2 \cdot \text{H}_2\text{O}$. The chloro-complexes are green to light blue in color and the tris-complex is bluish violet.

Microanalysis (C, H, N) (Table II.1) as well as chloride estimation (gravimetric method) of $[\text{Ni}(\text{R}_2\text{pp})_2\text{Cl}_2] \cdot x\text{H}_2\text{O}$ complexes justify the proposed formulation. The complex $[\text{Ni}(\text{H}_2\text{pp})_2\text{Cl}_2] \cdot 4\text{H}_2\text{O}$ displays $\nu(\text{OH})$ band at 3290 and 3150 (split band) cm^{-1} suggesting that the present water molecules are hydrogen bonded (Figure II.18). The complex $[\text{Ni}(\text{Me}_2\text{pp})_2\text{Cl}_2] \cdot 2\text{H}_2\text{O}$ displays $\nu(\text{OH})$ band at 3300 cm^{-1} indicating water molecules are present as solvent of crystallization (Figure II.19). The complex $[\text{Ni}(\text{H}_2\text{pp})_3](\text{ClO}_4)_2 \cdot \text{H}_2\text{O}$ displays $\nu(\text{OH})$ band at 3400 cm^{-1} and $\nu(\text{ClO}_4^-)$ at 1100 and 620 cm^{-1} . The IR spectrum of the tris-complex is shown in Figure II.20. The complexes $[\text{Ni}(\text{R}_2\text{pp})_2\text{Cl}_2] \cdot x\text{H}_2\text{O}$ are soluble in MeOH and EtOH (the solid state color, green/light blue is retained in solution). Unlike $[\text{Ni}(\text{H}_2\text{pp})_2\text{Cl}_2] \cdot 4\text{H}_2\text{O}$ the complex $[\text{Ni}(\text{Me}_2\text{pp})_2\text{Cl}_2] \cdot 2\text{H}_2\text{O}$ forms pink solutions in CH_2Cl_2 , MeCN and acetone. A nickel(II) complex synthesized following 1:1 metal-to-ligand stoichiometry, which is supposed to be $[\text{Ni}(\text{Me}_2\text{pp})(\text{S})_2\text{Cl}_2]$ (where $\text{S} = \text{EtOH}/\text{H}_2\text{O}$), also forms pink solutions in these solvents. The complex $[\text{Ni}(\text{H}_2\text{pp})_3](\text{ClO}_4)_2 \cdot \text{H}_2\text{O}$ is highly soluble in polar organic solvents. Electrical conductivity data in MeOH solutions shows 1:2

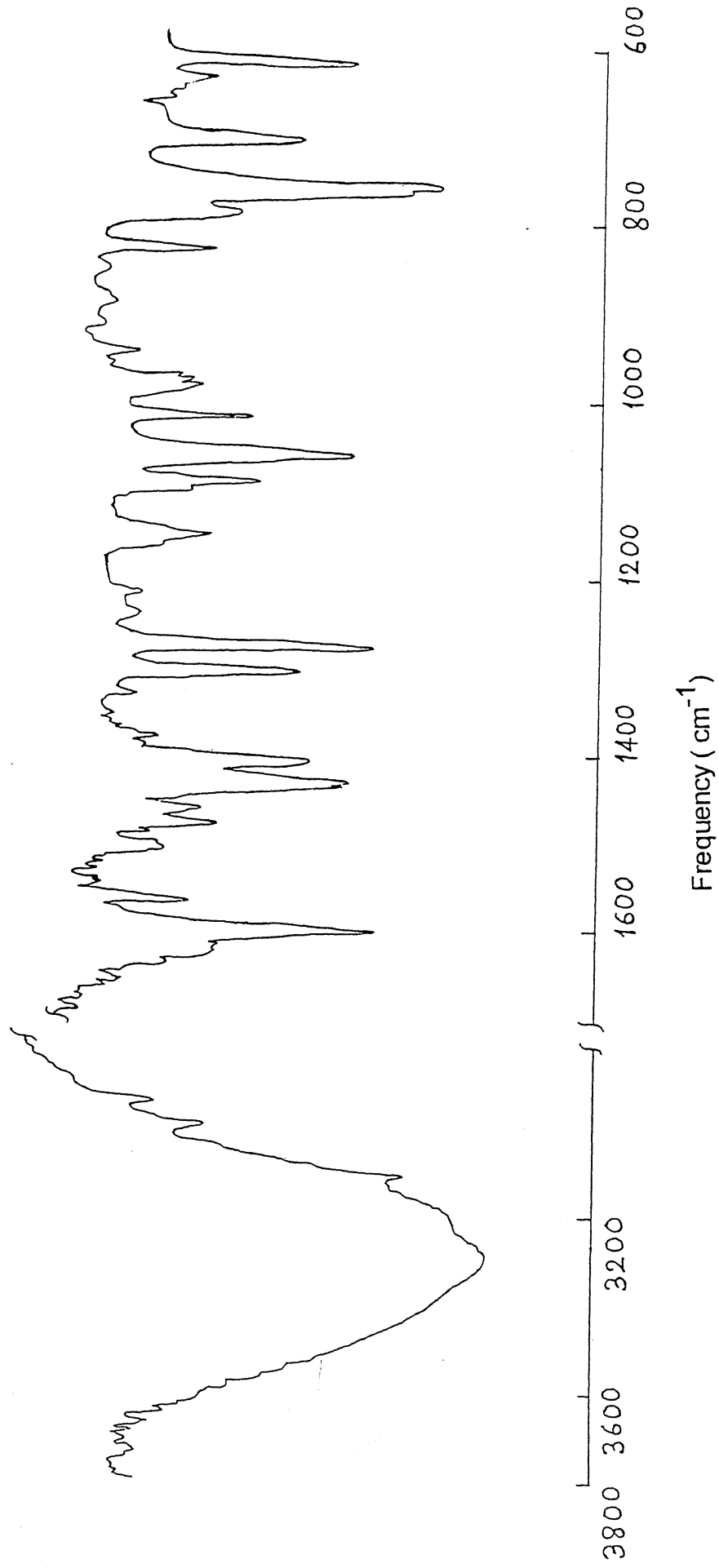


Figure II. 18 IR Spectrum of $[\text{Ni}(\text{H}_2\text{pp})_2\text{Cl}_2] \cdot 4\text{H}_2\text{O}$

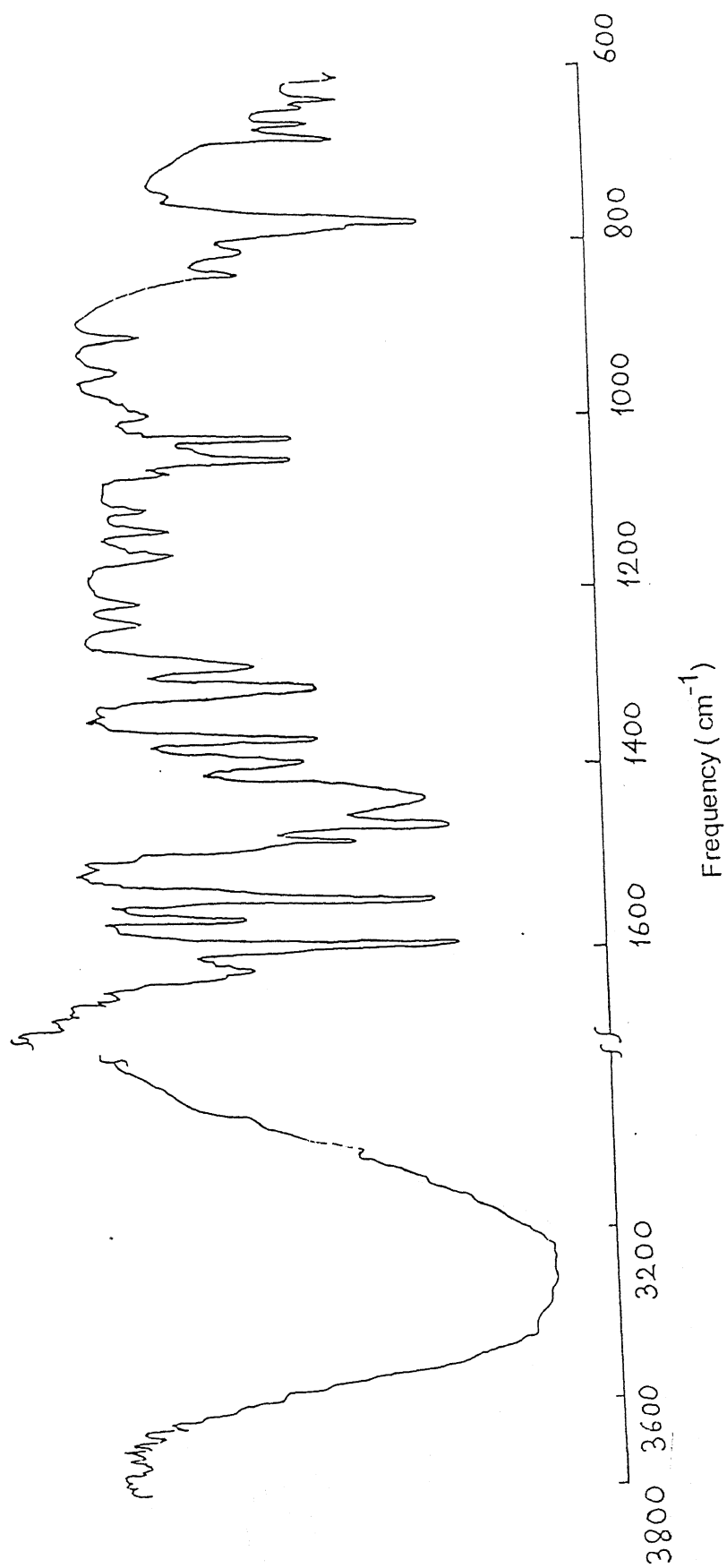


Figure II.19 IR Spectrum of $[\text{Ni}(\text{Me}_2\text{pp})_2\text{Cl}_2] \cdot 2\text{H}_2\text{O}$

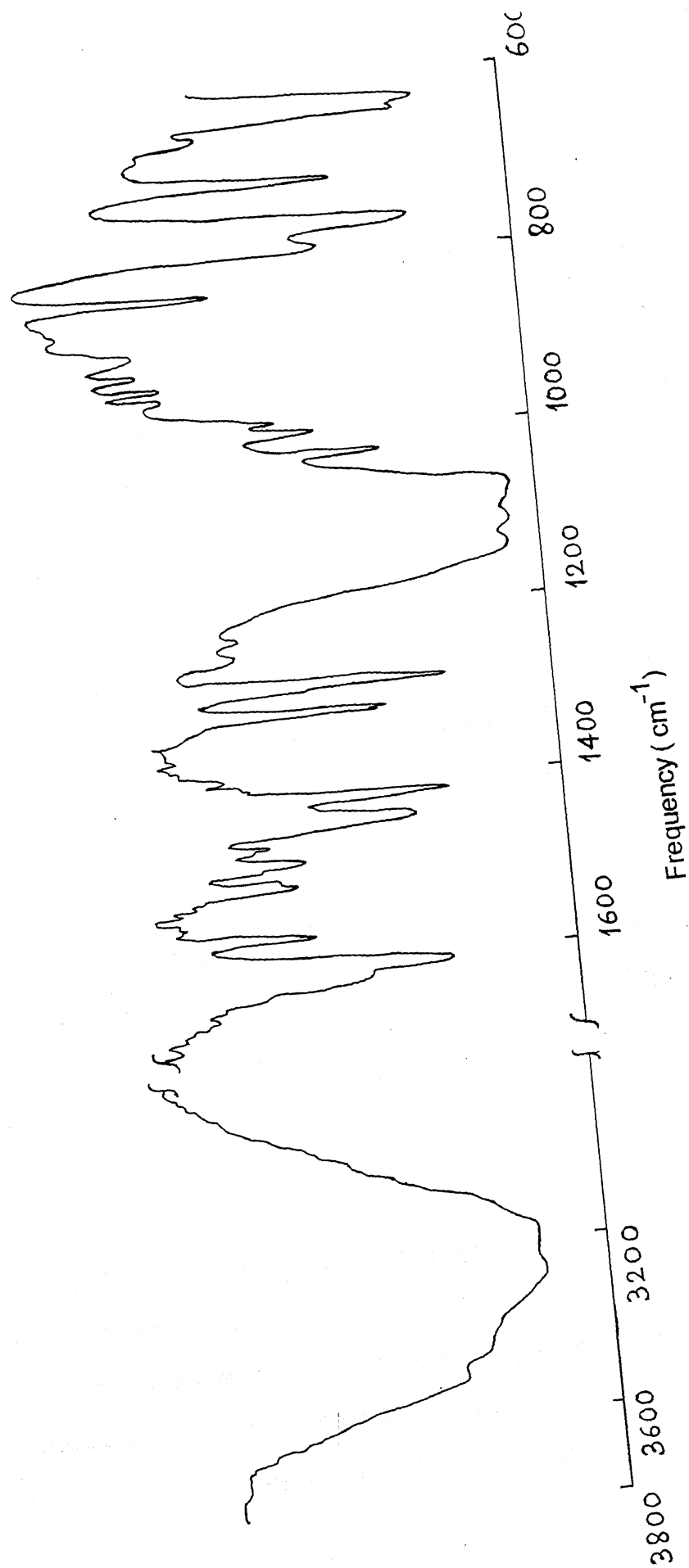


Figure II.20 IR Spectrum of $[\text{Ni}(\text{H}_2\text{pp})_3]\text{ClO}_4 \cdot 2\text{H}_2\text{O}$

electrolytic^{129a} behavior of $[\text{Ni}(\text{H}_2\text{pp})_3](\text{ClO}_4)_2 \cdot \text{H}_2\text{O}$. The complexes $[\text{Ni}(\text{R}_2\text{pp})_2\text{Cl}_2] \cdot x\text{H}_2\text{O}$ show close to 1:1 behavior^{129a} since their chlorides dissociate in solutions.

Solution-state magnetic susceptibility measurements using Evan's method reveal that the magnetic moments of the nickel(II) complexes are in the range $2.85\text{--}3.18 \mu_{\text{B}}$, which is within the accepted range of high-spin octahedral nickel(II) complexes with a ground term ${}^3\text{A}_{2\text{g}}$.^{135a} Solid state magnetic moments are in the range $2.98\text{--}3.02 \mu_{\text{B}}$ which is close to that in solution (Table II.2).

II.6.2.2 Absorption Spectra

The ligand field spectral properties of the Ni(II) complexes were examined in MeOH solutions. The behavior of the complexes are shown in Figures II.21-II.25 and spectral data are presented in Tables II.2, II.9a and II.9b. The spectra of these complexes are similar to those observed for *pseudo*-octahedral high-spin Ni(II) complexes.^{135a,135b} The absorption spectra in CH_2Cl_2 , MeCN and acetone solutions of the complexes $[\text{Ni}(\text{Me}_2\text{pp})_2\text{Cl}_2] \cdot 2\text{H}_2\text{O}$ and $[\text{Ni}(\text{Me}_2\text{pp})(\text{S})_2\text{Cl}_2]$ indicate that these complexes are present as a mixture of *pseudo*-octahedral and *pseudo*-tetrahedral^{135a,135b} species (see also Section II.4.2.1).

II.6.2.3 Solution Structure of the High-spin $\text{Ni}^{\text{II}}\text{N}_6$ Coordination Sphere by ${}^1\text{H}$ NMR Spectra

To elucidate the coordination geometry of the high-spin *pseudo*-octahedral 1:3 chelate nickel(II) complex, we have undertaken a ${}^1\text{H}$ NMR study (Figure II.26) focussing on paramagnetically

shifted $^{136-138}$ resonances. Assignments of the resonances (Table II.3) are made by comparison with the available data on coordinated pyridine ring proton resonances $^{138-141}$ as well as the spectra of Fe(II) and Ni(II) bis-complexes of closely similar tridentate ligands. 132,133 This result again demonstrates that as that in $[\text{Co}(\text{Me}_2\text{pp})\text{Cl}_2]$ the two heterocyclic rings are communicating electronically through the nickel(II) ion.

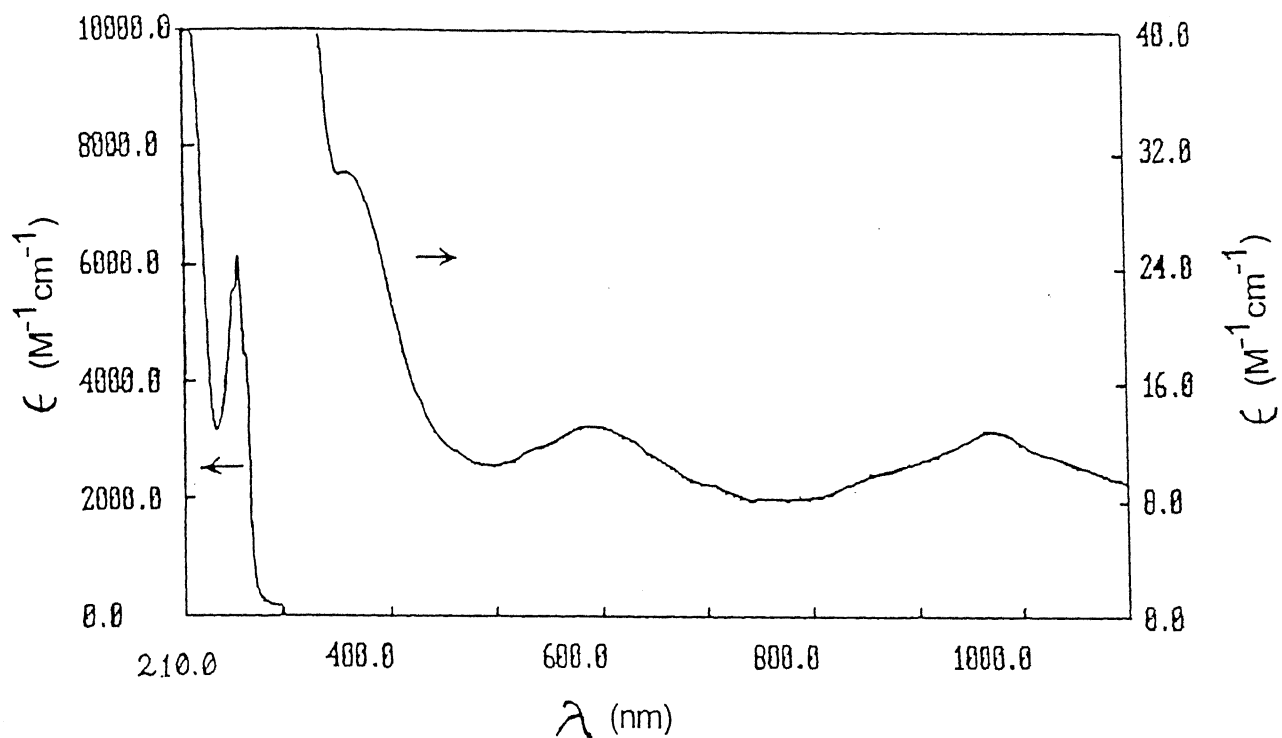


Figure II. 21 Electronic Spectrum of $[\text{Ni}(\text{H}_2\text{pp})_2\text{Cl}_2] \cdot 4\text{H}_2\text{O}$ in MeOH

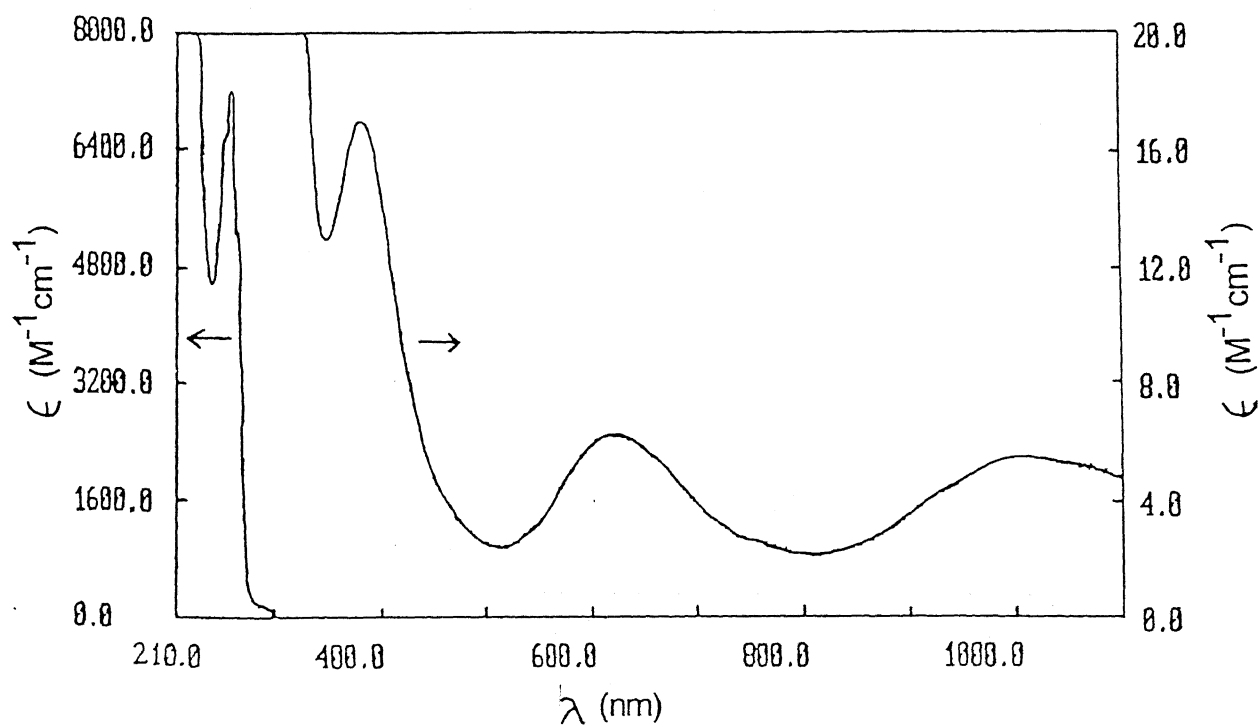


Figure II. 22 Electronic Spectrum of $[\text{Ni}(\text{Me}_2\text{pp})_2\text{Cl}_2] \cdot 2\text{H}_2\text{O}$ in MeOH

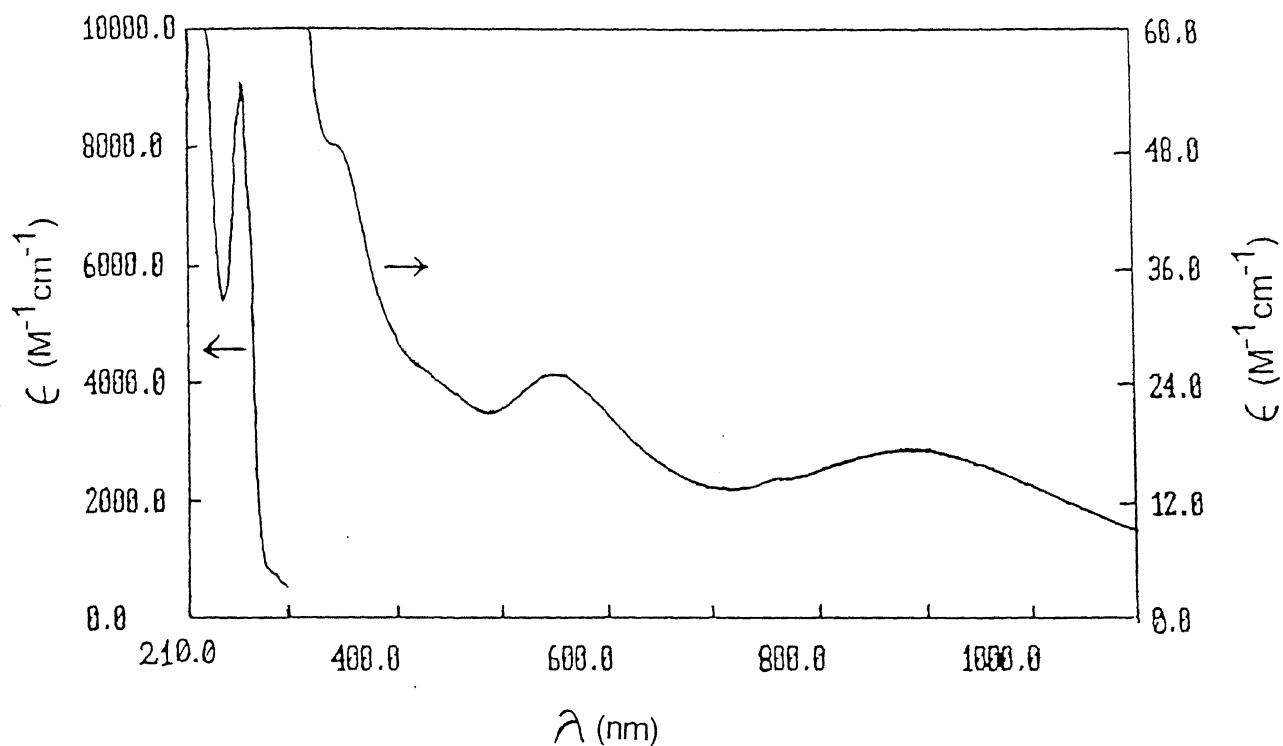


Figure II. 23 Electronic Spectrum of $[\text{Ni}(\text{H}_2\text{pp}')_3](\text{ClO}_4)_2 \cdot \text{H}_2\text{O}$ in MeCN

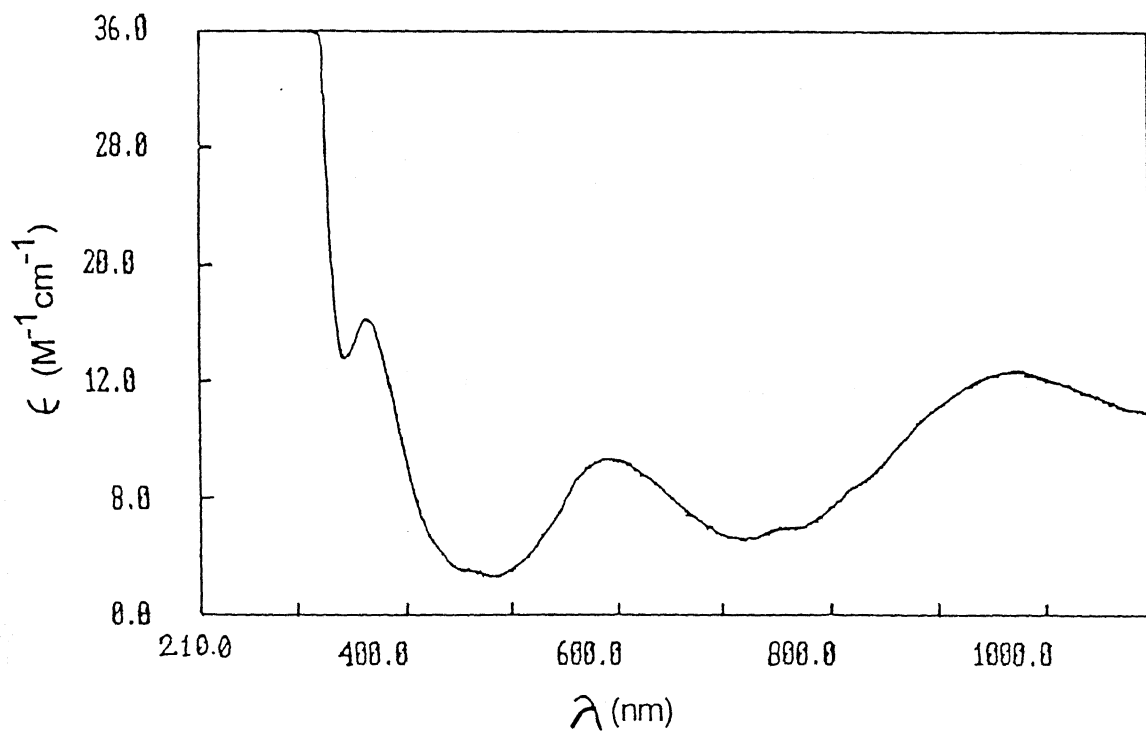


Figure II. 24 Electronic Spectrum of $[\text{Ni}(\text{H}_2\text{pp}')_3](\text{ClO}_4)_2 \cdot \text{H}_2\text{O}$ in MeOH

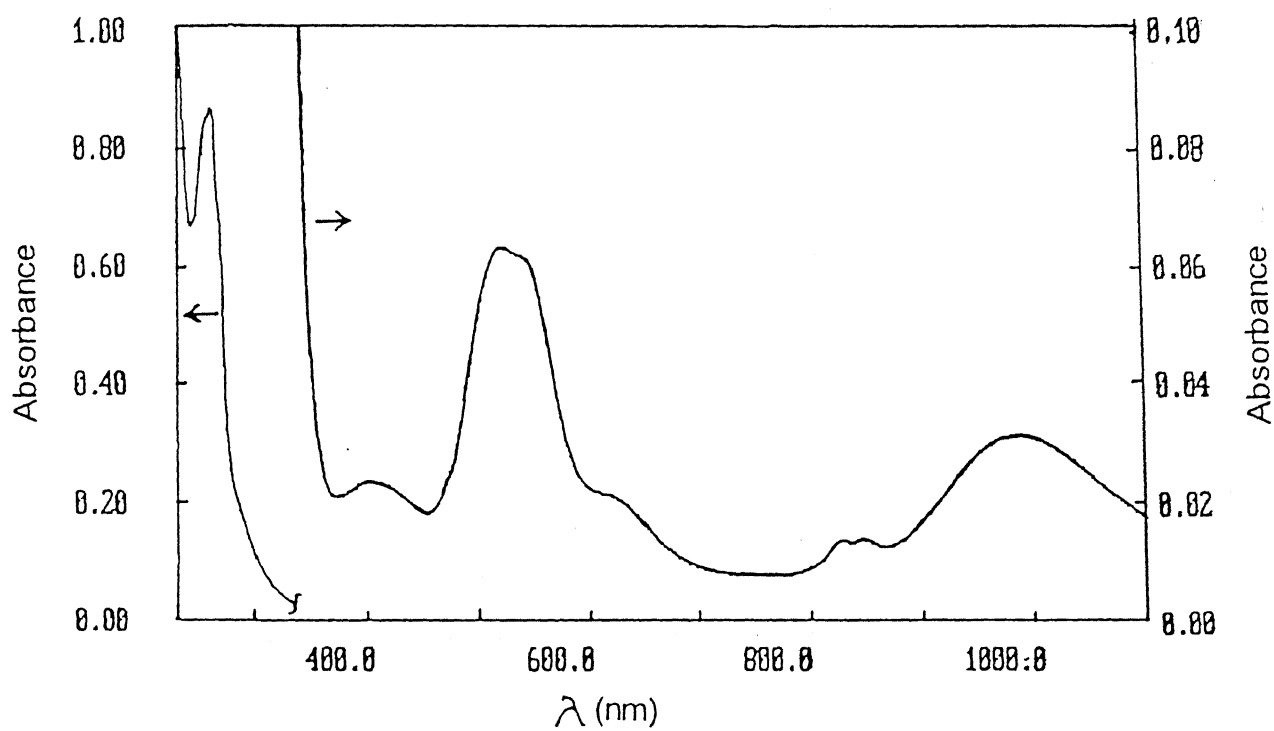


Figure II. 25 Electronic Spectrum of $[\text{Ni}(\text{Me}_2\text{pp})_2\text{Cl}_2] \cdot 2\text{H}_2\text{O}$ in CH_2Cl_2

Table II.9a Visible Spectral Data for the Nickel(II) Complexes in MeOH at 298 K

Complex	${}^3T_{2g} < \text{---} {}^3A_{2g}$		${}^3T_{1g}(F) < \text{---} {}^3A_{2g}$		${}^3T_{1g}(P) < \text{---} {}^3A_{2g}$	
	$\lambda, \text{ nm } \epsilon, \text{ M}^{-1}\text{cm}^{-1}$		$\lambda, \text{ nm } \epsilon, \text{ M}^{-1}\text{cm}^{-1}$		$\lambda, \text{ nm } \epsilon, \text{ M}^{-1}\text{cm}^{-1}$	
$[\text{Ni}(\text{H}_2\text{pp})_2]^{2-}$ $\text{Cl}_2] \cdot 4\text{H}_2\text{O}$	972	13	589	13	362	30
$[\text{Ni}(\text{Me}_2\text{pp})_2]^{2-}$ $\text{Cl}_2] \cdot 2\text{H}_2\text{O}$	1005	6	620	7	385	17
$[\text{Ni}(\text{H}_2\text{pp})_3]^{-}$ $(\text{ClO}_4)_2 \cdot \text{H}_2\text{O}$	974	17	591	11	366	21

Table II.9b Visible Spectral Data for the Nickel(II) Tris-Complex in MeOH at 298 K

Complex	${}^3T_{1g}(F) < \text{---} {}^3A_{2g}$		$D_q, \text{ cm}^{-1}$	$B, \text{ cm}^{-1}$
	$\lambda, \text{ nm}$			
	Expt.	Calcd.		
$[\text{Ni}(\text{H}_2\text{pp})_3]^-$ $(\text{ClO}_4)_2 \cdot \text{H}_2\text{O}$	366	342	1026.7	1027.4

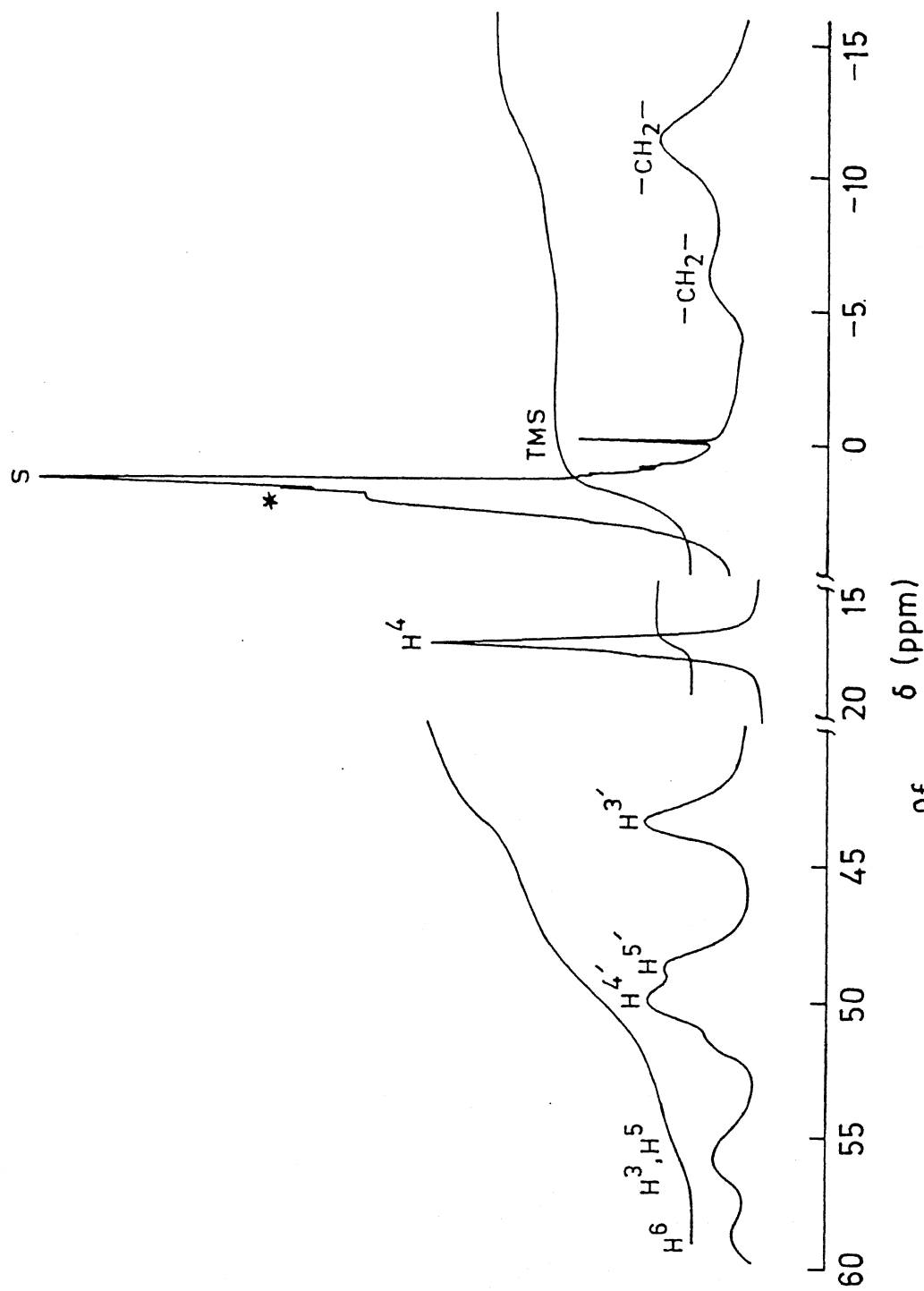


Figure 11.26 400 MHz ^1H NMR Spectrum of $[\text{Ni}(\text{H}_2\text{pp})_3](\text{ClO}_4)_2 \cdot 2\text{H}_2\text{O}$ in CD_3CN (Solvent and Water Peaks Marked by S and * Respectively)

II.7 Concluding Remarks

The salient features of the work described in this chapter are as follows:

(i) Synthesis and characterization of a new class of complexes having 1:1, 1:2, and 1:3 metal-to-ligand stoichiometries using a bidentate unsubstituted (H_2pp) and 1:1, 1:2 metal-to-ligand ratios using a bidentate substituted ligand (Me_2pp) have been achieved using Co(II) and Ni(II) as metal ions. Differences in the behavior of H_2pp and Me_2pp ligands must be due to the effect of methyl substituents at 3- and 5-positions of pyrazole ring. All the complexes are high-spin and the metal ions are in +2 oxidation state.

(ii) (a) Steric hindrance exerted by the ligand, Me_2pp in the coordination sphere of Co(II) complexes is manifested by the formation of only 1:1 stoichiometric stable complex, $[Co(Me_2pp)Cl_2]$; though $[Co(H_2pp)Cl_2]$ is also formed, it is moisture sensitive i.e. water molecule(s) can enter into the coordination sphere easily to form hexa-coordinated Co(II). Moreover, the former complex is not soluble in MeOH and EtOH whereas the latter complex is soluble in those solvents to form pink colored octahedral species.

To release the steric strain probably due to the presence of two ligands and two chloride ions, the complex $[Co(H_2pp)_2Cl_2] \cdot 4H_2O$ liberates chloride(s) in MeOH solution.

Due to steric reason tris-Co(II) complex of Me_2pp could not be prepared readily.

(b) Similarly, Ni(II)-tris-complex of Me_2pp could not

be prepared readily.

(iii) The predominance of steric over electronic is manifested by the steric barrier to the close approach of the Ni(II) to the donor atoms which causes an effective reduction in the field strength experienced by the metal and in the distortions in the coordination octahedron. This is revealed from the absorption spectral studies of Ni(II) complexes (Tables II.9a and II.9b).

(iv) ^1H NMR spectra of $[\text{Co}(\text{Me}_2\text{pp})\text{Cl}_2]$ and $[\text{Ni}(\text{H}_2\text{pp})_3](\text{ClO}_4)_2 \cdot \text{H}_2\text{O}$ suggest that the two heterocyclic rings are communicating electronically through Co(II) and Ni(II) respectively.

(v) Single-crystal X-ray analysis confirms the structure of $[\text{Co}(\text{Me}_2\text{pp})\text{Cl}_2]$ and $[\text{Co}(\text{H}_2\text{pp})_2\text{Cl}_2] \cdot 4\text{H}_2\text{O}$.

(vi) Four coordinate chloro-complexes of Co(II) act as very good oxidation catalysts for various types of organic substrates. This is an excellent achievement in this chapter.

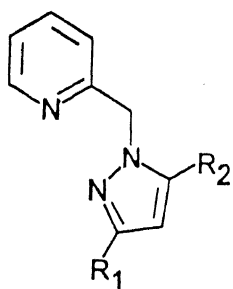
CHAPTER III

Cu(II) Complexes of Bidentate Pyrazolylmethylpyridine Ligands: Synthesis, Structure, and Redox Properties

In chapter II the effect of methyl substituents at the 3- and 5- positions of pyrazole rings of the pyrazolylmethylpyridine ligands H_2pp and Me_2pp has been explored on the formation of 1:1, 1:2, and 1:3 (metal-to-ligand ratio) complexes of Co(II) and Ni(II) complexes. With use of $Co(R_2pp)Cl_2$ complexes catalytic oxidation chemistry has also been explored.

The work presented in this chapter stems from the following observations:

(i) Investigations of the coordination chemistry of Cu(II) using nitrogen donor ligands gain impetus from their relevance to biological systems.¹⁴²⁻¹⁴⁴ Using a binucleating ligand providing two pyridyl nitrogen and an aliphatic nitrogen coordination to each Cu center, Karlin et al. demonstrated aromatic ring hydroxylation in their elegant work to model tyrosinase activity.¹⁴²⁻¹⁴⁴ Sorrell and coworkers, observed^{145,146} marked variations in the Cu(I)-dioxygen reactivity when substituting pyrazole for pyridine, partially or fully, as donor sites. The exact factors that account for the different reactivities are still not very clear.



$R_1 = R_2 = H$, H_2 bp

$R_1 = R_2 = Me$, Me_2 bp

(ii) Studies of structurally characterized mononuclear Cu(II) complexes having various degrees of nitrogen coordination using ligands of biological relevance are of great interest.¹⁴⁷⁻¹⁶¹ Such studies provide an opportunity to systematically identify the effect of ligand electronic and/or imposed steric factors responsible for providing subtle stereochemical preferences for a particular molecular structure, associated electronic structure, and reactivities.

Following these observations¹⁴²⁻¹⁶¹ and our recent activity¹⁶² demonstrating aromatic ring hydroxylation using a binucleating ligand providing a pyridyl nitrogen and an aliphatic nitrogen coordination to each Cu center, we have investigated Cu chemistry using chelating ligands having various combinations of both pyridyl and pyrazole donors in a given ligand system. Interestingly, such studies are rare.^{149,150} Additionally, mononuclear Cu complexes of nitrogen donor ligands with a substrate binding (nitrite ion) site is of current interest due to their relevance in copper containing nitrite reductases.

It has long been recognized that there are many subtly balanced factors^{163,164} influencing the formation of the highly complicated structures of Cu(II) complexes.¹⁶⁵ It is likely that frontier orbitals play an important role in determining the stereochemistry of complexes. Particularly, the geometry of complexes and the conformation of ligands are very sensitive to the energy levels and the order of d-orbitals.

Specifically, in this chapter (i) the effect of methyl substituents of pyrazole rings in H₂pp and Me₂pp on grossly Cu^{II}N₄ and Cu^{II}N₄X (X = Me₂pp, Cl⁻, SCN⁻, and N₃⁻) coordination spheres,

and (ii) structural/functional modeling for the substrate binding center of the active site of copper containing nitrite reductases have been described.

III.1 Experimental Section

III.1.1 Solvents and Reagents

Solvents and reagents were obtained from commercial sources and used without further purification unless otherwise stated. Details of solvent purification are described in chapter II (Section II.1.1).

III.1.2 Measurements

Details of spectroscopic measurements are given in chapter II (Section II.1.2). EPR simulations were carried out using a FORTRAN romb¹⁶⁶ program on HP 9000 series 486 PC.

III.2 Syntheses of Ligands

III.2.1 R₂pp (R = H, H₂pp; R = Me, Me₂pp)

Syntheses of these ligands are already described in chapter II.

III.3 Syntheses of complexes

III.3.1 [Cu^{II}(Me₂pp)₃](ClO₄)₂ (1) and [Cu^{II}(Me₂pp)₂](ClO₄)₂ · H₂O (2).

To an ethanolic solution (3 mL) of [Cu(H₂O)₆](ClO₄)₂ (0.10 g, 0.27 mmol) was added slowly while stirring an ethanolic solution (3 mL) of Me₂pp (0.10 g, 0.54 mmol). Within 5 min of stirring a green complex (1) started to precipitate out. Immediately the complex 2 was filtered and washed with ethanol and

dried under vacuo (Yield 42 mg). On standing for a further 5 min. a violet microcrystalline precipitate (2) started to appear. The precipitation is usually completed within 12 h. The solid thus obtained was filtered, washed thoroughly with ethanol and finally dried in vacuo (Yield 90 mg). The complex 2 was recrystallized from MeCN/EtOH to remove little amount of the green product (1).

III.3.2 $[\text{Cu}^{\text{II}}(\text{H}_2\text{pp})_2](\text{ClO}_4)_2 \cdot \text{H}_2\text{O}$ (2a)

This complex was synthesized following a similar procedure as that of 2, while using H_2pp in place of Me_2pp . Here only one complex (bluish-violet) is formed. (Yield 80 %).

III.3.3 $[\text{Cu}(\text{Me}_2\text{pp})_2(\text{NO}_2)](\text{ClO}_4)$ (3)

The violet complex 2, $[\text{Cu}(\text{Me}_2\text{pp})_2](\text{ClO}_4)_2 \cdot \text{H}_2\text{O}$ (0.10 g, 0.153 mmol) was dissolved in MeCN (8 mL) and an aqueous solution (2 mL) of NaNO_2 (.011 g, 0.153 mmol) was added to it dropwise while stirring. The reaction mixture which turned green was allowed to stand for three days in air. Green crystals thus obtained was washed thoroughly with water and dried in Abder Halden. Yield (70 mg, 78%). X-ray quality single crystals were obtained by slow evaporation of an MeCN/ H_2O (3:1) solution at room temperature.

The complex 3 can also be prepared from 1 following a similar method^{as} described above.

III.3.4 $[\text{Cu}(\text{Me}_2\text{pp})_2(\text{X})]\text{ClO}_4$ [$\text{X} = \text{Cl}^-$ (4), SCN^- (5), N_3^- (6)]

Complexes 4, 5 and 6 were synthesized in the same way as that of complex 3. The cations of the inorganic salts were tetraethylammonium, potassium and sodium respectively. Yields were 98%, 95% and 92% respectively.

Single crystals of X-ray quality were obtained by slow

evaporation of MeCN/H₂O (3:1) or MeCN/EtOH (3:1) solution for **4** and **5** respectively.

III.3.5 Preparation of Complexes **3**, **5** and **6** from **4**

An aqueous solution (1 mL) of NaNO₂ (0.0024 g, 0.035 mmol) was dropwise to an MeCN solution (3 mL) of **4** (0.02 g, 0.035 mmol) while stirring. The reaction mixture turned deep green which was allowed to stand for 2 days in air. Green crystals thus obtained was washed thoroughly with water and dried in air. Yield (20 mg, 98%)

Complexes **5** and **6** were prepared from **4** following a similar procedure as described above.

III.4 X-ray Data Collection and Structure Solution and Refinement

Crystals were mounted on glass fiber. Preliminary examination and data collection were performed with Mo K_α radiation ($\lambda = 0.71093 \text{ \AA}$) on an Enraf-Nonius CAD4 computer controlled diffractometer equipped with a graphite monochromator. Data at 293 K were collected for [Cu(Me₂pp)₂(NO₂)](ClO₄) at University of Louisville, Louisville, Kentucky and for [Cu(Me₂pp)₂(SCN)](ClO₄) at this Department of Chemistry, Indian Institute of Technology, Kanpur.

Cell constants and the orientation matrix for data collection were obtained from least-squares refinement, using the setting angles of 25 reflections in the range $30 < 2\theta < 36$ for [Cu(Me₂ppz)₂(NO₂)](ClO₄) and $12 < 2\theta < 20$ for [Cu(Me₂ppz)₂(SCN)](ClO₄). Experimental details of crystal data, intensity measurements, structure solution, and refinement were given in Table

Table III.1

EXPERIMENTAL DETAILS

A. Crystal Data

Empirical Formula	$\text{CuClO}_6\text{N}_7\text{C}_{22}\text{H}_{26}$
Formula Weight	583.49
Crystal Color, Habit	green, plate
Crystal Dimensions	0.090 X 0.410 X 0.490
Crystal System	monoclinic
Lattice Type	P
No. of Reflections Used for Unit Cell Determination (2θ range)	25 ($30.0 - 36.0^\circ$)
Omega Scan Peak Width at Half-height	0.50°
Lattice Parameters	$a = 13.186(5) \text{ \AA}$ $b = 20.824(7) \text{ \AA}$ $c = 9.677(4) \text{ \AA}$ $\beta = 90.19(3)^\circ$
	$V = 2657(1) \text{ \AA}^3$
Space Group	$P2_1/c$ (#14)
Z value	4
D_{calc}	1.458 g/cm^3
F_{000}	1204.00
$\mu(\text{MoK}\alpha)$	9.72 cm^{-1}

B. Intensity Measurements

Diffractometer	Cad4Mach
Radiation	$\text{MoK}\alpha$ ($\lambda = 0.71093 \text{ \AA}$) graphite monochromated

Attenuator	Zr foil (factor = 22.37)
Take-off Angle	2.8°
Detector Aperture	2.0 - 2.5 mm horizontal 2.0 mm vertical
Crystal to Detector Distance	21 mm
Temperature	22.0°C
Scan Type	ω -2 θ
Scan Rate	1.0°/min (in omega) (1 rescans)
Scan Width	$(0.80 + 0.35 \tan \theta)^\circ$
$2\theta_{max}$	50.0°
No. of Reflections Measured	Total: 5123 Unique: 4848 ($R_{int} = 3.46$)
Corrections	Lorentz-polarization Absorption (trans. factors: 0.8597 - 1.2079)

C. Structure Solution and Refinement

Structure Solution	Patterson Methods (DIRDIF92 PATTY)
Refinement	Full-matrix least-squares
Function Minimized	$\Sigma w(Fo - Fc)^2$
Least Squares Weights	$\frac{1}{\sigma^2(Fo)} = \frac{4Fo^2}{\sigma^2(Fo^2)}$
p-factor	0.014
Anomalous Dispersion	All non-hydrogen atoms
No. Observations ($I > 3.00\sigma(I)$)	3041
No. Variables	346
Reflection/Parameter Ratio	8.79
Residuals: R; Rw	0.052 ; 0.052
Goodness of Fit Indicator	2.32

Max Shift/Error in Final Cycle	0.02
Maximum peak in Final Diff. Map	$0.46 \text{ e}^-/\text{\AA}^3$
Minimum peak in Final Diff. Map	$-0.55 \text{ e}^-/\text{\AA}^3$

Table III.2

EXPERIMENTAL DETAILS

A. CRYSTAL DATA

Empirical Formula	$\text{CuClSO}_4\text{N}_7\text{C}_{23}\text{H}_{26}$
Formula Weight	596
Crystal Colour, Habit	Deep green, parallelopiped
Crystal dimensions (mm ³)	0.4 x 0.3 x 0.3
Crystal System	Monoclinic
No. of reflections used for unit cell determination (2 θ range)	25 reflections (12<2 θ <20)
Lattice parameters	a= 9.465(3), b= 18.364(7) _O c= 15.496(9) _O Å, $\alpha = \beta = \gamma = 90.00^\circ$ $\beta = 102.7(4)^\circ$ V= 2627.49(2.11) _O Å ³ P ₂ ₁ (No.4)
Space Group	
Z value	2 (celmol =2)
D _{calc} (g cm ⁻³)	1.506
F _{ooo}	1227.7

B. INTENSITY MEASUREMENTS

Diffractometer	Cad4Mach
Radiation	MoK α ($\lambda = 0.71073\text{\AA}$)
Temperature	293K
Scan Type	θ -2 θ
Scan Rate	variable
Scan Width	1.0 + 0.35tan θ
2 θ range(deg)	2 - 50
No. of reflections measured (2<2 θ <50)	5220
No. of unique reflections	4776
Corrections	L _p

C. STRUCTURE SOLUTION AND REFINEMENT

Structure Solution	Direct Method
Refinement	Full matrix, least ₂ squares
Function minimized	$\sum w(F_o - F_c)^2$
Anomalous dispersion	applied (for non H atoms)
No. of observations (I>2 σ (I))	2660
No. of variables	312
Reflection/Parameter ratio	8.80
Residuals: R; R _w	0.107; 0.096
Goodness of fit indicator	4.025
Max shift/error in final cycle	0.2629 X 10
Avg shift/error in final cycle	0.1926
Maximum ₃ peak in final diff. map(eÅ ⁻³)	2.04 near Cl(2a)
Minimum ₃ peak in final diff. map(eÅ ⁻³)	-1.33

III.1 and III.2 respectively. As a check on crystal and electronic stability three representative reflections were measured every 97 reflections. The intensities of these standards remained constant within experimental error throughout data collection. Intensities were corrected for Lorentz and polarization effect. Anomalous dispersion was applied for all non-hydrogen atoms. Analytical absorption correction was applied to the data. The structures were refined by a full-matrix least-squares method. All the non-hydrogen atoms with the exception of disordered atoms having occupancies less than 50%, were refined anisotropically. Hydrogen atoms were included but not refined. The function minimized was $\sum w(|F_o| - |F_c|)^2$ where F_o and F_c are the observed and calculated structure amplitudes, and the weight, w , is $4F_o^2/\sigma^2(F_o^2)$. Structure $[\text{Cu}(\text{Me}_2\text{pp})_2(\text{NO}_2)](\text{ClO}_4)$ was solved by heavy-atom Patterson methods¹⁶⁷ using the TEXSAN¹⁶⁸ software package and expanded using Fourier techniques.¹⁶⁹⁻¹⁷² All calculations for the complex $[\text{Cu}(\text{Me}_2\text{pp})_2(\text{SCN})](\text{ClO}_4)$ were performed using the Xtal 3.2 package¹²⁷ installed on a PC 486 computer. The final weighted R factors were 0.052, 0.107 and the unweighted R_w factors were 0.052, 0.11 for $[\text{Cu}(\text{Me}_2\text{pp})_2(\text{NO}_2)](\text{ClO}_4)$ and $[\text{Cu}(\text{Me}_2\text{pp})_2(\text{SCN})](\text{ClO}_4)$ respectively.

III.5 Results and Discussion

III.5.1 Syntheses and Preliminary Characterization

A. Bis-ligated Cu(II) Complexes

The bis-ligated Cu(II) complexes (violet complexes as

well as the green complex) were readily obtained when ethanolic solutions of the ligands and copper(II) perchlorate hexahydrate were mixed. Microanalyses of all the Cu(II) complexes confirm to the said formulation (Table III.3).

For complex 1 the presence of $\nu(\text{ClO}_4^-)$ bands at ~ 1100 and $\sim 620 \text{ cm}^{-1}$ and absence of $\nu(\text{OH})$ band in its IR spectrum suggest the presence of perchlorate as counter anion and absence of water as solvent of crystallization (Figure III.1). Both the complexes 2 and 2a display $\nu(\text{OH})$ band at $\sim 3400 \text{ cm}^{-1}$ and $\nu(\text{ClO}_4^-)$ bands at ~ 1100 and $\sim 620 \text{ cm}^{-1}$ in their IR spectra (Figure III.2 and III.3) indicate the presence of perchlorate counter anions and water as solvent of crystallization. For both the complexes the perchlorate bands are split (in nujol mull) suggesting the perchlorate coordination (vide infra). Electrical conductivity measurements in MeCN show that complexes 1, 2, and 2a are 1:2 electrolyte.^{129a} The IR spectral feature of 2 and 2a are very similar suggesting that these two complexes have similar solid state geometry. The violet complexes of expected composition $[\text{Cu}(\text{R}_2\text{pp})_2](\text{ClO}_4)_2 \cdot \text{H}_2\text{O}$ (2 and 2a) are soluble in MeCN, DMF, and H_2O and moderately soluble in MeNO_2 and acetone giving rise to blue solutions. The green complex of expected composition $[\text{Cu}(\text{Me}_2\text{pp})_3](\text{ClO}_4)_2$ (1) is soluble in MeOH, EtOH, CHCl_3 , and CH_2Cl_2 to form green solutions while it forms bluish green solutions in MeCN and DMF. This complex is also sparingly soluble in H_2O to form blue solution. Bluish coloration of the green complex 1 in MeCN, DMF and H_2O suggest (vide infra) dissociation of axially ligated one of the bidentate ligands which is acting as a monodentate ligand.

Table III.3: Microanalytical data of Copper(II) Complexes

Complexes	Empirical Formula	Analysis ^a		
		% C	% H	% N
[Cu(Me ₂ pp) ₃] (ClO ₄) ₂	C ₃₃ H ₃₉ Cl ₂ N ₉ O ₈ Cu	47.09 (47.84)	4.04 (4.82)	14.03 (14.94)
[Cu(Me ₂ pp) ₂] (ClO ₄) ₂ ·H ₂ O	C ₂₂ H ₂₈ Cl ₂ N ₆ O ₉ Cu	40.16 (40.34)	4.18 (4.28)	12.72 (12.84)
[Cu(H ₂ pp) ₂] (ClO ₄) ₂ ·H ₂ O	C ₁₈ H ₂₀ Cl ₂ N ₆ Cu	36.17 (36.09)	3.43 (3.34)	14.13 (14.04)
[Cu(Me ₂ pp) ₂ - (Cl)](ClO ₄)	C ₂₂ H ₂₆ Cl ₂ N ₆ O ₄ Cu	46.19 (46.12)	4.48 (4.54)	14.62 (14.67)
[Cu(Me ₂ pp) ₂ - (NO ₂)](ClO ₄)	C ₂₂ H ₂₆ ClN ₇ O ₆ Cu	44.90 (45.28)	4.30 (4.46)	16.72 (16.81)
[Cu(Me ₂ pp) ₂ - (SCN)](ClO ₄)	C ₂₃ H ₂₆ SCl ₂ N ₇ O ₄ Cu	46.46 (46.39)	4.43 (4.37)	16.52 (16.47)
[Cu(Me ₂ pp) ₂ - (N ₃)](ClO ₄)	C ₂₂ H ₂₆ ClN ₉ O ₄ Cu	45.56 (45.60)	4.42 (4.49)	21.71 (21.76)

^aCalculated values in parentheses.

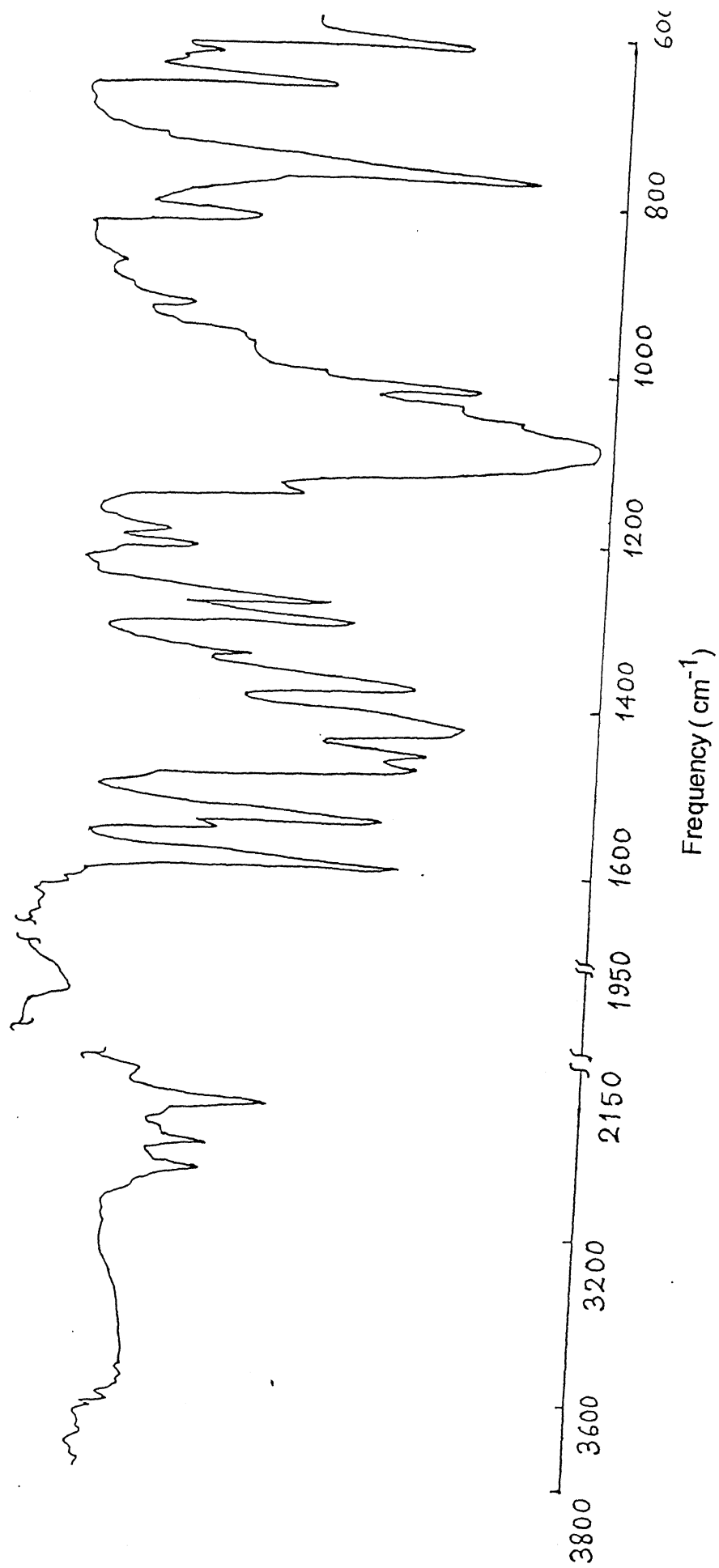


Figure III.1 IR Spectrum of $[\text{Cu}(\text{Me}_2\text{ppz})_3](\text{ClO}_4)$

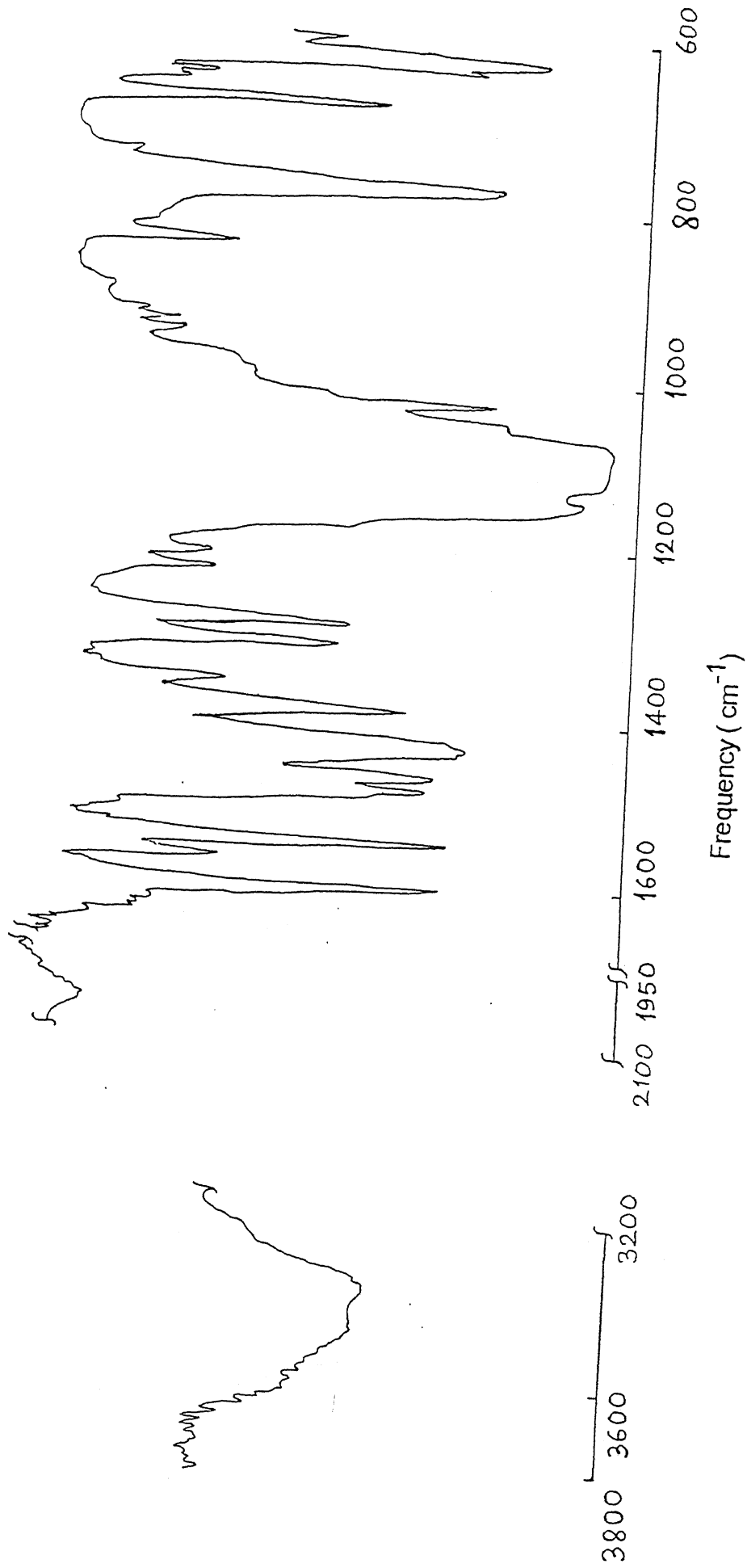


Figure III.2 IR Spectrum of $[\text{Cu}(\text{Me}_2\text{pp})_2](\text{ClO}_4)_2 \cdot \text{H}_2\text{O}$ in nujol mull

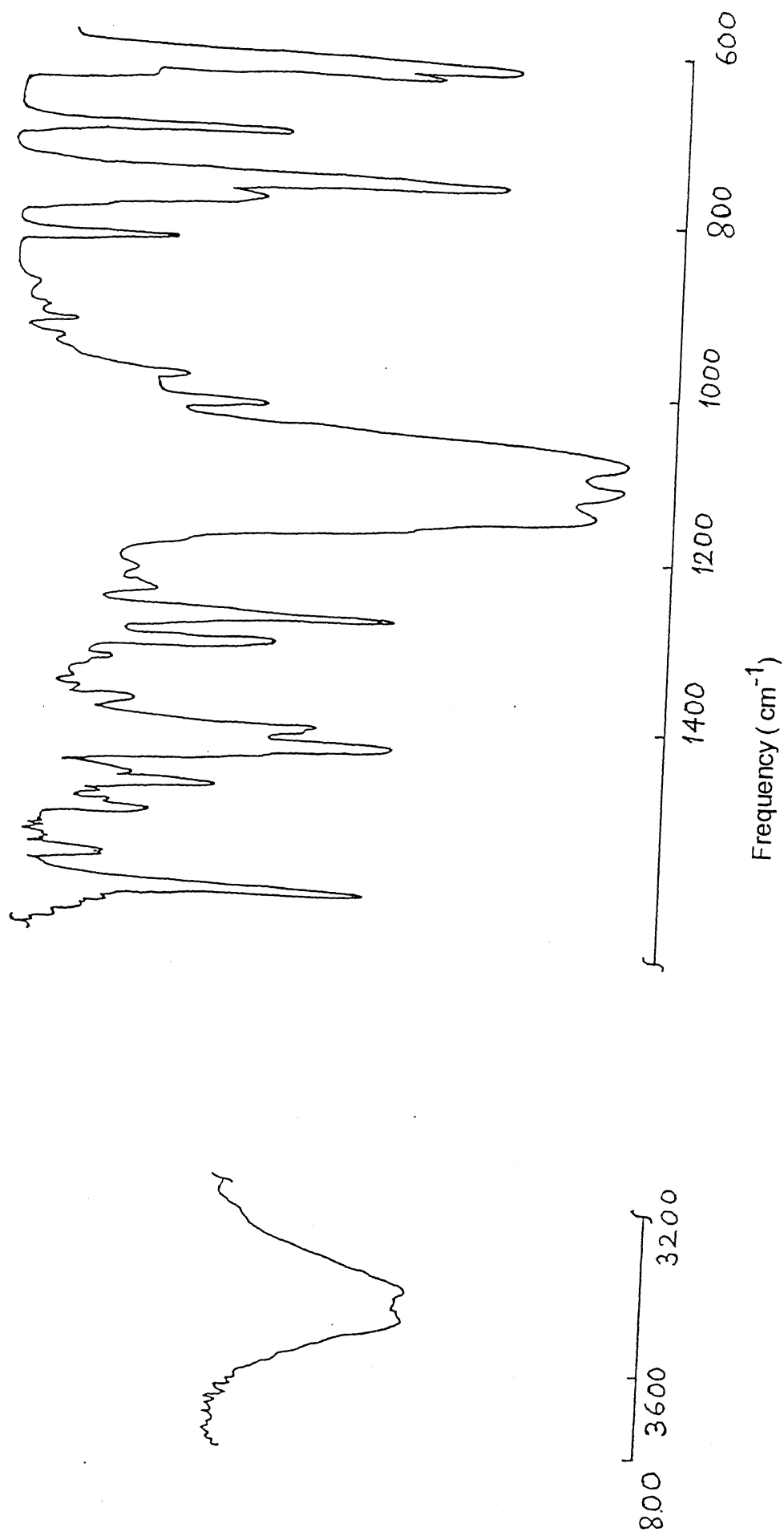


Figure III.3 IR Spectrum of $[\text{Cu}(\text{H}_2\text{pp})_2](\text{ClO}_4)_2 \cdot \text{H}_2\text{O}$ in nujol mull

Solution-state magnetic susceptibility measurements by Evans' method indicate (Table III.4) that the Cu(II) complexes, 2, and 2a are mononuclear since μ_{eff} values are in the range 1.84-1.87. Solid state μ_{eff} values are very close to that of the expected range (Table III.4).¹⁶⁵

B. Axially Ligated Five-Coordinate Copper(II) Complexes

An interesting point to be noted that whenever KBr pellets of 2 (violet complex) were made it turned to green. This observation indicate that 2 reacts with Br^- in the solid state! Thus five-coordinate complexes with $\text{Cu}^{\text{II}}\text{N}_4(\text{X})$ coordination spheres were prepared in aqueous MeCN.

The Cu(II) complexes having $\text{Cu}^{\text{II}}\text{N}_4\text{X}$ coordination sphere (X-ray structures of 3^{and 5}, Figures III.28 and III.29 were synthesized in a straightforward way by mixing appropriate salts of X^- in aqueous MeCN solutions of $[\text{Cu}(\text{Me}_2\text{pp})_2](\text{ClO}_4)_2 \cdot \text{H}_2\text{O}$. It is to be noted that the complex $[\text{Cu}(\text{Me}_2\text{pp})_3](\text{ClO}_4)_2$ (1) was obtained during the synthesis of $[\text{Cu}(\text{Me}_2\text{pp})_2](\text{ClO}_4)_2 \cdot \text{H}_2\text{O}$ (2).

All the complexes show bands in the range 1075-1090 cm^{-1} and at 620 cm^{-1} confirming the presence of perchlorate counter anions (Figures III.4, III.5, and III.6). The absence of $\nu(\text{OH})$ band precludes the presence of water as solvent of crystallization. In the IR spectrum of 3 (Figure III.4) presence of coordinated NO_2^- could not be identified as severe overlapping with ligand bands occur; however, an enhancement of bands in the expected range^{95g} (1210, 1305, 1360 and 1462 cm^{-1}) was clearly observed. It is finally confirmed by X-ray structural analysis.

In the IR spectrum of 5 bands at 2105 and 2060 cm^{-1} are

Table III.4 Molar Conductance, Magnetic Moment and Electronic Spectral Data of Copper(II) Complexes in MeCN at 298 K.

Complexes	Λ_M^a ($\Omega^{-1}\text{cm}^2\text{mol}^{-1}$)	$\mu_{\text{eff}}(\text{B.M.})^c$	$\lambda, \text{nm} (\epsilon, \text{M}^{-1}\text{cm}^{-1})$
$[\text{Cu}(\text{Me}_2\text{pp})_3] - (\text{ClO}_4)_2$	295 ^b	1.99	965(sh), 700, 364(sh), 362(sh), 288(sh), 269-(sh), 255 (975 (sh), 710, 370(sh), 263) ^d
$[\text{Cu}(\text{Me}_2\text{pp})_2] - (\text{ClO}_4)_2 \cdot \text{H}_2\text{O}$	286	1.87 (1.87)	950(sh) (25), 602(80) 350(sh) (720), 262(sh) - (1 1250) (975(sh), 635(sh), 505, 364, 273) ^d
$[\text{Cu}(\text{H}_2\text{pp})_2] - (\text{ClO}_4)_2 \cdot \text{H}_2\text{O}$	293	1.84 (1.90)	592(81), 325(sh) (868), 260(1 1300), 256(sh) - (1 1200) (535, 335(sh), 273) ^d
$[\text{Cu}(\text{Me}_2\text{pp})_2 - (\text{Cl})] (\text{ClO}_4)$	198	1.90	980(sh) (92), 710(155), 355(810), 280(sh) - (2 920), 260(8 272) (722, 626(sh), 368(sh), 271) ^d
$[\text{Cu}(\text{Me}_2\text{pp})_2 - (\text{NO}_2)] (\text{ClO}_4)$	142	1.90 (1.85)	975(sh) (195), 655(128), 390(1 100), 260(8 250) (965(sh), 676, 391(sh), 268) ^d
$[\text{Cu}(\text{Me}_2\text{pp})_2 - (\text{SCN})] (\text{ClO}_4)$	154	1.82	950(sh) (50), 690(141), 412(1 090), 54 - (11 470), 224(21 310) (712, 390, 268) ^d

Table III.4 contd.

$[\text{Cu}(\text{Me}_2\text{pp})_2^-$ $(\text{N}_3)](\text{ClO}_4)$	144	1.85	717(366), 425(1 9500), 417(2 355), 254(9 450) (800, 440, 270) ^d
---	-----	------	--

^aExpected range for 1:1 and 1:2 electrolytes in MeCN are 120-160 and 220-300 $\Omega^{-1}\text{cm}^2\text{M}^{-1}$

^bAfter addition of 3 equivalent of Me_2pp value obtained as 286

^cRoom temperature solid state values are in parentheses

^dRoom temperature solid state values are in parentheses

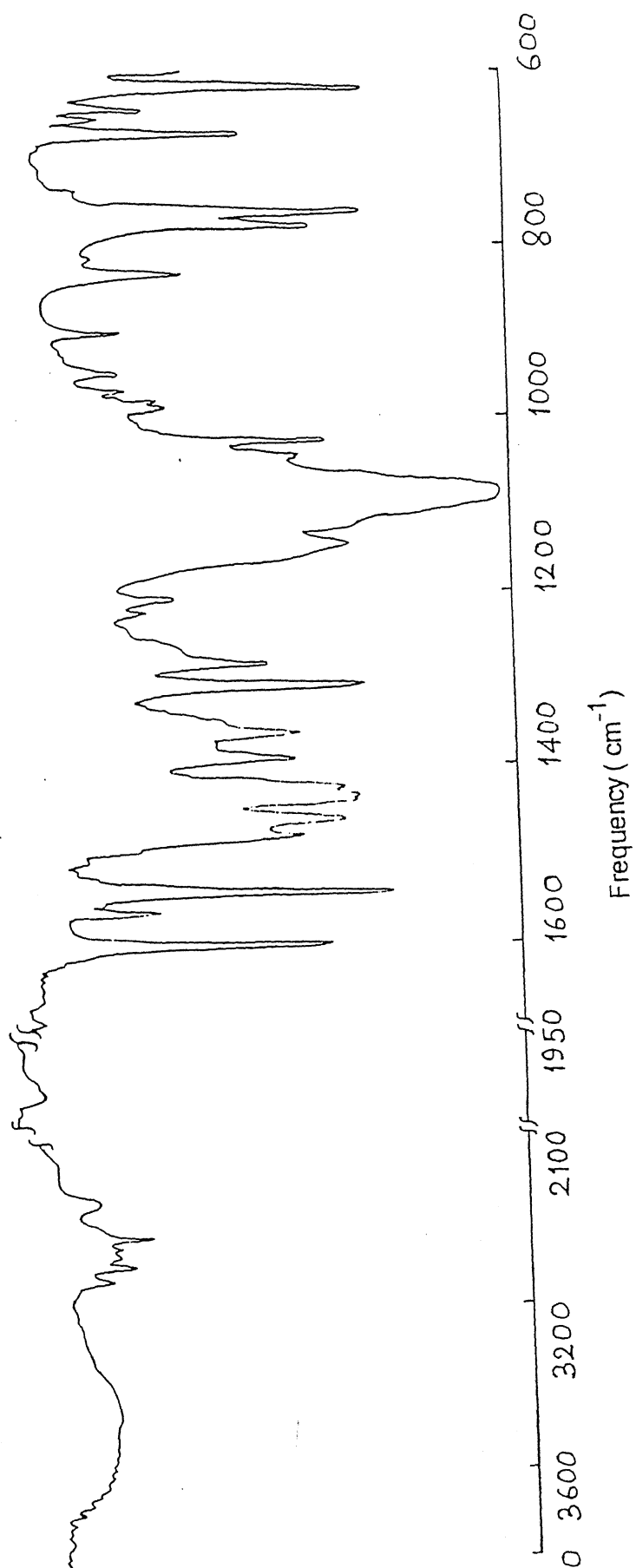


Figure III.4 IR Spectrum of $[\text{Cu}(\text{Me}_2\text{pp})_2(\text{NO}_2)](\text{ClO}_4)$

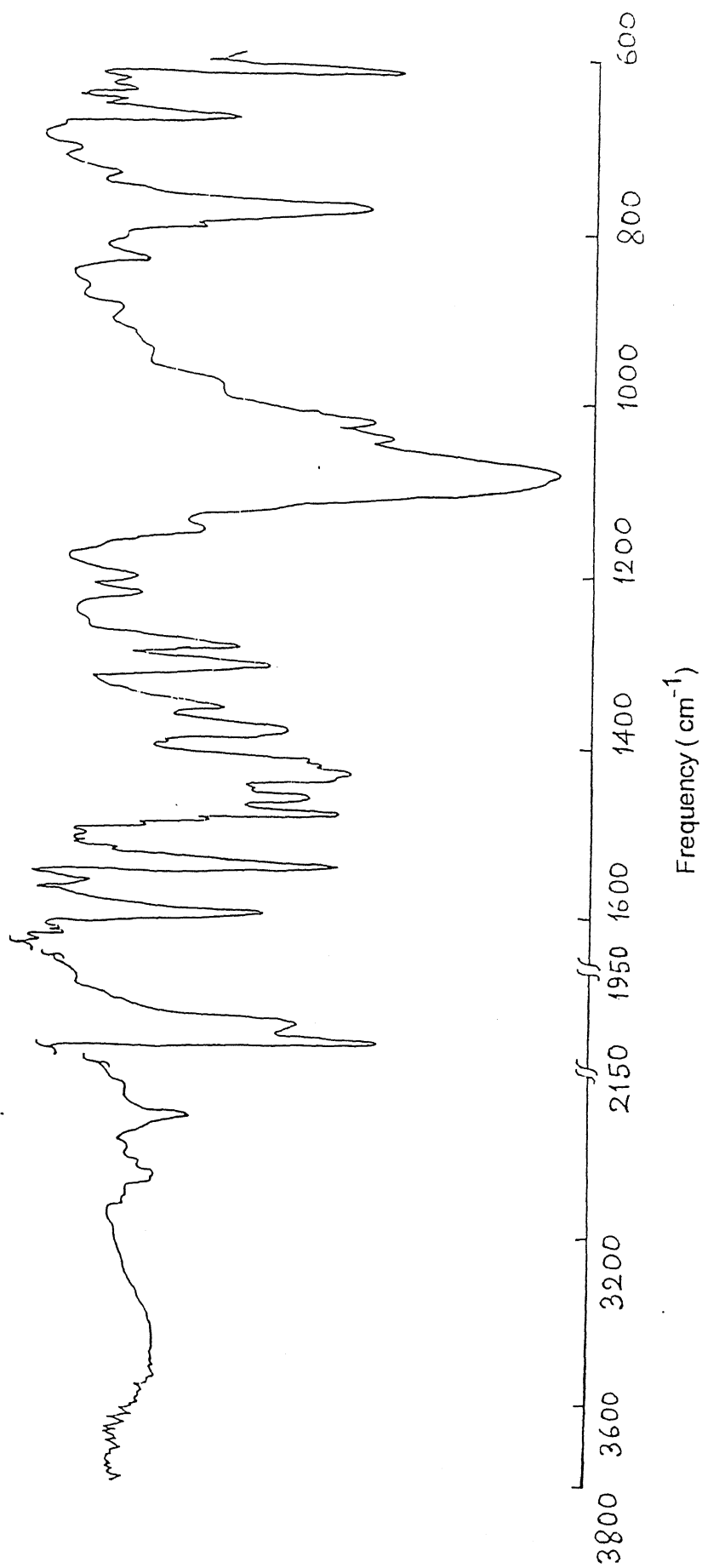


Figure III.5 IR Spectrum of $[\text{Cu}(\text{Me}_2\text{pp})_2(\text{SCN})](\text{ClO}_4)$

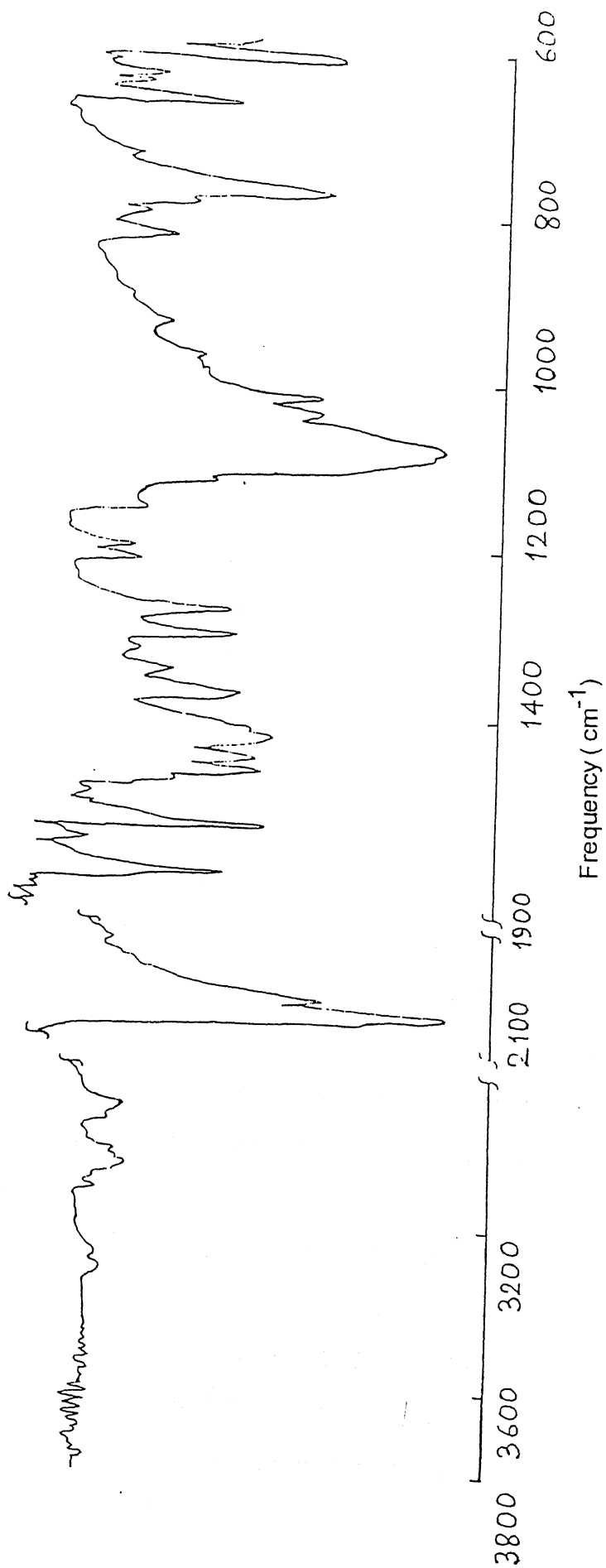


Figure III.6 IR Spectrum of $[\text{Cu}(\text{Me}_2\text{pp})_2(\text{N}_3)](\text{ClO}_4)$

suggestive of bound thiocyanate group (Figure III.5)¹⁷³ For 6 the IR bands at 2042 and 2005 cm^{-1} are indicative of bound azide group (Figure III.6).¹⁷⁴ The IR spectral feature of all these complexes are very simillar indicating that all these five-coordinate complexes have simillar solid state geometry. All the complexes are highly soluble in MeCN, DMF and CH_2Cl_2 and moderately soluble in MeOH to generate green solutions. Molar conductance values of all the complexes in MeCN solution show that these complexes are 1:1 electrolyte^{129a} (Table III.4).

Solution μ_{eff} values of these complexes are in the range 1.82-1.99 (Table III.4) which is expected for mononuclear Cu(II) complexes.¹⁶⁵ The solid state values are very close to the solution state values (Table III.4).

III.5.2 Absorption Spectra

A. Bis-ligated Cu(II) Complexes

The solid state reflectance spectra (in paraffin oil) of $[\text{Cu}(\text{R}_2\text{pp})_2](\text{ClO}_4)_2 \cdot \text{H}_2\text{O}$ (2 and 2a, violet complexes) display a broad band in the visible region (Table III.4; Figure III.7). The band maxima are 505 and 535 nm for 2 and 2a respectively. For 2 an additional ill-defined shoulder at 975 nm is also observed. This is could be due to distortions at the Cu(II) center arising from the steric constraint exerted by the substituted ligand, Me_2pp . For the complex 1 one broad band and a shoulder in the lower energy region is observed (Figure III.8). This is indicative of square pyramidal geometry¹⁶⁵ around Cu(II).

On going from solid to solution state (MeCN) (Table

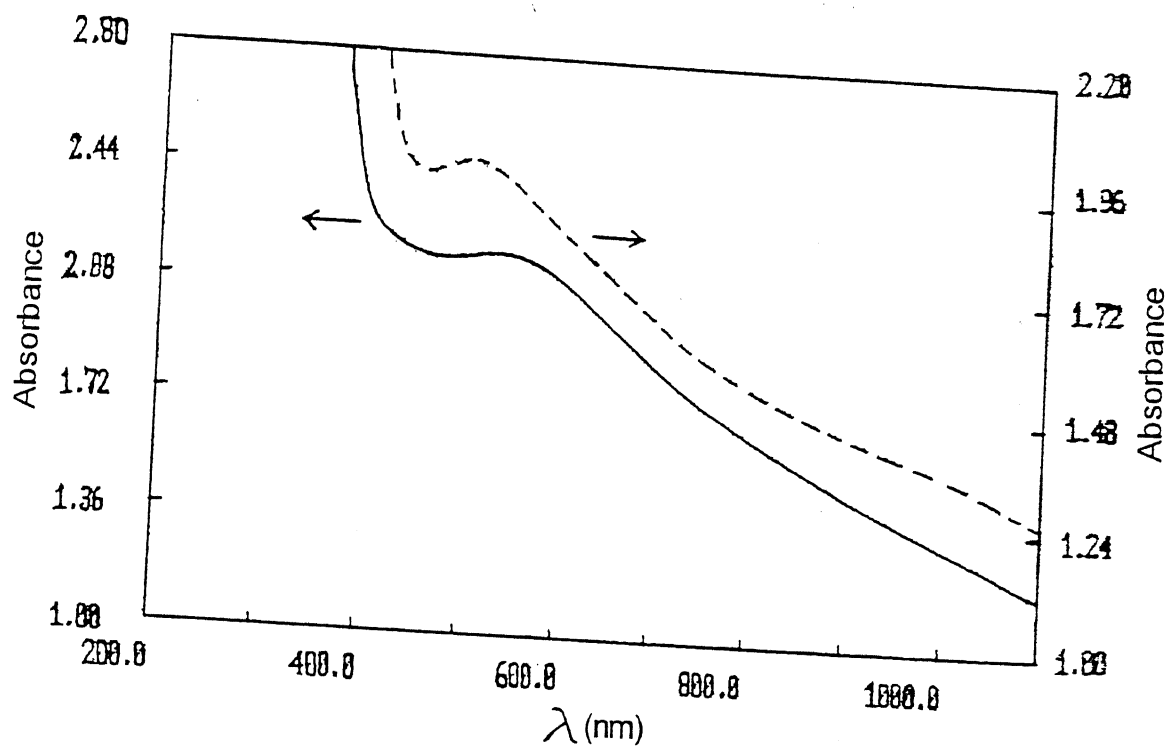


Figure III.7 Electronic Spectra of $[\text{Cu}(\text{H}_2\text{pp})_2](\text{ClO}_4)_2 \cdot \text{H}_2\text{O}$ (—) and $[\text{Cu}(\text{Me}_2\text{pp})_2](\text{ClO}_4)_2 \cdot \text{H}_2\text{O}$ (---) in paraffin oil.

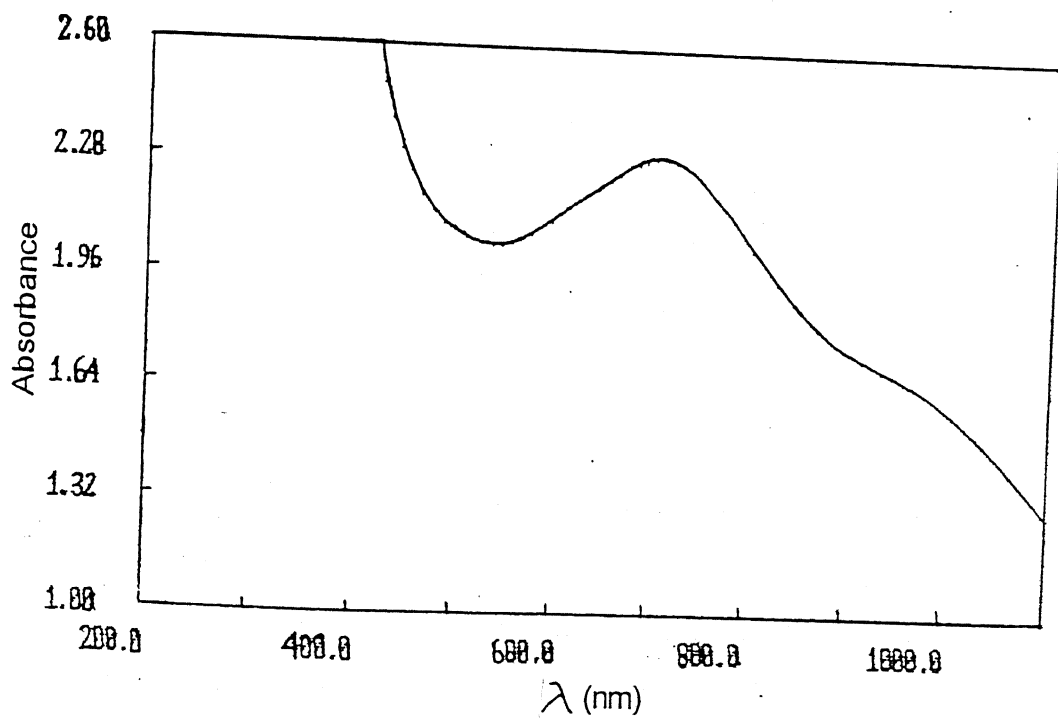


Figure III.8 Electronic Spectrum of $[\text{Cu}(\text{Me}_2\text{pp})_3](\text{ClO}_4)_2$ in paraffin oil

III.4, Figures III.9 and III.10) and also varying the nature of solvents from lower to higher coordinating ability (Table III.5) and in turn a bathochromic effect of the d-d band(s) for the complexes **2** and **2a** was observed. This indicates^{165,175} that the perchlorate groups are weakly bound in the axial positions. Thus these spectra are consistent with the tetragonal environments about the Cu(II) centers.^{165,175}

In MeCN solution $[\text{Cu}(\text{H}_2\text{pp})_2](\text{ClO}_4)_2 \cdot \text{H}_2\text{O}$ shows only one broad band whereas $[\text{Cu}(\text{Me}_2\text{pp})_2](\text{ClO}_4)_2 \cdot \text{H}_2\text{O}$ shows a broad band as well as two shoulders at lower energy in the visible region (Table III.4; Figures III.9 and III.10) indicating increased distortion in the latter case due to methyl substituents at 3- and 5- positions of the pyrazole ring of Me_2pp . For $[\text{Cu}(\text{R}_2\text{pp})_2](\text{ClO}_4)_2 \cdot \text{H}_2\text{O}$ in MeCN solution main bands are red-shifted (with a shoulder at lower energy for **2**) indicating that in solution the ligand field around Cu(II) decreases, suggesting axial solvent coordination.¹⁶⁵ This geometrical change is accompanied by a color change from violet to blue. In MeCN solutions shoulders at ca. 340 and 320 nm for **2** and **2a** are due to pyrazole \rightarrow Cu(II) charge transfer transitions.¹⁷⁶ All the Cu(II) complexes exhibit strong absorption bands in the UV region which are associated with intraligand charge transfer.

3. Axially Ligated Five-Coordinate Copper(II) Complexes

The reflectance spectral data of $[\text{Cu}(\text{Me}_2\text{pp})_2(\text{X})](\text{ClO}_4)$ show a single maximum in the visible region (Table III.4; Figures III.11-III.14) in the range 676-800 nm. In MeCN solutions all the five-coordinate complexes (except azido-complex) show one broad

Table III.5 Visible Spectral (d-d band) data of Cu(II) Complexes in Different Solvents at 298 K

Complexes	solvents	λ_{max} (nm)
[Cu(H ₂ pp) ₂] ⁻ (ClO ₄) ₂ ·H ₂ O	MeCN	592
	MeOH	625
	DMF	690
[Cu(Me ₂ pp) ₂] ⁻ (ClO ₄) ₂ ·H ₂ O	MeCN	602, 988 (sh)
	MeOH	680, 985
	DMF	680

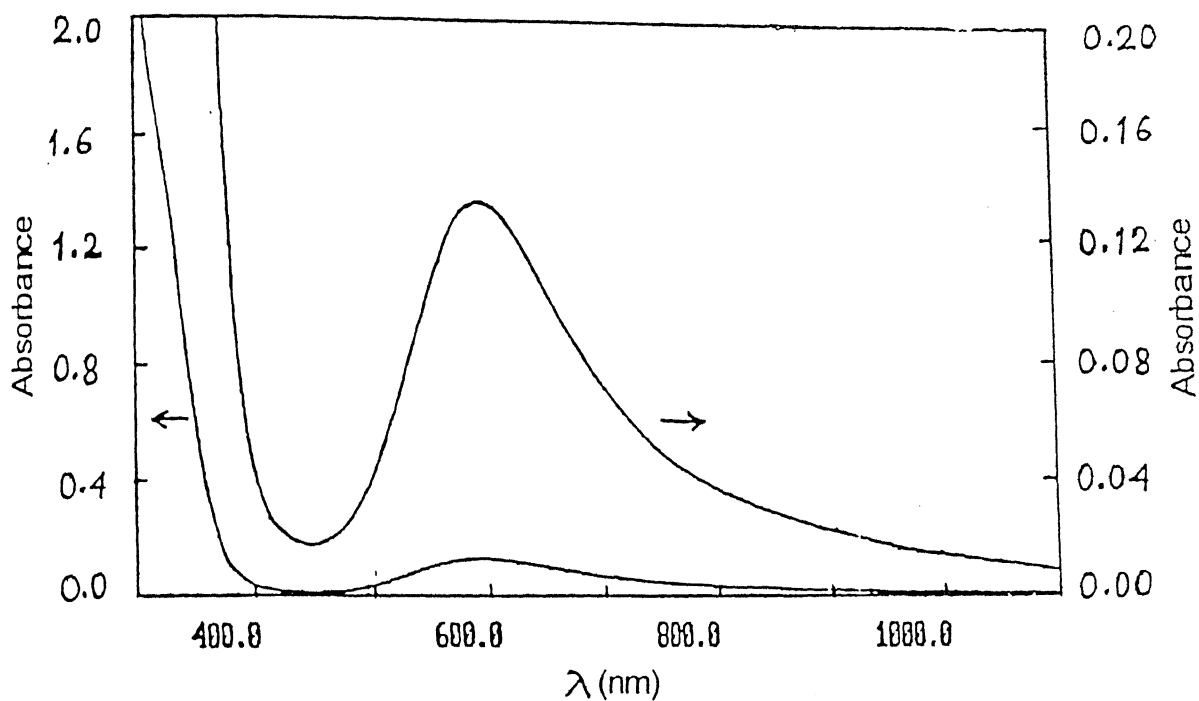


Figure III.9

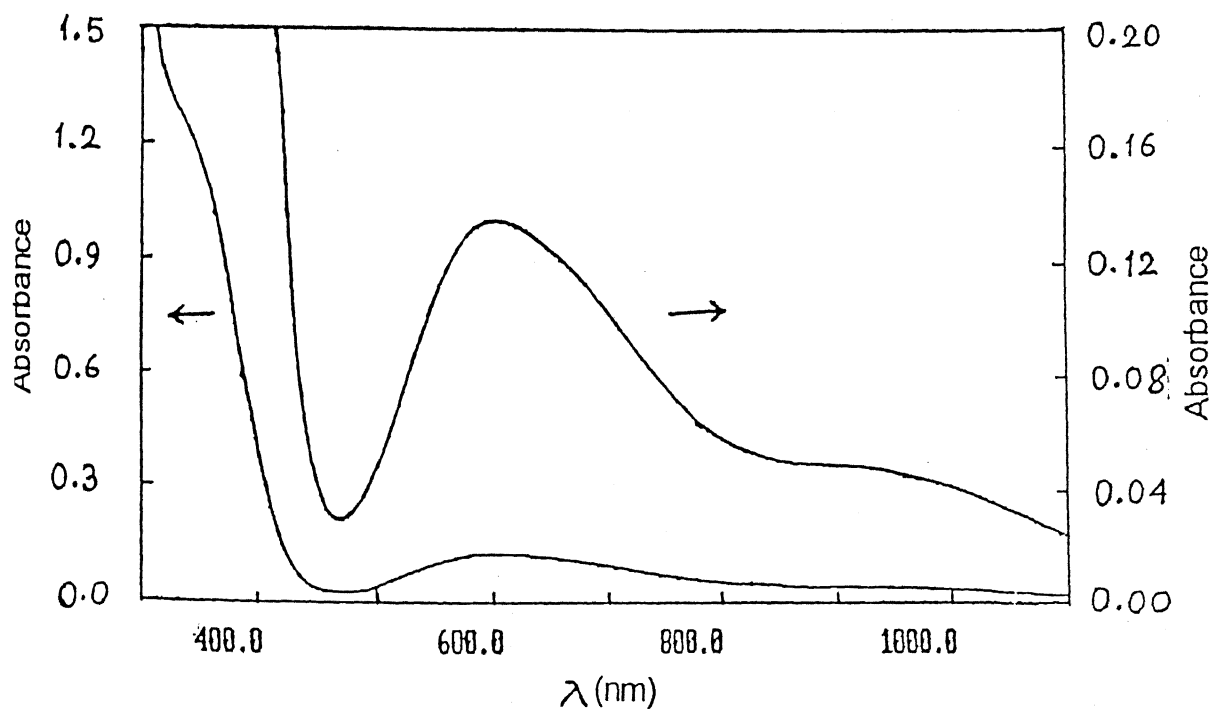
Electronic Spectrum of $[\text{Cu}(\text{H}_2\text{ppz})_2](\text{ClO}_4)_2 \cdot \text{H}_2\text{O}$ in MeCN

Figure III.10

Electronic Spectrum of $[\text{Cu}(\text{Me}_2\text{ppz})_2](\text{ClO}_4)_2 \cdot \text{H}_2\text{O}$ in MeCN

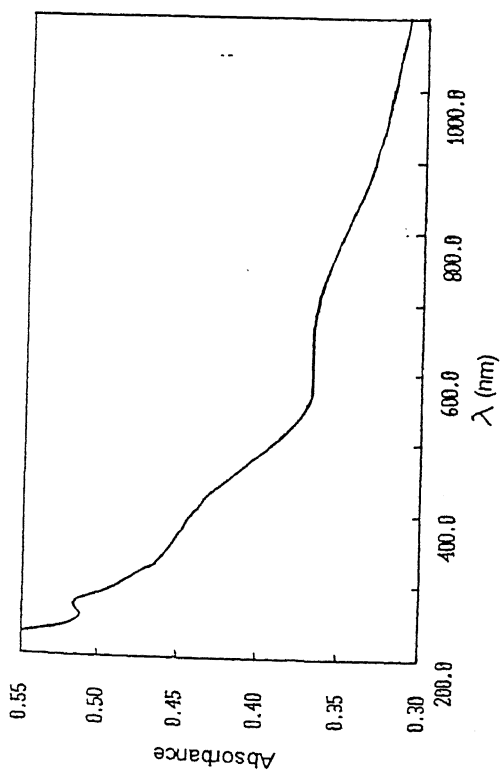


Figure III.11 Electronic Spectrum of $[\text{Cu}(\text{Me}_2\text{pp})_2(\text{NO}_2)](\text{ClO}_4)$ in paraffin oil

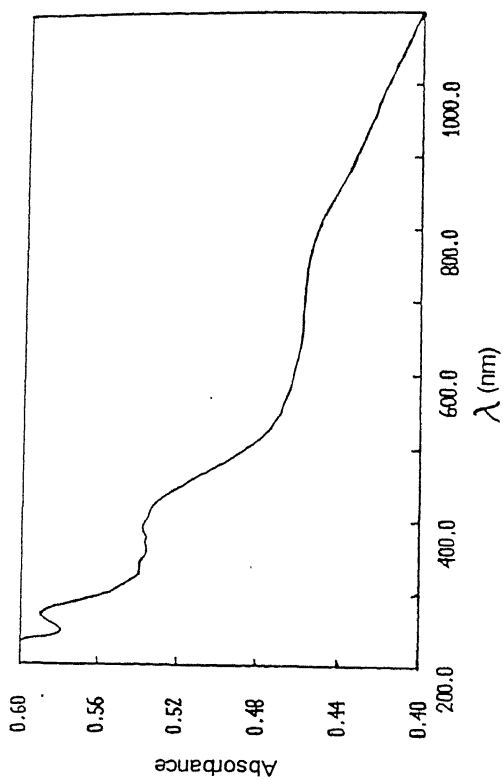


Figure III.13 Electronic Spectrum of $[\text{Cu}(\text{Me}_2\text{pp})_2(\text{SCN})](\text{ClO}_4)$ in paraffin oil

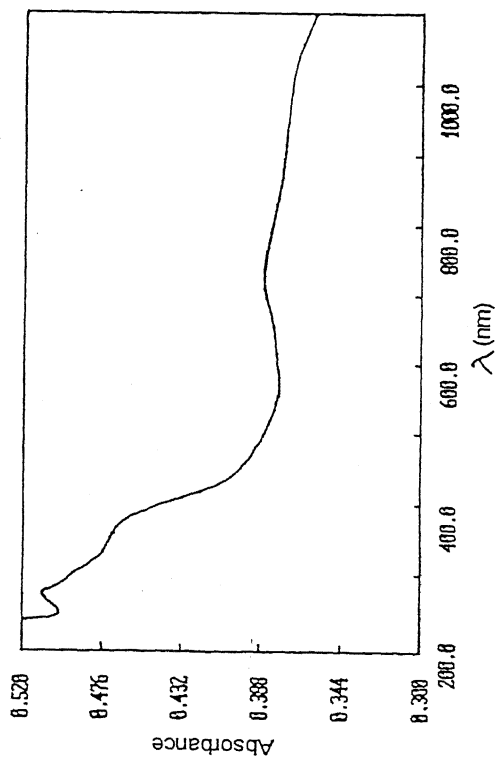


Figure III.12 Electronic Spectrum of $[\text{Cu}(\text{Me}_2\text{pp})_2(\text{Cl})](\text{ClO}_4)$ in paraffin oil

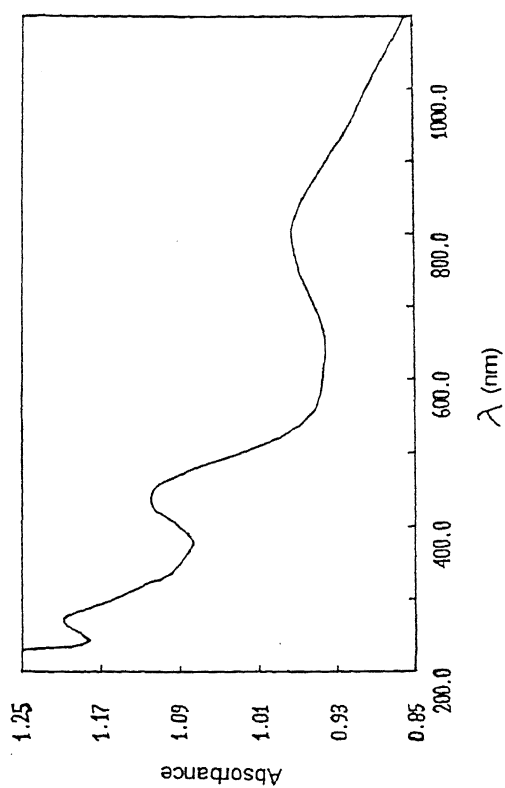


Figure III.14 Electronic Spectrum of $[\text{Cu}(\text{Me}_2\text{pp})_2(\text{N}_3)](\text{ClO}_4)$ in paraffin oil

band along with a shoulder at a lower energy in the visible region (Table III.4; Figures III.15-III.19). These observations indicate that the geometry around Cu(II) center is in between square pyramidal and trigonal bipyramidal.¹⁶⁵

In MeCN solution for all the five-coordinate complexes except 1 and 6 main bands are blue shifted compared to their solid state behavior. This may be due to a change in Cu(II) geometry which is now more towards square pyramidal for those cases.

III.5.3 EPR Spectral Studies

A. Bis-ligated Cu(II) Complexes

To extract complementary informations on the geometry of the Cu(II) complexes 1, 2, and 2a both in solid and solution state, EPR studies were performed. The EPR spectra of the polycrystalline complexes were recorded at 298 K as well as at 80 K and their g_{\parallel} and g_{\perp} values have been calculated. Following the equation $g_{av} = 1/3(g_{\parallel} + 2g_{\perp})$, g_{av} values are in the range 2.10-2.12, which are in agreement with an orbitally non-degenerate ground state.¹⁶⁵

In MeCN solutions the EPR spectra of the violet complexes $[Cu(R_{2pp})_2](ClO_4)_2 \cdot H_2O$ at 298 K are tetragonal (Figure III.20) with g_{av} and A_{av} are 2.123, 2.115 and 75, 65 G for unsubstituted and substituted respectively. Comparing the g values in solid state and solution state (Table III.6) it is observed that solvent has little effect on g values.

Simulated spectrum for 2 shown in Figure III.19 (broken line) and the parameters used are given in Table III.8A.

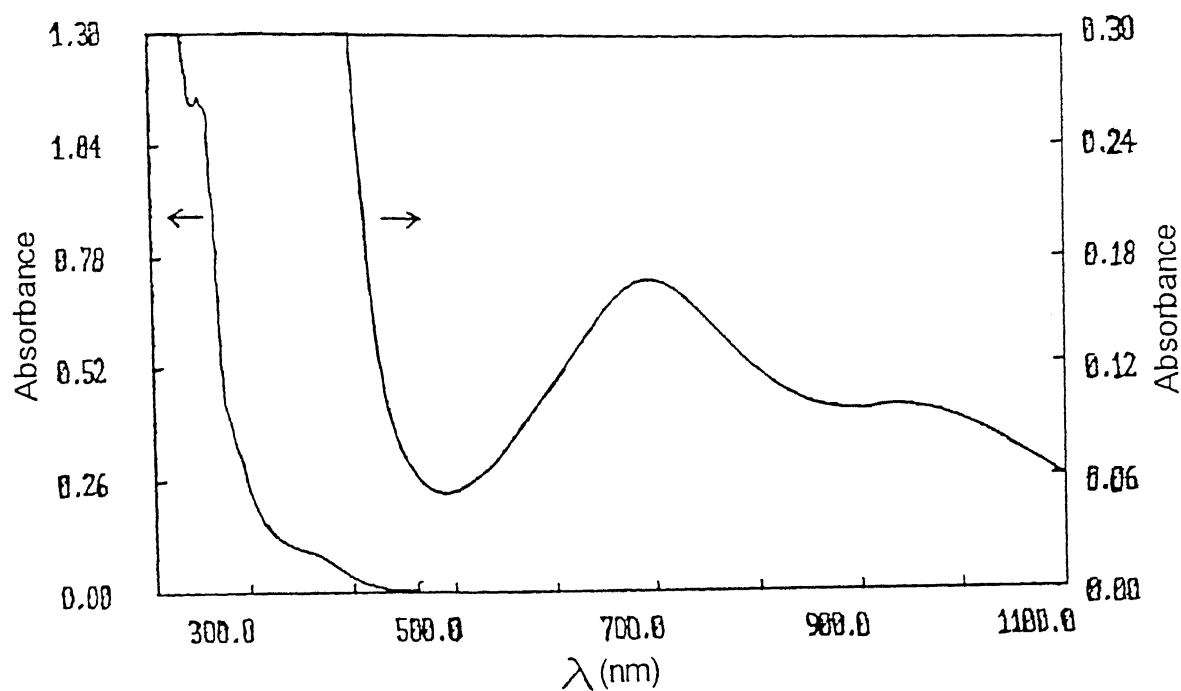


Figure III.15 Electronic Spectrum of $[\text{Cu}(\text{Me}_2\text{pp})_3](\text{ClO}_4)_2$ in MeCN

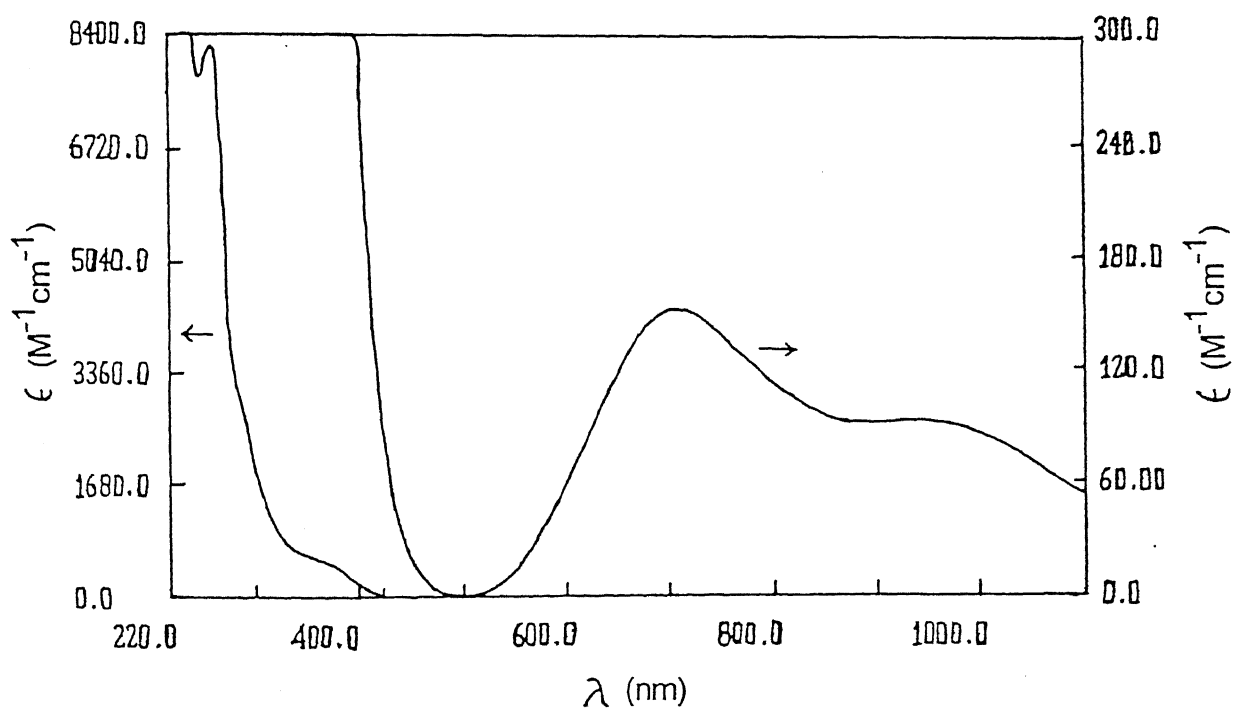


Figure III.16 Electronic Spectrum of $[\text{Cu}(\text{Me}_2\text{pp})_2(\text{Cl})](\text{ClO}_4)$ in MeCN

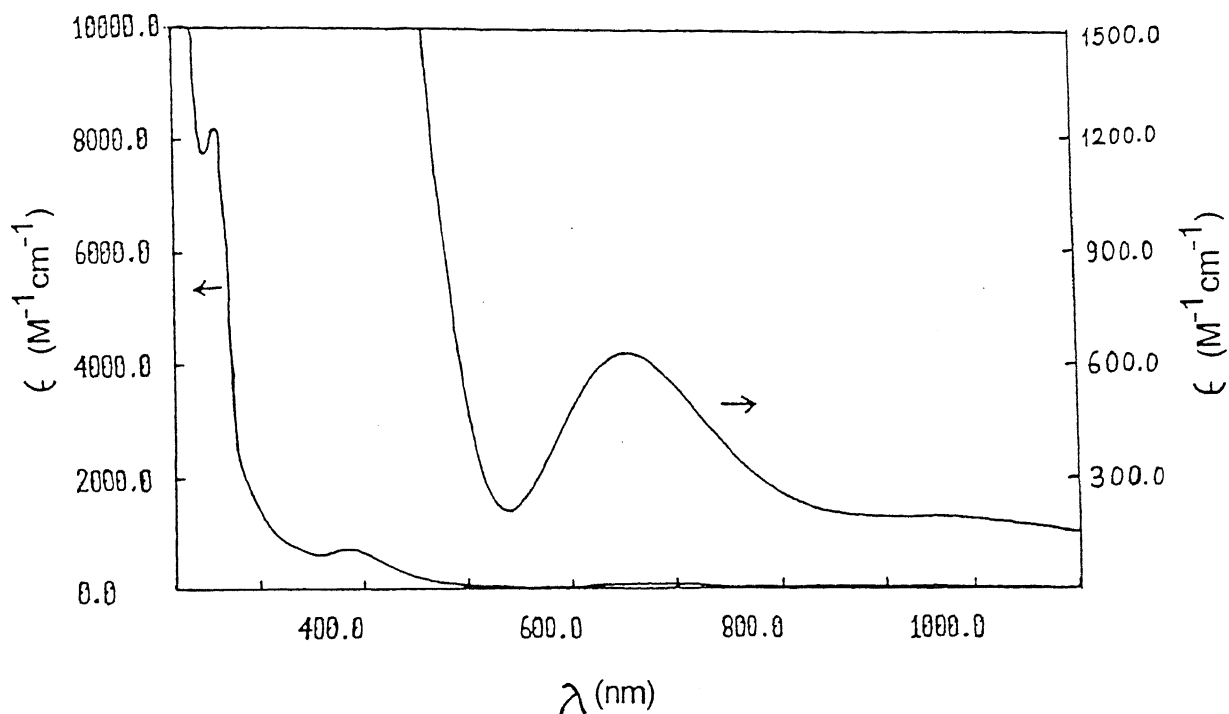
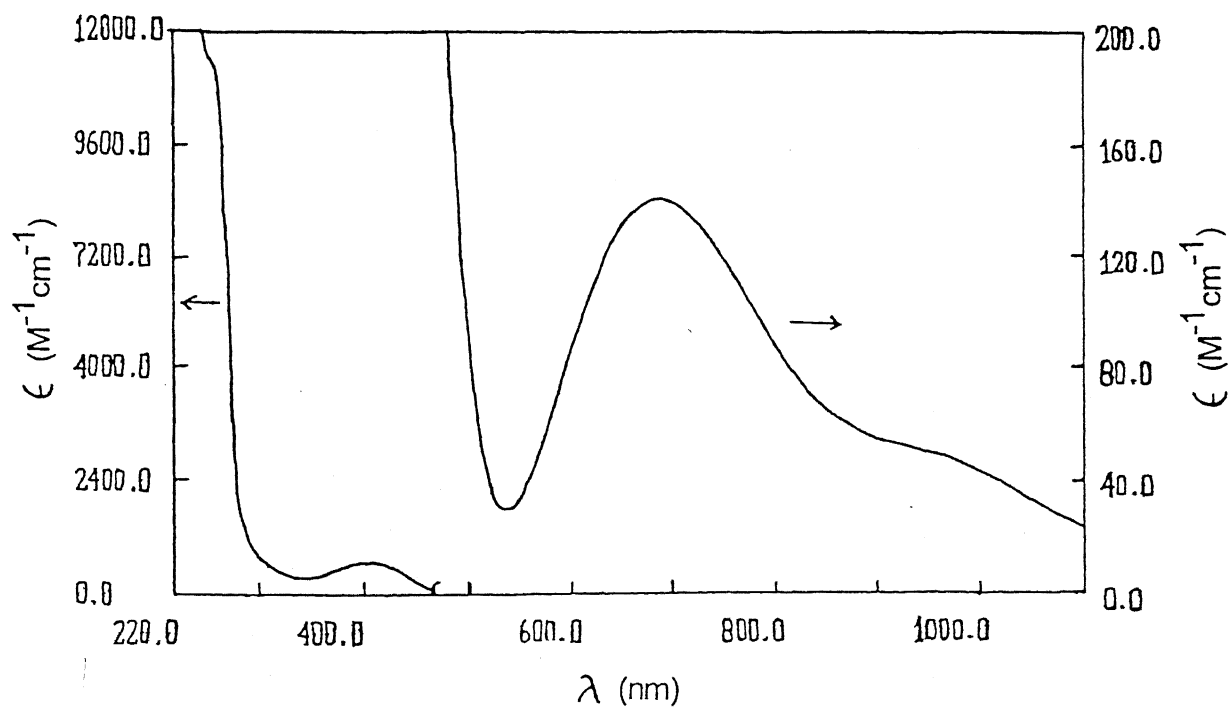


Figure III.17 Electronic Spectrum of $[\text{Cu}(\text{Me}_2\text{pp})_2(\text{NO}_2)](\text{ClO}_4)$ in MeCN



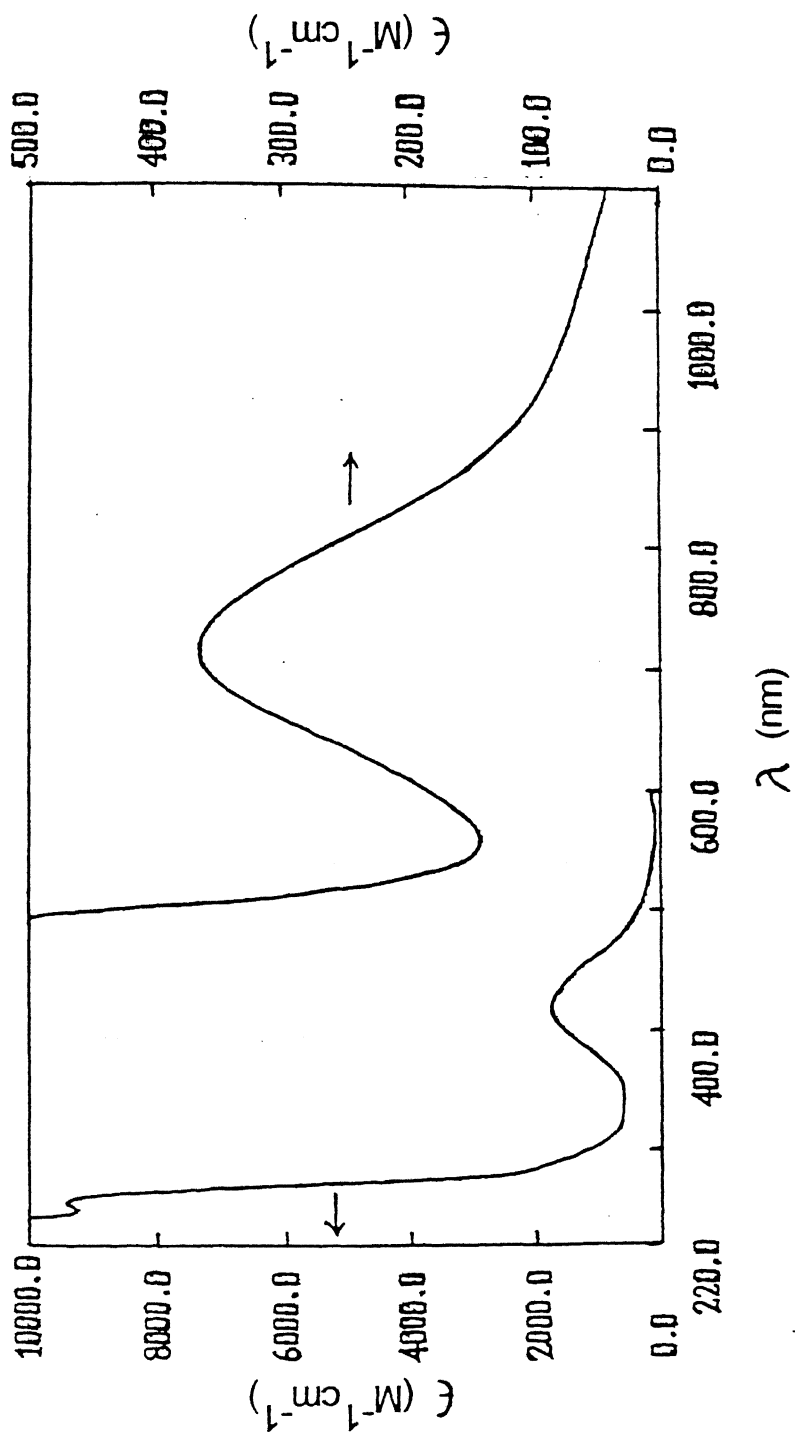


Figure III.19 Electronic Spectrum of $[\text{Cu}(\text{Me}_2\text{pp})_2(\text{N}_3)](\text{ClO}_4)$ in MeCN

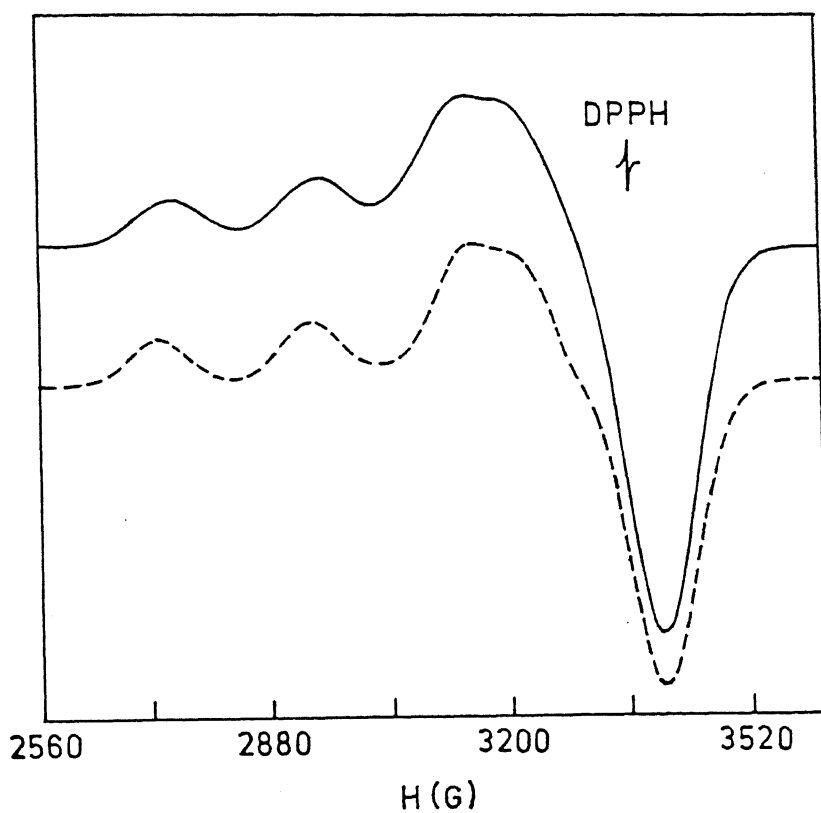


Figure III.20 EPR spectrum of $[\text{Cu}(\text{Me}_2\text{pp})_2](\text{ClO}_4)_2 \cdot \text{H}_2\text{O}$ (powder form at 298 K) (—), along with simulated spectrum (----).

Table III.6 X-Band EPR Spectral Data^a

Complex	g_{\parallel}	g_{\perp}	g_{av}^d	A_{\parallel} (G)
$[\text{Cu}(\text{H}_2\text{pp})_2] - (\text{ClO}_4)_2 \cdot \text{H}_2\text{O}$	2.214	2.067	2.117	200
$[\text{Cu}(\text{Me}_2\text{pp})_2] - (\text{ClO}_4)_2 \cdot \text{H}_2\text{O}$	2.214	2.048	2.105	200
	2.232 ^c	2.063 ^c	2.121 ^c	190 ^c
$[\text{Cu}(\text{Me}_2\text{pp})_2 - (\text{NO}_2)] (\text{ClO}_4)^b$	2.266	2.060	2.130	160
$[\text{Cu}(\text{Me}_2\text{pp})_2 - (\text{SCN})] (\text{ClO}_4)^b$	2.269	2.061	2.133	160

^aPolycrystalline powder form^bDichloromethane/toluene glass (80 K)^cFrozen acetonitrile (80 K)^d $g_{av} = (1/3(g_{\parallel}^2 + 2g_{\perp}^2))^{1/2}$

B. Axially Ligated Five-Coordinate Copper(II) Complexes

To extract information about the stereochemistry at the Cu(II) center in all five-coordinate complexes having $\text{Cu}^{\text{II}}\text{N}_4\text{X}$ coordination sphere, solid state, solution state and glass state EPR studies were performed. All the complexes (except the nitrito-compound (3)) show rhombic spectra in polycrystalline powder form at 298 K as well as at 80 K with three principal g values (Table III.7; Figures III.21-III.23). Rhombic nature of the EPR spectrum of **1** in polycrystalline state indicate that it's a five-coordinate Cu(II) complex (Table III.7; Figure III.24). In solutions they show tetragonal behavior at 298 K and isotropic at 80 K. In dichloromethane/ toluene glass at 80 K nitrito- and thiocyanato-complexes show well resolved tetragonal pattern (Figures III.25 and III.26). In dichloromethane glass at 80 K **1** shows tetragonal nature (Figure III.27). Simulated spectra are also shown in the respective experimental spectrum (broken line) and parameters used are compiled in Table III.8A and III.8B.

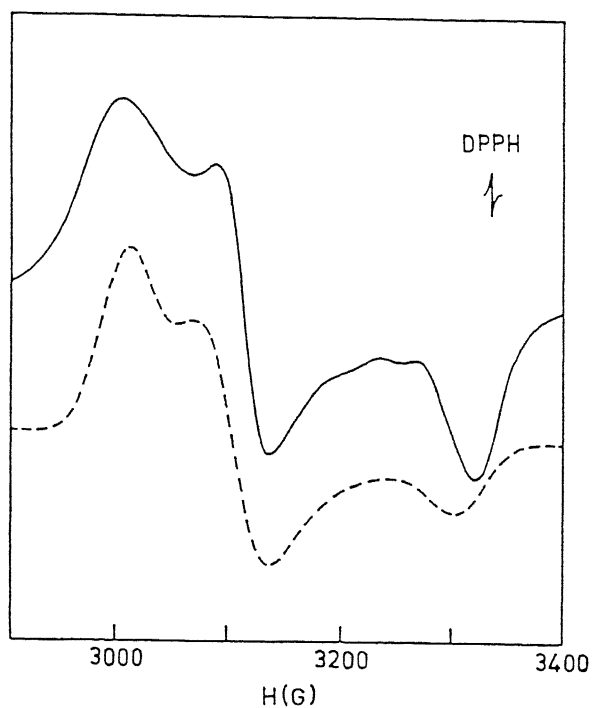


Figure III.21 EPR spectrum of $[\text{Cu}(\text{Me}_2\text{pp})_2(\text{Cl})](\text{ClO}_4)$ in solid state at 298K (—), along with simulated one(....)

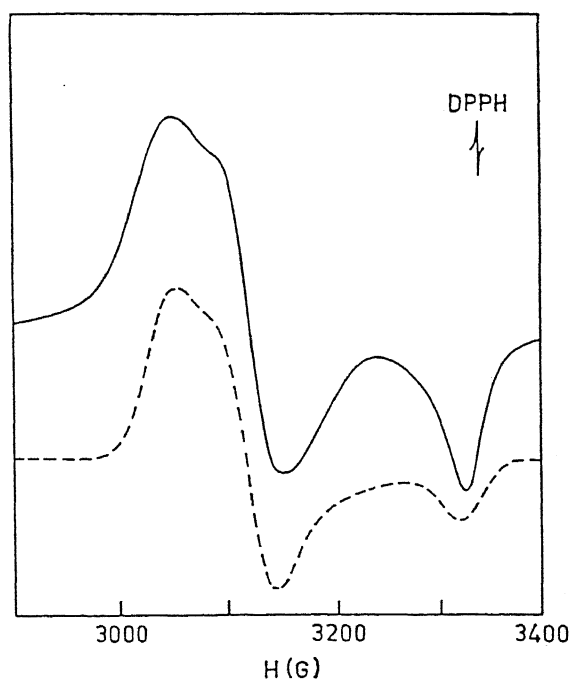


Figure III.22 EPR spectrum of $[\text{Cu}(\text{Me}_2\text{pp})_2(\text{SCN})](\text{ClO}_4)$ in solid state at 298K (—), along with simulated one(....)

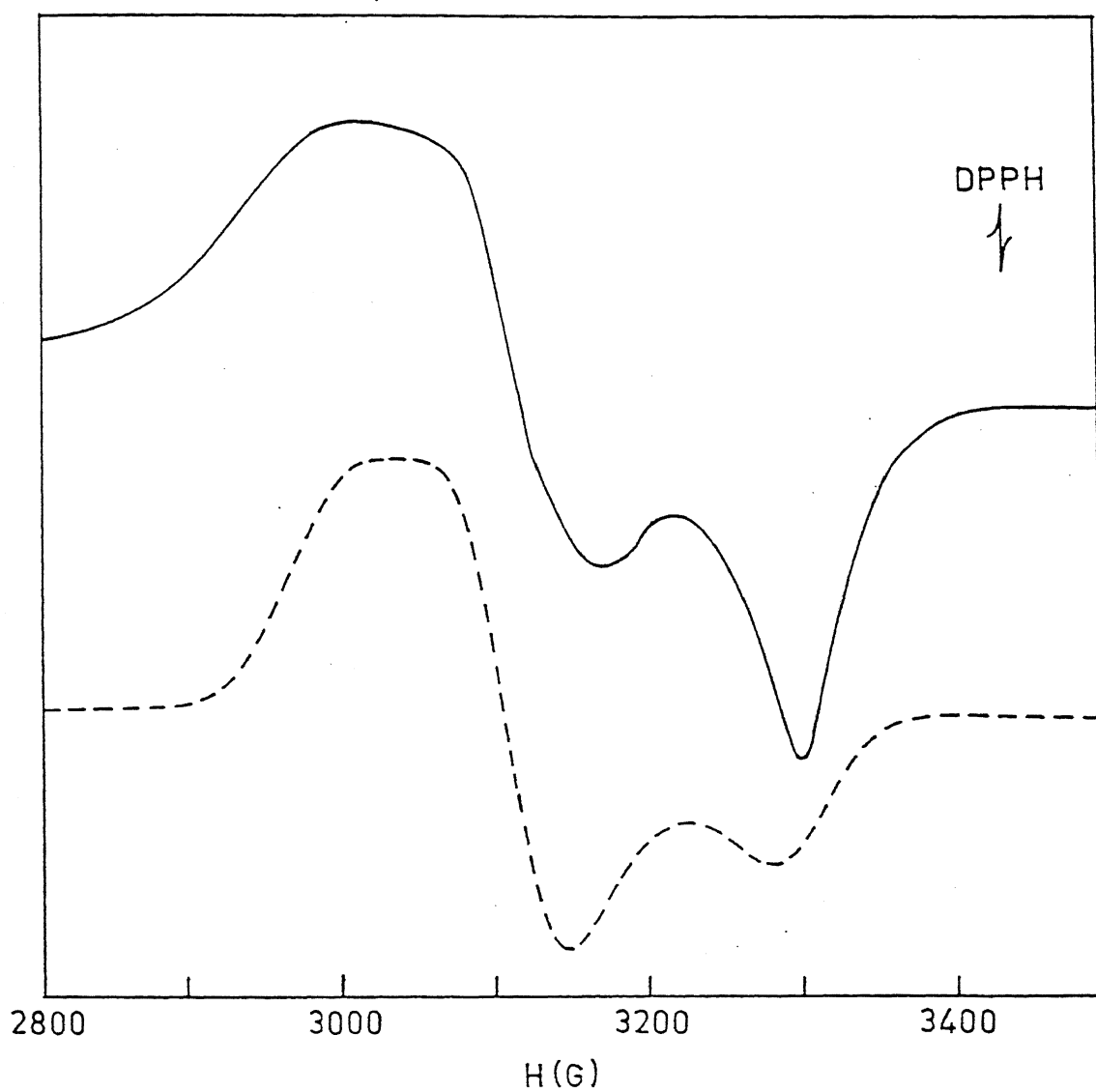


Figure III.23 EPR spectrum of $[\text{Cu}(\text{Me}_2\text{pp})_2(\text{N}_3)](\text{ClO}_4)$ in solid state at 298K (—) , along with simulated one(.....)

Table III.7 X-Band EPR Spectral Data^a for Five-Coordinate Cu(II) Complexes

Complex	g_1	g_2	g_3	g_{av}^b	Temperature (K)
$[\text{Cu}(\text{Me}_2\text{pp})_3]^- (\text{ClO}_4)_2$	2.013	2.150	2.206	2.125	298
	2.011 ^c	2.153 ^c	2.207 ^c	2.125 ^c	298
$[\text{Cu}(\text{Me}_2\text{pp})_2]^- (\text{Cl}) (\text{ClO}_4)$	2.018	2.150	2.220	2.131	298
$[\text{Cu}(\text{Me}_2\text{pp})_2]^- (\text{SCN}) (\text{ClO}_4)$	2.011	2.143	2.192	2.117	298
$[\text{Cu}(\text{Me}_2\text{pp})_2]^- (\text{N}_3) (\text{ClO}_4)$	2.083	2.207	2.284	2.193	80

^aPolycrystalline powder form

$$g_{av}^b = [1/3 (g_1^2 + g_2^2 + g_3^2)]^{1/2}$$

^cValues for the complex prepared from $[\text{Cu}(\text{Me}_2\text{pp})_2] (\text{ClO}_4)_2 \cdot \text{H}_2\text{O}$ + $3\text{Me}_2\text{pp}$

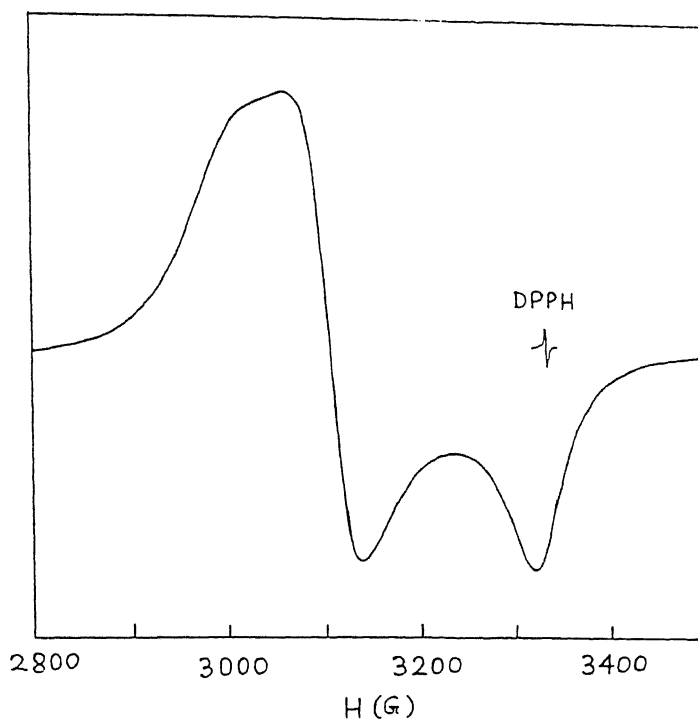


Figure III. 2^4 EPR spectrum of $[\text{Cu}(\text{Me}_2\text{pp})_3](\text{ClO}_4)_2$
in solid state at 298K

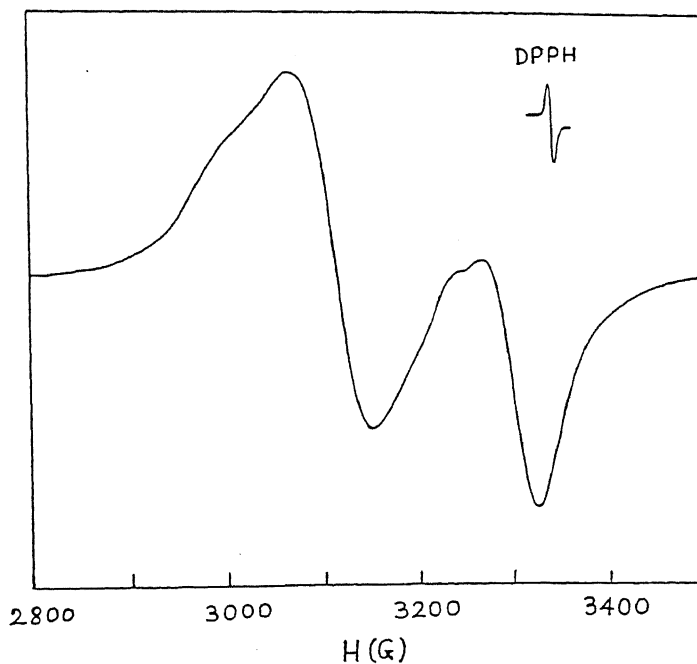


Figure III. 2^{4a} EPR spectrum of $[\text{Cu}(\text{Me}_2\text{pp})_3](\text{ClO}_4)_2$ (prepared
from $[\text{Cu}(\text{Me}_2\text{pp})_2](\text{ClO}_4)_2 \cdot \text{H}_2\text{O} + 3 \text{Me}_2\text{pp}$) in solid state at 298K

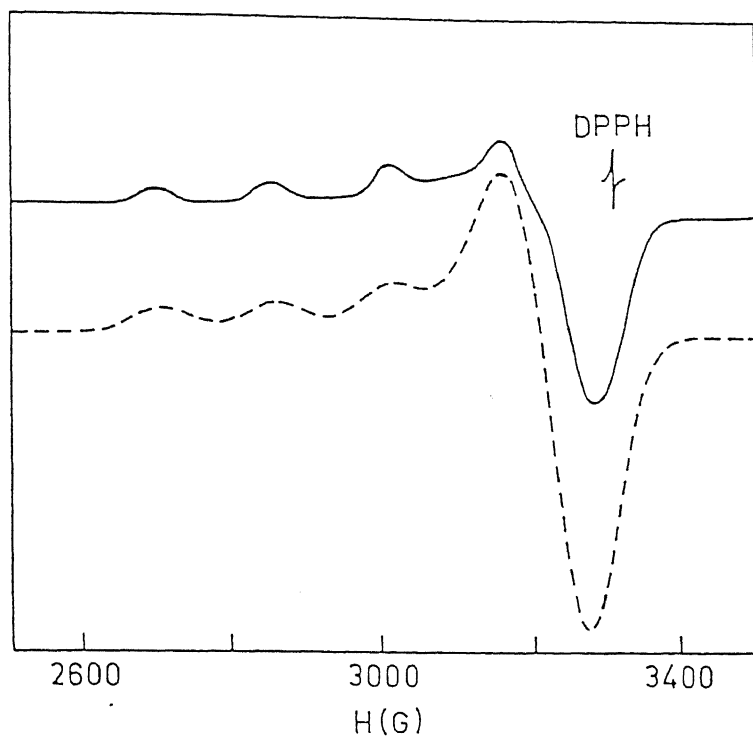


Figure III.25 EPR spectrum of $[\text{Cu}(\text{Me}_2\text{pp})_2(\text{NO}_2)](\text{ClO}_4)$ in dichloromethane-toluene (2:1) glass (80K) (—), along with simulated one(.....)

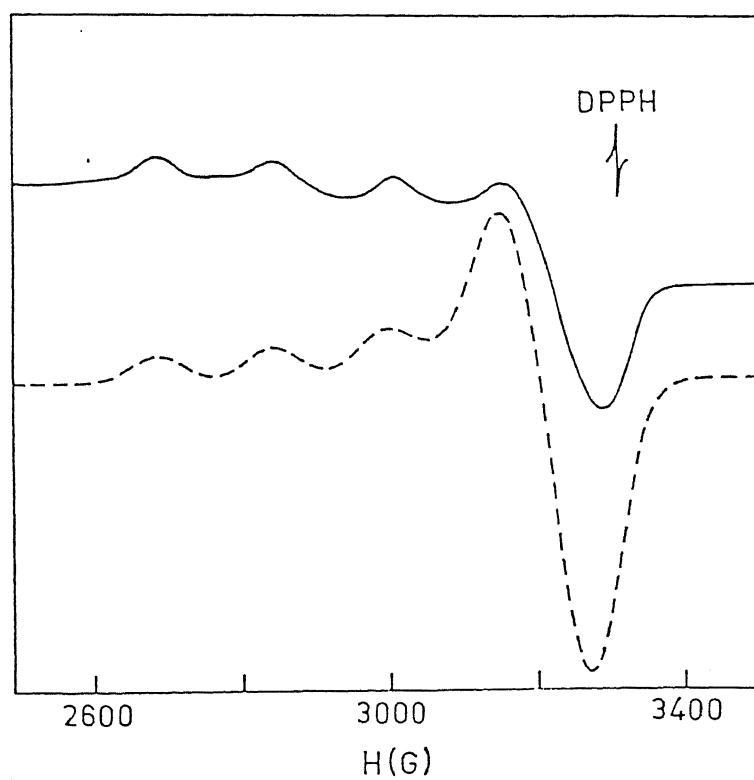


Figure III.26 EPR spectrum of $[\text{Cu}(\text{Me}_2\text{pp})_2(\text{SCN})](\text{ClO}_4)$ in dichloromethane-toluene (2:1) glass (80K) (—), along with simulated one(.....)

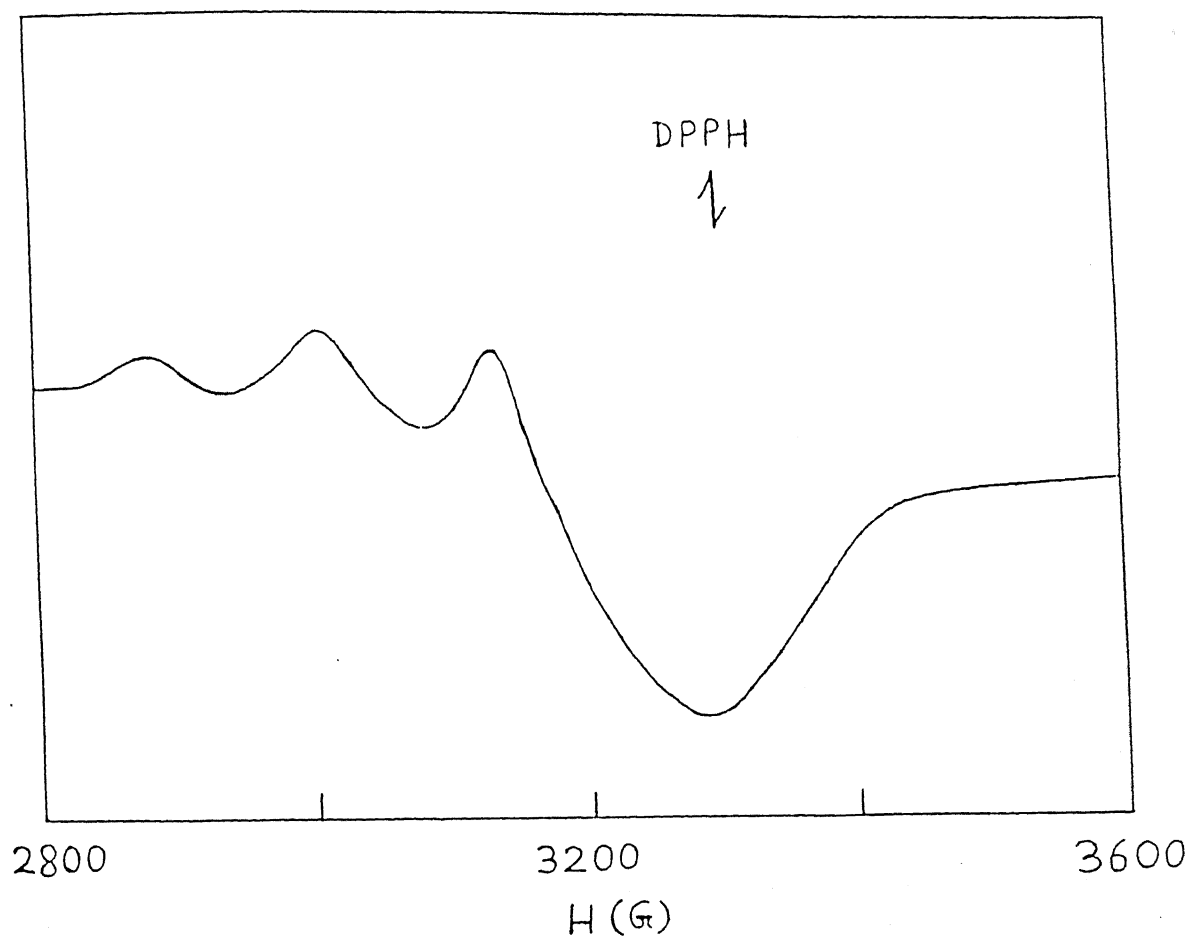


Figure III.27 EPR Spectrum of $[\text{Cu}(\text{Me}_2\text{ppz})_3](\text{ClO}_4)_2$ in CH_2Cl_2 glass (80K)

Table III.8A The EPR spectral parameters used in EPR simulations

Complex	$g_{ }$	g_{\perp}	$A_{ }$ (G)	Linewidth (G)		
				L_x	L_y	L_z
$[\text{Cu}(\text{Me}_2\text{pp})_2] - (\text{ClO}_4)_2 \cdot \text{H}_2\text{O}^a$	2.214	2.048	200	54	54	35.5
$[\text{Cu}(\text{Me}_2\text{pp})_2 - (\text{NO}_2)] (\text{ClO}_4)^b$	2.266	2.060	160	45	30	40
$[\text{Cu}(\text{Me}_2\text{pp})_2 - (\text{SCN})] (\text{ClO}_4)^b$	2.269	2.061	160	46	35	34

^aPolycrystalline powder form (298 K)^bDichloromethane/toluene glass (80 K)Table III.8B The EPR spectral parameters^a used in EPR simulations

Complex	g_1	g_2	g_3	A_1^b	A_2^b	A_3^b	Linewidth(G)		
							L_x	L_y	L_z
$[\text{Cu}(\text{Me}_2\text{pp})_2 - (\text{Cl})] (\text{ClO}_4)$	2.018	2.150	2.220	0.80	0.795	0.80	25	25	23
$[\text{Cu}(\text{Me}_2\text{pp})_2 - (\text{SCN})] (\text{ClO}_4)$	2.011	2.143	2.192	0.80	0.78	0.80	20	20	23
$[\text{Cu}(\text{Me}_2\text{pp})_2 - (\text{N}_3)] (\text{ClO}_4)^c$	2.083	2.207	2.284	0.80	0.79	0.80	30	30	40

^aPolycrystalline powder form at 298 K^bIn Gauss^cPolycrystalline powder form at 80 K

III.5.4 Solid state X-ray structure of the complex $[\text{Cu}(\text{Me}_2\text{pp})_2(\text{NO}_2)](\text{ClO}_4)$ (3)

To investigate whether or not 3 can be used as a structural model for copper containing nitrite reductase its X-ray structure was determined.

The asymmetric unit consists of one molecule of $[\text{Cu}(\text{Me}_2\text{pp})_2(\text{ONO})]^+$ and one non-coordinating perchlorate anion. The ORTEP view of the complex is depicted in Figure III.28. The Cu(II) is coordinated to four nitrogen atoms from two pyrazole and two pyridine rings of two Me_2pp ligands and one oxygen atom from NO_2^- group. Selected bond length and angles are given in Table III.9, and positional and isotropic thermal parameters are given in Table III.10. The environment around the Cu atom is best described as a distorted square pyramidal with a trigonal bipyramidal component of, $\tau = 0.29$ [$\tau = (\beta - \alpha)/60$, where $\beta = \text{N}(1)\text{-Cu-N}(4)$ 174.0° and $\alpha = \text{O}(1)\text{-Cu-N}(6)$ 156.6°]; for a perfect square pyramidal and trigonal bipyramidal geometries the value of τ is zero and unity respectively.¹⁷⁷ The basal plane of the square pyramid is defined by N(4) and N(6) atoms of a Me_2pp ligand, N(1) pyridine atom of the other ligand, and O(1) of the nitrite ion. The N(3) pyrazole nitrogen atom of the second ligand forms the axial bond. The Cu atom is displaced from the equatorial plane towards the axial pyrazole nitrogen by 0.25 Å. The two pyridyl nitrogens are trans to each other. There exists an inverse correlation¹⁶⁵ between the displacement parameter and the Cu-(apical) distance in square pyramidal copper(II) complexes. The present observation nicely fits in the expected trend.

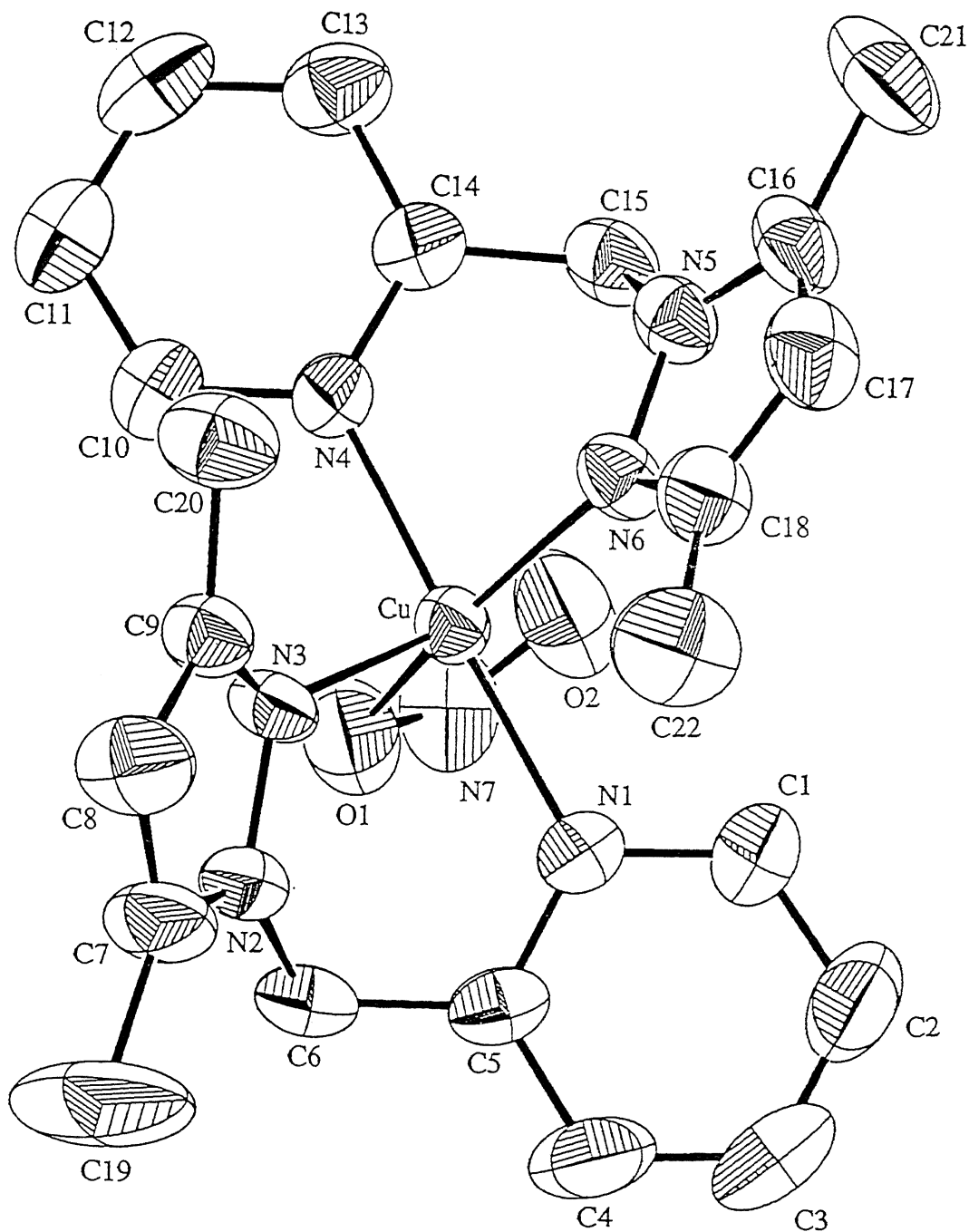


Figure III.28 ORTEP diagram of $[\text{Cu}(\text{Me}_2\text{pp})_2(\text{NO}_2)](\text{ClO}_4)$ showing the 50% probability thermal ellipsoids and atom labeling scheme

Table III.9 Selected Bond Lengths (Å) and Angles (deg) in the
cationic part of $[\text{Cu}(\text{Me}_2\text{pp})_2(\text{NO}_2)]\text{ClO}_4$ (3)

Cu-O(1)	2.091(5)	Cu-N(1)	2.007(4)
Cu-N(3)	2.155(4)	Cu-N(4)	2.002(4)
Cu-N(6)	2.063(4)	O(1)-N(7)	1.260(6)
		N(7)-O(2)	1.199(6)

O(1)-Cu-N(1)	86.6(2)	O(1)-Cu-N(3)	103.1(2)
O(1)-Cu-N(4)	89.2(2)	O(1)-Cu-N(6)	156.6(2)
N(1)-Cu-N(3)	89.0(2)	N(1)-Cu-N(4)	174.0(2)
N(1)-Cu-N(6)	94.9(2)	N(3)-Cu-N(4)	96.1(2)
N(3)-Cu-N(6)	100.3(2)	N(4)-Cu-N(6)	87.3(2)
Cu-O(1)-N(7)	110.3(4)		
O(1)-N(7)-O(2)	111.2(6)		

Table III. 10

Atomic coordinates and B_{iso}/B_{eq}

atom	x	y	z	B_{eq}
Cu()	0.20523(5)	0.16032(3)	0.01195(6)	3.00(1)
Cl()	0.6948(1)	0.15846(10)	0.5389(2)	5.89(5)
O(1)	0.2228(3)	0.2474(2)	-0.0928(4)	5.9(1)
O(2)	0.1960(4)	0.2757(3)	0.1045(5)	8.1(2)
O(3b)	0.759(2)	0.159(1)	0.415(3)	15.1(9)
O(3c)	0.694(1)	0.1830(9)	0.399(2)	6.4(4)
O(3a)	0.663(2)	0.209(1)	0.459(2)	10.5(6)
O(4b)	0.730(1)	0.2123(8)	0.610(2)	5.3(4)
O(4a)	0.687(2)	0.154(2)	0.686(3)	15.9(9)
O(4c)	0.703(1)	0.2045(8)	0.656(1)	4.1(3)
O(5b)	0.687(2)	0.096(1)	0.594(2)	11.2(6)
O(5c)	0.764(2)	0.1073(10)	0.560(2)	8.0(4)
O(5a)	0.803(1)	0.1418(9)	0.509(2)	7.5(4)
O(6b)	0.579(1)	0.1691(10)	0.528(2)	8.2(4)
O(6c)	0.600(2)	0.125(1)	0.560(2)	10.6(6)
O(6a)	0.642(2)	0.109(1)	0.480(3)	13.2(8)
N(1)	0.3557(3)	0.1624(2)	0.0431(4)	3.5(1)
N(2)	0.3167(3)	0.0940(2)	-0.2196(4)	3.8(1)
N(3)	0.2283(3)	0.0898(2)	-0.1479(4)	3.5(1)
N(4)	0.0549(3)	0.1679(2)	-0.0133(4)	3.1(1)
N(5)	0.0991(3)	0.1178(2)	0.2647(4)	3.5(1)
N(6)	0.1759(3)	0.1011(2)	0.1778(4)	3.4(1)
N(7)	0.2173(4)	0.2938(3)	-0.0094(6)	5.7(2)
C(1)	0.3916(4)	0.1708(3)	0.1713(6)	4.6(2)

Contd.

Atomic coordinates and B_{iso}/B_{eq} (continued)

atom	x	y	z	B_{eq}
C(2)	0.4921(6)	0.1739(4)	0.2013(7)	6.6(2)
C(3)	0.5602(5)	0.1685(4)	0.0960(9)	8.0(3)
C(4)	0.5247(5)	0.1602(4)	-0.0367(7)	6.2(2)
C(5)	0.4222(4)	0.1579(3)	-0.0617(6)	3.9(1)
C(6)	0.3793(4)	0.1512(3)	-0.2045(6)	4.3(1)
C(7)	0.3331(5)	0.0398(3)	-0.2931(6)	5.4(2)
C(8)	0.2530(5)	0.0003(3)	-0.2680(6)	5.5(2)
C(9)	0.1901(4)	0.0325(3)	-0.1782(5)	3.6(1)
C(10)	0.0155(4)	0.1677(3)	-0.1409(5)	4.0(1)
C(11)	-0.0862(5)	0.1732(3)	-0.1652(6)	5.1(2)
C(12)	-0.1499(5)	0.1811(3)	-0.0564(8)	5.7(2)
C(13)	-0.1107(4)	0.1819(3)	0.0769(7)	4.9(2)
C(14)	-0.0081(4)	0.1746(3)	0.0951(6)	3.6(1)
C(15)	0.0414(4)	0.1751(3)	0.2363(5)	3.9(1)
C(16)	0.0944(5)	0.0772(3)	0.3742(5)	4.4(2)
C(17)	0.1671(5)	0.0324(3)	0.3541(6)	5.0(2)
C(18)	0.2164(4)	0.0485(3)	0.2328(6)	4.4(2)
C(19)	0.4218(6)	0.0316(5)	-0.3868(9)	11.0(3)
C(20)	0.0936(5)	0.0093(3)	-0.1163(6)	5.2(2)
C(21)	0.0203(6)	0.0879(4)	0.4895(6)	6.9(2)
C(22)	0.3005(5)	0.0132(4)	0.1665(7)	6.8(2)

The average copper(II)-N(pyridine) distance of 2.005 Å is comparatively shorter than that found for similar complexes.^{95g,h} The copper(II)-O(nitrite) distance of 2.091(5) Å is appreciably longer than the closely similar copper(II)-nitrito complexes (2.012(5) Å^{95g} and 1.938(2) Å^{95h}). The equatorial copper(II)-N(pyrazole) distance of 2.063(4) Å is significantly longer than the related complexes^{156,160} and falls in the range for copper(II) complexes with sterically crowded tris(pyrazolyl)-hydroborate complexes.^{95a-c,e,f} Interestingly, the axial Cu-N(pyrazole) bond distance of 2.155(4) Å is quite long. Within the mononuclear copper(II) complexes of pyrazole donors this is the first report (see chapter IV) of a axially coordinated Cu(II)-N(pyrazole) bond. We believe that the observed bonding effect is the manifestation of the steric crowding created by the pyrazole ring methyl substituents near donor site of the Me₂pp ligands.

The pyridyl and pyrazole rings are each planar. However, a pyridyl ring of a given ligand is twisted to a pyrazole ring by an angle of 52.58° and 59.92°. Thus the six-membered chelate rings exist in boat conformations, as is observed in compounds of these kinds of ligands (see chapter IV).

It is worthnoting that this complex is the first example of a nitrite bound complex with the coordination sphere Cu^{II}N₄O where two bidentate pyrazolylmethylpyridine ligands are coordinated. The perchlorate was found to be disordered. Each of the oxygens was disordered over three positions and they were modelled accordingly. At convergence $R = 0.052$ and $R_w = 0.052$. Final difference Fourier maps showed no significant residual electron density.

III.5.5 Solid State X-ray structure of $[\text{Cu}(\text{Me}_2\text{pp})_2(\text{SCN})](\text{ClO}_4)$ (Table III.11a)

The asymmetric unit of this complex consists of two independent five-coordinate $[\text{Cu}(\text{Me}_2\text{pp})_2(\text{SCN})]^{1+}$ cations and two perchlorate anions. Figure III.29 provides a perspective view of the cationic parts. The structure reveals that the copper(II) ion is surrounded by two pyrazole nitrogens, two pyridine nitrogens, and one sulfur atom of NCS^- . The geometry around copper(II) is described as distorted trigonal bipyramidal with a very small square pyramidal component, considering the structural index τ ($= 0.74$ and 0.66) for two five-coordinate Cu centers (Table III.11), as described previously. It is worth noting here that the pentacoordinate complex is sulfur coordinated at the fifth coordination which is usually uncommon^{178,179} in mononuclear Cu(II) chemistry. Perchlorates are disordered. Bond distances and bond angles of the coordination spheres of Cu(1) and Cu(2) are compiled in Table III.11. Bond distances and angles of coordinated NCS^- are as follows: $(\text{S-C})_{\text{av}} = 1.67$ and $(\text{C-N})_{\text{av}} = 1.10 \text{ \AA}$; $(\text{Cu-S-C})_{\text{av}} = 106$ and $(\text{S-C-N})_{\text{av}} = 172^\circ$. Thus it is clear that NCS^- is sulfur bound. C-C, C-N, and N-N bonds are in the expected range. Our efforts are on to get the more converged structure.

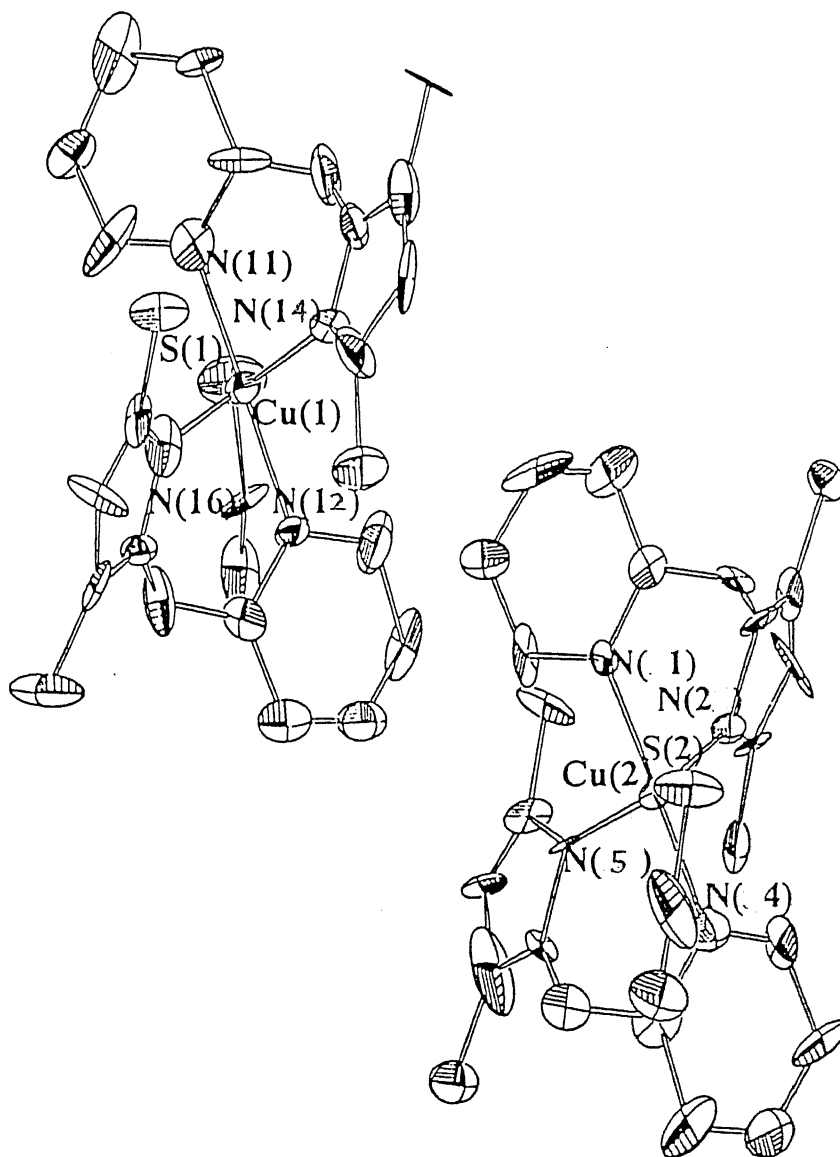


Figure III.29 ORTEP diagram of $[\text{Cu}(\text{Me}_2\text{pp})_2(\text{SCN})](\text{ClO}_4)$ showing the 50% probability thermal ellipsoids and atom labeling scheme

Table III.11 Bond Distances and Bond Angles of the Two Coordination Spheres of Copper for $[\text{Cu}(\text{Me}_2\text{pp})_2(\text{SCN})](\text{ClO}_4)$ (5)

atom	distance, Å	atom	angle, deg	atom	angle, deg
Cu1-N11	2.01 (2)	S1-Cu1-N11	90 (1)	N11-Cu1-N14	96 (1)
Cu1-N12	2.04 (3)	S1-Cu1-N12	84 (1)	N11-Cu1-N16	89 (1)
Cu1-N14	2.10 (3)	S1-Cu1-N14	130.2 (8)	N12-Cu1-N14	89 (1)
Cu1-N16	2.10 (3)	S1-Cu1-N16	129.6 (9)	N12-Cu1-N16	94 (1)
Cu1-S1	2.39 (2)	N11-Cu1-N12	174 (1)	N14-Cu1-N16	100 (1)
Cu2-N1	1.97 (3)	S2-Cu2-N1	89 (1)	N1-Cu2-N4	179 (1)
Cu2-N2	2.09 (3)	S2-Cu2-N2	121.6 (8)	N1-Cu2-N5	89 (1)
Cu2-N4	1.97 (2)	S2-Cu2-N4	90 (1)	N2-Cu2-N4	88 (1)
Cu2-N5	2.09 (3)	S2-Cu2-N5	139.8 (9)	N2-Cu2-N5	99 (1)
Cu2-S2	2.39 (2)	N1-Cu2-N2	94 (1)	N4-Cu2-N5	91 (1)

Table III. 11a

Atomic Positional and Isotropic Displacement Parameters

	x/a	y/b	z/c	U
Cu(1)	0.7160(4)	0.4226(4)	0.4800(2)	* 0.0359
Cu(2)	1.0093(4)	0.1133(4)	0.0024(3)	* 0.0343
S(1)	0.719(1)	0.5529(8)	0.4883(7)	* 0.0810
C(1s)	0.652(4)	0.588(2)	0.387(2)	* 0.0388
N(1s)	0.594(3)	0.616(2)	0.333(2)	* 0.0589
N(11)	0.684(3)	0.429(2)	0.347(1)	* 0.0361
N(12)	0.746(3)	0.428(2)	0.614(2)	* 0.0431
N(13)	1.005(2)	0.360(2)	0.570(2)	* 0.0369
N(14)	0.888(3)	0.348(1)	0.497(2)	* 0.0368
N(15)	0.428(3)	0.364(2)	0.392(2)	* 0.0349
N(16)	0.541(3)	0.350(2)	0.465(2)	* 0.0464
S(2)	1.049(1)	-0.0151(8)	-0.0048(7)	* 0.0793
C(2s)	0.928(4)	-0.039(2)	-0.096(3)	* 0.0830
N(2s)	0.839(3)	-0.057(2)	-0.158(2)	* 0.0636
N(1)	0.982(3)	0.119(2)	-0.127(2)	* 0.0594
N(2)	1.181(3)	0.187(1)	0.026(2)	* 0.0266
N(3)	1.312(3)	0.171(2)	0.101(2)	* 0.0551
N(4)	1.033(3)	0.106(2)	0.132(2)	* 0.0339
N(5)	0.839(3)	0.187(2)	-0.005(2)	* 0.0380
N(6)	0.723(3)	0.178(1)	-0.078(2)	* 0.0240
C(7)	1.299(4)	0.101(3)	0.145(2)	* 0.0493
C(11)	1.342(4)	0.285(3)	0.051(3)	* 0.0852
C(17)	0.840(4)	0.119(2)	-0.176(2)	* 0.0509
C(18)	0.913(3)	0.096(2)	0.164(3)	* 0.0496
C(19)	1.169(3)	0.100(2)	0.189(2)	* 0.0290
C(20)	1.214(4)	0.255(2)	0.002(2)	* 0.0320
C(24)	0.635(5)	0.241(3)	-0.080(4)	* 0.0901
C(31)	1.188(4)	0.106(2)	0.279(2)	* 0.0569
C(34)	0.804(5)	0.116(3)	-0.276(2)	* 0.0727
C(35)	0.692(5)	0.284(3)	-0.010(3)	* 0.0843
C(38)	1.113(4)	0.294(2)	-0.074(2)	* 0.0508
C(39)	0.810(4)	0.250(2)	0.032(2)	* 0.0439
C(47)	0.925(4)	0.093(2)	0.257(2)	* 0.0438
C(49)	1.073(6)	0.099(2)	0.306(2)	* 0.0799
C(55)	1.388(4)	0.232(2)	0.110(3)	* 0.0415
C(56)	0.925(4)	0.280(2)	0.113(3)	* 0.0661
C(59)	1.074(4)	0.121(2)	-0.260(2)	* 0.0571
C(68)	0.495(4)	0.247(2)	-0.151(2)	* 0.0681
C(77)	0.708(4)	0.115(2)	-0.133(2)	* 0.0395
C(82)	1.091(3)	0.117(3)	-0.166(2)	* 0.0455
C(88)	0.926(4)	0.122(3)	-0.312(2)	* 0.0607
C(89)	1.532(4)	0.226(2)	0.187(2)	* 0.0518
C(211)	0.622(5)	0.431(3)	0.648(2)	* 0.0715
C(491)	1.007(3)	0.425(3)	0.621(2)	* 0.0572
C(561)	0.547(3)	0.432(2)	0.296(2)	* 0.0392
C(601)	1.100(4)	0.299(2)	0.579(3)	* 0.0475
C(641)	0.529(4)	0.440(2)	0.198(2)	* 0.0593
C(931)	0.894(4)	0.416(2)	0.757(2)	* 0.0567

Contd.

C(871)	0.818(4)	0.259(2)	0.374(2)	* 0.0680
C(881)	0.773(4)	0.443(2)	0.215(3)	* 0.0507
C(801)	0.771(5)	0.417(2)	0.795(3)	* 0.0703
C(761)	0.628(4)	0.419(3)	0.733(2)	* 0.0645
C(721)	0.901(4)	0.282(2)	0.467(3)	* 0.0506
C(731)	1.223(4)	0.294(2)	0.657(2)	* 0.0489
C(691)	0.649(4)	0.447(2)	0.168(2)	* 0.0655
C(701)	1.035(4)	0.251(2)	0.509(3)	* 0.0390
C(631)	0.805(4)	0.433(3)	0.307(2)	* 0.0796
C(661)	0.883(4)	0.419(3)	0.665(2)	* 0.0566
C(811)	0.427(3)	0.426(3)	0.343(2)	* 0.0520
C(841)	0.623(4)	0.251(2)	0.573(3)	* 0.0493
C(101)	0.514(5)	0.280(3)	0.496(3)	* 0.0557
C(121)	0.331(4)	0.307(2)	0.380(2)	* 0.0393
C(991)	0.393(4)	0.252(2)	0.451(3)	* 0.0583
C(941)	0.178(5)	0.319(3)	0.314(2)	* 0.1028

III.5.6 Electrochemistry

The electrochemical studies of the present Cu(II) complexes have been done in MeCN using platinum electrode at room temperature. The results of the investigation are summarized in Table III.12.

A. Bis-ligated Cu(II) Complexes

complexes 2 and 2a exhibit two consecutive steps of reduction. The first response is assigned as Cu(II)/Cu(I) redox process and is quasireversible (Figure III.30, Table III.12), as the peak-to-peak separations (ΔE_p) increase with increase in the scan rate (Figure III.30). The separation of the anodic (E_{pa}) and cathodic (E_{pc}) peaks were 120 mV (scan rate 50 mV s^{-1}) and peak current ratios were near unity. The one-electron nature of these reduction processes were confirmed by controlled-potential coulometric measurements. The Cu(II) / Cu(I) reduction potentials are fairly positive. This result implies that the copper(II) state is significantly destabilized in these complexes. It has been well established^{160, 180-182} that for nitrogen donor ligands the following factors influence to destabilize Cu(II) center and hence to raise the Cu(II)/Cu(I) redox potential. They include: (i) reducing ligand field strength around copper(II) by decreasing ligand σ -donor ability, (ii) introduction of alkyl or aryl substituents near the ligand donor site, which effectively results in a more hydrophobic environment, and (iii) use of π -accepting ligands to favor copper(I) state. It is well-known that pyrazoles are poor π -accepting ligands. Moreover, for 2 and 2a due to presence of two axially-ligated MeCN molecules Cu(II)/Cu(I) redox potentials have

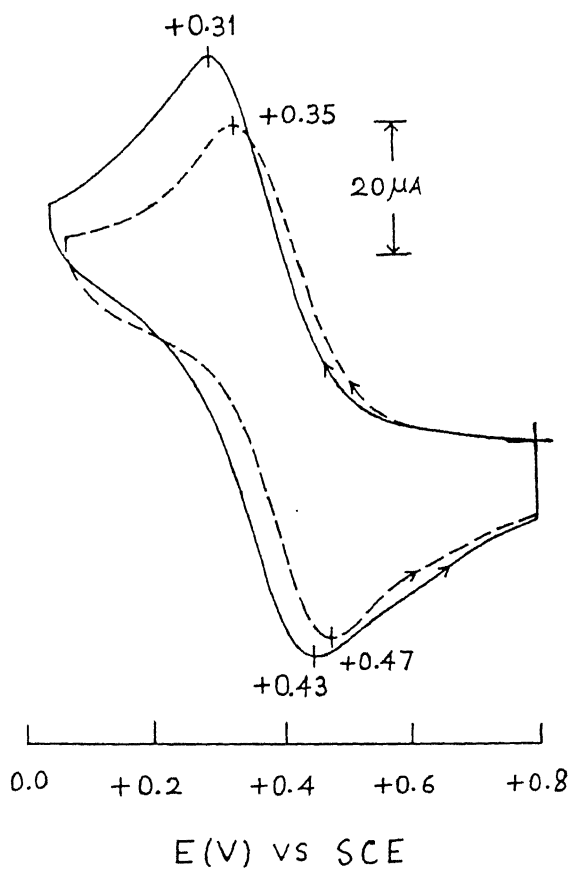


Figure III.30 Cyclic voltammograms (scan rate 50 mV s^{-1}) of $[\text{Cu}(\text{H}_2\text{pp})_2](\text{ClO}_4)_2 \cdot \text{H}_2\text{O}$ (—) and $[\text{Cu}(\text{Me}_2\text{pp})_2](\text{ClO}_4)_2 \cdot \text{H}_2\text{O}$ (---) at platinum electrode in MeCN; supporting electrolyte TBAP

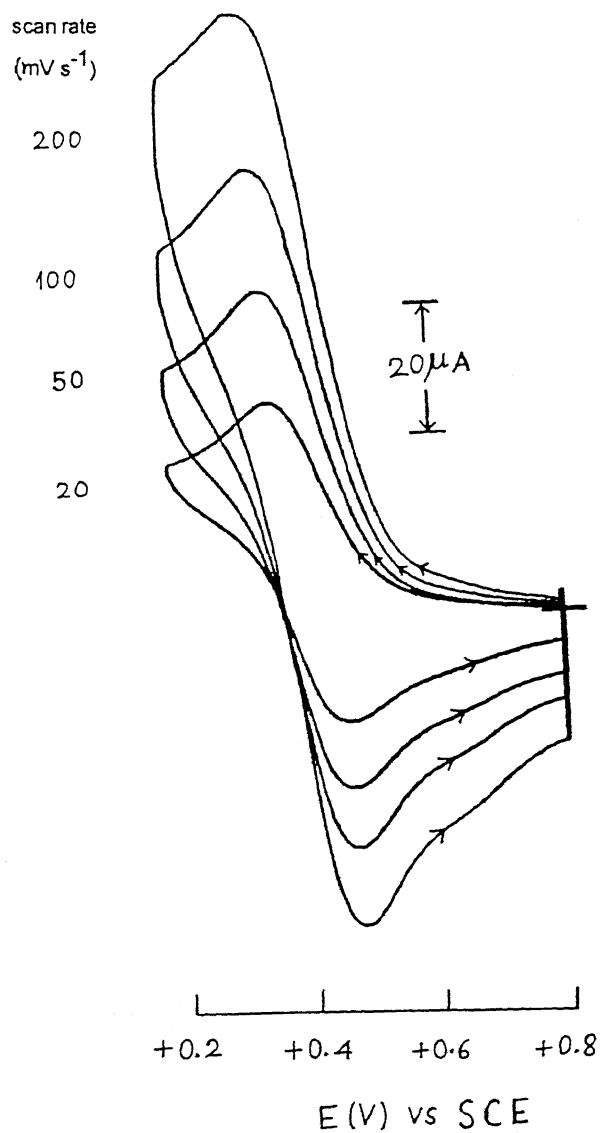


Figure III.30a Variable scan cyclic voltammograms of $[\text{Cu}(\text{Me}_2\text{pp})_2](\text{ClO}_4)_2 \cdot \text{H}_2\text{O}$ in MeCN at platinum electrode; supporting electrolyte TBAP

Table III.12 Electrochemical^a Data for the Copper(II) Complexes

Complex	Cu(II)/Cu(I) couple				Cu(I)/Cu(0) couple
	E_f /V	ΔE_p /mV	E_{pc} /V	E_{pa} /V	E_{pc} /V
[Cu(H ₂ pp) ₂] ⁻ (ClO ₄) ₂ ·H ₂ O	0.37	120	0.31	0.43	-0.52
[Cu(Me ₂ pp) ₂] ⁻ (ClO ₄) ₂ ·H ₂ O	0.41	120	0.35	0.47	-0.56
[Cu(Me ₂ pp) ₃] ⁻ (ClO ₄) ₂	0.40,	100,	0.36	0.46	-0.60
	0.20	240	0.08	0.32	-0.74
[Cu(Me ₂ pp) ₂] ⁻ (Cl)] (ClO ₄)	0.29	180	0.19	0.37	-0.66
[Cu(Me ₂ pp) ₂] ⁻ (NO ₂)] (ClO ₄)	0.01	660	-0.32	0.34	-0.58
[Cu(Me ₂ pp) ₂] ⁻ (SCN)] (ClO ₄)	0.35	160	0.23	0.37	-0.64
[Cu(Me ₂ pp) ₂] ⁻ (N ₃)] (ClO ₄)	0.19	260	0.06	0.32	-0.65

^aIn MeCN at 298 K

further been increased. Another interesting result is the observed small but measurable shift (30 mV) in the $E_{1/2}$ values of 2 and 2a. The more positive values for 2 and 2a are due to steric and/or "environment" effect.^{86-88,91,183}

The second redox process (Table III.12) is due to Cu(I)/Cu(0) process and is irreversible. The electrogenerated Cu(0) species gets adsorbed on the electrode surface, as is evident during re-oxidation step.

B. Axially Ligated Five-Coordinate Copper(II) Complexes

The purpose of electrochemical studies of these Cu(II) complexes was to investigate the sensitivity of the Cu(II)/Cu(I) redox potentials with change in the donor strength of the axial ligands. The voltammetric behavior of the complexes are presented in Figures III.31 - III.35.

Cyclic voltammograms of 1 clearly show (Figure III.31) that its third ligand (ligated axially as monodentate) is dissociated in solution. This explains why 1 forms bluish-green solution in MeCN. Thus we observe two Cu(II)/Cu(I) responses: one for the violet complex (2) and the other for the penta-coordinate green complex (1).

For 4, 5 and 6 the Cu(II)/Cu(I) reduction potentials are quite negative compare to their parent complex 2 (Table III.10) which indicates that axially ligated anions favour the stabilization of the Cu(II) state. For 6 an oxidative irreversible wave suggests oxidation of coordinated azide group (Figure III.34).

No distinct correlation between the Cu(II)/Cu(I) potentials and the nature of X^- has been achieved. For all the five-

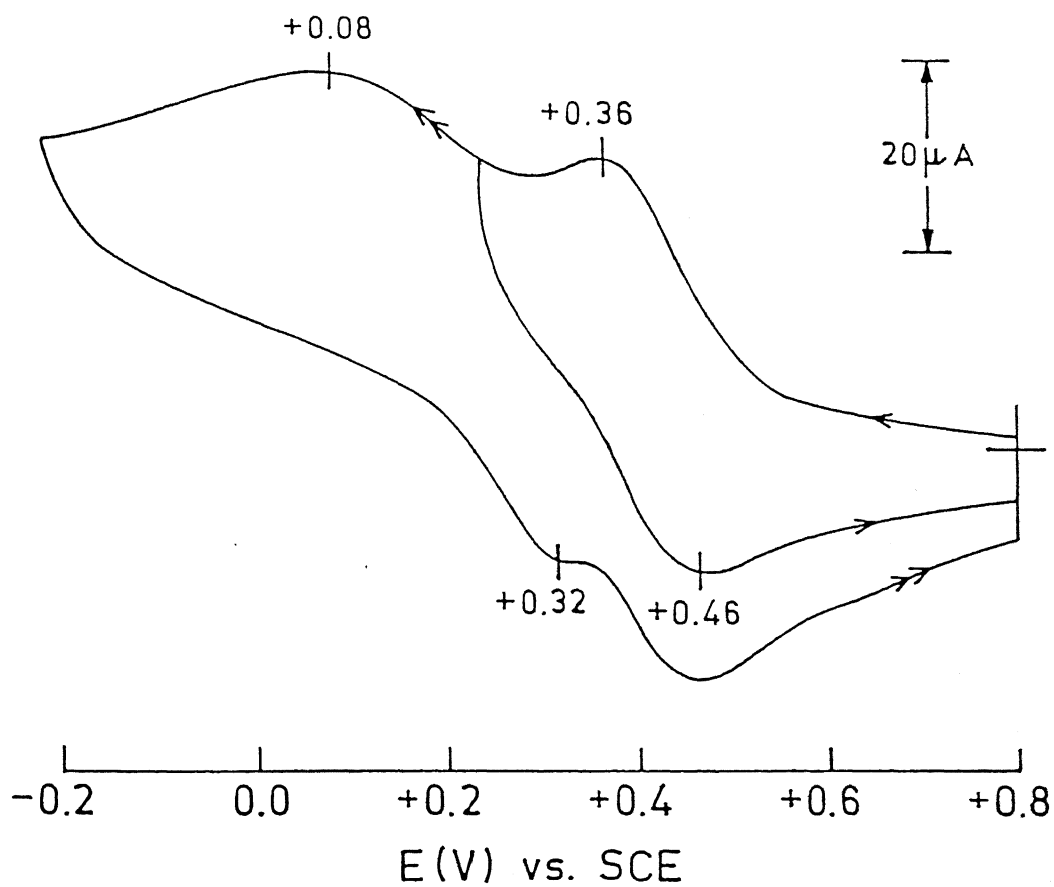


Figure III-31 Cyclic voltammograms (scan rate 50 mV s^{-1}) of $[\text{Cu}(\text{Me}_2\text{pp})_3]-(\text{ClO}_4)_2$ in MeCN at a platinum electrode ; supporting electrolyte TBAP

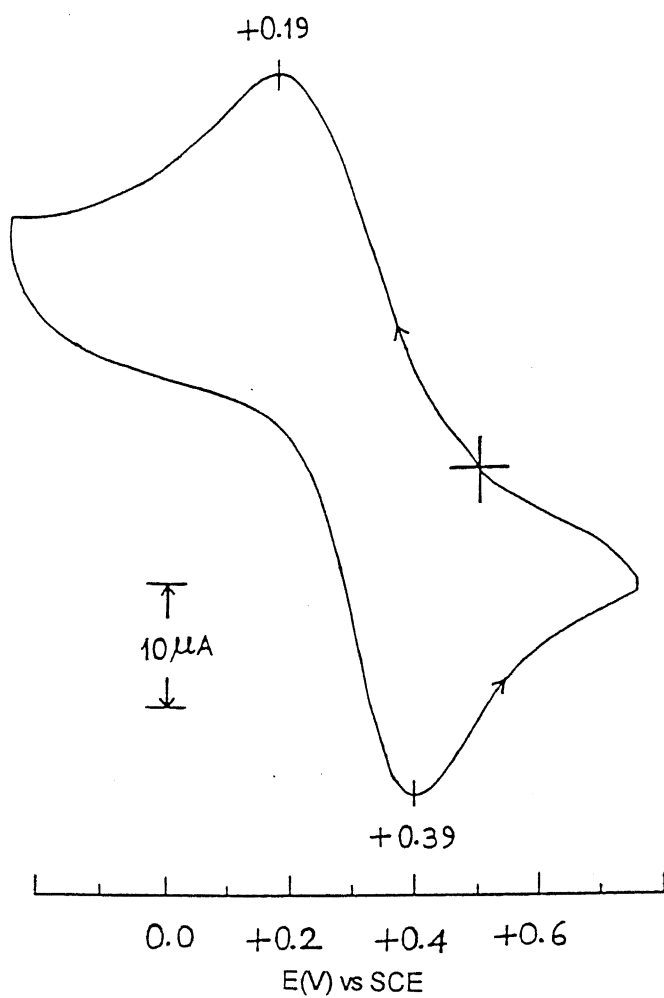


Figure III.32 Cyclic voltammogram (scan rate 50 mV s^{-1}) of $[\text{Cu}(\text{Me}_2\text{pp})_2(\text{Cl})](\text{ClO}_4)$ at platinum electrode in MeCN; supporting electrolyte TBAP

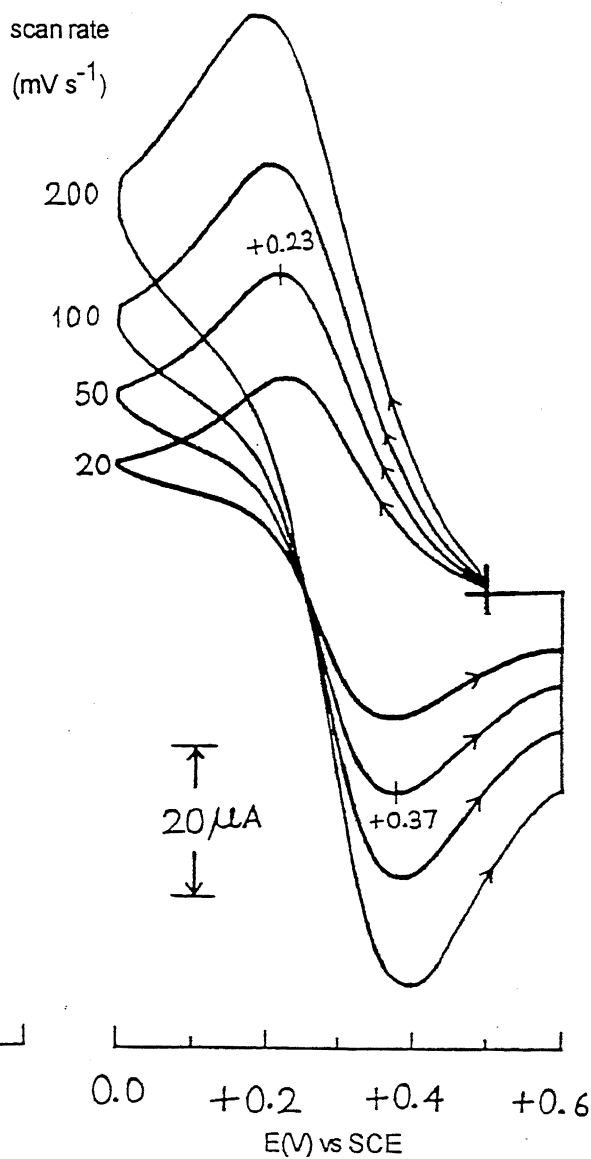


Figure III.33 Cyclic voltammograms of $[\text{Cu}(\text{Me}_2\text{pp})_2(\text{SCN})](\text{ClO}_4)$ in MeCN at platinum electrode; supporting electrolyte TBAP

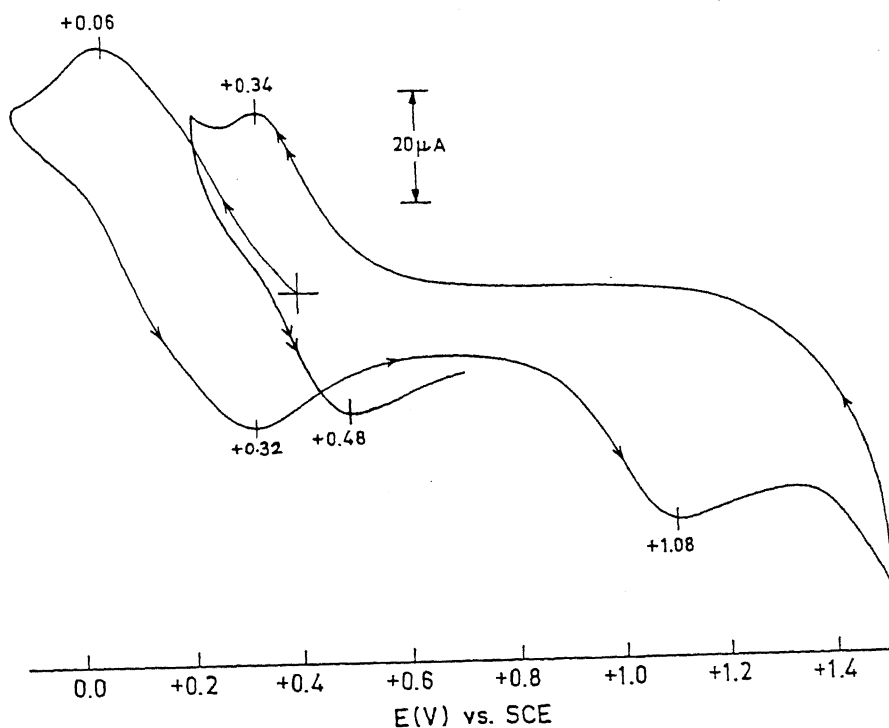


Figure III.34 Cyclic voltammogram (scan rate = 50 mV s^{-1}) of $[\text{Cu}(\text{Me}_2\text{ppz})_2(\text{N}_3)](\text{ClO}_4)$ at platinum electrode in MeCN; supporting electrolyte TBAP

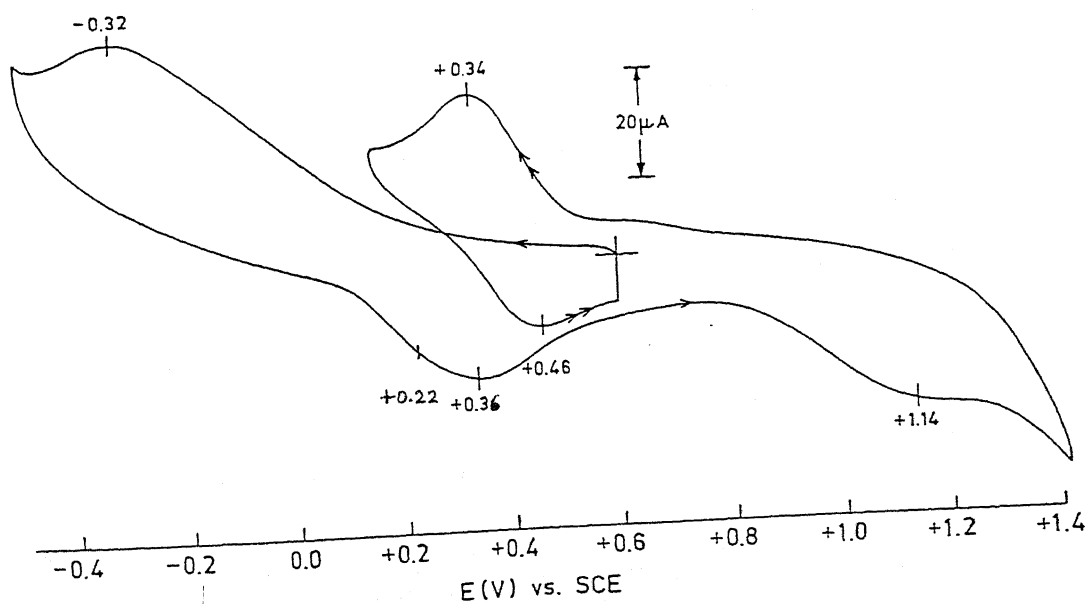


Figure III.35 Cyclic voltammogram (scan rate 50 mV s^{-1}) of $[\text{Cu}(\text{Me}_2\text{ppz})_2(\text{NO}_2)](\text{ClO}_4)$ at platinum electrode in MeCN; supporting electrolyte TBAP

coordinate complexes Cu(I)/Cu(0) process (Table III.12) occurs at moderately negative potential and is irreversible. The electrogenerated Cu(0) species gets adsorbed on the electrode surface, as is evidenced during re-oxidation step. The anodic stripping of the adsorbed Cu(0) species is observed in the -0.2 to -0.4 V range.

C. Redox Properties of $[\text{Cu}(\text{Me}_2\text{pp})_2(\text{NO}_2)](\text{ClO}_4)$ (3)

The electrochemistry of the nitrito complex 3 was thoroughly investigated to extract information regarding its use as a model for the copper containing nitrite reductases.

In MeCN solution 3 exhibit electrochemically irreversible ($E_{\text{pc}} = -0.32$ V) one-electron reduction (Table III.12, Figure III.35). The overlapping re-oxidative responses at 0.22 and 0.36 V could be due to O-bound and N-bound (copper(I)-nitrite species formed at the electrode surface) respectively. In fact, Tolman et al. have documented that their copper(I) model complex is N-bound^{95b} and it is expected to be so for its transformation to NO bound species. When the anodic scanning is continued further an irreversible response at 1.14 V is observed (Figure III.35). On scan reversal at 1.4 V, a well-behaved cyclic response at $E_{1/2} = 0.40$ V is identified (Figure III.35). This couple is due to the Cu(II)/-Cu(I) redox process for complex 2 (Table III.12). This behavior implies that complex 2 is generated at the electrode surface due to the irreversible oxidation of nitrite ion bound to copper(II). It has been shown that NO_3^- ion does not bind to complex 2. The one-electron nature of Cu(II)/Cu(I) reduction of 3 was confirmed by controlled potential coulometry at -0.5 V. Interestingly,

reduced solutions of 3 exhibit almost identical behavior (the oxidative response becomes broad and it is seen at ~ 0.6 V). This could be due to oxidation of N-bound NO_2^- . Coulometric re-oxidation of the reduced solutions give back the starting complex quantitatively, implying that the redox process is chemically reversible.

Two main results emerge from these experiments.

(i) Potential for nitrite-bound Cu(II)/Cu(I) couple of 3 is more negative (~ 700 mV) than the solvent bound couple of 2. This is the first observation of this effect for a nitrite-bound copper(II) model complex. (ii) The nitrite ion remains bound to the copper(I) state, probably as N-bound.

Thus the electrochemical behavior of 3 clearly demonstrates that this complex serves as a good model for the copper containing nitrite reductases.

III.6 Conclusions

(i) Syntheses of a number of Cu(II) complexes having effectively CuN_4 and $\text{CuN}_4(\text{X})$ coordination have been achieved using two pyrazolylmethylpyridine ligands H_2pp and Me_2pp , in a comparatively straightforward manner.

(ii) Various geometries namely tetragonal, distorted square pyramidal, and distorted trigonal bipyramidal have been identified by absorption and EPR spectral measurements.

(iii) Steric hindrance exerted by two methyl substituents at 3- and 5- positions of pyrazole ring of the ligand Me_2pp is reflected in electronic spectral studies (Table III.2). Moreover, predominance of steric effect over electronic effect is

indicated from the longer Cu(II)-N(pyrazole) distances compared to Cu(II)-N(pyridine) distances in the structure of nitrito- and thiocyanato- complexes.

(iv) For the first time the structure of a nitrite-bound mononuclear copper(II) complex having both pyridine and pyrazole donors has been determined. Thus 3 can be considered as a structural model for the copper containing nitrite reductases. Electrochemical experiments on this complex reveal that the nitrite ion remains bound during redox interconversions (Cu(II) to Cu(I) to Cu(II)) studies and thus the electrode process Cu(II)/Cu(I) is chemically reversible. This observation clearly demonstrates that 3 serves also as a functional model for the above-mentioned enzymes.

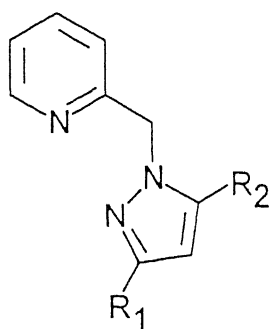
CHAPTER IV

Five-Coordinate Cu(II) Complexes Using Pyrazolylmethylpyridine and Bis(pyrazolylmethyl)pyridine Ligands: Synthesis, Structure, and Redox Properties

In the previous chapter (chapter III) the effect of methyl substituents at the 3- and 5- positions of pyrazole rings in the two bidentate ligands H_2pp and Me_2pp has been explored in terms of geometry and stereochemistry of the bis-ligated and penta-coordinated Cu(II) complexes.

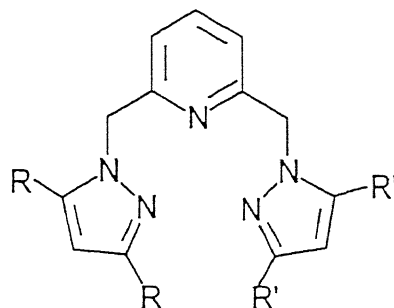
In continuation with the work described in chapter III in the present chapter an interesting chemistry of two mononuclear $Cu^{II}N_5$ complexes using pyrazolylmethylpyridine and bis(pyrazolylmethyl)pyridine ligands (R_2pp (I, II); R_4bpp (III, IV)) is described.

To our knowledge, there are only five structurally characterized complexes of this type and the nature of ligands used in these complexes is closely similar. The complexes are: $[Cu(appn)(dpa)]^{2+}$, ¹⁸⁴ $[Cu(appn)(bpy)]^{2+}$, ¹⁸⁴ $[Cu(dien)(bpy)]^{2+}$, ¹⁸⁵ $[Cu(dien)(phen)]^{2+}$, ¹⁸⁵ and $[Cu(dien)(dpa)]^{2+}$ ¹⁸⁶ [appn = N-(3-aminopropyl)-1,3-propanediamine, dpa = di-2-pyridylamine, bpy = 2,2'-bipyridine, dien = diethylenetriamine, phen = 1,10-phenanthroline].



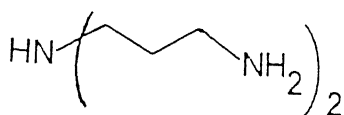
$R_1 = R_2 = H$, H_2bpp (I)

$R_1 = R_2 = Me$, Me_2bpp (II)

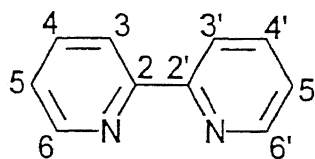


$R = R' = H$, H_4bpp (III)

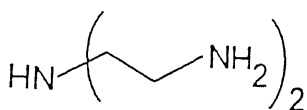
$R = R' = Me$, Me_4bpp (IV)



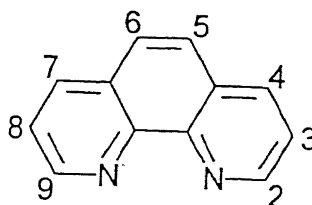
dppn



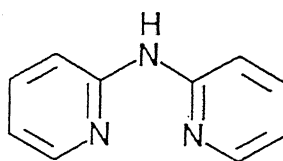
bpy



dien



phen



dpa

IV.1 Experimental Section

IV.1.1 Solvents and Reagents

Details of solvent purification are described in chapter II (Section II.1.1).

IV.1.2 Measurements

Details of spectroscopic measurements are given in chapter II (Section II.1.2).

IV.2 Synthesis of Ligands

Syntheses of the ligands H_2pp and Me_2pp are already described in chapter II.

IV.2.1 2,6-bis(pyrazol-1-ylmethyl)pyridine (H_4bpp)³⁹

A mixture of 2,6-bis(chloromethyl)pyridine hydrochloride (2.50 g, 0.012 mol), pyrazole (1.60 g, 0.024 mol), benzene (350 mL), 40% aqueous sodium hydroxide (60 mL) and 40% aqueous tetra-n-butylammonium hydroxide (30 drops) were refluxed with stirring for 8 h and then stirred at 298 K for 12 h. The organic layer was separated, dried over anhydrous sodium sulphate and evaporated under reduced pressure to yield H_4bpp as an oil (yield 2.54 g, 90%). 1H NMR; δ (ppm): 7.5 (m, 5H), 6.8 (d, $J = 8.0$ Hz, 2H), 6.2 (t, $J = 2.0$ Hz, 2H), and 4.5 (s, 4H).

IV.2.2 2,6-bis(3,5-dimethylpyrazol-1-ylmethyl)pyridine (Me_4bpp)

This ligand was prepared following a similar procedure as described for H_4bpp using 3,5-methylpyrazole instead of pyrazole (yield, 90%) (mp 115 $^{\circ}$ C). 1H NMR; δ (ppm): 7.4 (q, $J = 7.5$ Hz, 1H), 6.6 (d, $J = 8.0$ Hz, 2H), 5.9 (s, 2H), 5.3 (s, 4H), 2.3 (s, 6H), and 2.2 (s, 6H) (Figure IV.1).

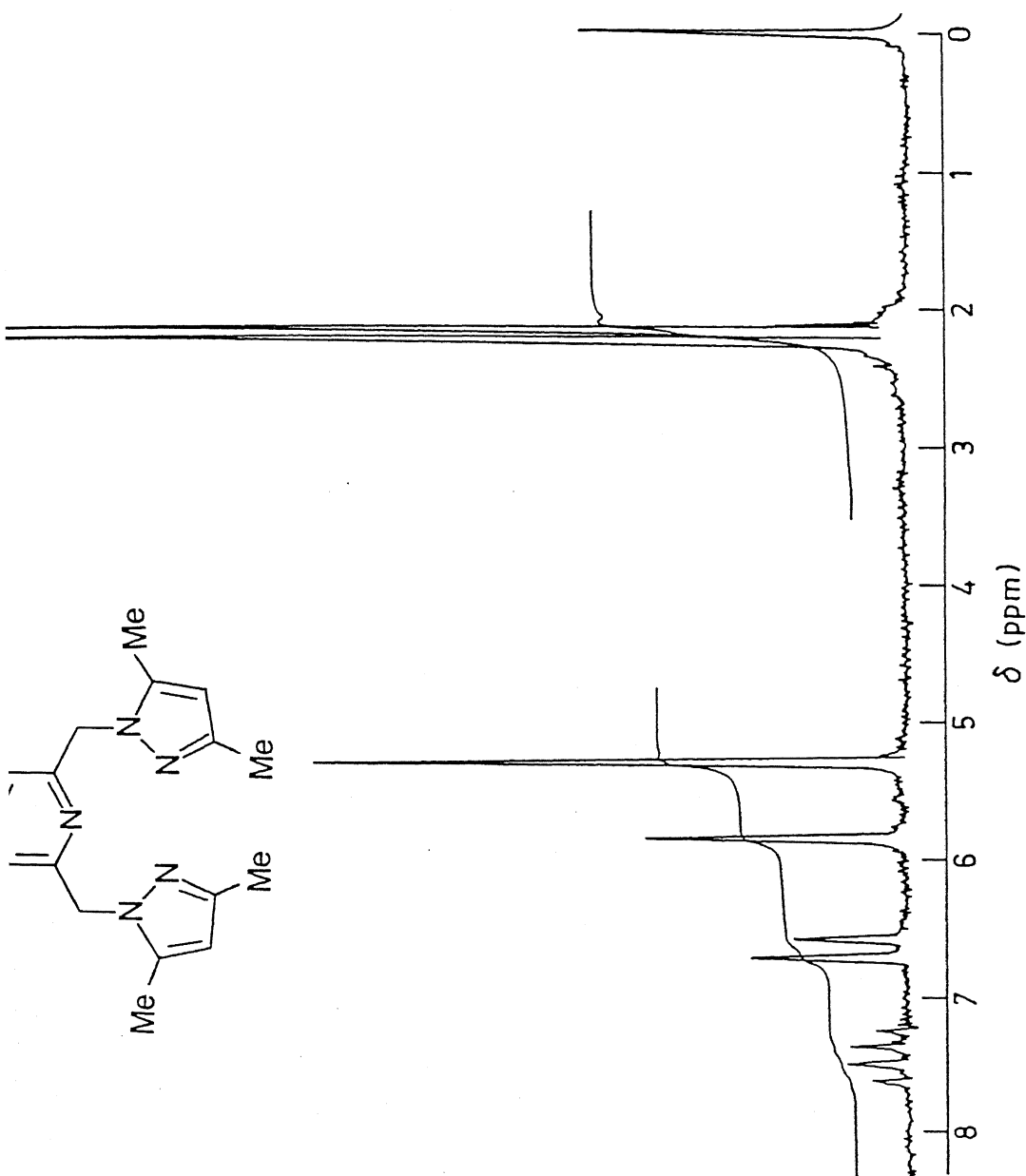


Figure IV.1 ^1H NMR spectrum of 2,6-bis(3,5-dimethylpyrazol-1-yl)-1-methylpyridine (Me_4bpp) in CDCl_3

IV.3 Synthesis of the Complexes

IV.3.1 $[\text{Cu}(\text{H}_2\text{pp})(\text{H}_4\text{bpp})](\text{ClO}_4)_2$ (1)

To an aqueous solution (2 mL) of $[\text{Cu}(\text{H}_2\text{O})_6](\text{ClO}_4)_2$ (0.1 g, 0.27 mmol) was added a methanolic solution of H_4bpp (0.065 g, 0.27 mmol) while stirring the solution at room temperature. The resulting solution turned blue. Stirring was continued for a further 10 min. A methanolic solution (2 mL) of H_2pp (0.043 g, 0.29 mmol) was added to the resulting reaction mixture. The resulting solution thus obtained was allowed to stand for slow evaporation overnight at room temperature. Blue crystals thus obtained were washed with water once and finally dried in air. Yield (0.15 g, 84%).

IV.3.2 $[\text{Cu}(\text{Me}_2\text{pp})(\text{Me}_4\text{bpp})](\text{ClO}_4)_2$ (2)

This complex was prepared following a similar procedure as that of complex 1 using appropriate ligands. Yield (0.12 g, 60%). Unlike the complex 1 it is green in color.

IV.3 X-ray Data Collection, Structure Solution and Refinement

The single crystal suitable for X-ray diffraction studies were grown by slow evaporation of an aqueous MeOH solution of 2. Crystals of the complex were mounted on a glass fiber. Preliminary examination and data collection were performed on a Enraf Nonius CAD4 Mach diffractometer fitted with a graphite monochromator (λ (MoK_α) = 0.71073 Å, θ -2 θ mode, $2\theta_{\text{max}} = 50^\circ$). Data at 293 K were collected at this Department, Indian Institute of Technology, Kanpur, India.

Cell constant and the orientation matrix for data collection were obtained from least-squares refinements, using the

setting angles of 25 reflections in the range $16 < 2\theta < 30$. Experimental details of crystal data, intensity measurements, structure solution, and refinement were given in Table IV.1. Other details are same as that describe in previous chapter.

The Structure was solved by direct methods and successive Fourier syntheses and refined by a full-matrix least-squares procedure on F , minimizing the function $\sum w(|F_o| - |F_c|)^2$. Of the 3492 measured reflections 2495 with $I > 3\sigma(I)$ were used in the analyses. One of the perchlorates was found to be severely disordered. For this approximately tetrahedral perchlorate ion, the apical oxygen atom was unique, but the remaining three oxygens were disordered over two positions, with 0.70 and 0.30 occupancy. With the model used the structure converged satisfactorily. Chiralities for the noncentrosymmetric structures were assigned on the basis of refinements in each enantiomorph. Non-hydrogen atoms except those of perchlorate oxygens were refined with anisotropic thermal parameters. Hydrogens were added in calculated positions and included without refinements with fixed isotropic thermal parameters. Six reflections (hkl : 0,0,6; 0,5,4; 0,6,0; 0,3,13; 2,1,15; 3,2,0) were omitted in the final stages of refinement as the peak profiles were extremely broad. These erroneous reflections were probably caused by the quality of crystal chosen for data collection. Some of the C-C [C(6)-C(7), C(7)-C(8), C(19)-C(20), C(20)-C(21)] and C-N [C(9)-N(3), C(22)-N(6)] bonds of the pyridine rings of both the ligands were restrained to have reasonable bond distances. Additionally, one bond N(2)-C(4) of the tridentate ligand and a perchlorate Cl(2)-O(7a) bond were restrained for the same reasons. At convergence $R = 0.074$ and $R_w =$

Table IV.1

EXPERIMENTAL DETAILS

A. CRYSTAL DATA

Empirical Formula	$\text{CuCl}_2\text{O}_8\text{N}_8\text{C}_{28}\text{H}_{34}$
Formula Weight	744.6
Crystal Colour, Habit	Green, block shaped
Crystal dimensions (mm^3)	0.5 x 0.4 x 0.3
Crystal System	Orthorhombic
No. of reflections used for unit cell determination (2θ range)	25 reflections ($16 < 2\theta < 30$)
Lattice parameters	$a = 9.582(4)$, $b = 11.937(4)$ $c = 29.147(6) \text{ \AA}$, $\alpha = \beta = \gamma = 90.00^\circ$ $V = 3333.82(1.74) \text{ \AA}^3$
Space Group	$P2_12_12_1$ (No. 19)
Z value	4
D_{calc} (g cm^{-3})	1.484
F_{000}	1539.7
$\mu(\text{MoK}\alpha)$ (mm^{-1})	0.88
Transm Coef	0.7708-0.7721

B. INTENSITY MEASUREMENTS

Diffractometer	Cad4Mach
Radiation	$\text{MoK}\alpha$ ($\lambda = 0.71073 \text{ \AA}$)
Temperature	293K
Scan Type	θ - 2θ
Scan Rate	variable
Scan Width	$1.0 + 0.35 \tan \theta$
2θ range (deg)	2 - 50
No. of reflections measured ($2 < 2\theta < 50$)	3492
No. of unique reflections	3291
Corrections	L_p , absorption (analytical)

C. STRUCTURE SOLUTION AND REFINEMENT

Structure Solution	Direct Method
Refinement	Full matrix, least squares
Function minimized	$\sum w(F_o - F_c)^2$
Anomalous dispersion	applied (for non H atoms)
No. of observations ($I > 3\sigma(I)$)	2495
No. of variables	396
Reflection/Parameter ratio	6.300
Residuals: $R; R_w$	0.074; 0.073
Goodness of fit indicator	5.315
Max shift/error in final cycle	0.3108×10^{-2}
Avg shift/error in final cycle	0.1481×10^{-3}
Maximum peak in final diff. map (e \AA^{-3})	0.96 near Cl(1)
Minimum peak in final diff. map (e \AA^{-3})	-0.91

0.073. The highest peak in the difference map was $0.96 \text{ e}\text{\AA}^{-3}$ near one disordered perchlorate oxygen.

IV.4 Results and Discussion

IV.4.1 Synthesis and characterization

The Cu(II) complexes were readily synthesized by the stoichiometric reaction of Cu(II) perchlorate hexahydrate with aqueous methanolic solutions of the appropriate ligands.

Microanalytical data (Table IV.2) confirm to the proposed formulations of 1 and 2. For 1 and 2 in the IR spectra characteristic ionic perchlorate absorptions were observed: $\nu(\text{ClO}_4^-)$ at 1105, 620; 1090, 620 cm^{-1} respectively. Solution electrical conductivity^{129a} data (Table IV.3) together with IR data suggest the proposed formulations of 1 and 2 are correct. Acetonitrile solution of the complex 1 is blue whereas MeCN solution of 2 is bluish green. The complex 1 is comparatively less soluble in MeCN. The magnetic moment of 1 in MeCN solution and the moments for 2 in the solid-state as well as in MeCN solution are $\sim 1.80 \mu_{\text{B}}$ (Table IV.3) which fall within the range $1.80\text{--}2.00 \mu_{\text{B}}$ found for other copper(II) complexes in a magnetically dilute environment.¹⁶⁵

Table IV.2: Microanalytical data of Copper(II) Complexes

Complexes	Empirical Formula	Analysis ^a		
		%C	%H	%N
[Cu(H ₂ pp) - (H ₄ bpp)] (ClO ₄) ₂	C ₂₂ H ₂₂ Cl ₂ N ₈ O ₈ Cu	39.68 (39.96)	3.41 (3.33)	16.67 (16.95)
[Cu(Me ₂ pp) - (Me ₄ bpp)] (ClO ₄) ₂	C ₂₈ H ₃₄ Cl ₂ N ₈ O ₈ Cu	45.22 (45.13)	4.91 (4.84)	15.10 (15.04)

^aCalculated values in parentheses

Table IV.3 Molar Conductance, Magnetic Moment and Electronic Spectral Data of Copper(II) Complexes in MeCN at 298 K.

Complexes	Λ_M^a ($\Omega^{-1} \text{cm}^2 \text{mol}^{-1}$)	μ_{eff} (B.M.) ^b	λ , nm (ϵ , $\text{M}^{-1} \text{cm}^{-1}$)
[Cu(H ₂ pp) - (H ₄ bpp)] (ClO ₄) ₂	250	1.84	870(sh) (20), 615(65), 320(sh) (915), 267(sh) - (9 800), 261(11 050) (885(sh), 603, 335(sh), 275) ^c
[Cu(Me ₂ pp) - (Me ₄ bpp)] (ClO ₄) ₂	300	1.80 (1.77)	900(sh) (25), 621(100), 350(sh) (735), 258(sh) - (10 200) (900(sh), 633, 375(sh), 275) ^c

^aExpected range for 1:1 and 1:2 electrolytes in MeCN are 120-160 and 220-300 $\Omega^{-1} \text{cm}^2 \text{M}^{-1}$ ^bRoom temperature solid state values are in parentheses^cSolid state (paraffin oil) values

IV.4.2 Absorption spectra

The visible spectra of the polycrystalline complexes were obtained in paraffin oil (Table IV.3). Each complex displays a broad band centred at ~ 630 nm with a shoulder at ~ 900 nm and are typical of square-pyramidal copper(II) complexes with nitrogen donors.¹⁶⁵ In MeCN solution a similar spectral feature (Figures IV.2 and IV.3; Table IV.3) was observed, demonstrating that the solid-state structures are retained in solution.

IV.4.3 EPR spectral studies

Complexes 1 and 2 exhibit EPR spectra of axial symmetry: $g_{\parallel} > g_{\perp} > 2.00$; (Figure IV.4); Table IV.4). This behaviour is typical of square-pyramidal copper(II) complexes with $d_{x^2-y^2}$ ground state.¹⁶⁵ Simulated spectrum of 2 is also shown in Figure IV.4). The EPR spectral parameters used in simulation are: $g_{\parallel} = 2.245$, $g_{\perp} = 2.062$, $A_{\parallel} = 175$ G, and linewidths (G) = 42 (L_x), 38 (L_y), and 35 (L_z).

IV.4.4 Description of the structure of 2 (Table IV.6)

(a) The Metal Atom Stereochemistry. The molecular structure consists of discrete five-coordinate $[\text{Cu}(\text{Me}_4\text{bpp})(\text{Me}_2\text{pp})]^{2+}$ cations and two perchlorate anions. Figure IV.5 provides a perspective view of the cationic part. The structure reveals that the copper(II) ion is surrounded by three pyrazole nitrogens and two pyridine nitrogens. The geometry around copper(II) is best described as square pyramidal with a very small trigonal-bipyramidal component, considering the structural index τ ($= 0.16$) for the five-coordinate geometry, as described in chapter III (section III.5.4) (Table IV.5). Four nitrogens from the pyrazole

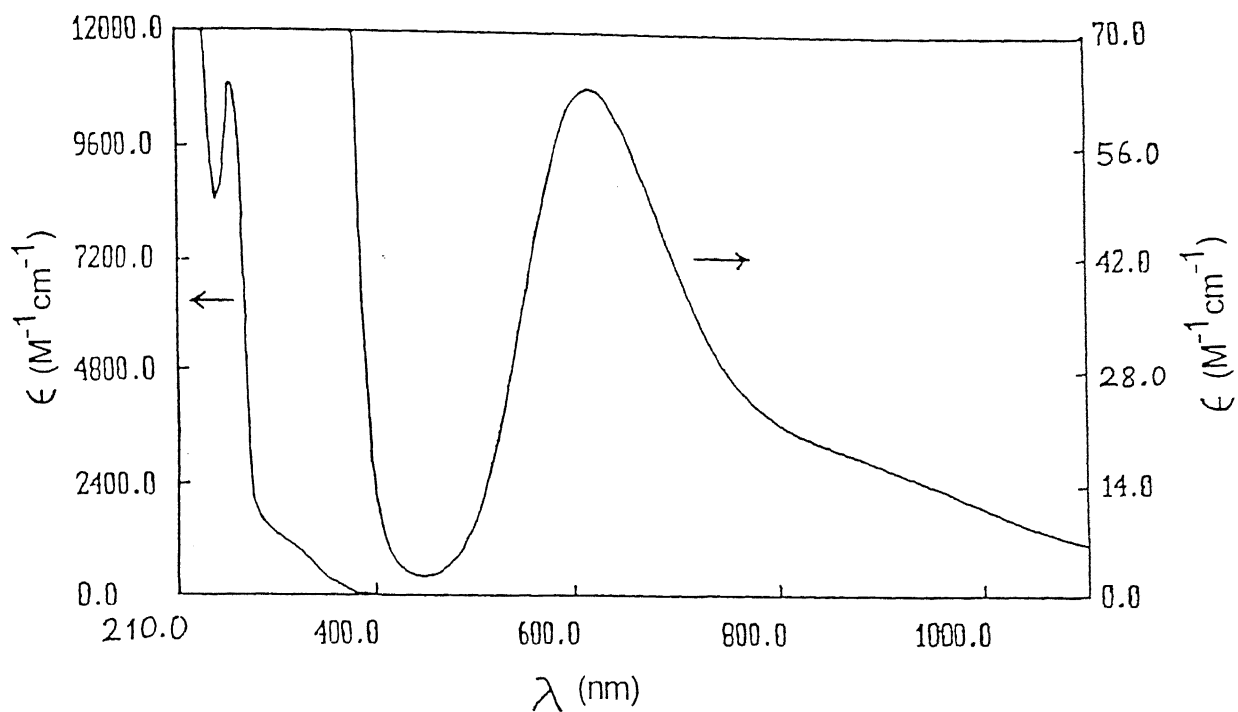


Figure IV. 2 Electronic Spectrum of $[Cu(H_2pp)(H_4bpp)](ClO_4)_2$ in MeCN

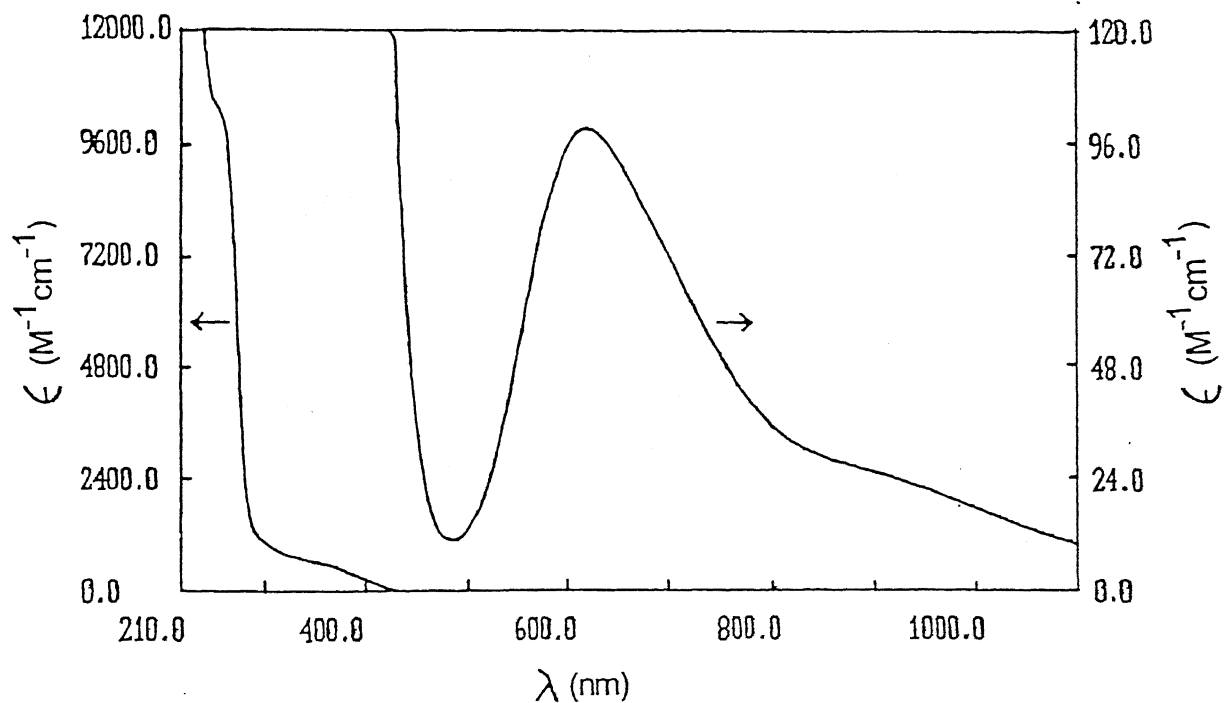


Figure IV. 3 Electronic Spectrum of $[Cu(Me_2pp)(Me_4bpp)](ClO_4)_2$ in MeCN

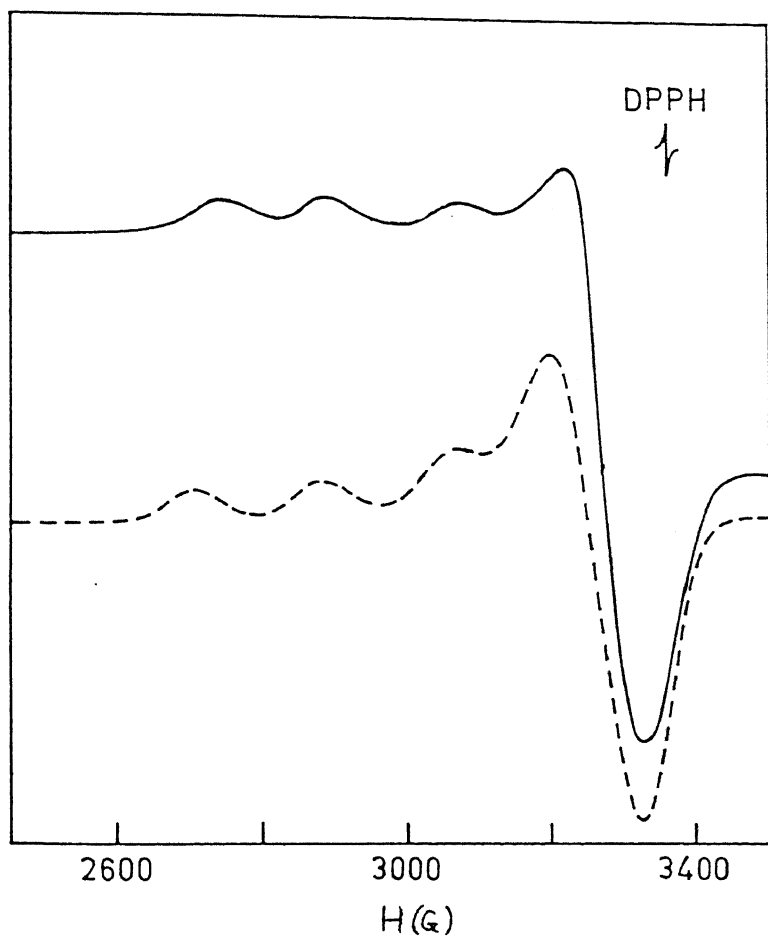


Figure IV.4 EPR spectrum of $[\text{Cu}(\text{Me}_2\text{pp})(\text{Me}_4\text{bpp})](\text{ClO}_4)_2$ in frozen (80K) MeCN solution (—), along with simulated spectrum (----) .

Table IV.4 X-Band EPR Spectral Data

Complex	g_{11}	g_{\perp}	g_{av}^d	A_{11} (G)
[Cu(H ₂ pp) - (H ₄ bpp)] (ClO ₄) ₂ ^a	2.256	2.062	2.129	175
	2.264 ^b	2.057 ^b	2.128 ^b	170 ^b
[Cu(Me ₂ pp) - (Me ₄ bpp)] (ClO ₄) ₂ ^c	2.245	2.062	2.124	175

^aPolycrystalline powder form (298 K)^bDMF solution (80 K)^cMeCN solution (80 K)

$$g_{av}^d = (1/3(g_{11}^2 + 2g_{\perp}^2))^{1/2}$$

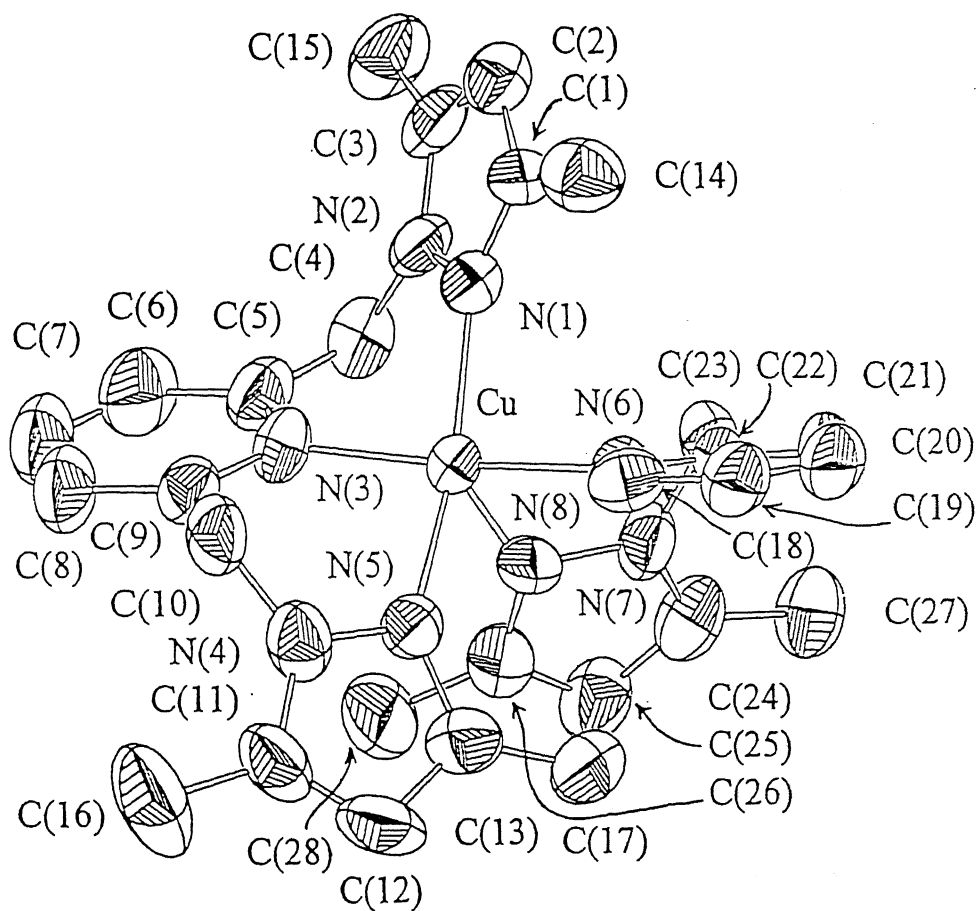


Figure IV.5 ORTEP diagram of $[\text{Cu}(\text{Me}_2\text{pp})(\text{Me}_4\text{bpp})](\text{ClO}_4)_2$ showing the 50% probability thermal ellipsoids and atom labeling scheme

Table IV.5 Selected Bond Lengths (Å) and Angles (deg) in the cationic part of $[\text{Cu}(\text{Me}_2\text{pp})(\text{Me}_4\text{bpp})](\text{ClO}_4)_2$ (2)

Cu-N(1)	2.04 (1)	Cu-N(3)	2.071 (9)
Cu-N(5)	2.03 (1)	Cu-N(6)	2.021 (9)
Cu-N(8)	2.22 (1)		
N(1)-Cu-N(3)	89.5 (4)	N(3)-Cu-N(5)	85.5 (4)
N(1)-Cu-N(5)	164.4 (4)	N(6)-Cu-N(8)	86.9 (4)
N(1)-Cu-N(6)	91.0 (4)	N(1)-Cu-N(8)	94.0 (4)
N(3)-Cu-N(6)	173.7 (4)	N(3)-Cu-N(8)	99.3 (4)
N(5)-Cu-N(6)	92.4 (4)	N(5)-Cu-N(8)	101.4 (4)

Table IV.6

Atomic Positional, Isotropic Displacement and Site Occupation Parameters

	x/a	y/b	z/c	U	PP
Cu	0.5474 (2)	0.5101 (1)	0.38741 (5)	* 0.0484 (4)	
Cl (1)	0.1276 (5)	0.4903 (4)	0.4548 (2)	* 0.095 (2)	
Cl (2)	1.0204 (5)	0.9378 (4)	0.3475 (2)	* 0.089 (2)	
O (1)	0.266 (1)	0.516 (1)	0.4437 (4)	0.102 (3)	
O (2)	0.109 (1)	0.372 (1)	0.4582 (4)	0.121 (4)	
O (3)	0.035 (2)	0.537 (1)	0.4246 (5)	0.167 (6)	
O (4)	0.115 (2)	0.543 (1)	0.4996 (6)	0.205 (8)	
O (5)	0.932 (2)	1.006 (1)	0.3733 (6)	0.191 (6)	
O (6)	1.066 (2)	0.842 (2)	0.3719 (7)	0.134 (8)	0.7000
O (6a)	1.027 (4)	0.879 (3)	0.389 (1)	0.09 (1)	0.3000
O (7)	1.147 (2)	1.003 (2)	0.3463 (7)	0.135 (6)	0.7000
O (7a)	1.116 (2)	0.972 (2)	0.3146 (8)	0.051 (7)	0.3000
O (8)	0.941 (2)	0.879 (2)	0.3128 (7)	0.154 (8)	0.7000
O (8a)	0.912 (3)	0.993 (3)	0.326 (1)	0.09 (1)	0.3000
N (1)	0.415 (1)	0.486 (1)	0.3334 (3)	* 0.060 (4)	
N (2)	0.323 (1)	0.5667 (9)	0.3223 (4)	* 0.065 (5)	
N (3)	0.536 (1)	0.6814 (7)	0.3766 (3)	* 0.051 (4)	
N (4)	0.729 (1)	0.6348 (8)	0.4505 (4)	* 0.055 (4)	
N (5)	0.631 (1)	0.5503 (8)	0.4492 (4)	* 0.058 (4)	
N (6)	0.541 (1)	0.3453 (7)	0.4030 (3)	* 0.051 (4)	
N (7)	0.821 (1)	0.3865 (9)	0.3621 (4)	* 0.062 (4)	
N (8)	0.738 (1)	0.4723 (8)	0.3467 (3)	* 0.056 (4)	
C (1)	0.411 (1)	0.412 (1)	0.2973 (5)	* 0.067 (6)	
C (2)	0.315 (2)	0.452 (1)	0.2656 (5)	* 0.085 (7)	
C (3)	0.262 (2)	0.552 (1)	0.2797 (6)	* 0.078 (7)	
C (4)	0.298 (1)	0.658 (1)	0.3542 (4)	* 0.062 (5)	
C (5)	0.423 (1)	0.729 (1)	0.3585 (4)	* 0.053 (5)	
C (6)	0.419 (2)	0.840 (1)	0.3459 (5)	* 0.083 (7)	
C (7)	0.531 (2)	0.904 (1)	0.3550 (5)	* 0.080 (6)	
C (8)	0.648 (2)	0.856 (1)	0.3739 (6)	* 0.088 (7)	
C (9)	0.651 (1)	0.745 (1)	0.3859 (5)	* 0.061 (5)	
C (10)	0.771 (2)	0.691 (1)	0.4079 (5)	* 0.061 (6)	
C (11)	0.769 (2)	0.655 (1)	0.4942 (5)	* 0.069 (6)	
C (12)	0.703 (2)	0.579 (1)	0.5201 (5)	* 0.071 (6)	
C (13)	0.618 (1)	0.517 (1)	0.4936 (4)	* 0.055 (5)	
C (14)	0.499 (2)	0.310 (1)	0.2943 (5)	* 0.099 (7)	
C (15)	0.156 (2)	0.628 (1)	0.2616 (7)	* 0.128 (9)	
C (16)	0.878 (2)	0.741 (1)	0.5051 (6)	* 0.092 (6)	
C (17)	0.523 (2)	0.428 (1)	0.5073 (5)	* 0.083 (6)	
C (18)	0.413 (1)	0.299 (1)	0.4091 (4)	* 0.062 (6)	
C (19)	0.394 (2)	0.189 (1)	0.4218 (5)	* 0.076 (6)	
C (20)	0.512 (2)	0.128 (1)	0.4313 (5)	* 0.091 (8)	
C (21)	0.643 (2)	0.173 (1)	0.4248 (5)	* 0.071 (6)	
C (22)	0.659 (1)	0.283 (1)	0.4114 (4)	* 0.053 (5)	
C (23)	0.795 (1)	0.340 (1)	0.4086 (5)	* 0.057 (5)	
C (24)	0.920 (2)	0.362 (1)	0.3311 (6)	* 0.076 (7)	
C (25)	0.901 (2)	0.431 (1)	0.2937 (5)	* 0.085 (7)	
C (26)	0.787 (1)	0.499 (1)	0.3048 (4)	* 0.069 (5)	
C (27)	1.027 (2)	0.272 (1)	0.3396 (6)	* 0.093 (7)	
C (28)	0.725 (2)	0.590 (1)	0.2777 (5)	* 0.094 (7)	

N(1), pyridine N(3), pyrazole N(5) and pyridine N(6) groups form the equatorial plane of a square-pyramid with the other pyrazole N(8) occupying the axial position. The copper is 0.2 Å above the N_4 plane towards the axially coordinated pyrazole nitrogen of the bidentate ligand Me_2pp . It should be mentioned here that an inverse correlation has been shown to exist between the displacement parameter and the Cu-(apical) distance in square-pyramidal copper(II) complexes.¹⁶⁵ Longer the apical distance lower the displacement and the structure tends toward square-pyramidal geometry. The tetragonality parameter T^5 which is defined as the ratio of the four in-plane Cu-N distances and the single long Cu-N distance, has a value of 0.92 for the present complex. This value is within the observed range of 0.90-0.96 for a large group of five-coordinate complexes.¹⁶⁵

An interesting feature in this structure is the axially coordinated pyrazole nitrogen. The Cu-N(8) bond is rather long (2.22(1) Å). It is worth noting here that there are only a handful¹⁸⁴⁻¹⁸⁶ of structurally characterized mononuclear square-pyramidal CuN_5 complexes with axially coordinated heterocyclic ring nitrogen donors from chelating ligands, there seems to be no report of axially coordinated pyrazole nitrogen.

For both Me_4bpp and Me_2pp the pyridine and pyrazole rings are each planar. For Me_4bpp the two pyrazole rings are tilted to each other by $\sim 75^\circ$ and they make an angle of $\sim 56^\circ$ and $\sim 59^\circ$ with the pyridine ring. For Me_2pp the angle between the two heterocyclic rings is $\sim 54^\circ$. Thus the six-membered chelate rings exist in boat conformations, as in compounds of these kinds of

ligands.^{39,79,92}

(b) Evidence of Steric Crowding. The Cu-N(pyridine) distances are normal. The Cu-N(pyrazole) distances are on the higher side.^{39,150,156,157,160} In fact, the average in-plane Cu-N(pyrazole) distance of 2.03 Å (Table IV.5) is similar to sterically crowded hydrotris(pyrazolyl)borate complexes.¹⁵³⁻¹⁵⁵ We believe that it is the manifestation of the interplay between the two factors: (i) presence of the pyrazole ring substituted methyl groups near the donor site and (ii) the forced axial coordination to the copper(II) center rendering the copper site sterically congested.

The angles between the *trans* equatorial nitrogens N(1)-Cu-N(5) and N(3)-Cu-N(6) are 164.4 and 173.7° respectively (Table 3). The values are in the observed range for square-pyramidal copper(II) complexes (160-170°) in which the copper atom is displaced out of the plane.^{165,158} In the present complex slightly larger *trans* equatorial angles is indicative of the presence of steric crowding created by the two ligands Me₄bpp and Me₂pp. In [Cu(NH₃)₅]²⁺ where no angular strains imposed by chelate rings are expected the angles between the *trans* amines are 164.0 and 165.4°. ¹⁹⁸

IV.4.5 Redox Behavior

When examined by cyclic voltammetry in MeCN solution at a platinum working electrode, complexes 1 and 2 exhibit two consecutive steps of reduction. The first response is assigned as Cu(II)/Cu(I) redox process and is quasireversible (Figure IV.6) as the peak-to-peak separations (ΔE_p) increase with increase in the scan rate (Figure IV.7). The ΔE_p value of complex 2 is larger than that of complex 1. This result implies that structural reorganization occurs due to reduction and the effect is more pronounced in the case of 2. The second redox process is due to Cu(I)/Cu(0) reductive response and is irreversible.

To our knowledge, within the family of mononuclear Cu^{II}N₅ complexes,^{147,148,158,180,187-191} 1 and 2 have the highest reduction potentials for the Cu(II)/Cu(I) couple, which deserve special attention. This result implies that the copper(II) state is significantly destabilized in these complexes. It is to be noted that in 1 and 2, three out of five coordinating atoms are pyrazole ring nitrogens and it is well known that pyrazoles are poor π -accepting ligands. Hence we believe that the present result is due to the reduced ligand field around Cu(II) created by the constrained nature of the coordination geometry, which favours Cu(I) state. In other words, the presence of a sterically congested coordination zone around Cu(II) has caused the ligands to behave as poor coordinating ligands, stabilizing copper(I) state. The X-ray structure of 2 augments our argument. The observed displacement of copper atom from the CuN₄ equatorial plane towards axial pyrazole nitrogen of the bidentate ligand

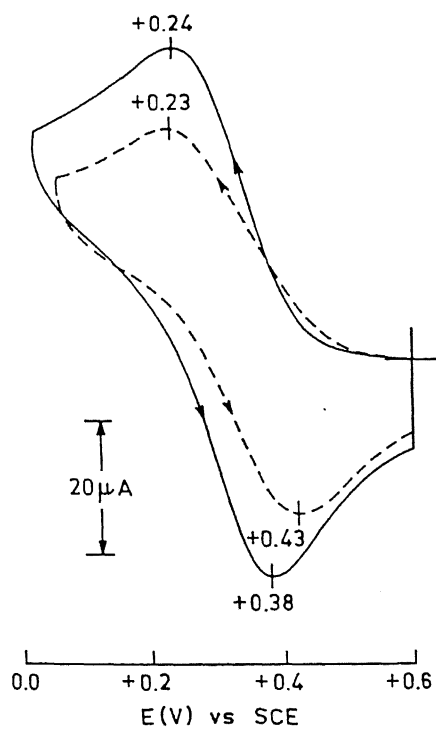


Figure IV.6 Cyclic voltammograms (scan rate 50 mV s^{-1}) of $[\text{Cu}(\text{H}_2\text{pp})(\text{H}_4\text{bpp})](\text{ClO}_4)_2$ (—) and $[\text{Cu}(\text{Me}_2\text{pp})(\text{Me}_4\text{bpp})](\text{ClO}_4)_2$ (---) at platinum electrode in MeCN; supporting electrolyte TBAP

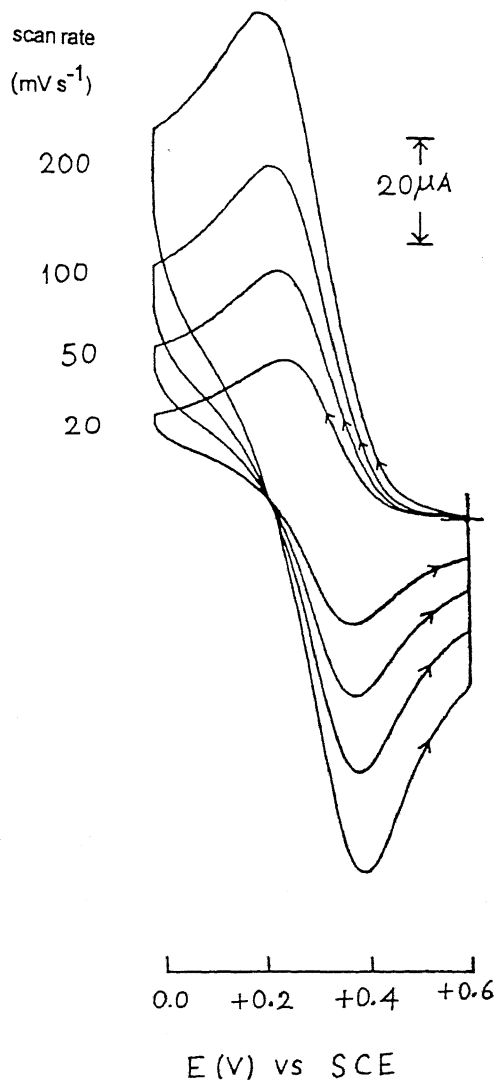


Figure IV.7 Variable scan cyclic voltammograms of $[\text{Cu}(\text{H}_2\text{pp})(\text{H}_4\text{bpp})](\text{ClO}_4)_2$ at platinum electrode in MeCN; supporting electrolyte TBAP

Me₂pp is caused by the forced axial pyrazole coordination, which in turn causes reduction in the ligand field around copper(II). Another interesting result is the observed small but measurable shift (20 mV) in the $E_{1/2}$ values of 1 and 2. The more positive value for 2 is due to steric and/or "environment" effect which is already described in chapter III (section III.5.6).

IV.4.6 Conclusions

(i) Syntheses of rare examples of penta-coordinate Cu(II) complexes with tridentate and bidentate nitrogen donor ligands have been achieved.

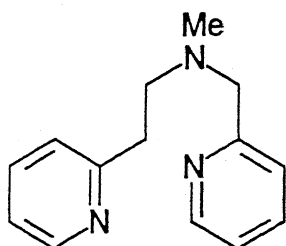
(ii) The first example of the crystal structure of such a complex with a sterically crowded coordination sphere where all the donor sites are provided by ring nitrogens have been provided.

(iii) These complexes exhibit, within CuN₅ family of complexes, the highest Cu(II)/Cu(I) redox potentials. The ligands chosen are such that they have provided a sterically congested coordination around copper(II) and a rather long forced axial pyrazole coordination. Such a forced pyrazole axial ligand coordination has not been observed previously. This has allowed to exert a decreased ligand field around copper(II) and hence to observe the highest Cu(II)/Cu(I) redox potential among all known CuN₅ family of complexes.

CHAPTER V

Chemistry of New Triply Bridged Dimanganese(III) and Dimanganese(IV) Complexes with $\{\text{Mn}^{\text{III}}_2(\mu\text{-O})(\mu\text{-OAc})_2\}^{2+}$ and $\{\text{Mn}^{\text{IV}}_2(\mu\text{-O})_2(\mu\text{-OAc})\}^{3+}$ Cores

In the last three chapters a rich chemistry of Co(II), Ni(II), and Cu(II) with pyrazolylmethylpyridine ligands has been described. This final chapter considers a dimanganese chemistry of relevance to biology. Specifically, in this chapter we have used a pyridine-rich facially capping tridentate ligand (MeL) to explore binuclear manganese chemistry at various oxidation levels. The binuclear chemistry of complexes having the core unit $\{\text{M}^{\text{III}}_2(\mu\text{-O})(\mu\text{-OAc})_2\}^{2+}$ (M = Fe, Ru) has already been explored from this laboratory.^{192, 193} Moreover, the chemistry of $\{\text{Mn}^{\text{III}}\text{Mn}^{\text{IV}}(\mu\text{-O})_2(\mu\text{-OAc})\}^{2+}$ core have already been done from our laboratory¹⁹⁴ using the same MeL ligand.



MeL

Introduction

Oxo-bridged binuclear manganese complexes are of great recent interest due to their demonstrated presence in the biological systems (chapter I, section I.2.2).

Recent interest in the synthetic complexes of manganese with structural unit $\{\text{Mn}^{\text{III}}_2(\mu\text{-O})(\mu\text{-OAc})_2\}^{2+}$ ¹⁹⁵⁻²⁰² is due to the fact that they serve as good models for the active sites of *pseudo*-catalases and the ribonucleotide reductases. The synthetic complexes with the structural unit $\{\text{Mn}^{\text{III}}\text{Mn}^{\text{IV}}(\mu\text{-O})_2(\mu\text{-OAc})\}^{2+}$ are of current interest since the $\text{Mn}^{\text{III}}\text{Mn}^{\text{IV}}$ unit is formed in the catalytic cycle of Mn-catalase²⁰³ and these are good models^{194,204} for the active site the photosynthetic oxygen evolving complex (OEC) of photosystem II (PSII).

The active-site Mn cluster of PSII is either^{205,206} tetranuclear^{207,208} or trinuclear with a nearby mononuclear site^{209,210}. Another possibility^{210,211} to describe the OEC in PSII is a cluster containing four Mn ions imbedded in a 'dimer of bis(μ -oxo) dimer' type structure with a short Mn-Mn distance of 2.7 Å and a longer Mn-Mn distance of 3.3 Å (Chap.I; Fig.I.9).

Crystal structure data are not available for any O_2 -evolving PSII complex. The $\text{Mn}_2(\mu\text{-O})_2$ core with higher oxidation states of manganese (III and IV) can be considered as a substructure of the biological aggregate. Because till now only this structural unit shown to be consistent with the relatively short Mn-Mn distance (i.e., 2.7 Å). And EPR spectrum of the S_2 state is most simply interpretable in terms of a dimeric mixed valence species with coupling to two manganese nuclei. Moreover, it is possible that critical step in photosynthetic water oxidation

involves O-O bond formation between two ligated O^{2-} or perhaps OH^- groups across the face of an Mn_2O_2 substructure of the active-site Mn-complex.

A number of research groups^{195-197, 204a, 211} have shown that $(\mu\text{-oxo})$ bis $(\mu\text{-acetato})$ dimanganese(III) complexes could be oxidized by following two pathways: i) sequential electrochemical oxidation to $Mn^{III}Mn^{IV}$ and Mn^{IV}_2 oxidation levels and ii) chemical transformations to $\{Mn^{III}Mn^{IV}(\mu\text{-O})(\mu\text{-OAc})_2\}^{+3}$ and $\{Mn^{III}Mn^{IV}(\mu\text{-O})_2(\mu\text{-OAc})\}^{2+}$ species. Disproportionation of the core under acidic conditions has been postulated previously.^{212, 213} And such disproportionation reactions have been demonstrated by R. Manchanda et al.²¹⁴ But we have isolated $\{Mn^{III}_2(\mu\text{-O})(\mu\text{-OAc})_2\}^{+2}$ core from $\{Mn^{III}Mn^{IV}(\mu\text{-O})_2(\mu\text{-OAc})\}^{+2}$ core in good yield using glacial acetic acid (acid promoted disproportionation reaction) for the first time. In this chapter a binuclear manganese chemistry of relevance to biology has been described. The possibility of various redox transformations has been investigated in considerable detail.

V.1 Experimental Section

V.1.1 Solvents and Reagents

Solvents and reagents were obtained from commercial sources and used without further purification unless otherwise stated. Details of solvent purification are discussed in chapter II (Section II.1.1).

V.1.2 Measurements

Details of spectroscopic measurements are given in

Variable-temperature magnetic susceptibility measurements were made on powdered samples over the temperature range $8.0 < T < 300$ K by the Faraday method using a locally built susceptometer in the laboratory of Professor S. Mitra, Chemical Physics Group, Tata Institute of Fundamental Research (TIFR), Bombay, India. The measurement were started at ~ 50.0 K and the sample was heated and held at the desired temperature during the measurement. This process was continued until the sample was attained at room temperature. Effective magnetic moments were calculated from $\mu_{\text{eff}} = 2.828 [\chi_M T]^{1/2}$, where χ_M is the corrected molar susceptibility. Diamagnetic corrections were made for the sample holder and for the diamagnetic contribution of the complex being measured. All measurements were made at a fixed field strength and field dependence of the magnetic susceptibility was not studied.

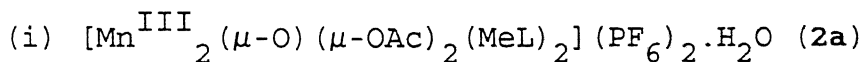
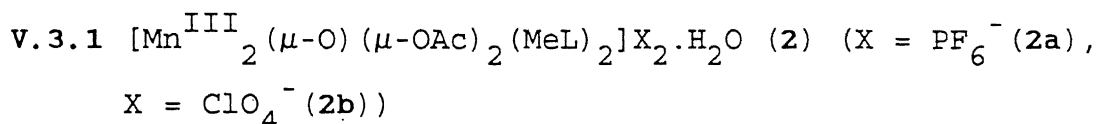
Positive ion FAB (FAB^+) mass spectra were recorded on a JEOL SX 102/DA-6000 Mass Spectrometer/Data System using Argon (6 KV, 10 mA) as the FAB gas. The accelerating voltage was 10 KV and spectra were recorded at room temperature using m-nitrobenzyl alcohol (3-NBA) as the matrix and MeCN as solvent.

V.2 Synthesis of (2-pyridylethyl)(2-pyridylmethyl)methylamine (MeL)

To a solution of 2-(2-methylaminoethyl)pyridine (3.34 g, 24.40 mmol) and NEt_3 (2.50 g, 24.70 mmol) in 90 mL of ethylacetate was added 10 mL of an ethanolic solution of 2-chloromethylpyridine (obtained by neutralization of the monohydrochloride (4.00 g, 24.40 mmol) with a 10% excess of a 2 mL saturated aqueous

K_2CO_3 solution with vigorous shaking). The mixture was allowed to stir at room temperature for 5 days. After filtration, the solvent was removed under reduced pressure to give a yellowish oil. To this, 20 ml of ethylacetate was added, filtered, and the volume of the filtrate was reduced down to 5 mL by rotary evaporation. The remaining solution was extracted with ethylacetate and dried over anhydrous Na_2SO_4 . After complete removal of the solvent the desired product was obtained as a yellowish brown liquid (Yield 4.50 g, 81%). 1H NMR (in $CDCl_3$): 8.57-6.83 (8H, m, aromatic), 3.85 (2H, s, NCH_2), 2.95 (4H, s NCH_2CH_2), 2.40 (3H, s, NCH_3). The 1H NMR spectrum of MeL is shown in Figure V.1.

V.3 Syntheses of Complexes



To a stirred mixture of $Mn(OAc)_3 \cdot 2H_2O$ (400 mg, 1.49 mmol) NH_4PF_6 (243 mg, 1.49 mmol) in 10 mL of MeCN was added MeL (339 mg, 1.49 mmol) dissolved in 10 mL of acetonitrile under dinitrogen atmosphere. The resulting mixture was stirred for 2 h at 298 K and filtered under dinitrogen atmosphere. The volume of the solution was reduced to ~10 mL. To the reduced solution was added 3 mL of glacial acetic acid and 10 mL of ethyl acetate and the resulted mixture was allowed to stand for 24 h at 273 K. The microcrystalline purplish brown product was collected by filtration and dried under vacuum at 298 K. Yield 896 mg, 60%. The perchlorate salt was prepared following a similar procedure using $NaClO_4 \cdot H_2O$ instead of NH_4PF_6 .

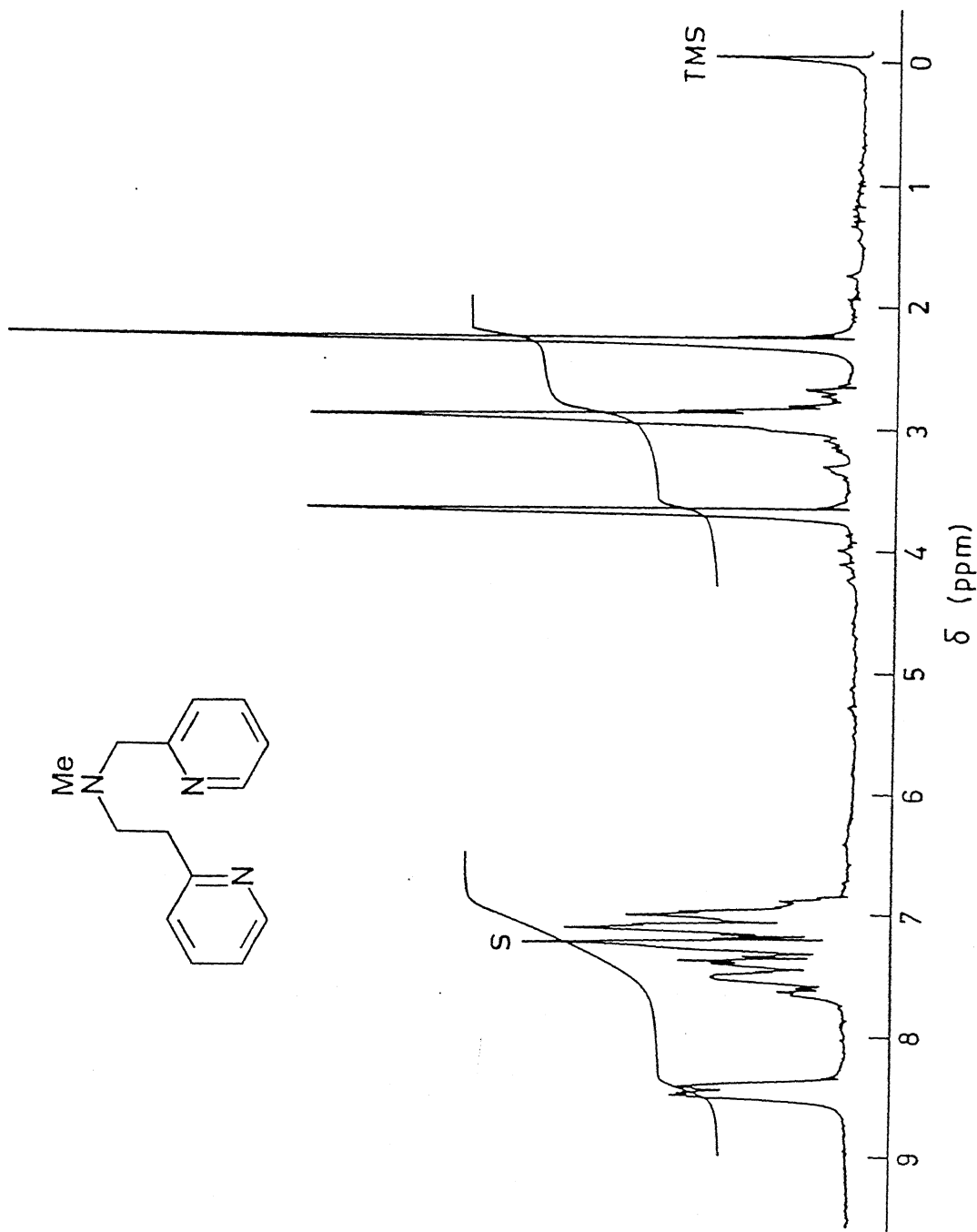
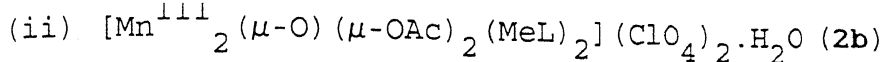


Figure V.1 ^1H NMR spectrum of 2-pyridylethyl(2-pyridylmethyl)methylamine (MeL) in CDCl_3



Method A. From $[\text{Mn}^{\text{III}}\text{Mn}^{\text{IV}}(\mu\text{-O})_2(\mu\text{-OAc})(\text{MeL})_2](\text{ClO}_4)_2 \cdot \text{H}_2\text{O}$ (1a) (this complex is already reported from our laboratory¹⁹⁴):

To an MeCN solution (5 mL) of **1** (25 mg, 0.0286 mmol) was added 1 mL of glacial acetic acid. The resulting mixture was stirred for 20 h and during this time the green solution turned to purplish-brown. After reducing the volume of the solution to 3 mL under reduced pressure 3 mL of ethylacetate was added and the mixture was allowed to stand at 273 K for 36 h. Purplish-brown precipitate collected by filtration. Yield: 20 mg (76%).

Method B. To a stirred mixture (5 mL) of $\text{Mn}(\text{OAc})_3 \cdot 2\text{H}_2\text{O}$ (200 mg, 0.746 mmol), NaOAc (61 mg, 0.746 mmol) and $\text{NaClO}_4 \cdot \text{H}_2\text{O}$ (210 mg, 2 mmol) in methanol was added a methanolic solution (5 mL) of MeL (169 mg, 0.746 mmol). Four drops of glacial acetic acid was added to prevent the formation of **1**. The reaction mixture was stirred for 15 min. Purplish-brown precipitate started to appear. The solid thus obtained was filtered and washed thoroughly with methanol. The product was dried in a vacuum desiccator. It was recrystallized from MeCN/ MeCO_2Et in presence of 4-6 drops of glacial acetic acid: After dissolving the compound in minimum amount of MeCN 4-6 drops of glacial acetic acid was added. To this solution an equal volume of MeCO_2Et was added and allowed to stand at 273 K for 1-2 days. Crystalline purplish-brown product was collected by filtration and dried in a vacuum desiccator. Yield 230 mg, 67%.

Method C. To a stirred mixture of $\text{Mn}(\text{OAc})_3 \cdot 2\text{H}_2\text{O}$ (370 mg, 1.38 mmol) and MeL (0.313 mg, 1.38 mmol) in methanol (8 mL) was added dropwise a methanolic (2 mL) solution of 0.12 mL 70% perchloric acid. The resulting mixture was stirred for 5 min. Purplish-brown precipitate started to appear. The solid thus obtained was filtered and washed thoroughly with methanol. The product was dried in a vacuum desiccator. It was recrystallized as described in (ii)

Method B. Yield 310 mg, 50%.

V.3.2 $[\text{Mn}^{\text{III}}\text{Mn}^{\text{IV}}(\mu\text{-O})_2(\mu\text{-OAc})(\text{MeL})_2](\text{ClO}_4)_2 \cdot \text{H}_2\text{O}$ (**1a**) (synthesis of this complex is already reported from our laboratory¹⁹⁴ using $\text{Mn}(\text{OAc})_3 \cdot 2\text{H}_2\text{O}$ as starting material under dinitrogen atmosphere).

Method A. (i) To a stirred solution of $\text{Mn}(\text{OAc})_3 \cdot 2\text{H}_2\text{O}$ (590 mg, 2.202 mmol) and MeL (500 mg, 2.202 mmol) in methanol (12 mL) was added dropwise a methanolic (3 mL) solution of 0.30 mL 70% perchloric acid. The resulting mixture was stirred for 45 min. Green precipitate started to appear. The green solid thus obtained was filtered and washed thoroughly with methanol. It was recrystallized from CH_2Cl_2 . The product was dried in a vacuum desiccator. Yield 350 mg, 37%.

(ii) $[\text{Mn}^{\text{III}}\text{Mn}^{\text{IV}}(\mu\text{-O})_2(\mu\text{-OAc})(\text{MeL})_2](\text{BF}_4)_2 \cdot 2\text{MeCN}$ (**1b**)

To a stirred mixture (5 mL) of $\text{Mn}(\text{OAc})_3 \cdot 2\text{H}_2\text{O}$ (100 mg, 0.372 mmol), NaOAc (62 mg, 0.746 mmol) and NaBF_4 (82 mg, 0.746 mmol) in MeCN was added a MeCN solution (5 mL) of MeL (84 mg, 0.372 mmol). The reaction mixture was stirred for 2 h and it was then filtered. The volume of the filtrate was reduced to ~ 5 mL. To this filtrate was added ~ 5 mL of MeCO_2Et slowly and kept at 273 K for 12 h. Green crystals thus obtained were filtered and

washed thoroughly with MeCO_2Et . The product was dried in a vacuum desiccator. Yield 60 mg, 35%. Single crystals suitable for X-ray diffraction studies were grown by slow diffusion of MeCO_2Et into a MeCN solution of **1b** (solvent layering). This complex was prepared only for X-ray diffraction studies.

Method B. From $[\text{Mn}^{\text{III}}_2(\mu\text{-O})(\mu\text{-OAc})_2(\text{MeL})_2](\text{ClO}_4)_2 \cdot \text{H}_2\text{O}$ (**2b**)

To an MeCN solution (10 mL) of **2b** (100 mg, 0.1092 mmol) was added $\text{NaClO}_4 \cdot \text{H}_2\text{O}$ (616 mg, 4.384 mmol) and 2 mL of water. The resulting reaction mixture was stirred at 298 K for 3-4 h. The black precipitate (probably MnO_2) obtained was rejected by filtration. The Volume of the resulting solution was reduced to ~ 5 mL and kept at 273 K overnight. Green crystalline precipitate thus obtained was filtered, thoroughly washed with water and dried in vacuo. Yield 15 mg, 16%.

V.3.3 $[\text{Mn}^{\text{IV}}_2(\mu\text{-O})_2(\mu\text{-OAc})(\text{MeL})_2](\text{ClO}_4)_3 \cdot \text{H}_2\text{O}$ (**3**)

Method A. This compound was prepared following Armstrong's method:²¹⁵ The ligand MeL (500 mg, 1.10 mmol), was dissolved in 15 mL of methanol. To this was added solid $\text{Mn}(\text{OAc})_3 \cdot 2\text{H}_2\text{O}$ (590 mg, 2.20 mmol) while stirring at 298 K. After stirring the reaction mixture for 15 min it was filtered (to reject insoluble black residue). To the stirred filtrate was added 0.6 mL of 70% perchloric acid (in 2 mL of methanol) dropwise. The resulted mixture was stirred for 45 min at 298 K. The greenish-brown precipitate was filtered and washed with methanol (2-3 times) and finally with CH_2Cl_2 to remove trace amount of **1**. The greenish-brown compound

thus obtained was dried in a vacuum desiccator. Yield 290 mg, 30%.

Method B. From $[\text{Mn}^{\text{III}}_2(\mu\text{-O})(\mu\text{-OAc})_2(\text{MeL})_2](\text{ClO}_4)_2 \cdot \text{H}_2\text{O}$ (**2b**)

To a methanolic suspension of **2** (100 mg in 4 mL) was added 70% perchloric acid (0.075 mL in 1 mL methanol) dropwise while stirred the reaction mixture. The suspension disappeared and greenish-brown precipitate started to appear. Stirring was continued for a further 45 min, filtered, washed with methanol and finally with CH_2Cl_2 to remove trace amount of **1**. The greenish-brown compound thus obtained was dried in a vacuum desiccator. Yield 16 mg, 15%.

Method C. From $[\text{Mn}^{\text{III}}\text{Mn}^{\text{IV}}(\mu\text{-O})_2(\mu\text{-OAc})(\text{MeL})_2](\text{ClO}_4)_2 \cdot \text{H}_2\text{O}$ (**1a**)

To a methanolic suspension of **1** (80 mg in 4 mL) was added 70% perchloric acid (0.04 mL in 1 mL methanol) dropwise while stirred the reaction mixture. Suspension disappeared and greenish-brown precipitate started to appear. Stirring was continued for a further 45 min, filtered, washed with methanol and finally with CH_2Cl_2 to remove trace amount of **1**. The greenish-brown compound thus obtained was dried in a vacuum desiccator. Yield 27 mg, 30%.

V.4 X-ray Data Collection and Structure Solution and Refinement

The single crystals suitable for X-ray diffraction studies were grown by slow diffusion of ethylacetate into the MeCN solution of a BF_4^- salt of the mixed valence dimer (**1b**) (solvent layering). Crystals of the complex were mounted on a glass fiber. Preliminary examination and data collection were performed with $^{40}\text{K}_\alpha$ radiation ($\lambda = 0.71073 \text{ \AA}$) on an Enraf-Nonius CAD4 Mach

computer controlled diffractometer equipped with a graphite monochromator. Data at 293 K were collected at this Department, Indian Institute of Technology, Kanpur, India

Cell constants and the orientation matrix for data collection were obtained from least-squares refinements, using the setting angles of 25 reflections in the range $16 < 2\theta < 24$. Experimental details of crystal data, structure solution, and refinement were given in Table V.1.

Intensities were corrected for Lorentz and polarization effect. Anomalous dispersion was applied for all non-hydrogen atoms. Analytical absorption correction was applied to the data. The compound crystallizes as $[\text{Mn}^{\text{III}}\text{Mn}^{\text{IV}}(\mu\text{-O})_2(\mu\text{-OAc})(\text{MeL})_2] \cdot (\text{BF}_4)_2 \cdot 2\text{MeCN}$ (**1b**) in the triclinic system. The structure was solved in the space group $P1$ (No.2) by direct methods¹²⁷ and refined by a full-matrix least-squares method with anisotropic thermal parameters used for only Mn, O, and N atoms except N atoms of MeCN molecules, all C atoms, and the BF_4^- anions. Hydrogens were added in their calculated positions with fixed isotropic thermal parameters and were not refined. Two boron atoms of counter anions were not refined. Both the tetrafluoroborates were severely disordered. For both of them, the apical fluorine atoms were unique, but the remaining three fluorines were disordered over three positions, with occupancies of 0.5, 0.25, and 0.25. All the C-N and C-C (N(4) - C(30)) bonds of one of the terminal MeL ligands were restrained and the two pyridine rings of the same terminal ligand were refined as rigid bodies to have reasonable bond distances and angles. With the model used the structure converged moderately satisfactorily. Four reflections (hkl:

Table V.1

EXPERIMENTAL DETAILS

A. CRYSTAL DATA

Empirical Formula	$\text{Mn}_2\text{B}_2\text{F}_8\text{O}_4\text{N}_8\text{C}_{34}\text{H}_{43}$
Formula Weight	910.6
Crystal Colour, Habit	Dark green, irregular shaped
Crystal dimensions (mm^3)	0.5 x 0.2 x 0.15
Crystal System	Triclinic
No. of reflections used for unit cell determination (2θ range)	25 reflections ($16 < 2\theta < 24$)
Lattice parameters	$a = 10.283(2)$, $b = 13.874(5)$ $c = 16.152(5)$ Å, $\alpha = 65.74(3)^\circ$ $\beta = 84.24(2)^\circ$, $\gamma = 78.06(2)^\circ$ $V = 2055.094(1.169)$ Å ³
Space Group	$P\bar{1}$ (No.2)
Z value	2
D_{calc} (g cm^{-3})	1.34
F_{000}	933.8
μ ($\text{MoK}\alpha$) (mm^{-1})	0.69

B. INTENSITY MEASUREMENTS

Diffractometer	Cad4Mach
Radiation	$\text{MoK}\alpha$ ($\lambda = 0.71073$ Å)
Temperature	293K
Scan Type	θ - 2θ
Scan Rate	variable
Scan Width	$1.0 + 0.35 \tan \theta$
2θ range (deg)	2 - 50
No. of reflections measured ($2 < 2\theta < 50$)	7894
No. of unique reflections	7220
Corrections	L_p , absorption (analytical)

C. STRUCTURE SOLUTION AND REFINEMENT

Structure Solution	Direct Method
Refinement	Full matrix, least squares
Function minimized	$\sum w(F_o - F_c)^2$
Anomalous dispersion	applied (for non H atoms)
No. of observations ($I > 3\sigma(I)$)	3738
No. of variables	333
Reflection/Parameter ratio	11.2
Residuals: $R; R_w$	0.121; 0.134
Goodness of fit indicator	5.232
Max shift/error in final cycle	0.3285×10^{-1}
Avg shift/error in final cycle	0.1195×10^{-2}
Maximum peak in final diff. map ($\text{e}\text{\AA}^{-3}$)	1.68 near C(21)
Minimum peak in final diff. map ($\text{e}\text{\AA}^{-3}$)	-1.05

1,-1,1; 1,0,-1; 2,0,0; 2,2,1) were omitted in the final stages of refinement as the peak profiles were extremely broad. These erroneous reflections were probably caused by the quality of crystal chosen for data collection. In fact, quality of crystals obtained were not good. Our efforts are on sort out this problems. Other details of X-ray structure determination are the same as that in chapter IV.

V.5 Results and Discussion

V.5.1 Syntheses of Tribridged Cores

(i) $\{\text{Mn}^{\text{III}}_2(\mu\text{-O})(\mu\text{-OAc})_2\}^{2+}$ core

The complexes **2a** and **2b** were synthesized following three procedures: (i) direct reaction between $\text{Mn}(\text{OAc})_3 \cdot 2\text{H}_2\text{O}$ and the facially capping ligand MeL in MeCN in the presence of glacial acetic acid. Thus it is a modified method than that reported by others,²⁰⁴⁻²⁰⁶ (ii) reaction between MeL and $\text{Mn}(\text{OAc})_3 \cdot 2\text{H}_2\text{O}$ in MeOH in presence of HClO_4 , and (iii) reaction between $\text{Mn}(\text{OAc})_3 \cdot 2\text{H}_2\text{O}$ and MeL in MeOH in presence of anhydrous sodium acetate and glacial acetic acid. When NH_4PF_6 was used as the counterion, complex **2a** was isolated in the solid state and the use of $\text{NaClO}_4 \cdot \text{H}_2\text{O}$ afforded **2b**. It has been observed that in MeCN solution complexes **2a** and **2b** are better stabilized in the presence of glacial acetic acid. It has also been noted that **2a** and **2b** are extremely moisture sensitive. In fact, with its presence **2a** and **2b** are converted to bis(μ -oxo) $\text{Mn}_2(\text{III,IV})$ core within 1-2 weeks.

(ii) $\{\text{Mn}^{\text{IV}}_2(\mu\text{-O})_2(\mu\text{-OAc})\}^{3+}$ core

For synthesis of 3 the reaction conditions used were similar to those employed previously by others.²¹⁵⁻²¹⁷ We believe that upon addition of HClO_4 the mixed-valent core $\text{Mn}_2(\text{III},\text{IV})$ (1a) forms initially and then it disproportionates to produce $\text{Mn}_2(\text{IV},\text{IV})$ along with a Mn^{II} species. This hypothesis is supported by three observations: (i) 3 can also be prepared from isolated 1a on treatment of HClO_4 in MeOH, (ii) the yield of 3 is quite low and (iii) the filtrate of the reaction mixture was lightly colored, suggesting that the remaining manganese is in a low oxidation state, which is confirmed by 6 line EPR spectrum of the filtrate.

V.5.2 Characterization of the Cores

A. $\text{Mn}_2(\text{III},\text{IV})$ Core

Characterization of this core using MeL as terminal ligand has already been done by C, H, N analysis, IR, and absorption spectroscopies.¹⁹⁴

B. $\text{Mn}_2(\text{III},\text{III})$ Core

The $\{\text{Mn}^{\text{III}}_2(\mu\text{-O})(\mu\text{-OAc})_2\}^{2+}$ core formulation results in a dipositively charged complex, which is consistent with the microanalysis data (Table V.2) and conductivity data (Table V.3). The characteristic IR bands (Figure V.2) of 2a is assignable to bridging acetate at 1435 and 1570 cm^{-1} for $\nu_s(\text{OAc})$ and $\nu_{as}(\text{OAc})$ respectively, the $\nu(\text{Mn}_2\text{O}_2)$ at 760 cm^{-1} , and $\nu(\text{PF}_6^-)$ at 835 cm^{-1} . For 2b, $\nu(\text{ClO}_4^-)$ bands are observed at 1200 and 625 cm^{-1} . For both

Table V.2 Microanalytical Data of Manganese Dimers

Complexes	Empirical Formula	Analysis ^a		
		%C	%H	%N
2a	$C_{32}H_{42}N_6O_6F_{12}P_2Mn_2$	37.96 (38.15)	4.10 (4.17)	8.82 (8.35)
2b	$C_{32}H_{42}N_6O_{14}Cl_2Mn_2$	41.67 (41.97)	4.80 (4.60)	9.28 (9.18)
3	$C_{30}H_{39}N_6O_{17}Cl_3Mn_2$	37.26 (37.06)	4.07 (4.00)	8.95 (8.65)

^aCalculated values in parentheses

Table V.3 Molar Conductance, Magnetic Moment and Electronic Spectral Data of Manganese Dimers in MeCN at 298 K

Complexes	Λ_M^a ($\Omega^{-1}\text{cm}^2\text{mol}^{-1}$)	μ_{eff} (B.M.) ^{b, c}	λ , nm(ϵ , $\text{M}^{-1}\text{cm}^{-1}$)
2a	293	4.97 (4.91)	875(sh) (112), 730(130), 563- (sh) (290), 521(422), 487(510) 375(sh) (1880), 285(sh) (15 470) 259(25 170)
3	344	2.48 (0.00)	896(sh) (35), 755(90), 720(sh) - (65), 602(355), 450(sh) (1 450), 300(sh) (13 760), 253(26 720)

^aExpected range for 1:2 and 1:3 electrolytes in MeCN are 220-300 and 340-420 $\Omega^{-1}\text{cm}^2\text{M}^{-1}$

^bValues per manganese

^cRoom temperature solid state values are in parentheses

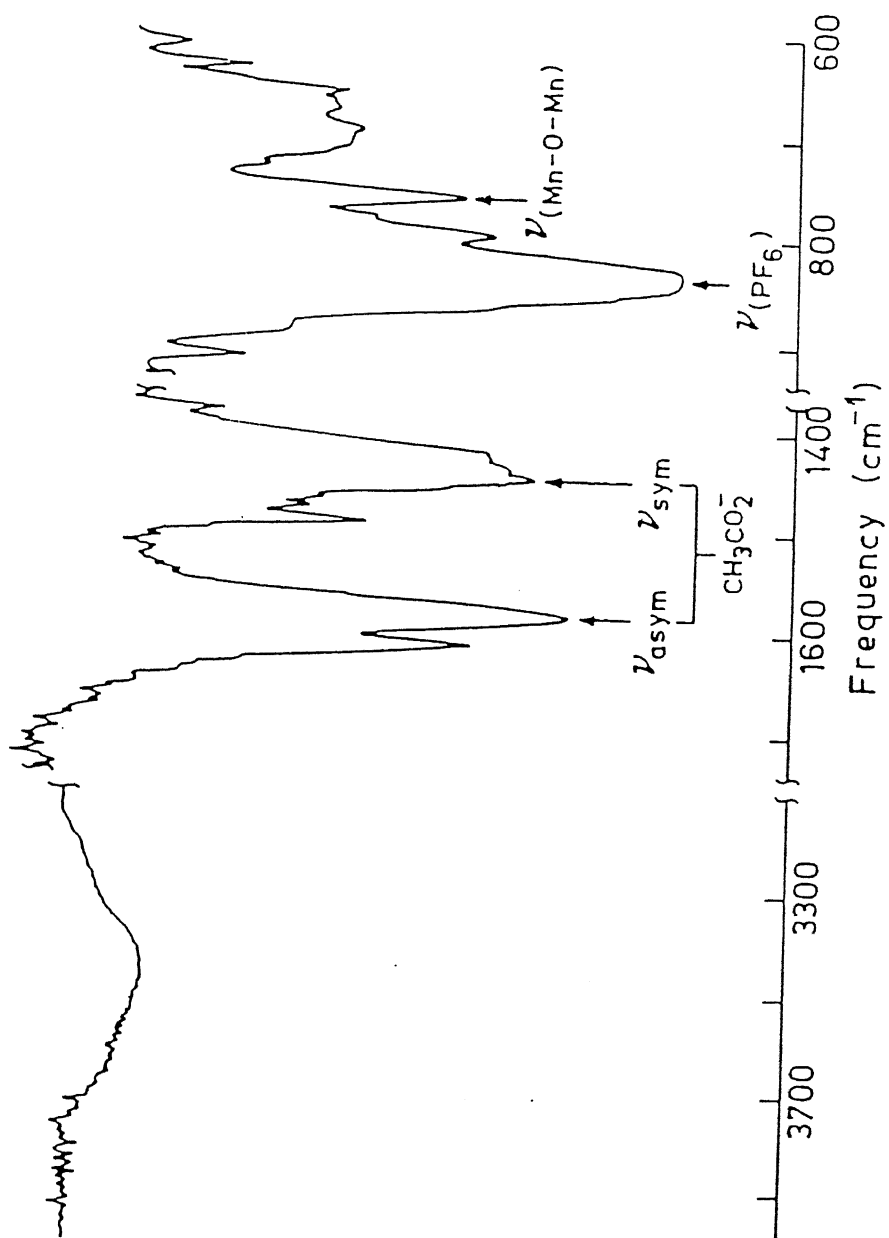


Figure V.2

IR Spectrum of $[\text{Mn}^{\text{III}}_2(\mu\text{-O})(\mu\text{-OAc})_2(\text{MeL})_2](\text{PF}_6)_2 \cdot \text{H}_2\text{O}$

the complexes the appearance of a broad band ($\nu(\text{OH})$) in the range 3420 - 3440 cm^{-1} indicates the presence of water as solvent of crystallization.

C. $\text{Mn}_2(\text{IV}, \text{IV})$ Core

For 3 microanalysis data (Table V.2) and conductivity data (Table V.3) suggest the tripositive charge of this complex. The characteristic bands in its IR spectrum (Figure V.3) are assignable for $\nu(\text{Mn}_2\text{O}_2)$ at 766, for $\nu_s(\text{OAc})$ at 1438, for $\nu_{as}(\text{OAc})$ at 1570, for $\nu(\text{OH})$ a broad band at 3420 and for $\nu(\text{ClO}_4^-)$ at 1088 and 624 cm^{-1} .

V.5.3 Absorption Spectra

A. $\text{Mn}_2(\text{III}, \text{IV})$ Core

Absorption spectroscopic studies of this core have already been done from our laboratory.¹⁹⁴

B. $\text{Mn}_2(\text{III}, \text{III})$ Core

The absorption spectrum of $[\text{Mn}^{\text{III}}_2(\mu\text{-O})(\mu\text{-OAc})_2(\text{MeL})_2]^- (\text{PF}_6)_2 \cdot \text{H}_2\text{O}$ (2a) in acetonitrile is shown in Figure V.4. It displays a characteristic spectral feature (Table V.3) similar to 195-200 those of the related structurally characterized binuclear manganese(III) complexes with $\{\text{Mn}^{\text{III}}_2(\mu\text{-O})(\mu\text{-OAc})_2\}^{2+}$ chromophore.

C. $\text{Mn}_2(\text{IV}, \text{IV})$ Core

For 3 the absorption spectra in MeCN is shown in Figure

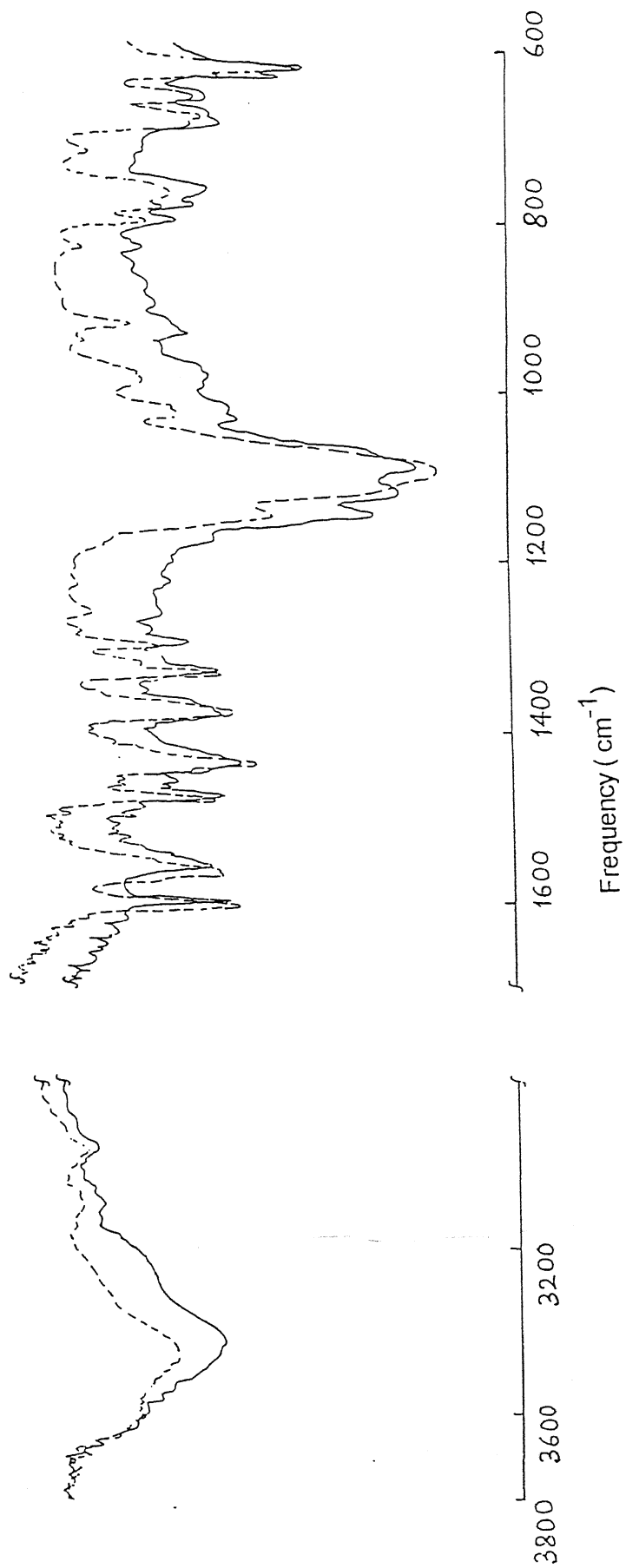


Figure v.3 IR Spectra of $[\text{Mn}^{\text{III}}]_{\text{Mn}^{\text{V}}}(\mu\text{-O})_2(\mu\text{-OAc})_2(\mu\text{-O})(\text{MeL})_2$ (—) and $[\text{Mn}^{\text{III}}]_{\text{Mn}^{\text{V}}}(\mu\text{-O})_2(\mu\text{-OAc})_2(\mu\text{-O})(\text{MeL})_2 \cdot \text{H}_2\text{O}$ (---).

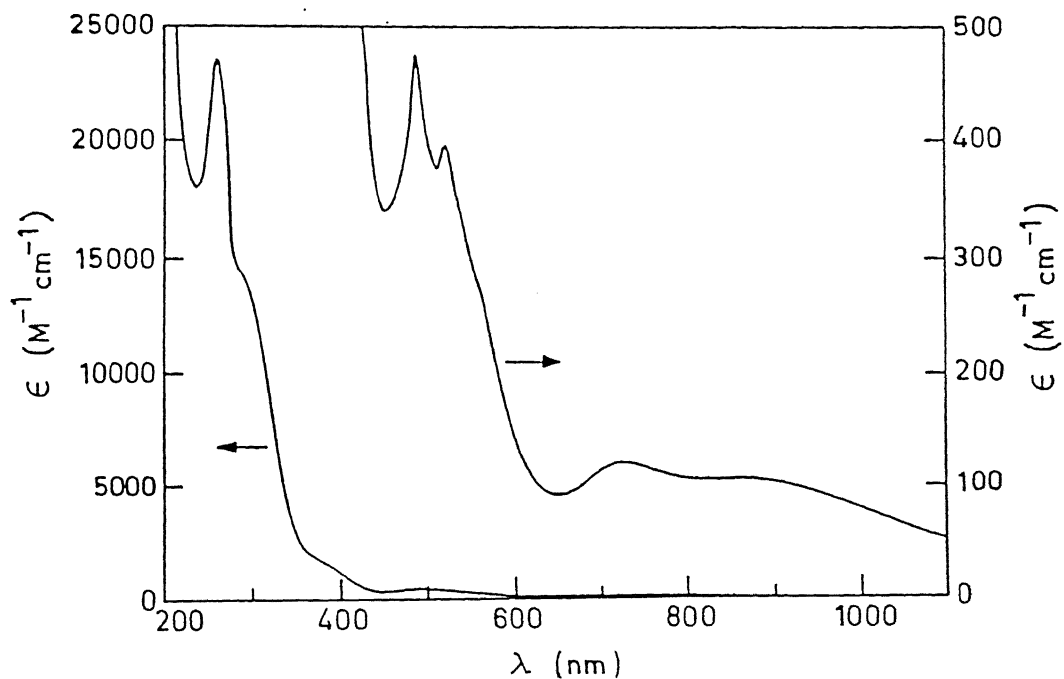


Figure V. 4 Electronic Spectrum of $[\text{Mn}^{\text{III}}_2(\mu\text{-O})(\mu\text{-OAc})_2(\text{MeL})_2](\text{PF}_6)_2 \cdot \text{H}_2\text{O}$ in MeCN

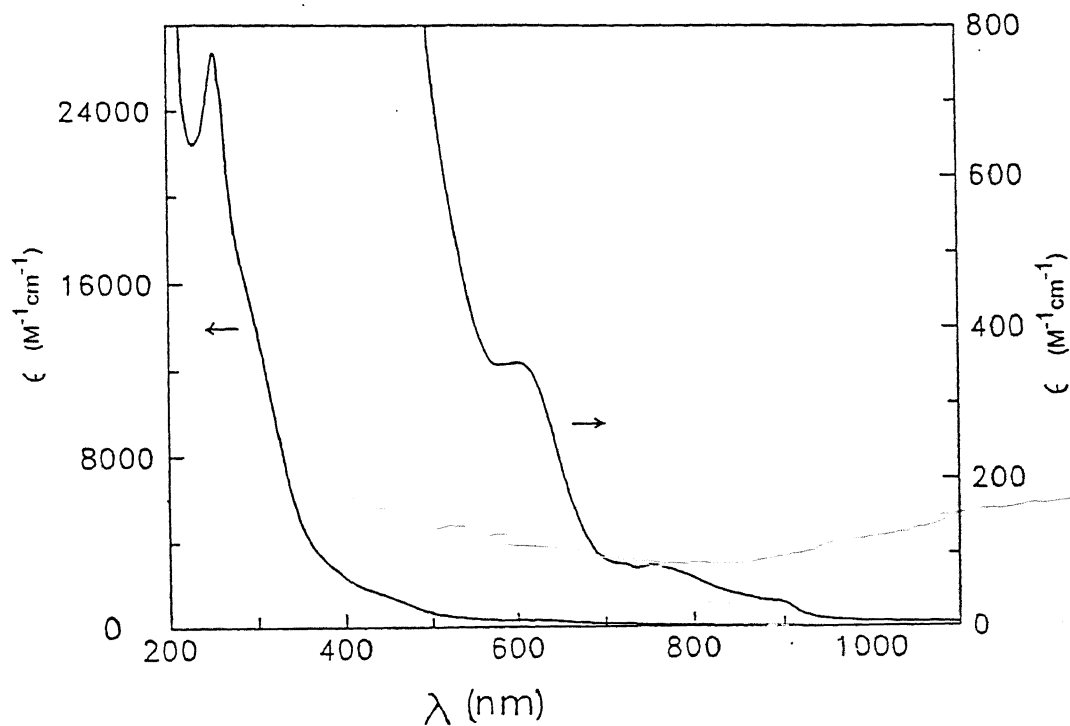


Figure V. 5 Electronic Spectrum of $[\text{Mn}^{\text{IV}}_2(\mu\text{-O})_2(\mu\text{-OAc})(\text{MeL})_2](\text{ClO}_4)_3 \cdot \text{H}_2\text{O}$

V.5. The electronic spectrum (Table V.3) is completely different than 1 and 2. Bands in the region 602 - 450 nm have been observed for other IV,IV dioxo-bridged Mn_2 complexes and assigned as $oxo \rightarrow metal\ d\pi^*$ charge-transfer transitions.^{216,217} The origin of the bands in the region 720-896 nm is not yet understood. Bands at 300 and 253 nm are due to intraligand charge transfer transitions.

V.5.4 FAB Mass Spectroscopy

The positive ion FAB mass spectrum of $[Mn^{III}_2(\mu-O)(\mu-OAc)_2(MeL)_2](PF_6)_2 \cdot H_2O$ (2a) is shown in Figure V.6. In this complicated spectrum (Figure V.6) the dipositive molecular ion $[Mn^{III}_2(\mu-O)(\mu-OAc)_2(MeL)_2]^{2+}$ (M/Z = 698) is observed and a monopositive molecular ion $[Mn^{III}_2(\mu-O)(\mu-OAc)_2(MeL)_2](PF_6)^+$ (M/Z = 843) with relatively low abundance is also observed. For 1a (Figure V.7) dipositive molecular ion $[Mn^{III}Mn^{IV}(\mu-O)_2(\mu-OAc)(MeL)_2]^{2+}$ (M/Z = 754) is observed. However, the complex 3 dissociates in the experimental conditions and only a very low abundant molecular ion peak of $[Mn^{IV}_2(\mu-O)_2(\mu-OAc)(MeL)_2]^{3+}$ (M/Z = 754) is observed (Figure V.8).

V.5.5 Magnetism

In order to have knowledge about the nature of coupling between the two Mn centers solid state as well as solution state magnetic susceptibility measurements were performed.

A. $Mn_2(III,IV)$ Core

Variable-temperature (19.8-300K) solid-state magnetic

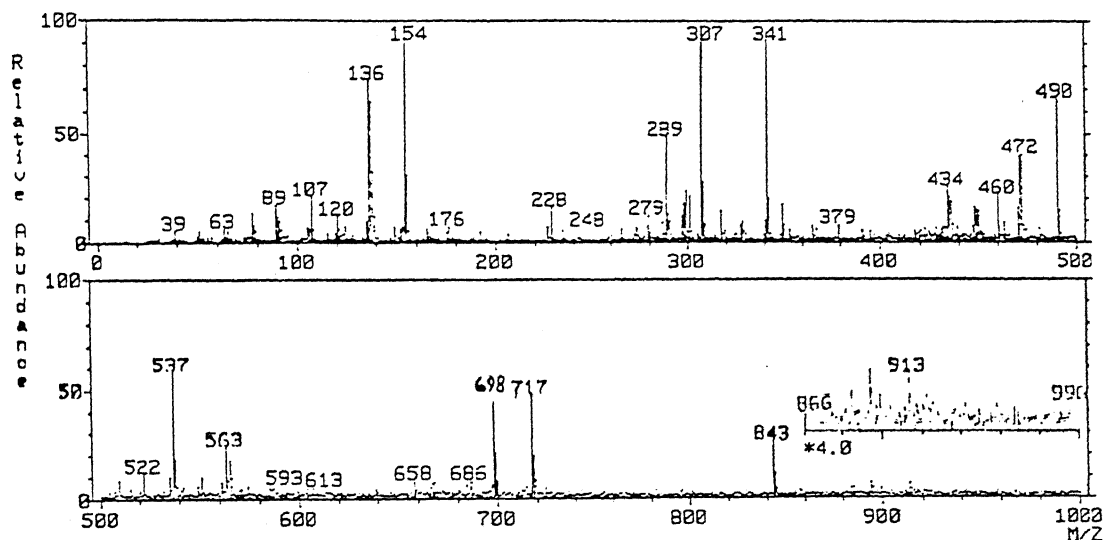


Figure V.6 FAB(positive) mass spectra of $[\text{Mn}^{\text{III}}_2(\mu\text{-O})(\mu\text{-OAc})_2(\text{MeL})_2](\text{ClO}_4)_2 \cdot \text{H}_2\text{O}$

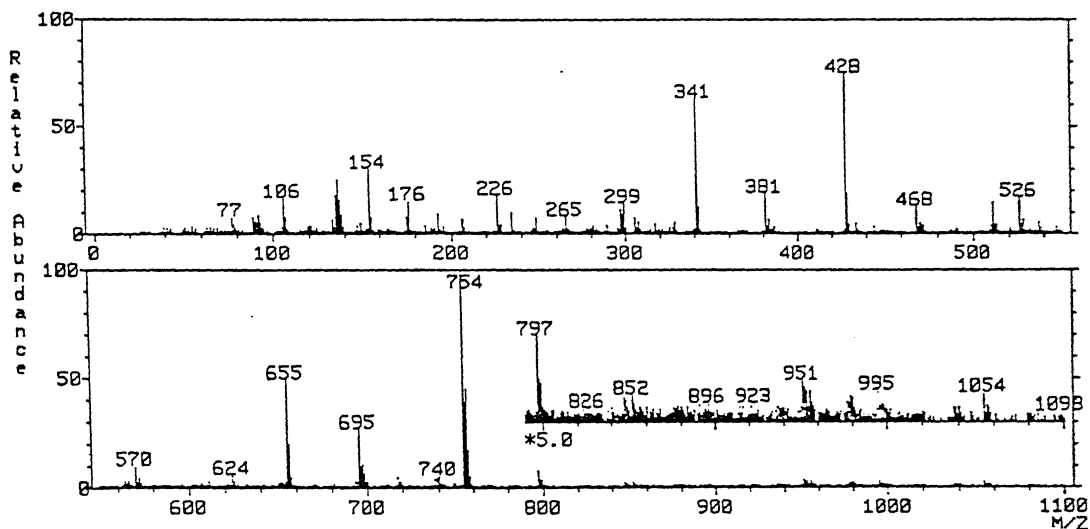


Figure V.7 FAB(positive) mass spectra of $[\text{Mn}^{\text{III}}\text{Mn}^{\text{IV}}(\mu\text{-O})_2(\mu\text{-OAc})(\text{MeL})_2](\text{ClO}_4)_2 \cdot \text{H}_2\text{O}$

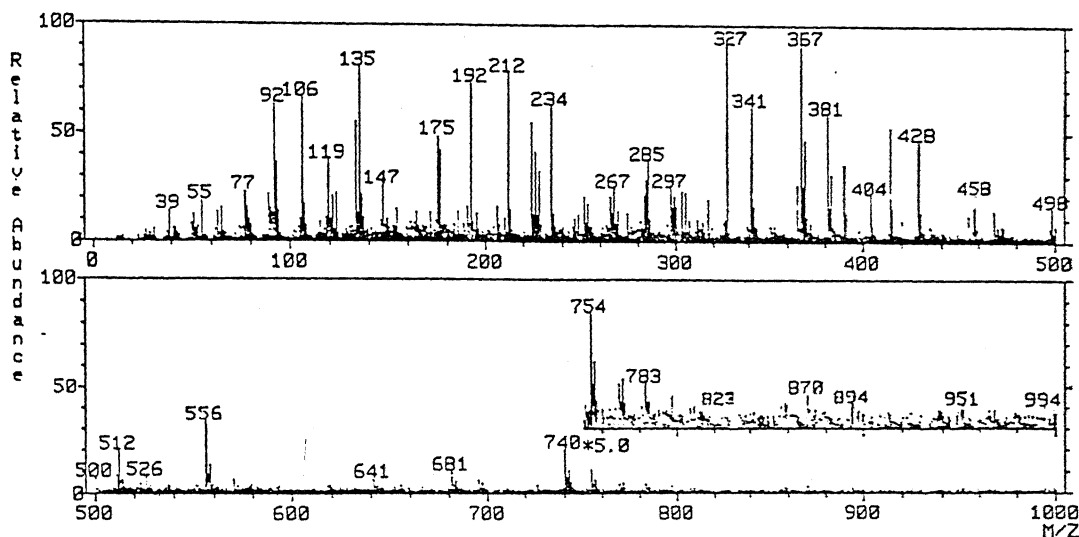


Figure V.8 FAB(positive) mass spectra of $[\text{Mn}^{\text{IV}}_2(\mu\text{-O})_2(\mu\text{-OAc})(\text{MeL})_2](\text{ClO}_4)_3 \cdot \text{H}_2\text{O}$

susceptibility data are consistent with a doublet ground state with $J = -144 \text{ cm}^{-1}$ (i.e. Mn(III) and Mn(IV) pair are antiferromagnetically coupled).

B. $\text{Mn}_2(\text{III}, \text{III})$ Core

Solution magnetic susceptibility measurements using the Evans' method^{129a} (MeCN, 300 K) gave magnetic moment of $5.0 \mu_B$ per manganese. This is very close to magnetically isolated Mn(III) (high spin d^4 system) ion $4.90 \mu_B$. In the temperature range 52-300 K molar magnetic susceptibilities (Table V.4) and magnetic moments per manganese of powdered sample of 2a (Faraday method) are also consistent with two isolated high spin Mn(III) centers. The magnetic moment of this complex was measured to be $4.91 \mu_B$ per manganese at 300 K, increasing slightly to $5.17 \mu_B$ per manganese at 52 K. Thus the magnetic data adhere closely to the Curie-Weiss law ($\mu = 5.03 \mu_B$; $\theta = -9.92 \text{ K}$; correlation coefficient = 0.9992). If the experimental χ_M^{-1} vs T (Figure V.9) data were fitted to the appropriate expression²²⁸ for Mn(III)-Mn(III) ($S = 2/S = 2$) pairs, only very weak ferromagnetic exchange coupling ($\sim +1 \text{ cm}^{-1}$) was obtained fixed $g = 2.0$; t.i.p. = $2.43 \times 10^{-4} \text{ cm}^3 \text{ M}^{-1}$; paramagnetic susceptibility from high spin Mn(III) impurity = $5.29 \times 10^{-3} \text{ cm}^3 \text{ M}^{-1}$). The observed magnetic behavior is similar to that encountered with related binuclear Mn(III) systems.^{195, 196, 201}

C. $\text{Mn}_2(\text{IV}, \text{IV})$ Core

For complex 3 room temperature solution magnetic moment per Mn is $2.48 \mu_B$ which is relatively higher than those of the related systems,²¹⁵⁻²¹⁸ implying the presence of weak coupling

Table V.4 Variable-Temperature Magnetic Susceptibility data of 2a

T, K	χ_M (exptl)	χ_M (calcd)	T, K	χ_M (exptl)	χ_M (calcd)
52	1.287E-01	1.288E-01	180	3.529E-02	3.480E-02
61	1.074E-01	1.083E-01	200	3.120E-02	3.125E-02
80	8.160E-02	8.097E-02	225	2.741E-02	2.772E-02
100	6.434E-02	6.398E-02	250	2.377E-02	2.491E-02
120	5.395E-02	5.288E-02	275	2.168E-02	2.262E-02
140	4.600E-02	4.507E-02	300	2.008E-02	2.072E-02
160	3.990E-02	3.927E-02			

χ_M in $\text{cm}^3 \text{mol}^{-1}$; $J = 9.99 \times 10^{-1}$; χ_{para} (high spin Mn(III) impurity) = $5.29 \times 10^{-3} (\text{cm}^3 \text{mol}^{-1})$; $g = 2.00$; TIP = $2.43 \times 10^{-4} \text{cm}^3 \text{mol}^{-1}$; Final residual error = 6.65×10^{-6} .

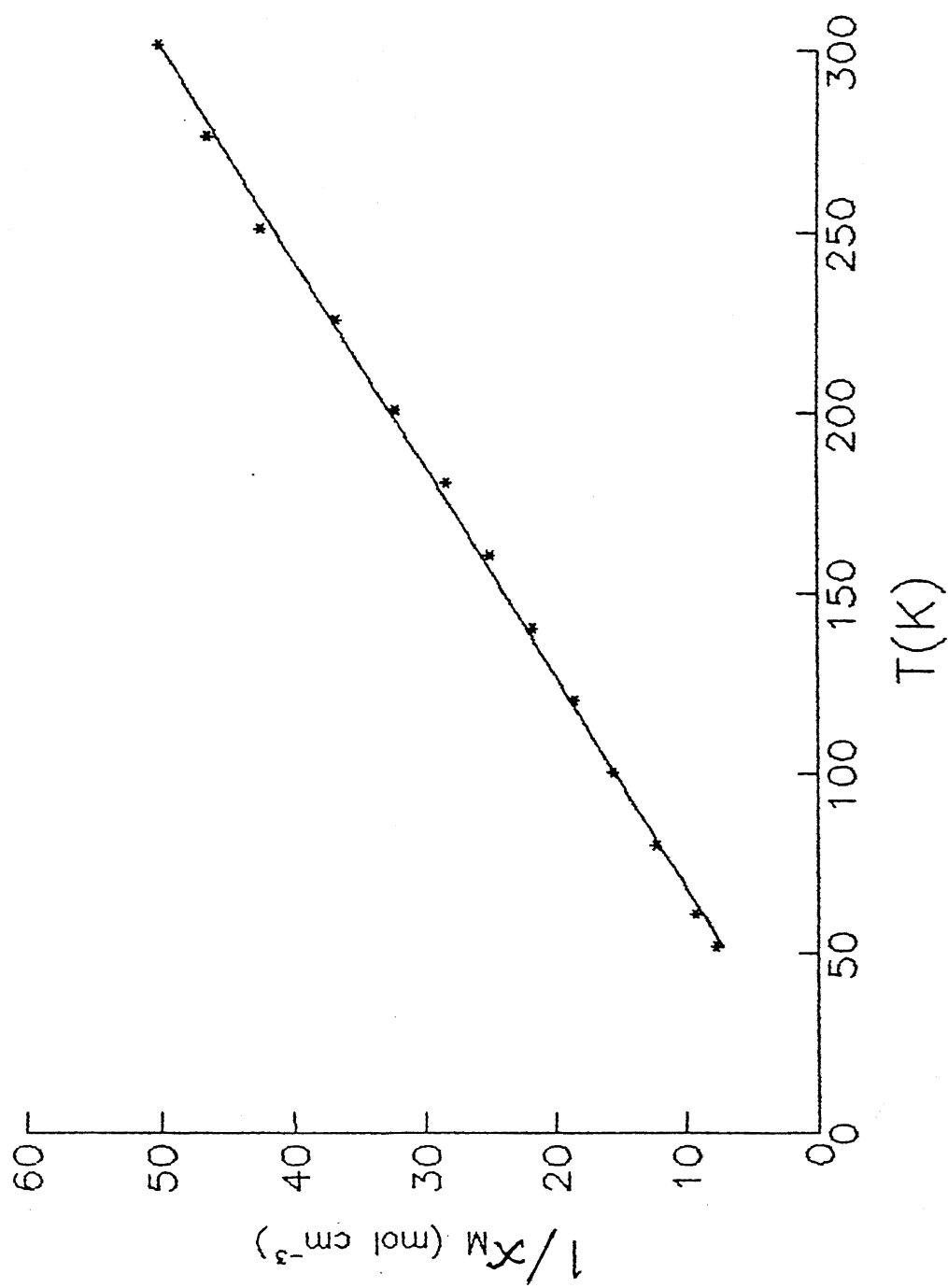


Figure V.9 Plot of χ_M^{-1} vs T for $[\text{Mn}^{\text{III}}_2(\mu\text{-O})(\mu\text{-OAc})_2(\text{MeL})_2](\text{PF}_6)_2 \cdot \text{H}_2\text{O}$

in 3. Detailed variable-temperature magnetic susceptibility measurements are planned for this complex.

V.5.6 Description of X-ray Structure of the $[\text{Mn}^{\text{III}}\text{Mn}^{\text{IV}}(\mu\text{-O})_2(\mu\text{-OAc})(\text{MeL})_2](\text{BF}_4)_2 \cdot 2\text{MeCN}$ (1a)

The ORTEP of the cationic part of **1a** is shown in Figure V.10. The ligand MeL binds each Mn atom in a facial configuration. The other three coordination sites of both the Mn atoms are occupied by the two bridged oxo groups and the oxygen atoms of the bridged acetate group. The Mn(IV) and Mn(III) ions (Mn(1) and Mn(2), respectively) are clearly distinguishable in **1a** on the basis of bond distances (Table V.5). The Mn...Mn distance (2.619(4) Å) is within the range (2.588(2)-2.741(1) Å) observed for other structurally characterized $\text{Mn}^{\text{III}}\text{Mn}^{\text{IV}}$ dioxo-bridged complexes.²⁰⁵ Bond angles (Table V.5) suggest that geometry around both the Mn-centers are distorted octahedral (Table V.6),

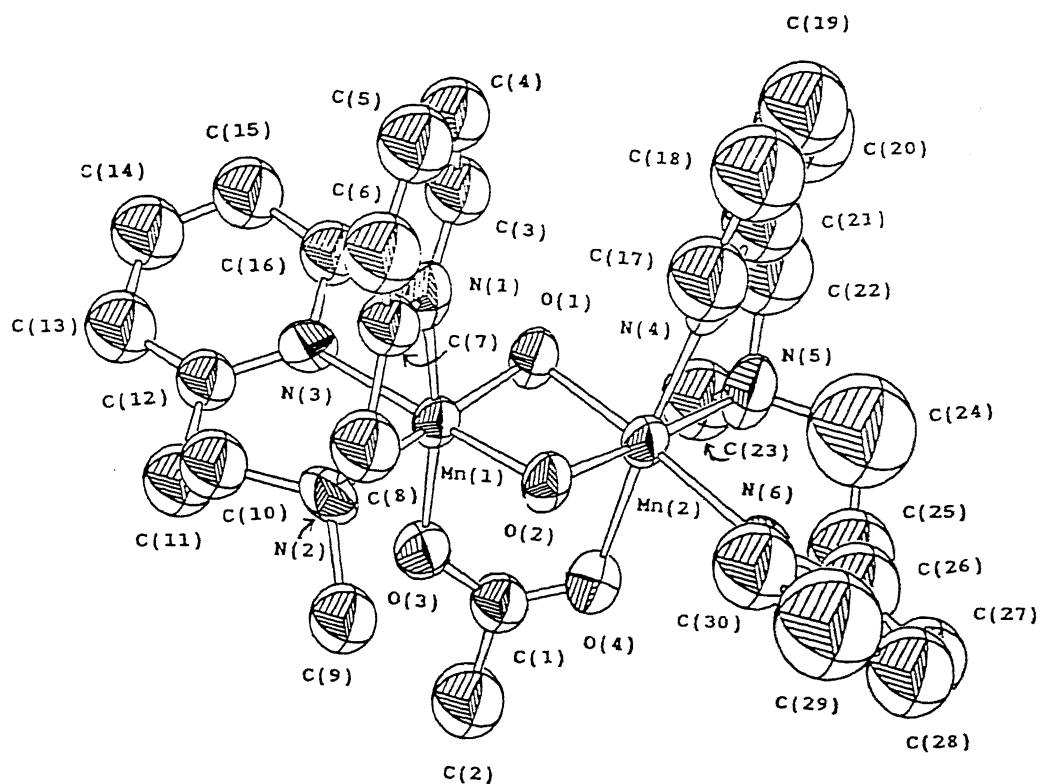


Figure V.10 ORTEP diagram of $[\text{Mn}^{\text{III}}\text{Mn}^{\text{IV}}(\mu\text{-O})_2(\mu\text{-OAc})(\text{MeL})_2](\text{BF}_4)_2 \cdot 2\text{MeCN}$ showing the 50% probability thermal ellipsoids and atom labeling scheme

Table V.5

Bond Distances

(Angstroms)

Mn1-Mn2	2.620 (4)	B2-F8a	1.28 (6)
Mn1-O1	1.772 (9)	B2-F8b	1.40 (4)
Mn1-O2	1.78 (1)	F5-F8b	1.08 (6)
Mn1-O3	1.944 (8)	F6-F6a	1.16 (6)
Mn1-N1	2.03 (1)	F6-F6b	1.04 (6)
Mn1-N2	2.14 (1)	F6a-F6b	.67 (7)
Mn1-N3	2.10 (1)	F6a-F8a	1.63 (9)
Mn2-O1	1.82 (1)	F6b-F8a	1.28 (9)
Mn2-O2	1.816 (9)	F7-F7b	.75 (7)
Mn2-O4	2.19 (1)	F7a-F8	1.22 (9)
Mn2-N4	2.20 (1)	F7a-F8b	.8 (1)
Mn2-N5	2.11 (1)	F8-F8a	1.02 (6)
Mn2-N6	2.12 (2)	N8-C33	1.06 (6)
O3-C1	1.27 (2)	C33-C34	1.44 (6)
O4-C1	1.19 (2)	B1-F1	1.38 (1)
N1-C3	1.35 (2)	B1-F2	1.27 (3)
N1-C7	1.36 (2)	B1-F2a	1.37 (5)
N2-C8	1.50 (2)	B1-F2b	1.40 (6)
N2-C9	1.47 (2)	B1-F3	1.42 (5)
N2-C10	1.47 (3)	B1-F3a	1.53 (5)
N3-C12	1.32 (2)	B1-F3b	1.44 (6)
N3-C16	1.34 (2)	B1-F4	1.39 (3)
N4-C17	1.32 (2)	B1-F4a	1.42 (4)
N4-C21	1.47 (2)	B1-F4b	1.38 (5)
N5-C22	1.55 (2)	F1-F3	1.62 (5)
N5-C23	1.48 (3)	F2-F4a	.97 (4)
N5-C24	1.46 (4)	F2-F4b	1.63 (7)
N6-C26	1.36 (3)	F2a-F2b	.75 (6)
N6-C30	1.36 (2)	F2a-F3a	1.55 (8)
C1-C2	1.47 (2)	F2a-F3b	.94 (8)
C3-C4	1.35 (2)	F2a-F4b	1.57 (6)
C4-C5	1.32 (2)	F2b-F3b	1.60 (8)
C5-C6	1.39 (3)	F2b-F4b	1.46 (6)
C6-C7	1.31 (2)	F3-F3a	1.34 (8)
C7-C8	1.50 (2)	F3-F4a	1.39 (5)
C10-C11	1.48 (2)	F3a-F3b	.71 (8)
C11-C12	1.52 (2)	F4-F4b	1.02 (5)
C12-C13	1.39 (3)	N7-C31	1.11 (4)
C13-C14	1.37 (2)	C31-C32	1.41 (4)
C14-C15	1.33 (3)		
C15-C16	1.40 (3)		
C17-C18	1.50 (3)		
C18-C19	1.31 (3)		
C19-C20	1.34 (3)		
C20-C21	1.28 (4)		
C21-C22	1.46 (3)		
C24-C25	1.50 (3)		
C25-C26	1.44 (3)		
C26-C27	1.40 (3)		
C27-C28	1.36 (3)		
C28-C29	1.35 (3)		
C29-C30	1.36 (4)		
B2-F5	1.24 (3)		
B2-F6	1.43 (3)		
B2-F6a	1.34 (5)		
B2-F6b	1.38 (4)		
B2-F7	1.38 (3)		
B2-F7a	1.42 (5)		
B2-F7b	1.36 (5)		
B2-F8	1.31 (5)		

Contd.

Bond Angles	(degrees)
Mn2-Mn1-O1	43.9 (3)
Mn2-Mn1-O2	43.8 (3)
Mn2-Mn1-O3	87.2 (4)
Mn2-Mn1-N1	101.2 (4)
Mn2-Mn1-N2	132.8 (4)
Mn2-Mn1-N3	135.2 (3)
O1-Mn1-O2	86.5 (5)
O1-Mn1-O3	93.5 (4)
O1-Mn1-N1	95.2 (4)
O1-Mn1-N2	174.3 (5)
O1-Mn1-N3	92.2 (5)
O2-Mn1-O3	94.0 (4)
O2-Mn1-N1	89.6 (5)
O2-Mn1-N2	89.5 (5)
O2-Mn1-N3	177.9 (4)
O3-Mn1-N1	170.8 (5)
O3-Mn1-N2	90.8 (4)
O3-Mn1-N3	87.7 (4)
N1-Mn1-N2	80.8 (4)
N1-Mn1-N3	88.9 (5)
N2-Mn1-N3	91.7 (5)
Mn1-Mn2-O1	42.5 (3)
Mn1-Mn2-O2	42.6 (3)
Mn1-Mn2-O4	81.0 (3)
Mn1-Mn2-N4	104.8 (4)
Mn1-Mn2-N5	133.3 (5)
Mn1-Mn2-N6	135.2 (4)
O1-Mn2-O2	83.9 (4)
O1-Mn2-O4	89.3 (4)
O1-Mn2-N4	93.1 (5)
O1-Mn2-N5	92.2 (5)
O1-Mn2-N6	177.1 (5)
O2-Mn2-O4	88.7 (4)
O2-Mn2-N4	97.6 (4)
O2-Mn2-N5	175.8 (6)
O2-Mn2-N6	94.2 (5)
O4-Mn2-N4	173.5 (4)
O4-Mn2-N5	89.7 (4)
O4-Mn2-N6	88.5 (5)
N4-Mn2-N5	84.1 (5)
N4-Mn2-N6	89.4 (5)
N5-Mn2-N6	89.6 (6)
Mn1-O1-Mn2	93.7 (4)
Mn1-O2-Mn2	93.7 (4)

Table V.6

Non-Hydrogen Positional, Isotropic Displacement and Site Occupation

Parameter

	x/a	y/b	z/c	U	PP
Mn(1)	0.2764(2)	0.7924(2)	0.1533(1)	* 0.043(1)	
Mn(2)	0.2350(2)	0.9578(2)	0.1980(2)	* 0.048(1)	
O(1)	0.1371(8)	0.8694(7)	0.1857(6)	* 0.050(5)	
O(2)	0.3756(8)	0.8593(7)	0.1881(6)	* 0.050(5)	
O(3)	0.2718(9)	0.8949(7)	0.0273(6)	* 0.053(5)	
O(4)	0.240(1)	1.0435(8)	0.0498(7)	* 0.068(5)	
N(1)	0.299(1)	0.6686(9)	0.2770(8)	* 0.058(6)	
N(2)	0.453(1)	0.6966(9)	0.1266(8)	* 0.059(6)	
N(3)	0.155(1)	0.7118(9)	0.1167(7)	* 0.047(6)	
N(4)	0.215(1)	0.8887(9)	0.3467(8)	* 0.066(7)	
N(5)	0.063(1)	1.068(1)	0.2046(9)	* 0.072(7)	
N(6)	0.355(1)	1.060(1)	0.2064(8)	* 0.078(8)	
N(7)	0.234(2)	0.427(2)	0.260(1)	* 0.159(7)	
N(8)	0.269(3)	1.079(2)	0.431(2)	* 0.18(1)	
C(1)	0.256(1)	0.996(1)	0.001(1)	0.051(4)	
C(2)	0.262(2)	1.056(1)	-0.098(1)	0.088(6)	
C(3)	0.203(2)	0.647(1)	0.343(1)	0.068(5)	
C(4)	0.232(2)	0.564(1)	0.424(1)	0.081(5)	
C(5)	0.353(2)	0.504(1)	0.438(1)	0.088(6)	
C(6)	0.450(2)	0.525(2)	0.370(1)	0.094(6)	
C(7)	0.422(2)	0.607(1)	0.292(1)	0.063(4)	
C(8)	0.521(2)	0.644(1)	0.217(1)	0.077(5)	
C(9)	0.538(2)	0.766(1)	0.059(1)	0.076(5)	
C(10)	0.430(2)	0.613(1)	0.099(1)	0.072(5)	
C(11)	0.334(2)	0.659(1)	0.025(1)	0.079(5)	
C(12)	0.191(1)	0.662(1)	0.061(1)	0.056(4)	
C(13)	0.109(2)	0.607(1)	0.041(1)	0.078(5)	
C(14)	-0.016(2)	0.608(1)	0.079(1)	0.080(5)	
C(15)	-0.055(2)	0.657(1)	0.134(1)	0.076(5)	
C(16)	0.033(2)	0.710(1)	0.154(1)	0.059(4)	
C(17)	0.304(2)	0.820(2)	0.407(1)	0.107(7)	
C(18)	0.261(2)	0.783(2)	0.505(1)	0.127(8)	
C(19)	0.137(3)	0.819(2)	0.522(1)	0.125(8)	
C(20)	0.049(2)	0.888(2)	0.459(2)	0.17(1)	
C(21)	0.079(2)	0.923(1)	0.374(1)	0.095(6)	
C(22)	0.000(2)	1.002(2)	0.296(1)	0.136(8)	
C(23)	-0.032(2)	1.095(2)	0.132(1)	0.100(6)	
C(24)	0.092(3)	1.157(2)	0.222(2)	0.21(1)	
C(25)	0.191(2)	1.206(2)	0.151(1)	0.127(8)	
C(26)	0.323(2)	1.167(2)	0.188(1)	0.125(8)	
C(27)	0.418(2)	1.223(1)	0.194(1)	0.108(7)	
C(28)	0.537(2)	1.162(2)	0.229(2)	0.127(8)	
C(29)	0.565(2)	1.054(2)	0.258(2)	0.21(1)	
C(30)	0.476(2)	1.005(1)	0.241(1)	0.112(7)	
C(31)	0.141(3)	0.421(2)	0.302(2)	0.131(9)	
C(32)	0.029(2)	0.415(2)	0.361(2)	0.130(8)	
C(33)	0.329(4)	1.124(3)	0.444(2)	0.20(2)	
C(34)	0.428(4)	1.183(3)	0.447(2)	0.22(1)	

Contd

B(1)	0.24109	0.62411	-0.20810	0.1000	
B(2)	-0.22272	0.72864	0.35818	0.1000	
F(1)	0.259(2)	0.533(1)	-0.128(1)	0.170(5)	
F(2)	0.228(3)	0.726(2)	-0.240(2)	0.143(9)	0.5000
F(2a)	0.271(4)	0.602(3)	-0.284(3)	0.06(1)	0.2500
F(2b)	0.226(4)	0.564(3)	-0.257(3)	0.08(1)	0.2500
F(3)	0.349(4)	0.625(3)	-0.160(3)	0.23(2)	0.5000
F(3a)	0.385(5)	0.624(3)	-0.242(4)	0.09(2)	0.2500
F(3b)	0.343(6)	0.630(4)	-0.277(3)	0.09(2)	0.2500
F(4)	0.104(3)	0.630(2)	-0.197(2)	0.135(9)	0.5000
F(4a)	0.237(3)	0.705(2)	-0.175(2)	0.037(7)	0.2500
F(4b)	0.132(5)	0.661(4)	-0.263(3)	0.10(1)	0.2500
F(5)	-0.197(3)	0.714(2)	0.436(2)	0.32(1)	
F(6)	-0.223(3)	0.841(2)	0.325(2)	0.17(1)	0.5000
F(6a)	-0.128(5)	0.786(3)	0.314(3)	0.08(2)	0.2500
F(6b)	-0.175(5)	0.805(4)	0.282(3)	0.07(1)	0.2500
F(7)	-0.353(3)	0.739(2)	0.388(2)	0.108(9)	0.5000
F(7a)	-0.125(6)	0.633(4)	0.382(5)	0.13(2)	0.2500
F(7b)	-0.351(5)	0.726(4)	0.347(3)	0.10(2)	0.2500
F(8)	-0.212(4)	0.652(3)	0.329(3)	0.18(1)	0.5000
F(8a)	-0.221(5)	0.728(5)	0.279(3)	0.11(2)	0.2500
F(8b)	-0.127(5)	0.655(4)	0.420(3)	0.09(1)	0.2500

V.5.7 A Comment on the Preliminary Single Crystal X-ray Structure of $[\text{Mn}_2^{\text{III}}(\mu\text{-O})(\mu\text{-OAc})_2(\text{MeL})_2](\text{ClO}_4)_2 \cdot \text{H}_2\text{O}$ (2b)

Even though we have been successful in growing crystals for this compound (from MeCN/MeCO₂Et layering at 273 K), so far we have not been able to solve the crystal structure due to (i) bad quality of crystals, (ii) crystallographic ambiguity in the assignment of the correct space group. However, considering orthorhombic space group $Pca2_1$ we have been able to have a rough idea about the coordination spheres of the two manganese atoms from the difference Fourier maps. It clearly indicates that the proposed tribridged core structure is correct. Our efforts are on to sort out the structural problems.

V.5.8 Electrochemistry

To investigate the redox properties of the Mn-dimers electrochemistry were performed in MeCN at a platinum working electrode using TBAP as supporting electrolyte. Understandably, an important test for the merit of any PSII model system is the thermodynamics of its redox reaction.

A. $\text{Mn}_2(\text{III}, \text{IV})$ Core

Electrochemical behavior of this core¹⁹⁴ is shown in Figure V.11. One reversible²⁴⁹³ oxidative response at +0.98 V (equation V.1) and another irreversible reductive response at -0.10 V (equation V.2) were observed.

B. $\text{Mn}_2(\text{III}, \text{III})$ Core

The redox behavior of complex 2a is very interesting.

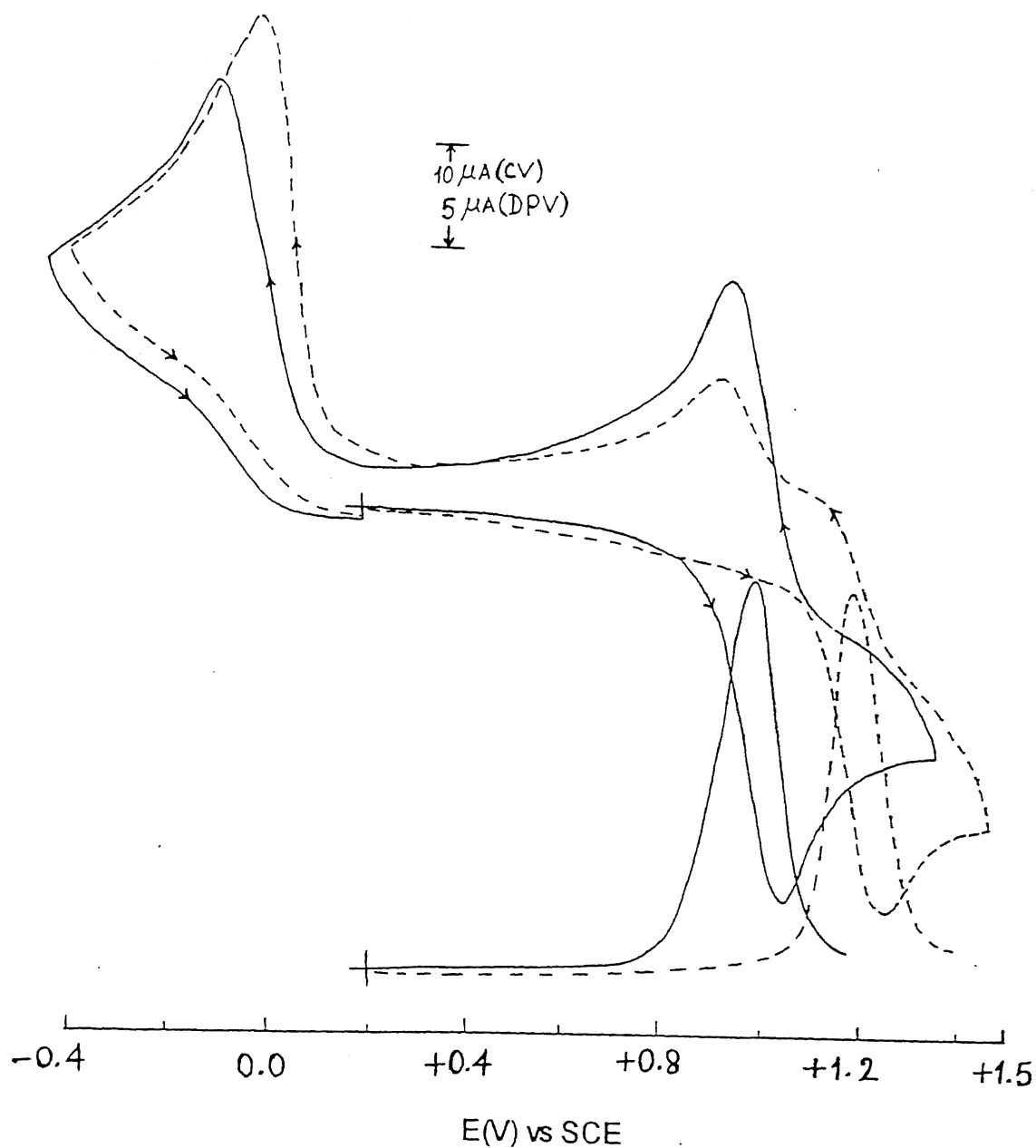
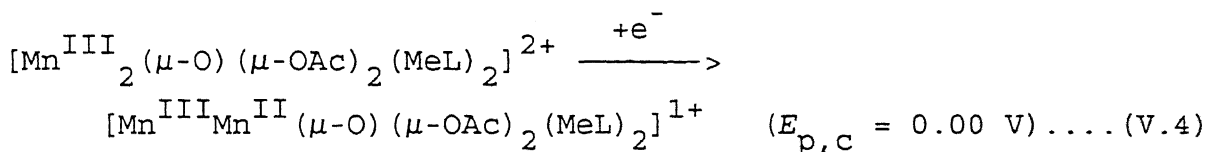
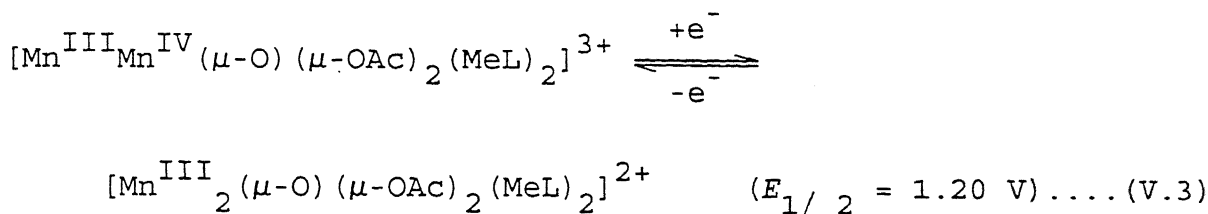
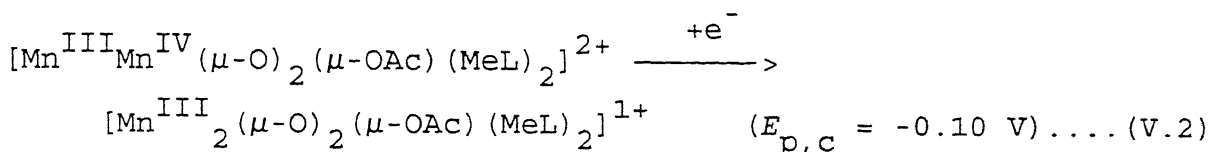
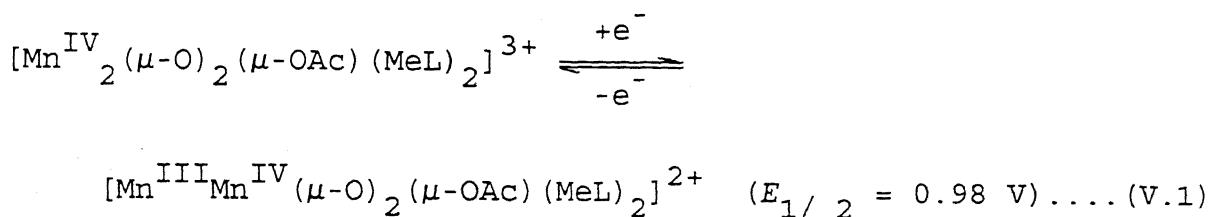


Figure V.11 Cyclic voltammograms (scan rate 50 mV s^{-1}) and differential pulse voltammograms (scan rate 5 mV s^{-1} , modulation amplitude 25 mV , drop time 0.5 s) of $[Mn^{III}_2(\mu-O)(\mu-OAc)_2(MeL)_2](ClO_4)_2 \cdot H_2O$ (---) $[Mn^{III}Mn^{IV}(\mu-O)_2(\mu-OAc)(MeL)_2](ClO_4)_2 \cdot H_2O$ (—) in MeCN at a platinum electrode; supporting electrolyte TBAP

The cyclic voltammetry of a 10^{-3} M MeCN solution of $[\text{Mn}^{\text{III}}_2(\mu\text{-O})(\mu\text{-OAc})_2(\text{MeL})_2]^{2+}$ in 0.2 M TBAP shows at a scan rate > 1000 mv/s a reversible oxidative response at +1.20 V ($\Delta E_p = 80$ mV and an irreversible reductive response at 0.00 V (Figure V.12). The electrode reactions for 1a and 2 are given in equations V.1, V.2 and equations V.3, V.4 respectively.



In order to estimate the thermodynamic stability of 2a we have calculated the comproportionation constant (K_{com} at 298 K; $\sim 1.0 \times 10^{21}$) of the reaction V.5 (the anodic wave of for the reductive response of 2a was not observed on scan reversal: the $E_{1/2}$ value is a rough estimate (cathodic peak potential + 40 mV ²³⁶)

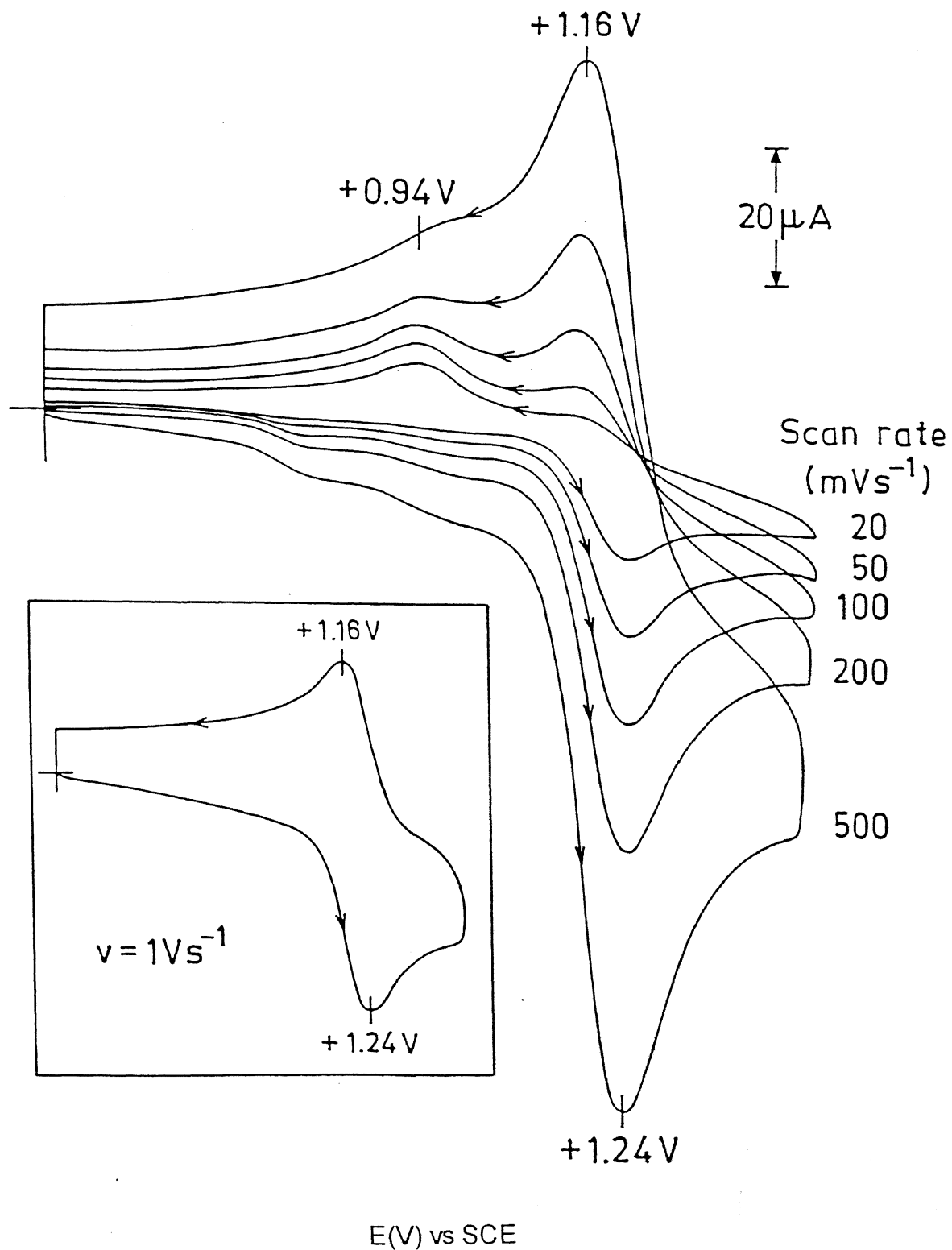
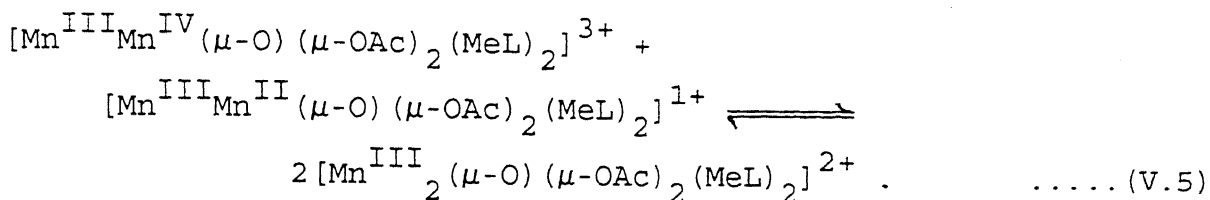


Figure V.12 Variable scan cyclic voltammograms of $[\text{Mn}^{\text{III}}_2(\mu\text{-O})(\mu\text{-OAc})_2(\text{MeL})_2](\text{ClO}_4)_2 \cdot \text{H}_2\text{O}$ in MeCN at platinum electrode; supporting electrolyte TBAP

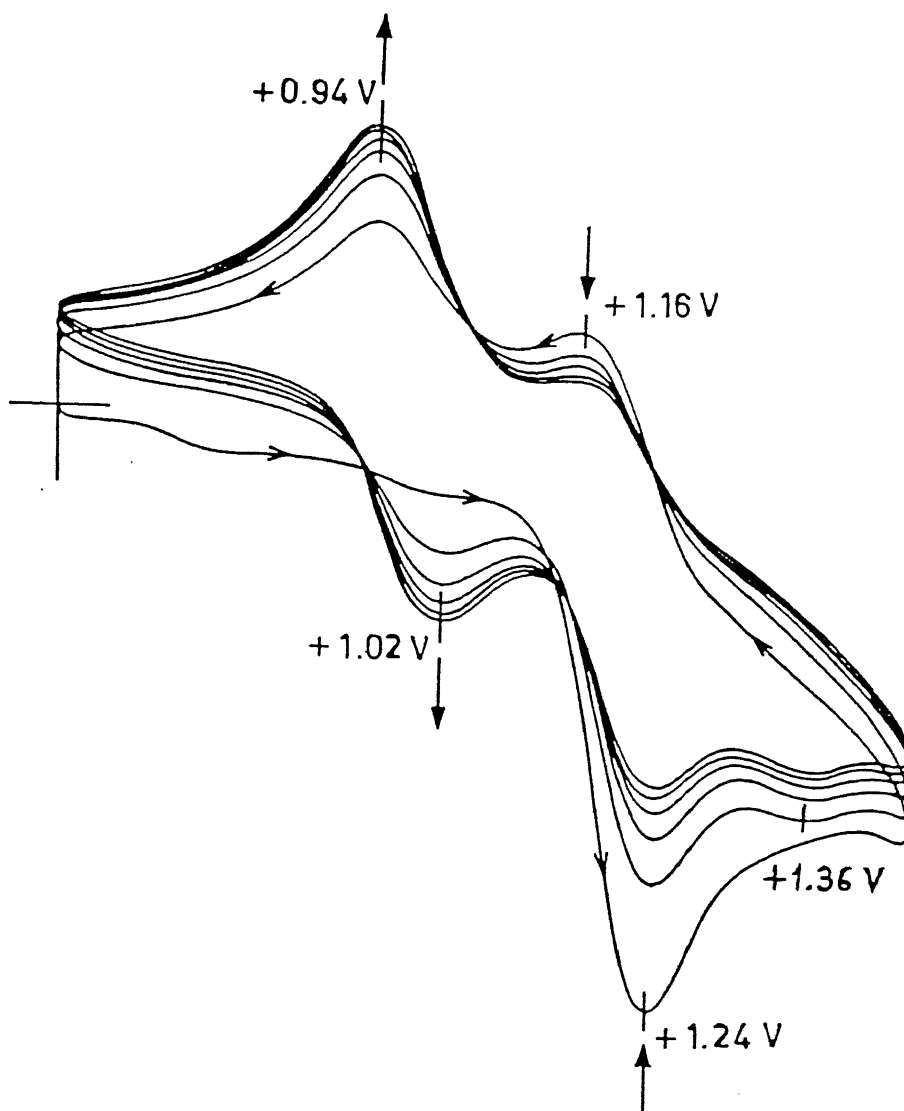


When the potential scan rates were in the range 20-500 mV/s, after initial scanning to monitor the oxidative response at +1.20 V during cathodic scan an additional ill-defined wave was observed at +0.94 V (Figure V.12).

The cyclic voltammetric results of **2a** are comparable to those of the reported complexes having similar core units. 195-197, 200

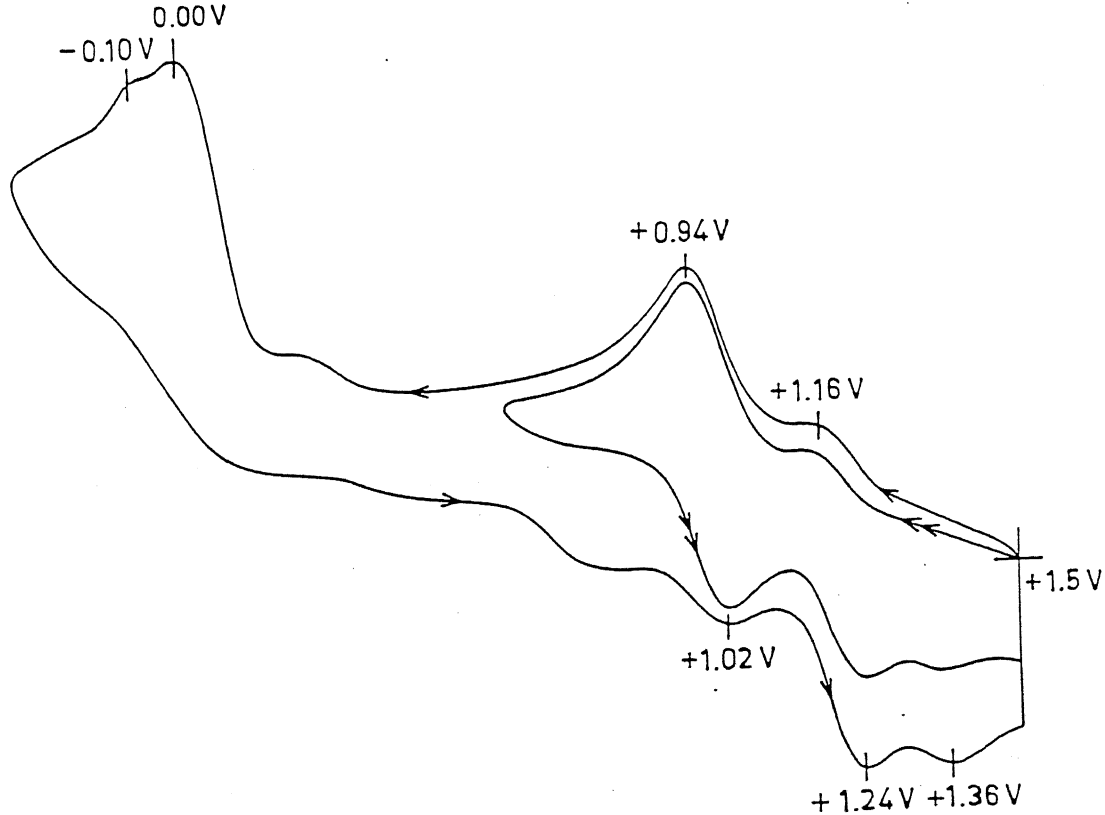
For **2a** on repetitive scanning of the potential between the limits 0.60-1.50 V, at the expense of the higher potential response (equation V.2) a new redox wave (equation V.1) is being formed which is due to the formation of **1a** at the electrode surface (Figure V.11, V.12 and V.13). An identical behavior is observed (Figure V.14), when examined by cyclic voltammetry, after holding the potential at +1.50 V for 30 s (in order to oxidize all of the $\text{Mn}_2(\text{III})$ complex in the double layer) scanning (at 50 mV/s scan rate) is done cathodically upto +0.60V.

It is worthnoting that in the two Figures V.13 and V.14 an additional irreversible response is observed at +1.36 V which is associated with the formation of the lower potential mixed-valent species. On scannig of the potential further down to -0.40 V, two irreversible reductive responses corresponding to electrode processes (equations V.2 and V.4) are observed (Figure V.14).



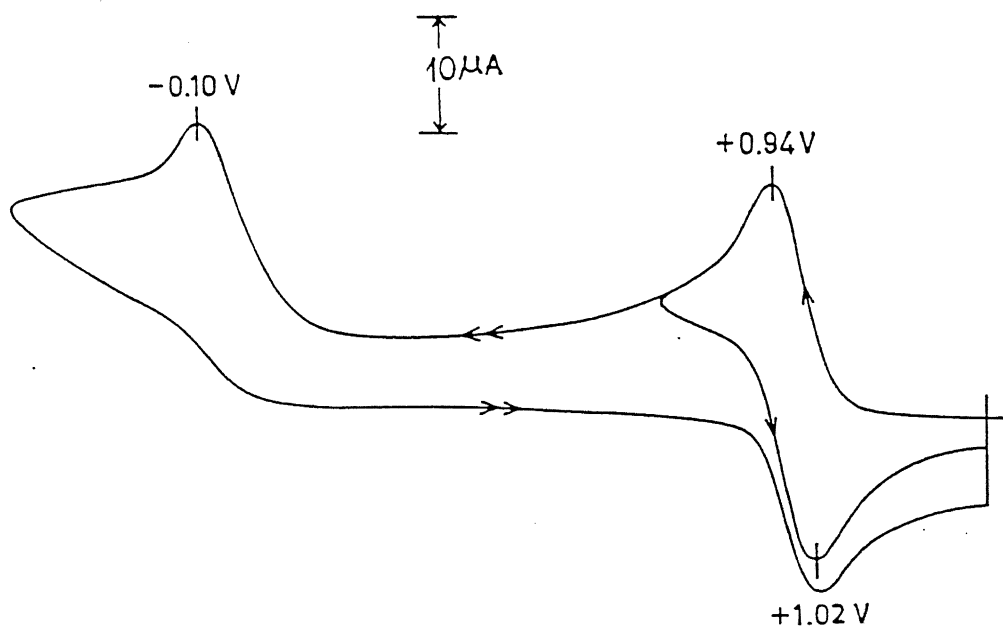
$E(\text{V})$ vs SCE

Figure V.13 Repetitive scan cyclic voltammograms of $[\text{Mn}^{\text{III}}_2(\mu\text{-O})(\mu\text{-OAc})_2(\text{MeL})_2](\text{ClO}_4)_2 \cdot \text{H}_2\text{O}$ in MeCN at platinum electrode; supporting electrolyte TBAP



E(V) vs SCE

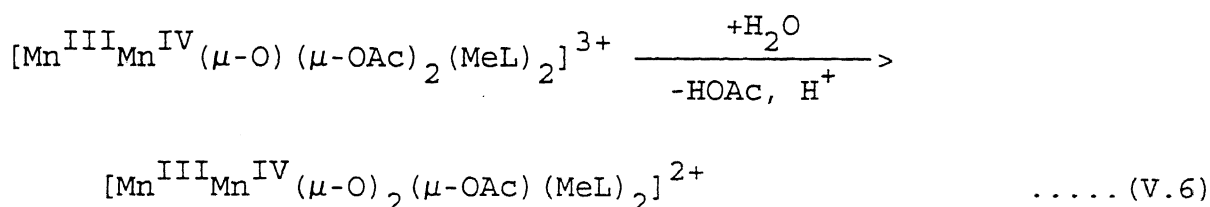
Figure V.14 Cyclic voltammograms of $[\text{Mn}^{\text{III}}_2(\mu\text{-O})(\mu\text{-OAc})_2(\text{MeL})_2](\text{ClO}_4)_2 \cdot \text{H}_2\text{O}$ (scan rate = 50 mV s^{-1}) at platinum electrode in MeCN; supporting electrolyte TBAP) after holding the potential at 1.50 V for 30 seconds



E(V) vs SCE

Figure V.15 Cyclic voltammograms (scan rate 50 mV s^{-1}) of $[\text{Mn}^{\text{IV}}_2(\mu\text{-O})_2(\mu\text{-OAc})-(\text{MeL})_2](\text{ClO}_4)_3 \cdot \text{H}_2\text{O}$ in MeCN at a platinum electrode; supporting electrolyte TBAP

The above two experiments point toward redox transformation of 2a to the one-electron oxidized form of 1a under oxidative conditions. Thus this is a clear case of an ECE mechanism²¹⁹ where removal of the second electron occurs with greater facility than removal of the first (compare equations V.1 and V.3). The chemical reaction after removal of the first electron from 2a could be as follows:



Thus, as the potential scanning is made upto the oxidative couple of 2a (equation V.3), $[\text{Mn}^{\text{III}}\text{Mn}^{\text{IV}}(\mu\text{-O})(\mu\text{-OAc})_2(\text{MeL})_2]^{2+}$ is oxidized to $[\text{Mn}^{\text{III}}\text{Mn}^{\text{IV}}(\mu\text{-O})(\mu\text{-OAc})_2(\text{MeL})_2]^{3+}$, which in turn transforms to 3. Coulometric oxidation of 2a at +1.50 V gives rise to an effective 2-electron transfer. For complete oxidation (at +1.50 V) of 5.29×10^{-4} mol of 2a, 0.99 C was observed. The value calculated for $n = 2$ is 1.02 C.

C. $\text{Mn}_2(\text{IV}, \text{IV})$ Core

For 3 on cathodic scanning starting from +1.40 V similar observations were obtained as that of equations V.1 and V.2 (Figure V.15).

V.5.9 EPR Spectra

Room temperature solid state EPR spectrum of 3 is shown in Figure V.16. There are two features in this spectrum to

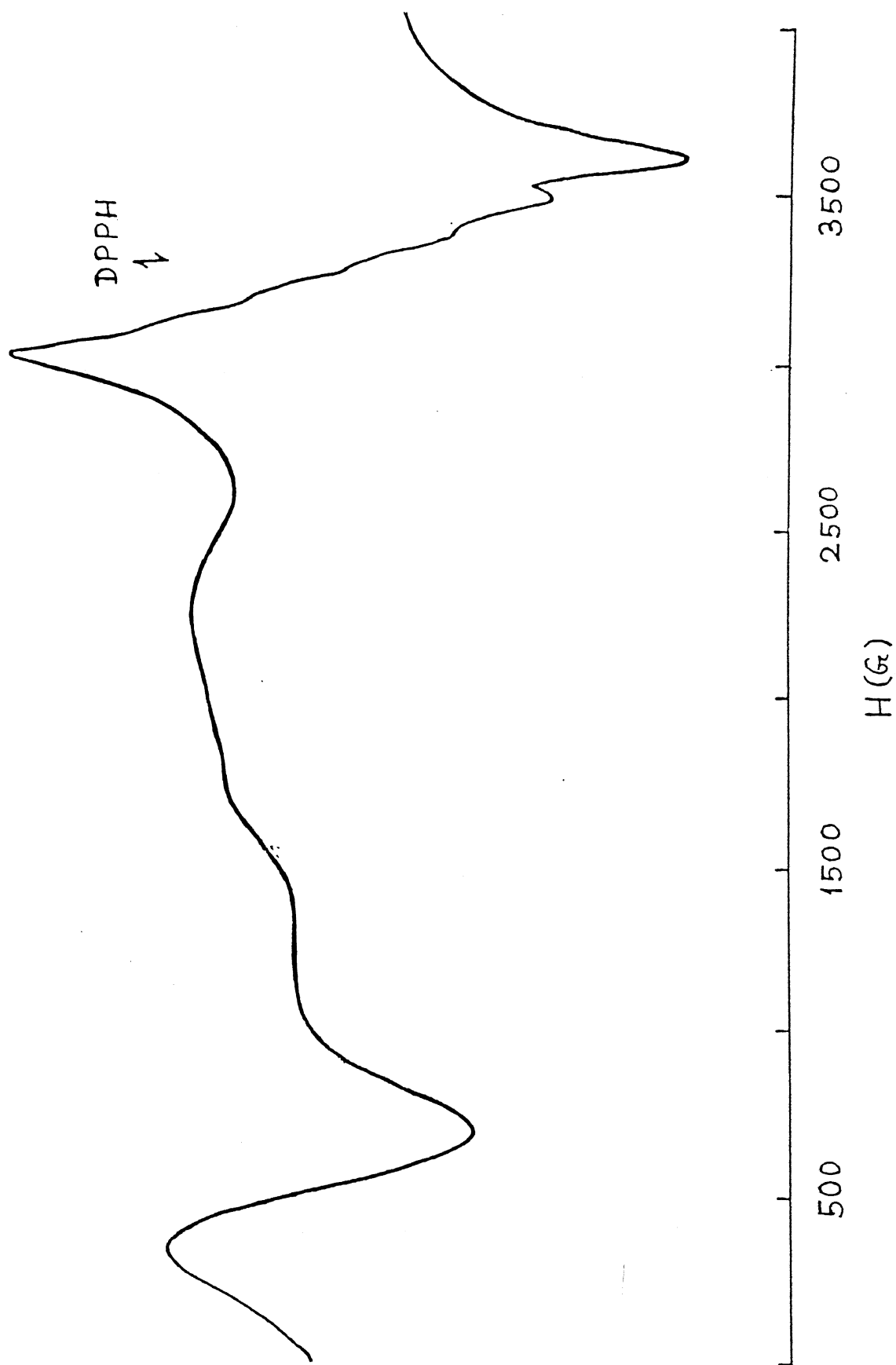


Figure V.16 EPR spectrum of $[\text{Mn}^{\text{IV}}_2(\mu\text{-O})_2(\mu\text{-OAc})(\text{MeL})_2](\text{ClO}_4)_3 \cdot \text{H}_2\text{O}$ (in powder form) at 298K

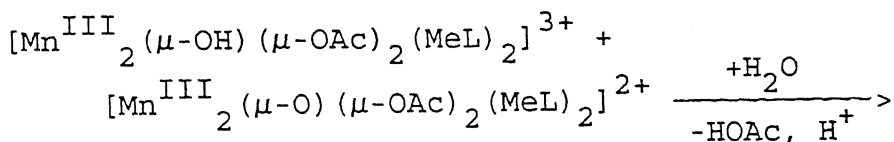
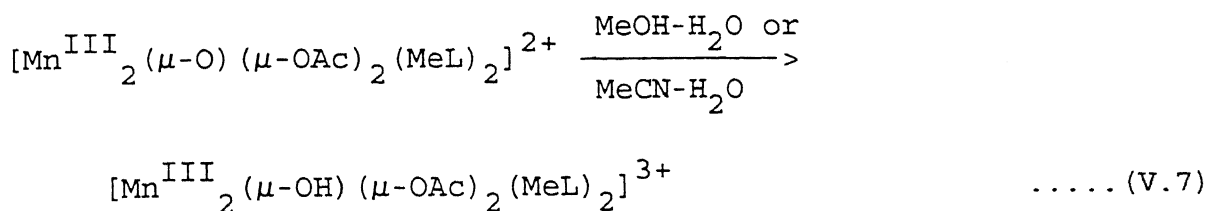
be noted: the broad high field signal ($g = 2$) is manganese hyperfine structured and another comparatively weak band at low field with g value of 11.88. The high field signal is due to the presence of trace amount of mononuclear Mn(II) and / or Mn(IV) impurities.^{220,224} The low field signal is indicative of weak dimer-dimer interactions.²²²⁻²²³ The low field signal disappears at 80 K implying that at 80 K such type of interaction vanishes.

V.5.10 Interconversions

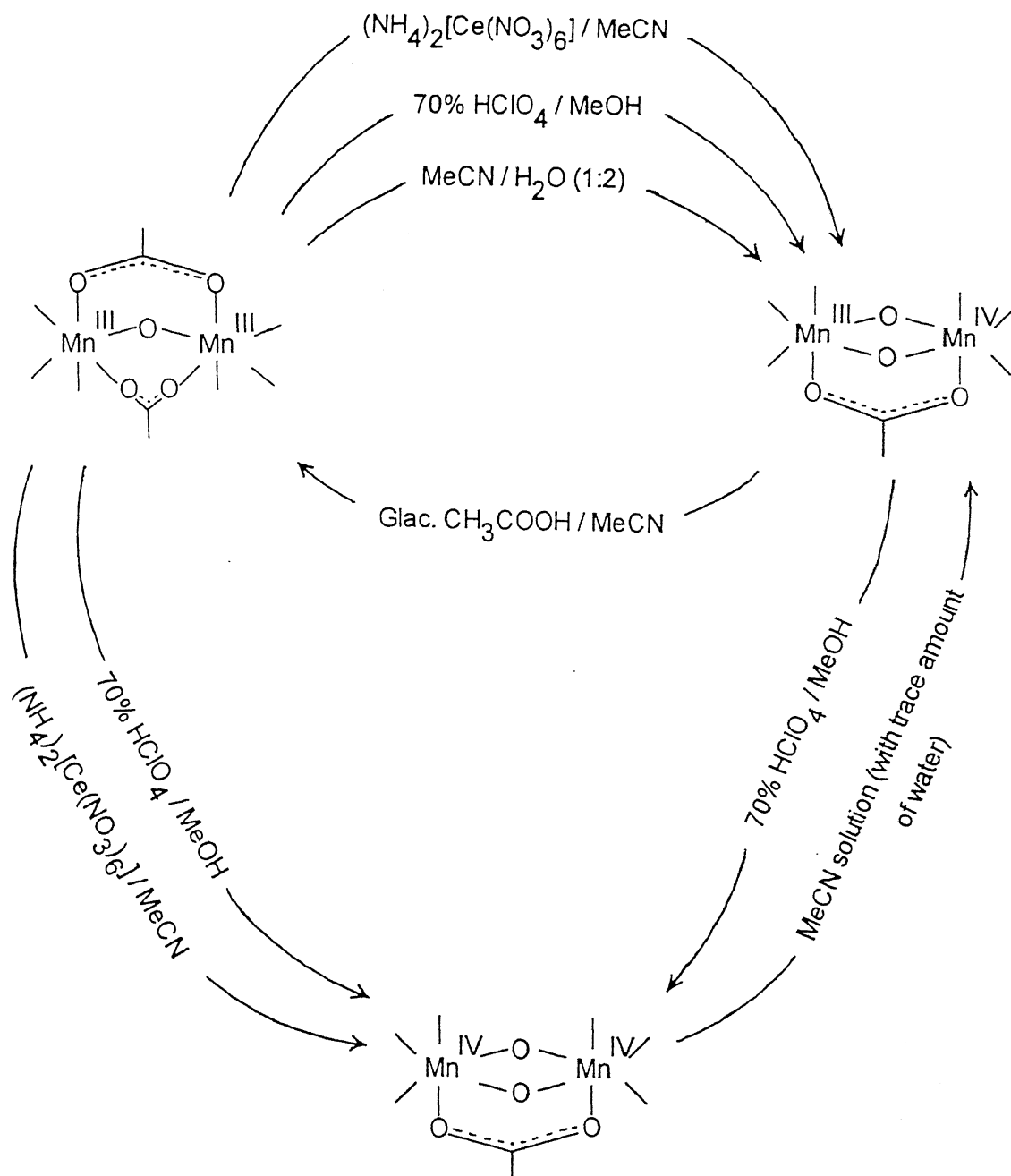
A very interesting point to note here is the facile transformation of one binuclear core to another among the three cores (Scheme V.1).

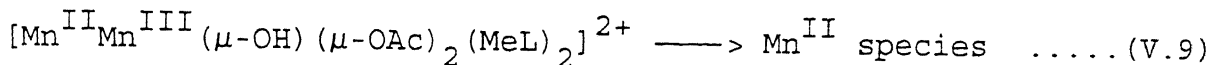
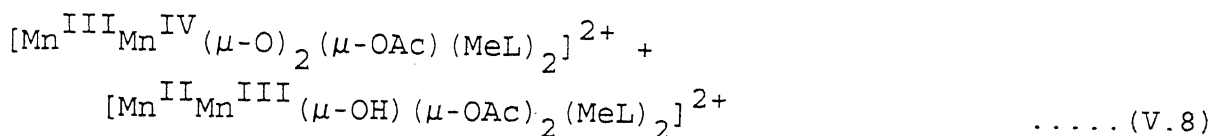


Disproportionation of $\text{Mn}_2(\text{III}, \text{III})$ to $\text{Mn}_2(\text{III}, \text{IV})$ and $\text{Mn}_2(\text{II}, \text{III})$ in protic solvents like aqueous MeOH and aqueous MeCN, as indicated by the following equations:



Scheme V.1

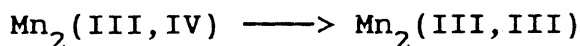
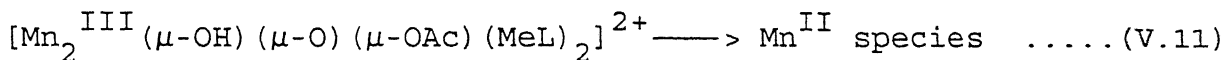
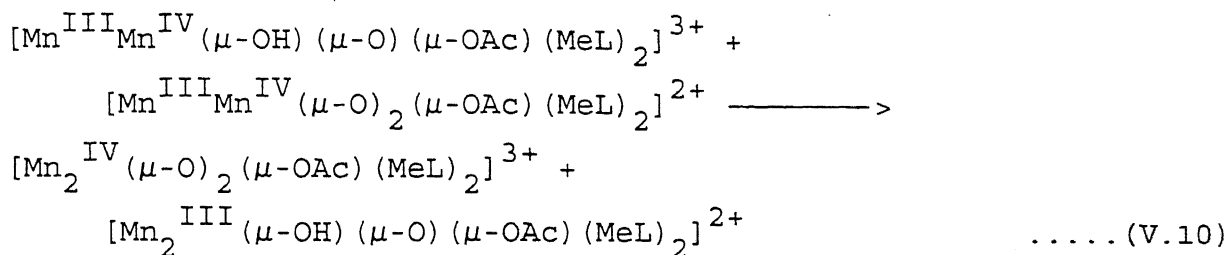




Formation of Mn(II) species (as shown in equation V.9) is confirmed by 6 line EPR spectrum (not shown) of the lightly colored filtrate.

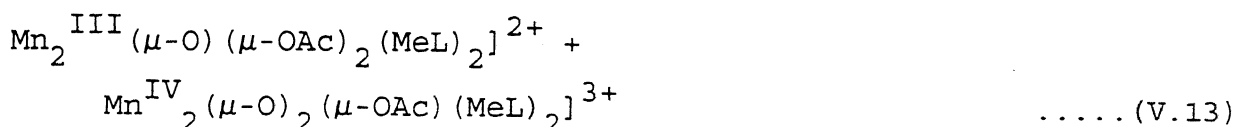
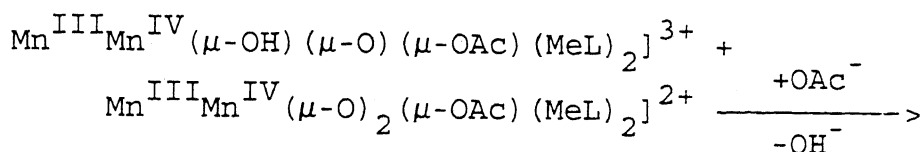
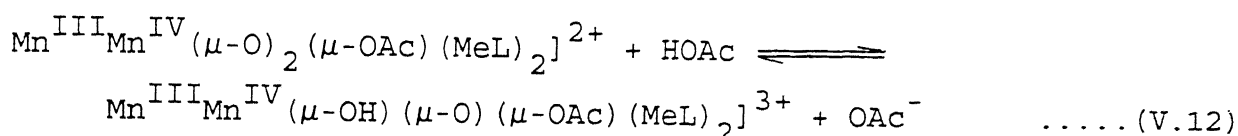


In this conversion initially $\text{Mn}_2(\text{III}, \text{III})$ is transformed to $\text{Mn}_2(\text{III}, \text{IV})$ and then to $\text{Mn}_2(\text{IV}, \text{IV})$ via formation of $[\text{Mn}^{\text{III}}\text{Mn}^{\text{IV}}(\mu\text{-OH})(\mu\text{-O})(\mu\text{-OAc})(\text{MeL})_2]^{3+}$ in presence of HClO_4 . The latter species oxidizes the $\text{Mn}_2(\text{III}, \text{IV})$ species as follows:

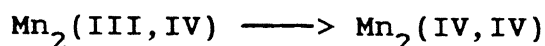


This conversion is an interesting observation of the present work. This transformation is brought about by glacial acetic acid in MeCN solution (as described in section V.3.2, (ii) Method B); through disproportionation reaction. Controlled experiments indicate the mechanism of this transformation is as

shown in equations V.12 and V.13.



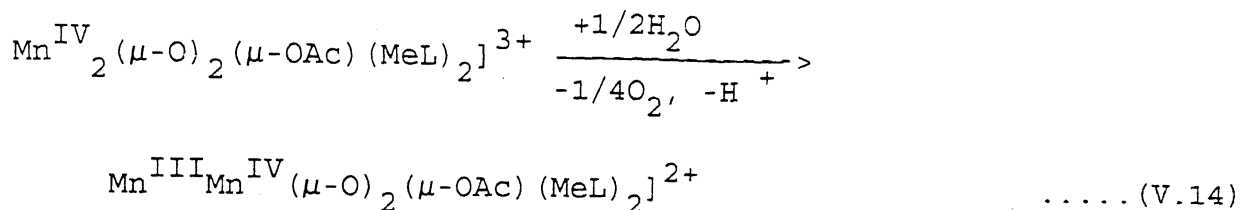
The $\text{Mn}_2(\text{IV}, \text{IV})$ thus formed²¹⁶ decomposes under the reaction conditions.



This conversion is already discussed in the transformation of $\text{Mn}_2(\text{III}, \text{III}) \longrightarrow \text{Mn}_2(\text{IV}, \text{IV})$.



The complex 3 is not as stable as that of 1a. The complex 3 in the solution state is only stable in absence of moisture. The color of MeCN solution of 3 (containing trace amount of water) changes from brown to green after ~1 week. Thus the $\text{Mn}_2(\text{IV}, \text{IV})$ species transformed to $\text{Mn}_2(\text{III}, \text{IV})$ species. This is clearly supported by characteristic electronic spectral feature and cyclic voltammetric behavior. The only possibility during this transformation is simultaneous oxidation of water as shown in equation V.14.



V.5.11 Reactivities of Chloride ions with the Dimanganese Cores

The reactivities of the Cl^- ions with the dimanganese cores have been demonstrated by electronic spectral measurements and cyclic voltammetric experiments.

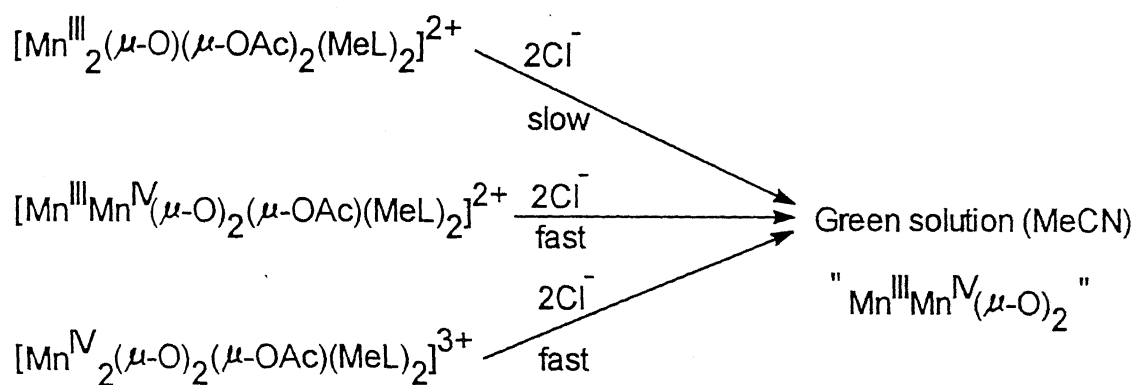
(i) Monitoring by Absorption Spectroscopy

When two equivalents of $\text{Et}_4\text{NCl} \cdot x\text{H}_2\text{O}$ was added to the MeCN solution of **1a** or **2b** or **3** the resulting solutions turned green (Scheme V.2). The electronic spectra of these green solutions are characteristics of a " $\text{Mn}^{\text{III}}\text{Mn}^{\text{IV}}(\mu\text{-O})_2$ " species. It has been observed that **2b** reacts rather slowly whereas **1a** and **3** react comparatively at a much faster rate. Changes in the electronic spectral feature after the addition of Cl^- is displayed in Figure V.17 for **2b**.

(ii) Monitoring by Cyclic Voltammetry

(a) During examination of a solution of **1a** and $\text{Et}_4\text{NCl} \cdot x\text{H}_2\text{O}$ (1:2 mole ratio) in MeCN by cyclic voltammetry at a platinum working electrode, scanning from 0.4 V to 1.40 V exhibits an oxidative response at ~1.00 V. The anodic peak height (i_{pa}) is larger than the cathodic one due to simultaneous oxidation of chloride ion ($\text{Cl}^- \xrightarrow{-e^-} 1/2 \text{Cl}_2$) (equations V.15; Figure V.18). The $\text{Mn}_2(\text{IV}, \text{IV})$ species thus generated at the electrode surface

Scheme v.2



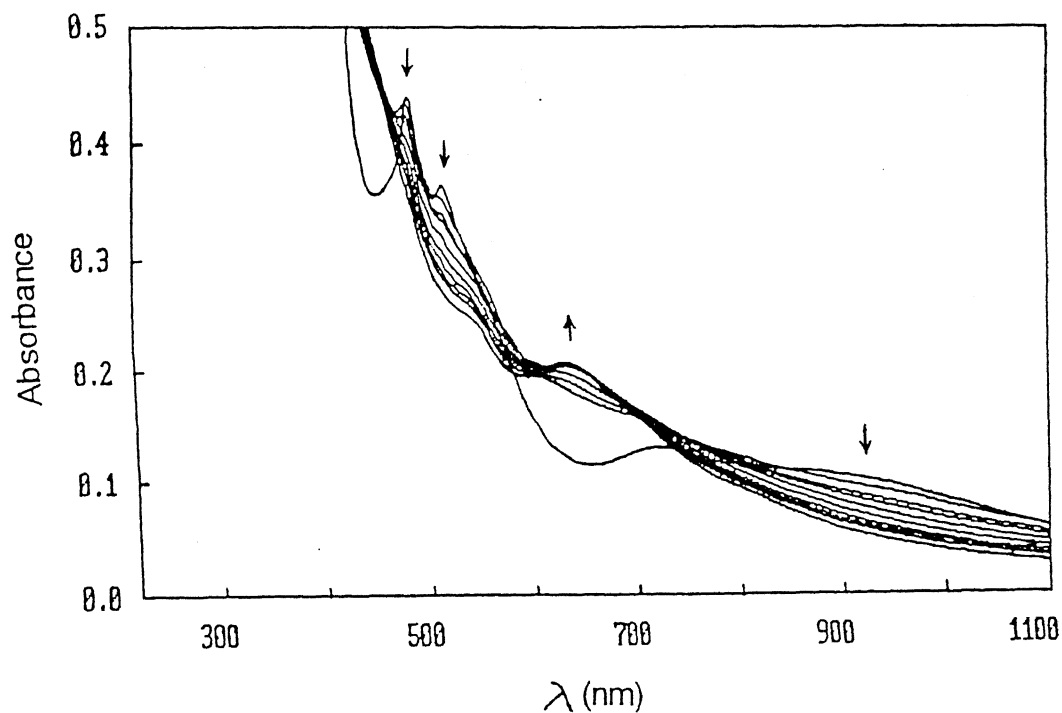
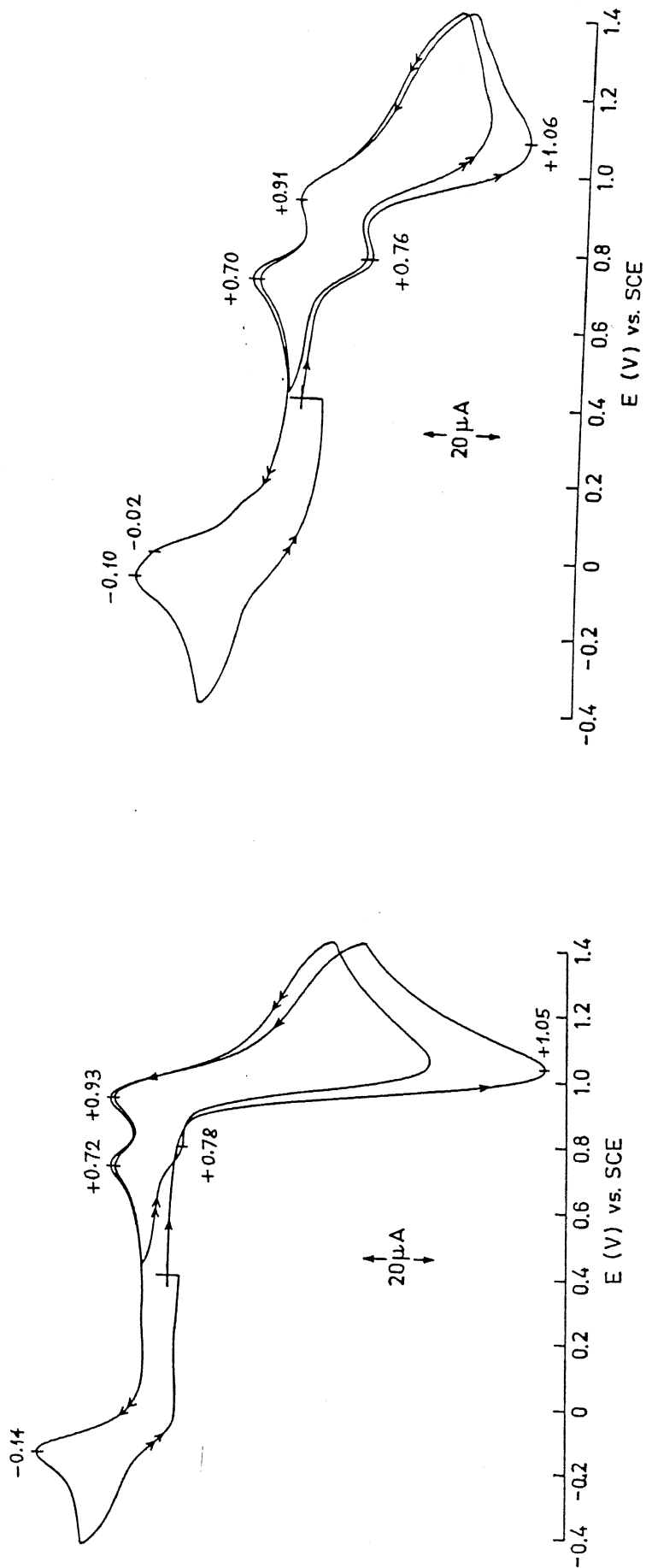


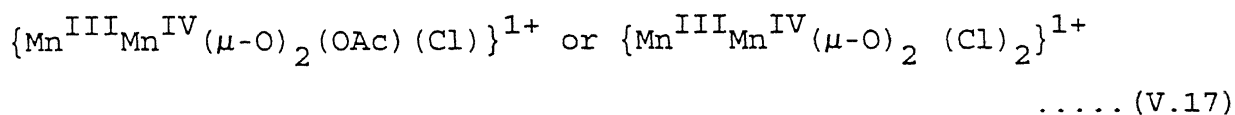
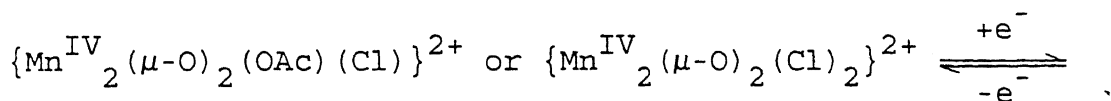
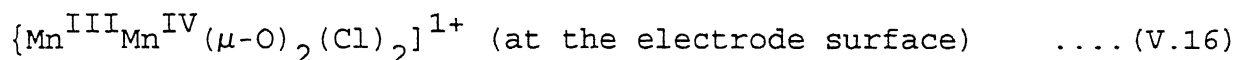
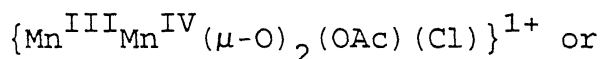
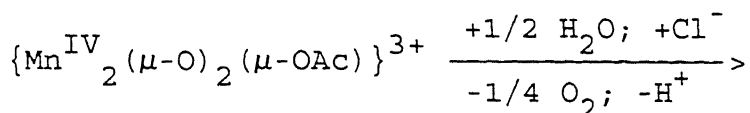
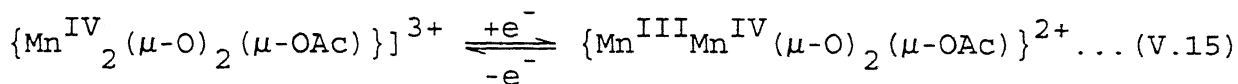
Figure V.17 Conversion of $[\text{Mn}^{\text{III}}_2(\mu\text{-O})(\mu\text{-OAc})_2(\text{MeL})_2]^{2+}$ to Chloride — ligated species in presence of 2 equivalents of $\text{Et}_4\text{NCl}\cdot x\text{H}_2\text{O}$ studied spectrophotometrically at a time interval of 5 min.



V.18 Cyclic voltammograms of a MeCN solution of $[\text{Mn}^{\text{III}}\text{Mn}^{\text{IV}}(\mu\text{-O})_2(\mu\text{-OAc})(\text{MeL})_2](\text{ClO}_4)_2 \cdot \text{H}_2\text{O}$ and $\text{Et}_4\text{NCl} \cdot x\text{H}_2\text{O}$ (1:2 mole ratio). Condition : Platinum working electrode, scan rate 50 mV s^{-1} , supporting electrolyte TBAP.

Figure V.19 Cyclic voltammograms of a MeCN solution of $[\text{Mn}_2^{\text{IV}}(\mu\text{-O})_2(\mu\text{-OAc})(\text{MeL})_2](\text{ClO}_4)_2 \cdot \text{H}_2\text{O}$ and $\text{Et}_4\text{NCl} \cdot x\text{H}_2\text{O}$ (1:2 mole ratio). Condition : Platinum working electrode, scan rate 50 mV s^{-1} , supporting electrolyte TBAP.

reacts with Cl^- and H_2O as shown in equation V.16. On reversal of the scan, an additional reductive wave was observed at 0.72 V (equation V.17). Since potential of the redox process presented in equation V.17 is much lower than that of the redox process presented in equation V.15 the chloride(s)-ligated species remains as $\text{Mn}_2(\text{IV}, \text{IV})$ at higher potential and thus being reduced on scan reversal. Again on reversal of the scan (i.e. again anodic scanning) a new oxidative wave at 0.80 V is observed. This new quasi-reversible response



$E_{1/2} = 0.76 \text{ V}$ ($\Delta E_p = 80 \text{ mV}$) (equation V.17) is associated with a new species. We believe that this species has at least one coordinated chloride ion (Cl^-) and which is being formed at the electrode surface between the reaction of 3 and Cl^- in the presence of H_2O (from $\text{Et}_4\text{NCl} \cdot x\text{H}_2\text{O}$). The above mechanism is

supported by two facts: (i) when Cl_2 gas was bubbled into an MeCN solution of **1a** we did not observe any reaction, (ii) in the presence of a trace amount of water MeCN solution of **3** changes to a solution of **1a** (equation V.14). On scanning of the potential further down to -0.40 V one irreversible reductive response was observed at -0.14 V which is more negative than that of **1a** (equation V.2). This is because Cl^- is expected to stabilize higher oxidation states. Recently, Armstrong et al.²⁰⁵ have synthesized and structurally characterized chloride-ligated $\{\text{Mn}_2^{\text{IV}}(\mu\text{-O})_2(\text{Cl})_2\}^{2+}$ species using similar type of symmetrical ligand (bpea) and the $E_{1/2}$ value ($+0.74$ V) of their chloride-ligated species is very close to that of our's.

(b) In MeCN solution containing two equivalents of $\text{Et}_4\text{NCl}\cdot x\text{H}_2\text{O}$, **3** exhibits at a platinum working electrode two successive oxidative waves (scanning in the range 0.4 to 1.4 V) at 0.80 V and 1.04 V (equations V.17 and V.16; Figure V.19). Unlike the situation in case (a) here in solution (i.e. not at the electrode surface) the chloride(s)-ligated species is formed. On reversal of the scan two reductive waves at ~ 1.00 V and 0.72 V were observed. The net effect is that we observed two responses with $E_{1/2}$ values of 0.76 V and ~ 1.00 V.

V.5.12 Concluding Remarks

(a) This is the first time a $\{\text{Mn}^{\text{III}}_2(\mu\text{-O})(\mu\text{-OAc})_2\}^{2+}$ core in high yield from a $\{\text{Mn}^{\text{III}}\text{Mn}^{\text{IV}}(\mu\text{-O})_2(\mu\text{-OAc})\}^{2+}$ core using glacial acetic acid has been isolated.

(b) Redox interconversions among all the three dimanganese cores (III,III; III,IV; IV,IV) have been achieved which can

be correlated with the S-states in PSII as a sub-structural model.

(c) X-ray structure of a novel binuclear trapped valence complex of the facially capping ligand MeL having the $\{\text{Mn}_2\text{O}_2^-(\text{OAc})\}^{2+}$ core has been determined. This represents a rare example of an asymmetric dioxo-dimanganese(III,IV) core.²⁰⁵ In fact, this is the first example of a structurally characterized dimanganese core where an asymmetric ligand (MeL) has been used as a facially capping ligand.

(d) Variable-temperature magnetic susceptibility measurements for the $\text{Mn}_2(\text{III},\text{III})$ core indicate that two Mn(III) centers are almost uncoupled.

(e) Even though we have failed so far to isolate halide-ligated dioxo-bridged dimer, we have shown by cyclic voltammetry the formation of chloride-ligated dioxo-bridged dimer in solution.

(f) The $\text{Mn}_2(\text{IV},\text{IV})$ core as well as the $\text{Mn}_2(\text{III},\text{IV})$ core can be used as potent oxidants.

References

1. McWhinnie, W. R.; Miller, J. D. *Adv. Inorg. Chem. Radiochem.* 1969, 12, 135.
2. Summers, L. A. *Adv. Heterocycl. Chem.* 1984, 35, 281 and references therein.
3. Albery, W. J.; Foulds, A. W. *Photochem.* 1979, 10, 41.
4. Crosby, G. A. *Acc. Chem. Res.* 1975, 8, 231.
5. Ford, P. C.; Wink, B.; DiBenedetto, J. *Prog. Inorg. Chem.* 1983, 30, 213.
6. McClanahan, S. F.; Dallinger, R. F.; Holler, F. J.; Kincaid, J. R. *J. Am. Chem. Soc.* 1985, 107, 4853.
7. Skorbogaty, A.; Smith, T. D. *Coord. Chem. Rev.* 1984, 53, 55.
8. Young, R. C.; Nagle, J. K.; Meyer, T. J.; Whitten, D. G. *J. Am. Chem. Soc.* 1978, 100, 4773.
9. Collin, J. -P.; Guillerez, S.; Sauvage, J. -P. *J. Chem. Soc. Chem. Commun.* 1989, 776.
10. Llobet, A.; Doppelt, P.; Meyer, T. J. *Inorg. Chem.* 1988, 27, 514.
11. Potts, K. T.; Usifer, P. A. Guadalupe, A.; Abruna, H. D. *J. Am. Chem. Soc.* 1987, 109, 3961.
12. Thompson, M. S.; Meyer, T. J. *J. Am. Chem. Soc.* 1982, 104, 5070.
13. Phifer, C. C.; McMillin, D. R. *Inorg. Chem.* 1986, 25, 1329.
14. Kirchoff, J. R.; McMillin, D. R.; Marnot, P. A.; Sauvage, J. -P. *J. Am. Chem. Soc.* 1985, 107, 1138 and references therein.
15. Collin, J. -P.; Sauvage, J. -P. *Inorg. Chem.* 1986, 25, 135.
16. Jameson, D. L.; Goldsby, K. A. *J. Org. Chem.* 1990, 55, 4992.
17. Jameson, D. L.; Blacho, . K.; Kruger, K. T.; Goldsby, K. A. *Inorg. Chem.* 1989, 28, 4312.
18. Veal, J. M.; Rill, R. L. *Biochemistry* 1988, 27, 1822.
19. Dietrich-Buchecker, C. O.; Marnot, P. A.; Sauvage, J. -P.; Kirchoff, J. R.; McMillin, D. R. *J. Chem. Soc. Chem. Commun.* 1983, 513.
20. Marnot, P. A.; Ruppert, R. R.; Sauvage, J. -P. *Nouv. J. Chim.* 1981, 5, 543.
21. Bailey, C. L.; Drago, R. S. *J. Chem. Soc. Chem. Commun.* 1987, 179.
22. Meyer, T. J. *Acc. Chem. Res.* 1978, 11, 94.

23. Gillard, R. D. *Coord. Chem. Rev.* **1983**, *50*, 303.
24. Juris, A.; Balzani, V.; Barigelletti, F.; Campanga, S. Belser, P.; Zelewsky, A. V. *Coord. Chem. Rev.* **1988**, *84*, 85 and references therein.
25. Fabian, R. H.; Klassen, D. M.; Sonntag, R. W. *Inorg. Chem.* **1980**, *19*, 1977 and references therein.
26. Araki, K.; Fuse, M.; Kishii, N.; Shiraishi, S.; Kodama, T.; Uchida, Y. *Bull. Chem. Soc. Jpn.* **1990**, *63*, 1299.
27. Case, F. H. *J. Am. Chem. Soc.* **1946**, *68*, 2574.
- 28a. Cagle, F. W. Jr.; Smith, G. F. *J. Am. Chem. Soc.* **1947**, *69*, 1860.
- 28b. Suzuki, T. M.; Kimura, T. *Bull. Chem. Soc. Jpn.* **1977**, *50*, 391.
29. Nakamura, K. *Bull. Chem. Soc. Jpn.* **1982**, *55*, 2697.
- 30a. Charlton, R. J.; Harris, C. M.; Patil, H.; Stephenson, N. C. *Inorg. Nucl. Chem. Lett.* **1966**, *2*, 409.
- 30b. Harris, C. M.; Patil, H. R. H.; Sinn, E. *Inorg. Chem.* **1967**, *6*, 1102.
- 30c. Harris, C. M.; Kokot, S.; Patil, H. R. H.; Sinn, E.; Wong, H. *Aust. J. Chem.* **1972**, *25*, 1631.
- 30d. Klassen, D. M. *Inorg. Chem.* **1976**, *15*, 3166 and references therein.
- 30e. Onggo, D.; Hook, J. M.; Rae, A. D.; Goodwin, H. A. *Inorg. Chim. Acta* **1990**, *173*, 19.
- 30f. Craig, D. C.; Goodwin, H. A.; Onggo, D. *Aust. J. Chem.* **1988**, *41*, 1157.
- 30g. Goodwin, H. A.; Kucharski, E. S.; White, A. H. *Aust. J. Chem.* **1983**, *36*, 1115.
- 30h. Abushamleh, A. S.; Goodwin, H. A.; Benson, C. G.; Long, G. J. *Aust. J. Chem.* **1984**, *37*, 281.
31. Constable, E. C. *Adv. Inorg. Chem. Radiochem.* **1986**, *30*, 69 and references therein.
32. Dietrich-Buchecker, C. O.; Marnot, P. A.; Sauvage, J. -P.; Kintinger, J. P.; Maltese, P. *Nouv. J. Chim.* **1984**, *8*, 573.
33. Kirchhoff, J. R.; McMillin, D. R. Marnot, P. A.; Sauvage, J. -P.; *J. Am. Chem. Soc.* **1985**, *107*, 1138.
34. Sprintschnik, G.; Sprintschnik, H. W.; Krisch, P. P. Whitten, D. G. *J. Am. Chem. Soc.* **1977**, *99*, 4947.

- 35a. Leising, R. A.; Takueuchi, K. J. *J. Am. Chem. Soc.* 1988, 110, 4079.
- 35b. Leising, R. A.; Kubow, S. A.; Churchill, M. R.; Buttrey, L. A. Ziller, J. W.; Takueuchi, K. J. *Inorg. Chem.* 1990, 29, 130
- 35c. Leising, R. A.; Kubow, S. A.; Takueuchi, K. J. *Inorg. Chem.* 1990, 29, 4569.
36. Thummel, R. P.; Hegde, V.; Jahng, Y. *Inorg. Chem.* 1989, 28, 3264.
- 37a. Thummel, R. P.; Decloitre, Y. *Inorg. Chim. Acta* 1987, 128, 245.
- 37b. Thummel, R. P.; Jahng, Y. *Inorg. Chem.* 1986, 25, 2527.
38. Downard, A. J.; Honey, G. E.; Steel, P. J. *Inorg. Chem.* 1991, 30, 3733.
39. Watson, A. A. House, D. A.; Steel, P. J. *Inorg. Chim. Acta* 1987, 130, 167.
40. Jameson, D. L.; Blaho, J. K.; Kruger, K. T.; Goldsby, K. A. *Inorg. Chem.* 1989, 28, 4312.
41. Jameson, D. L.; ; Goldsby, K. A. *J. Org. Chem.* 1990, 55, 4992.
42. Watson, A. A. House, D. A.; Steel, P. J. *J. Org. Chem.* 1991, 56, 4072.
- 43a. Konig, E.; Kannellakopulos, B.; Powietzka, B.; Goodwin, H. A. *Inorg. Chem.* 1989, 28, 3993.
- 43b. Abushamleh, A. S.; Goodwin, H. A. *Aust. J. Chem.* 1988, 41, 873.
44. Sanni, S. B.; Behm, H. J.; Beurskens, P. T.; van Albada, G. A.; Reedijk, J.; Lenstra, A. T. H.; Addison, A. W.; Palaniandavar, M. J. *J. Chem Soc. Dalton Trans.* 1988, 1429.
45. Piguet, C.; Bocquet, B.; Muller, E.; Williams, A. F. *Helv. Chim. Acta*, 1989, 72, 323.
46. Constable, E. C.; Henney, R. P. G.; Tocher, D. A. *J. Chem. Soc. Chem. Commun.* 1989, 913.
- 47a. Che, C. -M.; Leung, W. -H.; Li, C. -K.; Poon, C. -K. *J. Chem. Soc. Dalton Trans.* 1991, 379.
- 47b. Che, C. -M.; Lee, W. -O. *J. Chem. Soc. Chem. Commun.* 1988, 881.
- 47c. Che, C. -M.; Ho, C.; Lau, T. -C. *J. Chem. Soc. Dalton Trans.* 1991, 1901.
- 47d. Cheng, W. -C.; Yu, W. -Y.; Cheung, K. -K.; Che, C. -M.

J. Chem. Soc. Dalton Trans. 1994, 57 and references therein.

48. Che, C.-M.; Yam, V. W. -W. *J. Am. Chem. Soc.* 1987, 109, 1262. and references therein.
49. Goldstein, A. S.; Drago, R. S. *J. Chem. Soc. Chem. Commun.* 1991, 21 and references therein.
50. Gupta, N.; Grover, N.; Neyhart, G. A.; Singh, P.; Thorp, H. H. *Inorg. Chem.* 1993, 32, 310 and references therein.
- 51a. Haq, I.; Lincoln, P.; Suh, D.; Norden, B.; Chowdhry, B. Z.; Chaires, J. B. *J. Am. Chem. Soc.* 1995, 117, 4788.
- 51b. Linkletter, B.; Chin, J. *Angew. Chem. Int. Ed. Engl.* 1995, 34, 472.
- 51c. Pallenberg, A. J.; Koenig, K. S.; Barnhart, D. M. *Inorg. Chem.* 1995, 34, 2833.
52. Steel, P. J.; Lahousse, F.; Lerner, D.; Marzin, C. *Inorg. Chem.* 1983, 22, 1488.
53. Canty, A. J.; Lee, C. V. *Organometallics* 1982, 1, 1063.
- 54a. Baker, A. T.; Ferguson, N. J.; Goodwin, H. A.; Rae, A. D. *Aust. J. Chem.* 1989, 42, 623.
- 54b. Constable, E. C.; Steel, P. J. *Coord. Chem. Rev.* 1989, 93, 205.
- 54c. Sugiyarto, K. H.; Goodwin, H. A. *Aust. J. Chem.* 1988, 41, 1645.
55. McWhinnie, W. R. *J. Chem. Soc.* 1964, 5165.
56. Johnson, J. E.; Beineke, T. A.; Jacobson, R. A. *J. Chem. Soc. A* 1971, 1371.
57. Jensen, W. P.; Jacobson, R. A. *Inorg. Chim. Acta* 1981, 49, 199.
58. Cinquantini, A.; Opromolla, G.; Zanello, P. *J. Chem. Soc. Dalton Trans.* 1991, 3161.
59. Pyrka, G. J.; Seeney, R. J.; Pinkerton, A. A. *Acta Crystallogr. Sect C* 1991, 47, 510.
60. Geldard, J. F.; Gouge, E. D. *Inorg. Chem.* 1978, 17, 270.
- 61a. Huang, W. L.; Segers, D. P.; DeArmond, M. K. *J. Phys. Chem.* 1981, 85, 2080.
- 61b. Segers, D. P.; DeArmond, M. K. *J. Phys. Chem.* 1982, 86, 3768.
62. Morris, D. E.; Ohsawa, Y.; Segers, D. P.; DeArmond, M. K. *Inorg. Chem.* 1984, 23, 3010.
63. Blakley, R. L.; DeArmond, M. K. *J. Am. Chem. Soc.* 1987, 109,

4895.

64. Canty, A. J.; George, E. E.; Lee, C. V. *Aust. J. Chem.* 1983, 36, 413.
65. Bhaduri, S.; Sapre, N. Y.; Jones, P. G. *J. Chem. Soc. Dalton Trans.* 1991, 2539 and references therein.
66. Spodine, E.; Manzur, J.; Garland, M. T.; Fackler, J. P. Jr.; Staples, R. J.; Bancroft, B. T. *Inorg. Chim. Acta* 1993, 203, 73.
67. Canty, A. J.; Stevens, E. A. *Inorg. Chim. Acta* 1981, 55, L57.
68. Canty, A. J.; Hayhurst, G.; Chaichut, N.; Gatehouse, B. M. *J. Chem. Soc. Chem. Comm.* 1980, 316.
69. Canty, A. J.; Chaichut, N.; Gatehouse, B. M.; George, E. E.; Hayhurst, G. *Inorg. Chem.* 1981, 20, 2414.
70. Canty, A. J.; Minchin, N. J.; Skelton, B. W.; White, A. H. *J. Chem. Soc. Dalton Trans.* 1986, 2205.
71. Byers, P. K.; Canty, A. J.; Honeyman, R. T.; Watson, A. A. *J. Organomet. Chem.* 1990, 385, 429.
- 72a. Trofimenko, S. *J. Am. Chem. Soc.* 1970, 92, 5118.
- 72b. Trofimenko, S. *J. Am. Chem. Soc.* 1966, 88, 1842.
- 72c. Trofimenko, S. *Prog. Inorg. Chem.* 1986, 34, 115.
- 72d. Niedenzu, K.; Trofimenko, S. *Top. Curr. Chem.* 1986, 131, 1.
- 72e. Niedenzu, K.; Trofimenko, S. *Chem. Rev.* 1993, 93, 943.
73. Julia, S.; Sala, P.; Mazo, J. D.; Sancho, M.; Ochoa, C.; Elguero, J.; Fayet, J. -P.; Vertut, M. -C. *J. Heterocycl. Chem.* 1982, 19, 1141.
74. Minghetti, G.; Cinellu, M. A.; Bandini, A. L.; Banditelli, G.; Demartin, F.; Manassero, M. *J. Organomet. Chem.* 1986, 315, 387.
- 75a. Reedijk, J.; Verbiest, J. *Transition Met. Chem.* 1979, 4, 239.
- 75b. Reedijk, J.; Verbiest, J. *Transition Met. Chem.* 1978, 3, 51.
76. Lorenzotti, A.; Bonati, F.; Cingolani, A.; Lobbia, G. G.; Leonesi, D.; Bovio, B. *Inorg. Chim. Acta* 1990, 170, 199.
77. Shiu, K. -B.; Lin, S. -T.; Fung, D. -W.; Chan, T. -J.; Peng, S. -M.; Cheng, M. -C.; Chou, J. L. *Inorg. Chem.* 1995, 34, 854.
78. Fischer, B. E.; Sigel, H. *Inorg. Chem.* 1979, 18, 425.
79. House, D. A.; Steel, P. J.; Watson, A. A. *Aust. J.*

- Chem.* 1986, 39, 1525.
80. Botteghi, C.; Caccia, G.; Chelucci, G.; Soccolini, F. J. *Org. Chem.* 1984, 49, 4290.
 81. Chelucci, G.; Soccolini, F.; Botteghi, C. *Synth. Commun.* 1985, 15, 807.
 82. Brunner, H.; Riepl, G. *Angew. Chem. Int. Ed. Engl.* 1982, 21, 377.
 83. Botteghi, C.; Chelucci, G.; Chessa, G.; Delogu, G.; Gladiali, S.; Soccolini, F. J. *Organomet. Chem.* 1986, 304, 217.
 84. Halterman, R. L.; Vollhardt, K. P. C. *Tetrahedron Lett.* 1986, 27, 1461.
 85. Brunner, H. *Angew. Chem. Int. Ed. Engl.* 1983, 22, 897.
 86. Mahapatra, S.; Gupta, N.; Mukherjee, R. N. *J. Chem. Soc. - Dalton Trans.* 1991, 2911.
 87. Mahapatra, S.; Bhuniya, D.; Mukherjee, R. N. *Polyhedron* 1992, 11, 2045.
 88. Mahapatra, S.; Mukherjee, R. N. *J. Chem. Soc. Dalton Trans.* 1992, 2337.
 89. Mahapatra, S.; Mukherjee, R. N. *Indian J. Chem.* 1993, 32A, 64.
 90. Mahapatra, S.; Mukherjee, R. N. *Polyhedron* 1993, 12, 1603.
 91. Mahapatra, S.; Lal, T. K.; Mukherjee, R. N. *Polyhedron* 1993, 12, 1477.
 92. Mahapatra, S.; Butcher, R. J.; Mukherjee, R. N. *J. Chem. Soc. Dalton Trans.* 1993, 3723.
 93. Averill, B. A. *Angew. Chem. Int. Ed. Engl.* 1994, 33, 2057 and referenes therein.
 94. Godden, J. W.; Turley, S.; Teller, D. C.; Adman, E. T.; Liu, M. Y.; Payne, W. J.; LeGall, J. *Science* 1991, 253, 438.
 - 95a. Tolman, W. B. *Inorg. Chem.* 1991, 30, 4878.
 - 95b. Carrier, S. M.; Ruggiero, C. E.; Tolman, W. B.; Jameson, G. B. *J. Am. Chem. Soc.* 1992, 114, 4407.
 - 95c. Ruggiero, C. E.; Carrier, S. M.; Artholime, W. E.; Whittaker, J. W.; Cramer, C. J.; Tolman, W. B. *J. Am. Chem. Soc.* 1993, 115, 11285.
 - 95d. Halfen, J. A.; Mahapatra, S.; Olmstead, M. M.; Tolman, W. B.

- J. Am. Chem. Soc.* 1994, 116, 2173.
- 95e. Halfen, J. A.; Tolman, W. B. *J. Am. Chem. Soc.* 1994, 116, 5475.
- 95f. Ruggiero, C. E.; Carrier, S. M.; Tolman, W. B. *Angew. Chem. Int. Ed. Engl.* 1994, 33, 895.
- 95g. Jiang, F.; Conry, R. R.; Bubacco, L.; Tyeklar, Z.; Jacobson, R. R.; Karlin, K. D.; Peisach, J. *J. Am. Chem. Soc.* 1993, 115, 2093.
- 95h. Komeda, N.; Nagao, H.; Adachi, G.; Suzuki, M.; Uehara, A.; Tanaka, K. *Chem. Lett.* 1993, 1521.
- 96a. Renger, G. *Angew. Chem. Int. Ed. Engl.* 1987, 26, 643.
- 96b. Renger, G.; Wydrzynski, T. *Biol. Met.* 1991, 4, 73.
- 96c. Debus, R. J. *Biochim. Biophys. Acta* 1992, 1102, 269.
- 96d. Hansson, O.; Wydrzynski, T. *Photosynth. Res.* 1990, 23, 131.
97. Ghanotakis, D. F.; Yocum, C. F. *Annu. Rev. Plant Physiol. Plant Mol. Biol.* 1990, 41, 255.
98. Vincent, J. B.; Christou, G. *Adv. Inorg. Chem.* 1989, 33, 197.
99. Brudvig, G. W.; Crabtree, R. H. *Prog. Inorg. Chem.* 1989, 37, 99.
100. Brudvig, G. W.; Beck, W. F. *Annu. Rev. Biophys. Biophys. Chem.* 1989, 18, 25.
101. Volkov, A. G. *Bioelectrochem. Bioenerg.* 1989, 21, 3.
102. Rutherford, A. W. *Trends Biochem. Sci.* 1989, 14, 227.
103. Renger, G. *Photosynthetica* 1987, 21, 203.
104. Babcock, G. T. In *New Comprehensive Biochemistry: Photosynthesis*; Ames, J. Ed.; Elsevier: New York, 1987, 125.
105. Dismukes, G. C. *Photochem. Photobiol.* 1986, 43, 99.
106. Govindjee *Mendeleev Chem. J. (Engl. Transl.)* 1986, 31, 52.
107. Govindjee; Coleman, W. J. *Sci. Am.* 1990, 50.
108. Thorp, H. H.; Brudvig, G. W. *New J. Chem.* 1991, 15, 479.
109. Joliot, P.; Barbieri, G.; Chabaud, R. *Photochem. Photobiol.* 1969, 10, 309.
110. Kok, B.; Forbush, B.; McGloin, M. *Photochem. Photobiol.* 1970, 11, 457.
111. Boussac, A.; Zimmermann, J. -L.; Rutherford, A. W. *Biochemistry* 1989, 28, 8984.
112. Boussac, A.; Zimmermann, J. -L.; Rutherford, A. W. *FEBS Lett.* 1990, 227, 69.

113. Sivaraja, M.; Tso, J.; Dismukes, G. C. *Biochemistry* 1989, 28, 9459.
114. Tso, J.; Sivaraja, M.; Dismukes, G. C. *Biochemistry* 1991, 30, 4734.
115. Tso, J.; Sivaraja, M.; Philo, J. S.; Dismukes, G. C. *Biochemistry* 1991, 30, 4740.
116. Boussac, A.; Zimmermann, J. -L.; Rutherford, A. W.; Lavongne, J. *Nature* 1990, 397, 303.
117. Krishtalik, L. I. *Biochim. Biophys. Acta* 1986, 849, 162.
118. Brudvig, G. W.; dePaula, J. C. In *Progress in Photosynthesis Research* Biggins, J. Ed. M. Nijhoff : Boston, 1987, 1, 491.
119. Krishtalik, L. I. *Bioelectrochem. Bioenerg.* 1990, 23, 249.
120. Sawyer, D. T.; Roberts, J. L., Jr., 'Experimental Electrochemistry for Chemists', Wiley: New York, 1974.
121. Ray, M.; Mukerjee, S.; Mukherjee, R. N. *J. Chem. Soc. Dalton Trans.* 1990, 3635.
122. Evans, D. F. *J. Chem. Soc.* 1959, 2003.
123. van Geet, A. L. *Anal. Chem.* 1968, 40, 2227.
124. Gerger, W.; Mayer, U.; Gutmann, V. *Monatsh. Chem.* 1977, 108, 417.
125. O'Connor, C. J. *Prog. Inorg. Chem.* 1982, 29, 203.
126. Ramesh, K.; Mukherjee, R. N. *J. Chem. Soc. Dalton Trans.* 1992, 83.
127. Hall, S. R.; Flack, H. D.; Stewart, J. M. Eds.; University of Western Australia, Geneva and Maryland, 1992
- 128a. Bhatia, S.; Punniyamurthy, T.; Bhatia, B.; Iqbal, J. *Tetrahedron* 1993, 49, 6101.
- 128b. Punniyamurthy, T.; Iqbal, J. *Tetrahedron Letters* 1994, 35, 4003.
- 128c. Reddy, M. M.; Punniyamurthy, T.; Iqbal, J. *Tetrahedron Letters* 1995, 36, 159.
- 129a. Geary, W. J. *Coord. Chem. Rev.* 1971, 7, 81.
- 129b. Cotton, F. A.; Wilkinson, G. 'Advanced Inorganic Chemistry', 5th ed., Wiley: New York. Chichester. Brisbane. Toronto. Singapore, 1988, p. 729.
130. Mahapatra, S; Lal, T. K.; Mukherjee, R. N. *Polyhedron* 1993, 12, 1477.
131. Figgis, B. N. 'Introduction To Ligand Fields', 1st ed.,

- Wiley: New Delhi. Bangalore, 1966, p. 223 and 234.
132. Mahapatra, S.; Gupta, N. and Mukherjee, R. N. *J. Chem. Soc. Dalton Trans.* 1991, 2911.
 133. Mahapatra, S.; Mukherjee, R. N. *Indian J. Chem.* 1993, 32A, 64.
 134. Tan, J. D.; Hudson, S. E.; Brown, S. J.; Olmstead, M. M.; Mascharak, P. K. *J. Am. Chem. Soc.* 1992, 114, 3841.
 - 135a. Cotton, F. A.; Wilkinson, G. 'Advanced Inorganic Chemistry' 5th ed., Wiley: New York. Chichester. Brisbane. Toronto. Singapore, 1988, p. 744.
 - 135b. Figgis, B. N. 'Introduction To Ligand Fields', 1st ed., Wiley: New Delhi. Bangalore, 1966, p. 241.
 136. (a) DeW. Horrocks, W., Jr., in 'N.M.R. of Paramagnetic Molecules', Eds., La Mar, G. N.; DeW. Horrocks, W.; Holm, R. H. Academic Press: New York, 1973, pp. 127-177; (b) La Mar, G. N. *ibid.* p. 85-126.
 137. Bertini, I.; Luchinat, C.; Messori, L. in 'Metal Ions in Biological Systems. Applications of N.M.R. to paramagnetic Species', Vol. 21, Marcel Dekker: New York and Basel, 1987, p. 47-86.
 138. Wilson, L. J.; Georges, D.; Hoselton, M. A. *Inorg. Chem.* 1975, 14, 2968.
 139. Wicholas, M. *Inorg. Chem.* 1971, 10, 1086.
 140. Wandiga, S. O.; Sarneski, J. E.; Urbach, F. L. *Inorg. Chem.* 1972, 11, 1349.
 141. Larsen, E.; La Mar, G. N.; Wagner, B. E.; Parks, J. E.; Holm, R. H. *Inorg. Chem.* 1972, 11, 2652.
 142. Kitajima, N. *Adv. Inorg. Chem.* 1992, 39, 1.
 143. Karlin, K. D.; Tyeklar, Z. *Adv. Inorg. Biochem.* 1993, 9, 123.
 144. Kitajima, N.; Moro-oka, Y. *Chem. Rev.* 1994, 94, 737.
 145. Sorrell, T. N.; Vankai, V. A.; Garrity, M. L. *Inorg. Chem.* 1991, 30, 207.
 146. Sorrell, T. N. *Tetrahedron* 1989, 45, 3.
 147. Goodwin, J. A.; Stanbury, D. M.; Wilson, L.J.; Eigenbrot, C. W.; Scheidt, W. R. *J. Am. Chem. Soc.* 1987, 109, 2979.
 148. Knapp, S.; Keenan, T.P.; Zhang, X.; Fikar, R.; Potenza, J. A.; Schugar, H. J. *J. Am. Chem. Soc.* 1990, 112, 3452.
 149. Watson, A. A.; House, D. A.; Steel, P. J. *Inorg. Chim.*

Acta 1987, 130, 167.

150. Masood, Md. A.; Hodgson, D. J. *Inorg. Chem.* 1993, 32, 4839.
151. Oberhausen, K. J.; O'Brien, R. J.; Richardson, J. F.; Buchanan, R. M.; *Inorg. Chim. Acta* 1990, 173, 145.
152. Chen, S.; Richardson, J. F.; Buchanan, R. M. 1994, 33, 2376.
153. Kitajima, N.; Fujisawa, K.; Moro-oka, Y. *Inorg. Chem.* 1990, 29, 357.
154. Kitajima, N.; Katayama, T.; Fujisawa, K.; Iwata, Y.; Moro-oka, Y. *J. Am. Chem. Soc.* 1993, 115, 7872.
155. Tolman, W. B. *Inorg. Chem.* 1991, 30, 4877. Wei, N.; Murthy, N. N.; Karlin, K. D. *Inorg. Chem.* 1994, 33, 6093.
156. van Berkel, P. M.; Driessen, W. L.; Hamalaenen, R.; Reedijk, J.; Turpeinen, U. *Inorg. Chem.*, 1994, 33, 5920.
157. Driessen, W. L.; de Graaff, R. A. G.; Parlevliet, F. J.; Reedijk, J.; de Vos, R. M. *Inorg. Chim. Acta* 1994, 216, 43.
158. McLachlan, G. A.; Fallon, G. D.; Martin, R. L.; Spiccia, L. *Inorg. Chem.* 1995, 34, 254.
159. Satcher, J. H.; Droege, M. W.; Weakley, T. J. R.; Taylor, R. T. *Inorg. Chem.*, 1995, 34, 3317.
160. Martens, C. F.; Schenning, A. P. H. J.; Feiters, M. C.; Berens, H. W.; van der Linden, J. G. M.; Admirral, G.; Beurskens, P. T.; Kooijman, H.; Spek, A. L.; Nolte, R. J. M. *Inorg. Chem.* 1995, 34, 4735.
161. Itoh, S.; Konado, T.; Komtatsu, M.; Ohshiro, Y.; Li, C.; Kanehisa, N.; Kai, Y.; Fukuzumi, S. *J. Am. Chem. Soc.* 1995, 117, 4714.
162. Ghosh, D.; Lal, T. K.; Ghosh, S.; Mukherjee, R. N. *J. Chem. Soc., Chem. Commun.* 1996, 13.
163. Hathaway, B. J.; Billing, D. E. *Coord. Chem. Rev.* 1970, 5, 143.
164. Hathaway, B. J. in *Essays in Chemistry* (Edited by J. N. Bradley and R. D. Gillard), p. 61-96. Academic Press, New York (1971).
165. Hathaway, B. J. in *Comprehensive Coordination Chemistry* (Edited by G. Wilkinson, R. D. Gollard and J. A. McCleverty), Vol. 5, p. 533, 594, Pergamon Press, Oxford (1987) and references therein.
166. Venable, J. H. jun., Ph. D. Thesis, Yale University,

Michigan, 1966.

167. Beurskens, P. T.; Admiraal, G.; Beurskens, G.; Bosman, W. P.; Garcia-Granda, S.; Gould, R. O.; Smits, J. M. M. and Smykalla, C. PATTY (1992) and DIRDIF92. The DIRDIF program system, Technical report of the Crystallography Laboratory, University of Nijmegen, The Netherlands.
168. TEXSAN: Crystal Structure Analysis Package, Molecular Structure Corp.: The Woodlands, TX, 1985 & 1992.
169. Walker, N.; Stuart, D. *Acta Crystallogr.* 1983, A39, 158.
170. Cromer, D.T ; Waber, J. T. *International Tables for X-ray Crystallography*; The Kynoch Press: Birmingham, U.K., 1974; Vol. IV, Table 2.2 A.
171. Ibers, J. A.; Hamilton, W. C. *Acta Crystallogr.* 1964, 17, 781.
172. Creagh, D. C.; McAuley, W. J. *International Tables for X-ray Crystallography*; Kluwer Academic Publishers: Boston, 1992; Vol. C, Table 4.2.6.8, (Wilson, A. J. C., ed.).
173. Sadasivan, N.; Kernohan, J. A.; Endicott, J. E. *Inorg. Chem.* 1967, 6, 770 and references therein.
174. Mak, S. T.; Wong, W. T.; Yam, V. W. W.; Lai, T. F.; Che, C. M. *J. Chem. Soc. Dalton Trans.* 1991, 1915 and references therein.
175. Stergiou, A. C.; Papastephanou, S.; Tsiamis, C. *Polyhedron*, 1994, 13, 2285 and references therein.
176. Bernarducci, E.; Schwindinger, W. E.; Hugby, J. L. IV; Krogh-Jespersen, K.; Schugar, H. J. *J. Am. Chem. Soc.* 1981, 103, 1686.
177. Addison, A. W.; Rao, T. N.; Reedijk, J.; Rijn, J. van; Verschoor, G. C. *J. Chem. Soc., Dalton Trans.* 1984, 1349.
178. Laskowski, E. J.; Duggan, D. M.; Hendrickson, D. N. *Inorg. Chem.* 1975, 14, 2449.
179. Bouwman, E.; deGraaff, P. E. R.A G.; Kooijman, H.; Roinsot, R.; Rabu, R.; Reedijk, J.; Spek, A. *Inorg. Chem.* 1995, 34, 6303.
180. Wei, N.; Murthy, N. N.; Karlin, K. D. *Inorg. Chem.* 1994, 33, 6093.
181. Patterson, G. S.; Holm, R. H. *Bioinorg. Chem.* 1975, 4, 257.

182. Yokoi, H.; Addison, A. W. *Inorg. Chem.* 1977, 16, 1341.
183. Sorrell, T. N.; Jameson, D. L. *Inorg. Chem.* 1982, 21, 1014.
184. Ray, N. J.; Hathaway, B. G. *Acta Cryst.* 1978, B34, 3224.
185. Druhan, G.; Hathaway, B. G. *Acta Cryst.* 1979, B35, 344.
186. Ray, N. J.; Hulett, L.; Sheahan, R.; Hathaway, B. J. *J. Chem. Soc., Dalton Trans.* 1981, 1463.
187. Addison, A. W.; Hendricks, H. M. J.; Reedijk, J.; Thompson, L. K. *Inorg. Chem.* 1981, 20, 103.
188. Miyoshi, K.; Tanaka, H.; Kimura, E.; Tsuboyama, S.; Murata, S.; Shimizu, H.; Ishizu, K. *Inorg. Chim. Acta* 1983, 78, 23.
189. Fabbrizzi, L.; Poggi, A.; Zanello, P. *J. Chem. Soc., Dalton Trans.* 1983, 2191.
190. Oka, H.; Nakao, Y.; Suzuki, S.; Mori, W.; Kinoshita, I.; Ooi, S.; Ichimura, A. *Inorg. Chim. Acta.* 1989, 165, 111.
191. Murali, M.; Palaniandavar, M.; Pandiyan, T. *Inorg. Chim. Acta* 1994, 224, 19.
192. Mahapatra, S.; Gupta, N.; Mukherjee, R. N. *J. Chem. Soc. Dalton Trans* 1992, 3041.
193. Gupta, N.; Mukherjee, S.; Mahapatra, S.; Ray, M.; Mukherjee, R. N. *Inorg. Chem.* 1992, 31, 139.
194. Mahapatra, S.; Das, P.; Mukherjee, R. N. *J. Chem. Soc. Dalton Trans.* 1993, 217 and references therein.
195. Sheats, J. E.; Czernuszewicz, R. S.; Dismukes, G. C.; Rheingold, A. L.; Petrouleas, V.; Stubbe, J.; Armstrong, W. H.; Beer, R. H.; Lippard, S. J. *J. Am. Chem. Soc.* 1987, 109, 1435.
196. Wieghardt, K.; Bossek, U.; Ventur, D.; Weiss, J. *J. Chem. Soc., Chem. Commun.* 1985, 347.
197. Wieghardt, K.; Bossek, U.; Nuber, B.; Weiss, J.; Bonvoisin, J.; Corbella, M.; Vitols, S. E.; Girerd, J.-J. *J. Am. Chem. Soc.* 1988, 110, 7398.
198. Bossek, U.; Wieghardt, K.; Nuber, B.; Weiss, W. *Inorg. Chim. Acta* 1989, 165, 123.
199. Menage, S.; Girerd, J.-J.; Gleizes, A. *J. Chem. Soc., Chem. Commun.* 1988, 431.
200. Wu, F.-J.; Kurtz, D. M., Jr.; Hagen, K. S.; Nyman, P. D.;

- Debrunner, P. G.; Vankai, V. A. *Inorg. Chem.* 1990, 29, 5174.
201. Toftlund, H.; Markiewicz, A.; Murray, K. S. *Acta Chem. Scand.* 1990, 44, 443.
202. Blackman, A. G.; Huffman, J. C.; Lobkovsky, E. B.; Christou, G. J. *Chem. Soc., Chem. Commun.* 1991, 989.
- 203a. Fronko, R. M.; Penner-Hahn, J. E. *J. Am. Chem. Soc.* 1988, 110, 7554.
- 203b. Khangulov, S.; Sivaraja, M.; Barynin, V. V.; Dismukes, G. C. *Biochemistry*, 1993, 32, 4912..
- 204a. Wieghardt, K.; Bossek, U.; Zsolnai, L.; Huttner, G.; Blondin, G.; Girerd, J.-J.; Babonneau, F. J. *Chem. Soc., Chem. Commun.* 1987, 651.
- 204b. Bashkin, J. S.; Schake, A. R.; Vincent, J. B.; Chang, H. -R.; Li, Q.; Huffman, J. C.; Christou, J.; Hendrickson, D. N. *J. Chem. Soc., Chem. Commun.* 1988, 700.
- 204c. Pal, S.; Gohdes, J. W.; Wilisch, W. C. A.; Armstrong, W. H. *Inorg. Chem.* 1992, 31, 713.
205. Pal, S.; Olmstead, M. M.; Armstrong, W. H. *Inorg. Chem.* 1995, 35, 4708 and references therein.
206. Randall, D. W.; Sturgeon, B. E.; Ball, J. A.; Lorigan, G. A.; Chan, M. K.; Klein, M. P.; Armstrong, W. H.; Britt, R. D. *J. Am. Chem. Soc.* 1995, 117, 11780 and references therein.
207. Brudvig, G. W.; Thorp, H. H.; Crabtree, R. H. *Acc. Chem. Res.* 1991, 24, 311 and references therein.
208. Sauer, K.; Yachandra, V. K.; Britt, R. D.; Klein, M. P.; In *Manganese Redox Enzymes*; Pecoraro, V. L., Ed.; VCH Publishers: New York, 1992, pp 141.
209. Klein, M. P.; Yachandra, V. K. *J. Inorg. Biochem.* 1991, 43, 363.
210. Chan, K. M.; Armstrong, W. H. *J. Am. Chem. Soc.* 1991, 113, 5055 and references therein.
211. Wieghardt, K.; Bossek, U.; Bonvoisin, J.; Beauvillain, P.; Girerd, J.-J.; Nuber, B.; Weiss, J.; Heinze, J. *Angew. Chem., Int. Ed. Engl.* 1986, 25, 1030.
212. Cooper, S. R.; Calvin, M. J. *Am. Chem. Soc.* 1977, 99, 6623.
213. Sarneski, J. E.; Thorp, H. H.; Brudvig, G. W.; Crabtree, R. H.; Schulte, G. K. *J. Am. Chem. Soc.* 1990, 112, 7255.

- 214a. Manchanda, R.; Brudvig, G. W.; Crabtree, R. H. Sarneski, J. E.; Didiuk, M. *Inorg. Chim. Acta* 1993, 212, 135.
- 214b. Sarneski, J. E.; Brzezinski, L. J.; Anderson, B.; Didiuk, M.; Manchanda, R.; Crabtree, R. H.; Brudvig, G. W.; Schulte, G. K. *Inorg. Chem.* 1993, 32, 3265.
215. Pal, S.; Chan, M. K.; Armstrong, W. H. *J. Am. Chem. Soc.* 1992, 114, 6398 and references therein.
216. Pal, S.; Armstrong, W. H. *Inorg. Chem.* 1992, 31, 5417.
217. Okai, A. R.; Glerup, J.; Hodgson, D. J. *Inorg. Chem.* 1990, 29, 2435.
218. Goodson, P. A.; Glerup, J.; Hodgson, D. J.; Michelsen, K.; Weihe, H. *Inorg. Chem.* 1991, 30, 4909 and references therein.
219. Bard, A. J.; Faulker, L. R. *Electrochemical Methods: Fundamentals and Applications*; Wiley: New York, 1980.
220. Reddy, K. R.; Rajasekharan, M. V.; Padhye, S.; Dahan, F.; Tuchagues, J.-P. *Inorg. Chem.* 1994, 33, 428.
221. Glerup, J.; Goodson, P. A.; Hazell, A.; Hazell, R.; Hodgson, D. J.; McKenzie, C. J.; Michelsen, K.; Rychlewska, U.; Toftlund, H. *Inorg. Chem.* 1994, 33, 4105.
222. Hendrickson, D. N.; Christou, G.; Schmitt, E. A.; Libby, E.; Bashkin, J. S.; Wang, S.; Tsai, H.-L.; Vincent, J. B.; Boyd, P. D. W.; Huffman, J. C.; Folting, K.; Li, Q.; Streib, W. E. *J. Am. Chem. Soc.* 1992, 114, 2455.
223. Wemple, M. W.; Tsai, H.-L.; Folting, K.; Hendrickson, D. N.; Christou, G. *Inorg. Chem.* 1993, 32, 2025.

PLANE CALCULATIONS FOR THE COMPLEX [Co(Me₂pp)Cl₂]

PLANE NUMBER 1

=====

EQUATION OF PLANE AS AX+BY+CZ=D, XYZ IN FRACTIONAL AND ORTHOGONAL UNITS

	A	B	C	D	ESDA	ESDB	ESDC	ESDD
	6.7813	-.7038	-3.2978	1.0666	.0033	.0089	.0052	.0052
	.9515	-.0134	-.3074	1.0666	.0005	.0011	.0005	.0052

ATOM		DIST(A)	ESDD	X	Y	Z
Co	DEFINING	-.0000	.0013	.3095	.2775	.2537
Cl1	DEFINING	.0000	.0015	.2548	.4987	.0941
Cl2	DEFINING	.0000	.0014	.3958	.3310	.4198

PLANE NUMBER 2

=====

EQUATION OF PLANE AS AX+BY+CZ=D, XYZ IN FRACTIONAL AND ORTHOGONAL UNITS

	A	B	C	D	ESDA	ESDB	ESDC	ESDD
	3.0457	-.6426	9.8988	3.2757	.0101	.0126	.0059	.0059
	.2361	-.3045	.9228	3.2757	.0013	.0016	.0006	.0059

ANGLE BETWEEN PLANES/LINES 1 2 93.151 ESD .078

ATOM		DIST(A)	ESDD	X	Y	Z
Co	DEFINING	.0000	.0011	.3095	.2775	.2537
N1	DEFINING	-.0000	.0037	.4900	.0822	.1855
N3	DEFINING	-.0000	.0037	.1227	.1421	.3024

PLANE NUMBER 3

=====

EQUATION OF PLANE AS AX+BY+CZ=D, XYZ IN FRACTIONAL AND ORTHOGONAL UNITS

	A	B	C	D	ESDA	ESDB	ESDC	ESDD
	6.2051	2.6644	8.5871	4.8458	.0082	.0120	.0101	.0032
	.5830	.1388	.8005	4.8458	.0011	.0015	.0009	.0032

<CHI**2>	<GOODNESS OF FIT>	<N-3>
14.7609	2.2182	3

ANGLE BETWEEN PLANES/LINES 1 3 72.136 ESD .094

ANGLE BETWEEN PLANES/LINES 2 3 33.479 ESD .125

ATOM		DIST(A)	ESDD	X	Y	Z
N1	DEFINING	.0062	.0031	.4900	.0822	.1855
C1	DEFINING	-.0096	.0042	.6154	.1124	.0837
C2	DEFINING	.0004	.0050	.7383	-.0152	.0356
C3	DEFINING	.0089	.0049	.7305	-.1813	.0937
C4	DEFINING	-.0053	.0046	.5991	-.2156	.1977
C5	DEFINING	-.0038	.0038	.4808	-.0802	.2413

Contd.

PLANE NUMBER 4

=====

EQUATION OF PLANE AS $AX+BY+CZ=D$, XYZ IN FRACTIONAL AND ORTHOGONAL UNITS

A	B	C	D	ESDA	ESDB	ESDC	ESDD
.0380	1.8949	10.4482	3.4318	.0137	.0137	.0041	.0022
-.2265	.0005	.9740	3.4318	.0018	.0017	.0004	.0022

<CHI**2>	<GOODNESS OF FIT>	<N-3>
.6476	.5690	2

ANGLE BETWEEN PLANES/LINES	1	4	120.994 ESD	.102
ANGLE BETWEEN PLANES/LINES	2	4	32.307 ESD	.126
ANGLE BETWEEN PLANES/LINES	3	4	49.630 ESD	.132

ATOM		DIST(A)	ESDD	X	Y	Z
N2	DEFINING	-.0014	.0033	.1674	-.0318	.3335
N3	DEFINING	.0015	.0032	.1227	.1421	.3024
C9	DEFINING	-.0015	.0039	-.0465	.1761	.2965
C8	DEFINING	.0003	.0041	-.1058	.0260	.3241
C7	DEFINING	.0013	.0041	.0314	-.1050	.3475

PLANE NUMBER 1

=====

EQUATION OF PLANE AS $AX+BY+CZ=D$, XYZ IN FRACTIONAL AND ORTHOGONAL UNITS

A	B	C	D	ESDA	ESDB	ESDC	ESDD
6.6272	-3.4284	-3.8916	6.6272	.0086	.0243	.0301	.0085
.7622	-.5214	-.3836	6.6272	.0019	.0030	.0030	.0085

ATOM		DIST(A)	ESDD	X	Y	Z
N1	DEFINING	-.0000	.0095	.8690	-.0247	-.2014
N3	DEFINING	.0000	.0092	1.1596	.2750	.0295
Co	DEFINING	.0000	.0010	1.0000	.0000	.0000

PLANE NUMBER 2

=====

EQUATION OF PLANE AS $AX+BY+CZ=D$, XYZ IN FRACTIONAL AND ORTHOGONAL UNITS

A	B	C	D	ESDA	ESDB	ESDC	ESDD
-4.5686	6.5102	3.7759	-4.8891	.0254	.0283	.0443	.0216
-.2896	.8818	.3722	-4.8891	.0043	.0036	.0044	.0216

<CHI**2> <GOODNESS OF FIT> <N-3>
 .3720 .4313 2

ANGLE BETWEEN PLANES/LINES 1 2 145.423 ESD .319

ATOM		DIST(A)	ESDD	X	Y	Z
N2	DEFINING	.0010	.0084	.9614	.0813	-.2715
N1	DEFINING	-.0021	.0080	.8690	-.0247	-.2014
C1	DEFINING	.0042	.0104	.6777	-.1165	-.2728
C2	DEFINING	-.0042	.0124	.6454	-.0727	-.3896
C3	DEFINING	.0012	.0122	.8303	.0555	-.3857

PLANE NUMBER 3

=====

EQUATION OF PLANE AS $AX+BY+CZ=D$, XYZ IN FRACTIONAL AND ORTHOGONAL UNITS

A	B	C	D	ESDA	ESDB	ESDC	ESDD
7.0021	-2.7927	.8996	7.3801	.0051	.0312	.0398	.0113
.9489	-.3027	.0887	7.3801	.0020	.0039	.0039	.0113

<CHI**2> <GOODNESS OF FIT> <N-3>
 1.5977 .7298 3

ANGLE BETWEEN PLANES/LINES 1 3 32.103 ESD .291

ANGLE BETWEEN PLANES/LINES 2 3 120.582 ESD .344

ATOM		DIST(A)	ESDD	X	Y	Z
N3	DEFINING	-.0020	.0076	1.1596	.2750	.0295
C5	DEFINING	.0067	.0094	1.1985	.3352	-.0769
C6	DEFINING	-.0052	.0114	1.2633	.5078	-.0589
C7	DEFINING	-.0047	.0131	1.2925	.6225	.0710
C8	DEFINING	.0090	.0120	1.2566	.5643	.1848
C9	DEFINING	-.0036	.0101	1.1889	.3905	.1577

Table of Least-Squares Planes for $[\text{Cu}(\text{Me}_2\text{PP})_2(\text{NO}_2)](\text{ClO}_4)$

----- Plane number 1 -----

Atoms Defining Plane	Distance	esd
N(1)	0.0047	0.0046
C(1)	-0.0033	0.0064
C(2)	-0.0029	0.0080
C(3)	0.0034	0.0094
C(4)	0.0044	0.0078
C(5)	-0.0071	0.0059

Mean deviation from plane is 0.0043 angstroms
Chi-squared: 3.0

----- Plane number 2 -----

Atoms Defining Plane	Distance	esd
N(2)	-0.0006	0.0044
N(3)	0.0003	0.0043
C(7)	0.0014	0.0068
C(8)	-0.0011	0.0070
C(9)	0.0000	0.0054

Mean deviation from plane is 0.0007 angstroms
Chi-squared: 0.1

Dihedral angles between least-squares planes

plane	plane	angle
2	1	59.92

----- Plane number 3 -----

Atoms Defining Plane	Distance	esd
N(4)	0.0009	0.0043
C(10)	0.0080	0.0057
C(11)	-0.0117	0.0065
C(12)	0.0036	0.0070
C(13)	0.0072	0.0063
C(14)	-0.0068	0.0053

Mean deviation from plane is 0.0064 angstroms
Chi-squared: 7.5

Dihedral angles between least-squares planes

plane	plane	angle
3	1	171.47
3	2	112.50

Contd

Table of Least-Squares Planes (continued)

----- Plane number 4 -----

Atoms Defining Plane	Distance	esd
N(5)	-0.0085	0.0041
N(6)	0.0075	0.0043
C(16)	0.0131	0.0057
C(17)	-0.0073	0.0062
C(18)	-0.0042	0.0059

Mean deviation from plane is 0.0081 angstroms

Chi-squared: 13.0

Dihedral angles between least-squares planes

plane	plane	angle
4	1	119.16
4	2	60.84
4	3	52.58

PLANE CALCULATIONS FOR THE COMPLEX [Cu(Me2pp) (Me4bpp)] (ClO4)2

PLANE NUMBER 1

=====

EQUATION OF PLANE AS AX+BY+CZ=D, XYZ IN FRACTIONAL AND ORTHOGONAL UNITS

A	B	C	D	ESDA	ESDB	ESDC	ESDD
.7755	11.5369	-7.1013	3.5590	.0469	.0164	.1589	.0768
.0809	.9665	-.2436	3.5590	.0049	.0014	.0055	.0768

ATOM		DIST(A)	ESDD	X	Y	Z
N1	DEFINING	-.0000	.0162	.4152	.4858	.3334
Cu	DEFINING	.0000	.0015	.5474	.5101	.3874
N8	DEFINING	-.0000	.0148	.7381	.4723	.3467

PLANE NUMBER 2

=====

EQUATION OF PLANE AS AX+BY+CZ=D, XYZ IN FRACTIONAL AND ORTHOGONAL UNITS

A	B	C	D	ESDA	ESDB	ESDC	ESDD
-8.2323	1.0640	14.6876	1.9132	.0193	.0453	.0994	.0541
-.8591	.0891	.5039	1.9132	.0020	.0038	.0034	.0541

<CHI**2>	<GOODNESS OF FIT>	<N-3>
130.079	11.4052	1

ANGLE BETWEEN PLANES/LINES	1	2	96.094 ESD	.350
----------------------------	---	---	------------	------

ATOM		DIST(A)	ESDD	X	Y	Z
N1	DEFINING	.0820	.0141	.4152	.4858	.3334
N3	DEFINING	-.0720	.0129	.5363	.6814	.3766
N5	DEFINING	.0759	.0133	.6309	.5503	.4492
N6	DEFINING	-.0813	.0142	.5412	.3453	.4030
Cu	NON-DEFINING	-.1870	.0016	.5474	.5101	.3874
N8	NON-DEFINING	-2.3946	.0107	.7381	.4723	.3467

PLANE NUMBER 3

=====

EQUATION OF PLANE AS AX+BY+CZ=D, XYZ IN FRACTIONAL AND ORTHOGONAL UNITS

A	B	C	D	ESDA	ESDB	ESDC	ESDD
-7.0638	-6.0276	13.0859	-1.4933	.0501	.0806	.2055	.0887
-.7372	-.5049	.4490	-1.4933	.0052	.0067	.0071	.0887

<CHI**2>	<GOODNESS OF FIT>	<N-3>
3.1851	1.2620	2

ANGLE BETWEEN PLANES/LINES	1	3	131.077 ESD	.520
----------------------------	---	---	-------------	------

ANGLE BETWEEN PLANES/LINES	2	3	35.453 ESD	.495
----------------------------	---	---	------------	------

ATOM		DIST(A)	ESDD	X	Y	Z
N1	DEFINING	-.0052	.0136	.4152	.4858	.3334
C1	DEFINING	-.0032	.0170	.4109	.4121	.2973
C2	DEFINING	.0195	.0211	.3150	.4519	.2656
C3	DEFINING	-.0251	.0205	.2620	.5520	.2797
N2	DEFINING	.0116	.0145	.3233	.5667	.3223

Contd.

PLANE NUMBER 4

=====

EQUATION OF PLANE AS $AX+BY+CZ=D$, XYZ IN FRACTIONAL AND ORTHOGONAL UNITS

A	B	C	D	ESDA	ESDB	ESDC	ESDD
-3.3672	2.5863	26.5472	9.9647	.0569	.0691	.0748	.0695
-.3514	.2167	.9108	9.9647	.0059	.0058	.0026	.0695

<CHI**2>	<GOODNESS OF FIT>	<N-3>
3.5564	1.0888	3

ANGLE BETWEEN PLANES/LINES 1 4 92.347 ESD .455

ANGLE BETWEEN PLANES/LINES 2 4 38.722 ESD .426

ANGLE BETWEEN PLANES/LINES 3 4 56.043 ESD .572

ATOM		DIST(A)	ESDD	X	Y	Z
N3	DEFINING	-.0104	.0122	.5363	.6814	.3766
C5	DEFINING	.0156	.0147	.4226	.7289	.3585
C6	DEFINING	-.0183	.0194	.4189	.8402	.3459
C7	DEFINING	.0083	.0195	.5314	.9043	.3550
C8	DEFINING	-.0075	.0194	.6480	.8557	.3739
C9	DEFINING	.0113	.0163	.6513	.7446	.3859

PLANE NUMBER 5

=====

EQUATION OF PLANE AS $AX+BY+CZ=D$, XYZ IN FRACTIONAL AND ORTHOGONAL UNITS

A	B	C	D	ESDA	ESDB	ESDC	ESDD
-7.0792	7.9052	3.6400	1.5110	.0462	.0637	.2086	.1214
-.7388	.6622	.1249	1.5110	.0048	.0053	.0072	.1214

<CHI**2>	<GOODNESS OF FIT>	<N-3>
4.8664	1.5599	2

ANGLE BETWEEN PLANES/LINES 1 5 56.645 ESD .488

ANGLE BETWEEN PLANES/LINES 2 5 40.826 ESD .460

ANGLE BETWEEN PLANES/LINES 3 5 74.555 ESD .602

ANGLE BETWEEN PLANES/LINES 4 5 58.878 ESD .540

ATOM		DIST(A)	ESDD	X	Y	Z
N5	DEFINING	.0076	.0129	.6309	.5503	.4492
N4	DEFINING	-.0134	.0130	.7290	.6348	.4505
C11	DEFINING	.0283	.0182	.7685	.6554	.4942
C12	DEFINING	-.0190	.0186	.7028	.5786	.5201
C13	DEFINING	.0014	.0157	.6178	.5172	.4936

Contd.

PLANE NUMBER 6

=====

EQUATION OF PLANE AS $AX+BY+CZ=D$, XYZ IN FRACTIONAL AND ORTHOGONAL UNITS

A	B	C	D	ESDA	ESDB	ESDC	ESDD
5.9174	7.9656	12.1348	12.3338	.0555	.0701	.2046	.0441
.6176	.6673	.4163	12.3338	.0058	.0059	.0070	.0441

<CHI**2>	<GOODNESS OF FIT>	<N-3>
.3843	.4384	2

ANGLE BETWEEN PLANES/LINES	1	6	53.595 ESD	.559
ANGLE BETWEEN PLANES/LINES	2	6	105.147 ESD	.472
ANGLE BETWEEN PLANES/LINES	3	6	127.250 ESD	.624
ANGLE BETWEEN PLANES/LINES	4	6	72.136 ESD	.553
ANGLE BETWEEN PLANES/LINES	5	6	87.842 ESD	.597

ATOM		DIST(A)	ESDD	X	Y	Z
N8	DEFINING	.0030	.0125	.7381	.4723	.3467
N7	DEFINING	-.0051	.0144	.8205	.3865	.3621
C24	DEFINING	.0080	.0197	.9197	.3617	.3311
C25	DEFINING	-.0027	.0193	.9014	.4310	.2937
C26	DEFINING	-.0026	.0189	.7866	.4994	.3048

PLANE NUMBER 7

=====

EQUATION OF PLANE AS $AX+BY+CZ=D$, XYZ IN FRACTIONAL AND ORTHOGONAL UNITS

A	B	C	D	ESDA	ESDB	ESDC	ESDD
-.0669	3.5107	27.8572	12.4073	.0603	.0709	.0534	.0330
-.0070	.2941	.9557	12.4073	.0063	.0059	.0018	.0330

<CHI**2>	<GOODNESS OF FIT>	<N-3>
3.1348	1.0222	3

ANGLE BETWEEN PLANES/LINES	1	7	87.087 ESD	.479
ANGLE BETWEEN PLANES/LINES	2	7	59.081 ESD	.423
ANGLE BETWEEN PLANES/LINES	3	7	73.397 ESD	.574
ANGLE BETWEEN PLANES/LINES	4	7	20.500 ESD	.504
ANGLE BETWEEN PLANES/LINES	5	7	71.380 ESD	.551
ANGLE BETWEEN PLANES/LINES	6	7	53.853 ESD	.556

ATOM		DIST(A)	ESDD	X	Y	Z
N6	DEFINING	-.0038	.0134	.5412	.3453	.4030
C18	DEFINING	.0125	.0166	.4134	.2994	.4091
C19	DEFINING	-.0194	.0186	.3944	.1891	.4218
C20	DEFINING	.0224	.0210	.5121	.1280	.4313
C21	DEFINING	-.0090	.0185	.6427	.1731	.4248
C22	DEFINING	.0030	.0159	.6586	.2833	.4114

PLANE CALCULATIONS FOR THE COMPLEX [Mn₂(III, IV) (O)₂ (OAc) (MeL)₂] (BF₄)₂·2MeCN

PLANE NUMBER 1

=====

EQUATION OF PLANE AS AX+BY+CZ=D, XYZ IN FRACTIONAL AND ORTHOGONAL UNITS

A	B	C	D	ESDA	ESDB	ESDC	ESDD
-.3359	-5.2734	11.0902	-2.5715	.0587	.0728	.0666	.0735
.0311	-.7264	.6866	-2.5715	.0059	.0060	.0041	.0735

ATOM		DIST(A)	ESDD	X	Y	Z
Mn1	DEFINING	-.0000	.0025	.2764	.7924	.1533
O1	DEFINING	-.0000	.0137	.1371	.8694	.1857
O2	DEFINING	-.0000	.0137	.3756	.8593	.1881

PLANE NUMBER 2

=====

EQUATION OF PLANE AS AX+BY+CZ=D, XYZ IN FRACTIONAL AND ORTHOGONAL UNITS

A	B	C	D	ESDA	ESDB	ESDC	ESDD
-.2121	-1.6848	13.8096	1.0704	.0588	.0751	.0457	.0843
-.0125	-.5185	.8550	1.0704	.0059	.0061	.0028	.0843

ANGLE BETWEEN PLANES/LINES 1 2 15.575 ESD .444

ATOM		DIST(A)	ESDD	X	Y	Z
Mn2	DEFINING	-.0000	.0026	.2350	.9578	.1980
O1	DEFINING	-.0000	.0137	.1371	.8694	.1857
O2	DEFINING	-.0000	.0137	.3756	.8593	.1881

PLANE NUMBER 3

=====

EQUATION OF PLANE AS AX+BY+CZ=D, XYZ IN FRACTIONAL AND ORTHOGONAL UNITS

A	B	C	D	ESDA	ESDB	ESDC	ESDD
-.2826	-3.4732	12.5949	-.8896	.0587	.0211	.0155	.0324
.0082	-.6260	.7798	-.8896	.0058	.0017	.0010	.0324

<CHI**2> <GOODNESS OF FIT> <N-3>
418.230 20.4507 1

ANGLE BETWEEN PLANES/LINES 1 3 7.960 ESD .327

ANGLE BETWEEN PLANES/LINES 2 3 7.615 ESD .314

ATOM		DIST(A)	ESDD	X	Y	Z
Mn1	DEFINING	-.0099	.0029	.2764	.7924	.1533
O1	DEFINING	.1699	.0121	.1371	.8694	.1857
Mn2	DEFINING	-.0101	.0030	.2350	.9578	.1980
O2	DEFINING	.1682	.0120	.3756	.8593	.1881

PLANE NUMBER 4

=====

EQUATION OF PLANE AS AX+BY+CZ=D, XYZ IN FRACTIONAL AND ORTHOGONAL UNITS

A	B	C	D	ESDA	ESDB	ESDC	ESDD
4.8692	12.3818	11.0200	12.7827	.0724	.0480	.0886	.0064
.2894	.6714	.6823	12.7827	.0072	.0045	.0055	.0064

contd.

<CHI**2>	<GOODNESS OF FIT>	<N-3>
.5517	.4289	3

ANGLE BETWEEN PLANES/LINES	1	4	90.586 ESD	.537
ANGLE BETWEEN PLANES/LINES	2	4	76.610 ESD	.531
ANGLE BETWEEN PLANES/LINES	3	4	83.450 ESD	.456

ATOM		DIST(A)	ESDD	X	Y	Z
N1	DEFINING	.0019	.0160	.2986	.6686	.2770
C3	DEFINING	-.0042	.0202	.2032	.6471	.3427
C4	DEFINING	-.0018	.0226	.2322	.5639	.4236
C5	DEFINING	.0102	.0233	.3527	.5043	.4385
C6	DEFINING	-.0126	.0243	.4502	.5247	.3704
C7	DEFINING	.0033	.0199	.4217	.6065	.2924

PLANE NUMBER 5

=====

EQUATION OF PLANE AS AX+BY+CZ=D, XYZ IN FRACTIONAL AND ORTHOGONAL UNITS

A	B	C	D	ESDA	ESDB	ESDC	ESDD
2.5496	-7.1108	8.1559	-3.7121	.0678	.0801	.0985	.0646
.3483	-.7897	.5049	-3.7121	.0068	.0069	.0061	.0646

<CHI**2>	<GOODNESS OF FIT>	<N-3>
.8602	.5355	3

ANGLE BETWEEN PLANES/LINES	1	5	21.383 ESD	.524
ANGLE BETWEEN PLANES/LINES	2	5	33.190 ESD	.520
ANGLE BETWEEN PLANES/LINES	3	5	27.004 ESD	.467
ANGLE BETWEEN PLANES/LINES	4	5	94.872 ESD	.576

ATOM		DIST(A)	ESDD	X	Y	Z
N3	DEFINING	-.0016	.0139	.1552	.7118	.1167
C12	DEFINING	-.0060	.0179	.1914	.6619	.0614
C13	DEFINING	.0133	.0213	.1094	.6066	.0411
C14	DEFINING	-.0073	.0215	-.0160	.6076	.0787
C15	DEFINING	-.0045	.0210	-.0547	.6571	.1343
C16	DEFINING	.0078	.0182	.0328	.7095	.1542

PLANE NUMBER 6

=====

EQUATION OF PLANE AS AX+BY+CZ=D, XYZ IN FRACTIONAL AND ORTHOGONAL UNITS

A	B	C	D	ESDA	ESDB	ESDC	ESDD
4.9438	13.2433	7.4500	15.4099	.0923	.0421	.1226	.0486
.2883	.8391	.4612	15.4099	.0092	.0048	.0076	.0486

<CHI**2>	<GOODNESS OF FIT>	<N-3>
.8015	.5169	3

ANGLE BETWEEN PLANES/LINES	1	6	106.490 ESD	.589
ANGLE BETWEEN PLANES/LINES	2	6	92.542 ESD	.582
ANGLE BETWEEN PLANES/LINES	3	6	99.397 ESD	.515

Contd.

ANGLE BETWEEN PLANES/LINES 4 6 15.949 ESD .638

ANGLE BETWEEN PLANES/LINES 5 6 109.230 ESD .640

ATOM		DIST(A)	ESDD	X	Y	Z
N4	DEFINING	.0053	.0153	.2151	.8887	.3467
C17	DEFINING	-.0170	.0264	.3039	.8200	.4068
C18	DEFINING	.0105	.0277	.2609	.7830	.5049
C19	DEFINING	-.0048	.0301	.1369	.8185	.5219
C20	DEFINING	.0052	.0366	.0490	.8877	.4586
C21	DEFINING	-.0071	.0248	.0792	.9232	.3738

PLANE NUMBER 7

=====

EQUATION OF PLANE AS AX+BY+CZ=D, XYZ IN FRACTIONAL AND ORTHOGONAL UNITS

A	B	C	D	ESDA	ESDB	ESDC	ESDD
-3.0986	2.2942	14.6249	4.3666	.0981	.1224	.0635	.1564
-.3588	-.2267	.9055	4.3666	.0099	.0098	.0039	.1564

<CHI**2>	<GOODNESS OF FIT>	<N-3>
10.5330	1.8738	3

ANGLE BETWEEN PLANES/LINES 1 7 39.176 ESD .657

ANGLE BETWEEN PLANES/LINES 2 7 26.341 ESD .671

ANGLE BETWEEN PLANES/LINES 3 7 32.325 ESD .613

ANGLE BETWEEN PLANES/LINES 4 7 68.793 ESD .661

ANGLE BETWEEN PLANES/LINES 5 7 59.254 ESD .721

ANGLE BETWEEN PLANES/LINES 6 7 82.879 ESD .708

ATOM		DIST(A)	ESDD	X	Y	Z
N6	DEFINING	-.0147	.0188	.3546	1.0604	.2064
C26	DEFINING	.0559	.0264	.3227	1.1673	.1877
C27	DEFINING	-.0267	.0249	.4182	1.2228	.1935
C28	DEFINING	-.0140	.0286	.5369	1.1618	.2291
C29	DEFINING	.0707	.0366	.5651	1.0539	.2578
C30	DEFINING	-.0148	.0265	.4757	1.0050	.2407

An extensive coordination chemistry of cobalt(II), nickel(II), and copper(II) with pyrazolylmethylpyridine ligands has been described (chapters II - IV). A fascinating catalytic oxidation chemistry has been demonstrated using *pseudo*-tetrahedral cobalt(II) complexes. Future scope lies in (i) identifying the oxygenated cobalt species responsible for the oxidation chemistry, (ii) structural characterization of violet and green copper(II) complexes, and (iii) developing the copper(I) chemistry as the Cu(II)/Cu(I) redox potentials are fairly positive.

The electrochemistry of **3** which has been described (Chapter III) can be extended to model the other species of relevance to nitrite reductases.

The oxo-bridged dimanganese chemistry described in chapter V is quite involved and sets ground for future scopes of this work. They include: (i) structural characterization of $\text{Mn}_2(\text{III}, \text{III})$ and $\text{Mn}_2(\text{IV}, \text{IV})$ complexes, and (ii) temperature-dependent magnetic susceptibility studies on the $\text{Mn}_2(\text{IV}, \text{IV})$ complex, (iii) isolation of the chloride-ligated Mn-complexes in the solid state, and (iv) the final goal of functional modeling, such as oxidation of water using these complexes.